Alternative catalysts and technologies for NOx removal from biomass- and wastefired plants.

Schill, Leonhard; Fehrmann, Rasmus; Jensen, Anker Degn

Publication date:
2014

Document Version
Publisher's PDF, also known as Version of record

Technical University of Denmark

Alternative catalysts and technologies for NO_x removal from biomass- and waste-fired plants

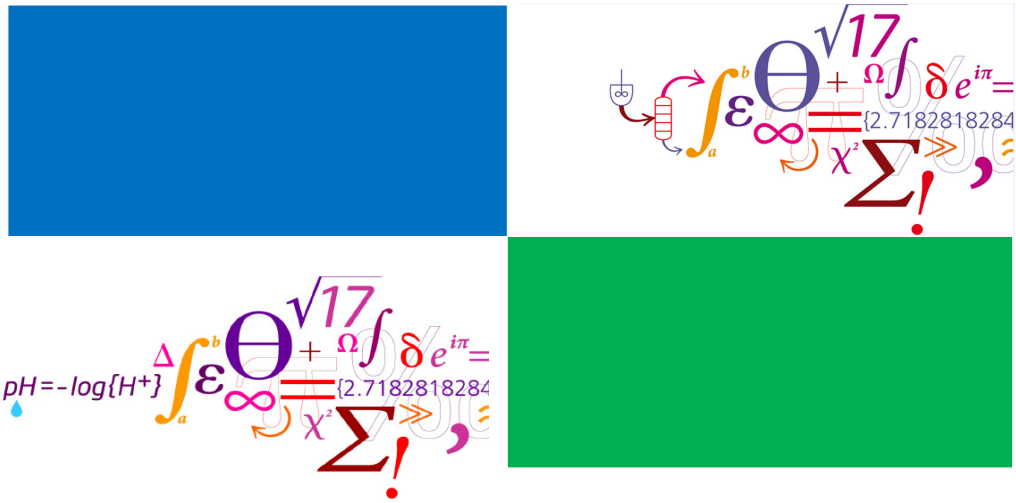

DTU Chemistry
Department of Chemistry

Ph.D. Thesis
Leonhard Schill
February 2014

Preface

This thesis has been submitted in candidacy for the Ph.D. degree in Chemistry from the Technical University of Denmark (DTU). The work summarized herein was mostly carried out at the Department of Chemistry in the Centre for Catalysis and Sustainable Chemistry (CSC) and to some extent at the Department of Chemical Engineering in the Centre for Combustion and Harmful Emission Control (CHEC), from January 2011 to January 2014. The work was jointly supervised by Prof. Rasmus Fehramnn (CSC) and Anker Degn Jensen (CHEC) and financed by Energinet.dk through the PSO Project 10521.

First and foremost I would like to thank my two supervisors, Rasmus Fehrmann and Anker Degn Jensen for having given me the opportunity to work on this project and for the good supervision. Great thanks also to Siva Sankar Reddy Putluru for good collaboration and strong support. Without him the project would not have culminated in a patent application.

I would further like to thank my supervisors at CSIC, Pedro Ávila and Søren Birk Rasmussen for a great external stay in Madrid. Also Ricardo and Miguel A. Bañares should be acknowledged for running some Raman samples.

It was a pleasure working at the CSC group. The pleasant and productive atmosphere is simply a result of the people working there. So a great thanks to all of them. Here some of the people I would like to point out. Bodil for running countless BET and TGA samples; Steffen Buus Kristensen for good deNO$_x$ advice ; Anders Theilgaard Madsen for good office companionship and for trying to teach the Danish language to me.

I am also grateful for the discussions with our collaborators from the power generating sector.

Last but not least I would like to thank my family for all the support during

and before the years of this project. Without them I would never had the chance to submit this thesis.

Abstract

The objective of this thesis has been to investigate alternative catalysts and technologies which are able to handle the challenging off-gases from biomass- and waste-fired units. Nitrogen oxides are unwanted by-products formed to some extent during almost any combustion. These by-products are usually removed with the selective catalytic reduction (SCR) using a vanadia-tungsta-titania (VWT) catalyst and ammonia (NH_3) as reductant. For application in coal- and gas-fired power plants this technology is mature. However, when firing biomass the flue gas contains potassium in large amounts which deactivates the VWT catalyst very rapidly. Firing of biomass increased strongly over the past decade and is expected to increase even further in the near future. Also waste incineration creates flue gases that are very challenging to the SCR catalyst. Therefore, SCR units in waste incineration plants are commonly placed at the so-called tail-end position, just before being released through the stack. At this position, the flue gas is very clean, so the catalyst has a long lifetime. However, tail-end placement usually requires costly reheating of the flue gas.

Two approaches were undertaken to solve the alkali poisoning problem: Use of Ag/Al_2O_3 as catalyt with hydrocarbons (ethanol, propene) as reductants (HC-SCR), and by developing low-temperature catalysts for NH_3-SCR to be used in the tail-end position at 150 °C, making costly reheating redundant.

The hope that HC-SCR is insensitive to potassium has been in vain. The deNO_x activity over Ag/Al_2O_3 used in ethanol-SCR is practically as much reduced as in the NH_3-SCR case over the traditional VWT catalyst. Furthermore, poisoning with potassium leads to unselective oxidation of the hydrocarbons instead of NO reduction and SO_2 concentrations as low as 20 ppm can heavily deactivate the Ag/Al_2O_3 catalyst. Therefore we concluded that HC-SCR is unfit for potassium containing flue gases.

The efforts at developing a catalyst to be used at the tail end position were

more fruitful and culminated in a patent application due to which only limited information can be disclosed. At 150 °C, in the presence of 10 % H_2O, the catalyst under patenting matches the activity of the commercial VWT one at 220 °C. However, flue gases at the tail-end position can contain up to 20 % H_2O, increasing the temperature of activity parity to 180 °C. Furthermore, the catalyst is also sensitive to SO_2, even at low concentrations.

One of the causes for the catalyst's high activity in NO reduction, the high concentration of chemisorbed surface oxygen, might be exploited in the removal of volatile organic compounds (VOC), another growing environmental technology. Preliminary tests are under planning.

Dansk Resumé

Formålet med denne afhandling har været at undersøge alternative katalysatorer og teknologier som er i stand til at håndtere de udfordrende røggasser fra biomasse- og affaldsfyrede anlæg. Nitrogenoxider er uønskede biprodukter, der dannes under næsten enhver forbrænding. Disse biprodukter fjernes ved selektiv katalytisk reduktion (SCR) ved hjælp af en vanadium-wolfram-titandioxid (VWT) katalysator og ammoniak (NH_3) som reduktionsmiddel. I kulfyrede anlæg er denne teknologi meget moden. Men røggasser fra biomasse-fyrede anlæg indeholder masser af kalium som deaktivere VWT katalysatoren meget hurtigt. Fyring af biomasse er vokset markant i løbet af det sidste årti og forventes at vokse endnu mere i den nærmeste fremtid.

Også røggasser fra affaldsforbrænding er en stor udfordring for SCR-katalysatorer. Derfor er SCR-enheder i affaldsforbrændingsanlæg almindeligvis placeret på den såkaldte tail-end position, lige før skorstenen. På dette sted er røggassen meget ren hvilket fører til at katalysatoren har en lang levetid. Men placering af SCR anlæg på dette sted kræver dyr genopvarmning af røggassen.

To fremgangsmåder blev foretaget for at løse alkali forgiftning problemet: Brug af Ag/Al_2O_3 som katalysator i forbindelse med kulbrinter (ethanol, propene) som reduktionsmiddel, og ved at udvikle lav temperatur katalysatorer for at brug ved 150 °C i NH_3-SCR anlæg på den tail-end position, så den dyre genopvarmning er overflødig.

Håbet om, at HC-SCR skulle være ufølsom over for kalium har været forgæves. Den Ag/Al_2O_3 katalysator der er blevet brugt i forbindelse med ethanol er næsten ligeså påvirket af kalium som den konventionel VWT katalysator. Desuden forårsager kalium uselektive oxidation af kulbrinter i stedet for reduktion af NO og SO_2. Koncentrationer så lave som 20 ppm kan ødelægge katalysatoren meget hurtigt. Derfor konkluderer vi, at HC-SCR er uegnet til kalium indeholdende

røggasser.

De bestræbelser på at udvikle en katalysator, der skal bruges ved tail-end position var mere frugtbare og kulminerede i en patentansøgning. Påbaggrund af denne ansøgning må vi ikke oplyse alle detaljer. I tilstedevrelse af 10 % vand er aktiviteten af vores katalysator ved 150 °C lige så høj som aktiviteten af den kommercielle VWT katalysator ved 220 °C. Røggasser ved tail-end position kan dog indeholde op til 20 % vand hvorfor temperaturen øges til 180 °C for at opnå sammenligningsgrundlag. Desuden er katalysator meget flsom overfor SO_2, ogs ved lave koncentrationer.

En af årsagerne til katalysatorens høje aktivitet i NO reduktion, er den høje koncentration af chemisorbed overflade oxygen, som muligvis udnyttes til fjernelse af flygtige organiske forbindelser (VOC), en anden voksende miljøteknologi. Foreløbige test er under planlægning.

Contents

Chapter 1

Nitrogen oxides

This chapter gives an introduction to the sources and environmental effects of nitrogen oxides (NO_x) and the legislation designed to curb their emission. The formation of NO_x during combustion is also presented.

1.1 Sources of nitrogen oxides

The abbreviation NO_x comprises the following seven nitrogen oxides which are considered to be atmospheric pollutants: NO, NO_2, NO_3, N_2O, N_2O_3, N_2O_4 and N_2O_5. Since emissions from the combustion of fuels mainly consist of NO and NO_2, with NO representing between 90 and 95 %, the focus will be on these two gases [1]. While there are also natural processes contributing to the emission of NO_x, such as fixation by lightning, volcanic activity, the oxidation of ammonia in the troposphere and ammonia oxidation from decomposition of proteins, the major soucres of NO_x emission are combustion of fossil fuels and burning of biomass. Man-made NO_x emissions account for three quarters of total emissions [1, 2].
The man-made NO_x sources can be subdivided into mobile and stationary sources. Mobile sources are predominantly found in the transportation sector, i.e. automobiles, ships, airplanes and locomotives. Stationary sources are power plants burning coal, natural gas or biomass, as well as waste incineration units and certain industrial processes (e.g. nitric acid production). Figure 1.1 shows the NOx emissions by sector in the USA and Europe. In both regions, the transportation sector is making the biggest contribution. Power generation is another important contributor and this thesis will deal with possible NO_x reduction technologies for

that sector.

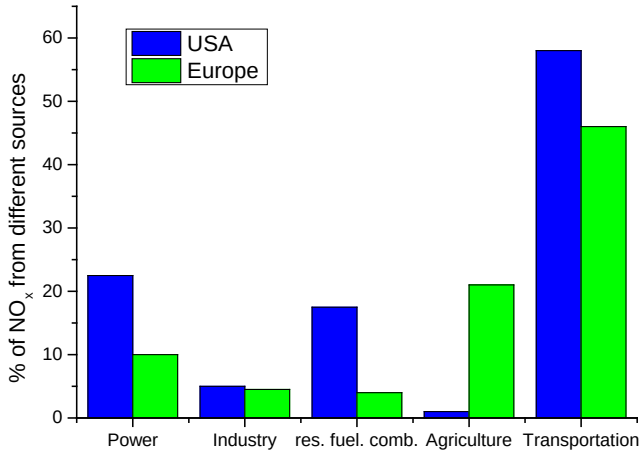

Figure 1.1: NO_x emissions by source category in the USA and European countries (based on data from 1993 to 2006). Adapted from [2]

1.2 Environmental effects of nitrogen oxides

NO_x gases are affecting the environment in many ways. They contribute to acid rain formation, ground level ozone (town smog) and ozone depletion.

Acid rain is formed by NO reacting with water in the atmosphere, see equation 1.1.

$$4\,NO + 3\,O_2 + 2\,H_2O \longrightarrow 4\,HNO_3 \tag{1.1}$$

Ground level ozone (O_3) is created in the troposhere by the reaction of nitrogen oxides (NO_x) with volatile organic compounds (VOC) in the presence of

sunlight and constitutes the main component of smog. The chemistry of ground level ozone formation involving volatile organic compounds, NO and peroxy radicals ($OH^{\bullet}$) is complex, but the critical step is the oxidation of NO to NO_2 by $OH^{\bullet}$ radicals. Chronic effects of ground level ozone exposure are increased incidence of asthma, decreased lung function growth and lung cancer [3].

NO_x gases contribute to stratospheric ozone depletion in a catalytic manner [4]. NO first reacts with ozone (O_3) to form oxygen (O_2) and NO_2. The consumed NO is recovered by the reaction of an oxygen radical $O^{\bullet}$ with NO_2. Since the NO is recovered, it can engage in many more cycles of ozone destruction, hence the catalytic nature of the process.

$$NO + O_3 \longrightarrow NO_2 + O_2 \tag{1.2}$$

$$NO_2 + O^{\bullet} \longrightarrow NO + O_2 \tag{1.3}$$

$$Net : O^{\bullet} + O_3 \longrightarrow 2O_2 \tag{1.4}$$

Decreased levels of ozone in the stratosphere lead to increased levels of UV radiation from the sun [4]. UV radiation destroys DNA and proteins in all living organisms. In humans, increased levels of UV radiation may cause increased incidence of squamous cell skin cancer and basal cell cancer and possibly melanoma, immune system deficiencies, and cataracts [4]. Furthermore,the productivity of ocean phytoplankton and certain crop plants is decreased.

1.3 Legislation

Due to the environmental damage caused by NO_x gases, many regulations designed to limit their emission were proposed and some have been adopted. The emissions regulations vary from country to country in type and extent. Here some examples of the more significant, adopted regulations. In November 1999, the Gothernburg Protocol to abate acidification, eutrophication and ground-level ozone was established, hereby setting emission ceilings for sulphur, NO_x, VOCs and ammonia in 2010. The protocol was signed by the USA, Canada and 29 European countries, with each of the signees setting their emission reduction goals. In terms of NO_x, Europe committed itself to a reduction of 41 % compared to 1990 [2,5]. The protocol was reviewed and in 2012 more stringent emission reduction commitments for 2020 were agreed upon. In 2012, to honour its commitment, the Danish government increased the NO_x tax for stationary NO_x sources from 5 Dkr pr. kg NO_x to 25 Dkr pr. kg [6]. Also other countries with significant

NO_x emissions like China are trying to reduce emissions despite rapid economic growth. The Chinese government is aiming at an emission reduction of 10 % (compared to 2010) during the 12th Five Year Plan (2011 to 2015) [7].

1.4 NO_xformation

Nitrogen oxides formed by combustion of fossil fuels or biomass can be categorised depending on the underlying formation mechanism [1]. The three types are: *thermal* NO_x, *fuel* NO_x and *prompt* NO_x.

Thermal NO_x are formed by the oxidation of atmospheric nitrogen at high temperatures, which can be described by equation 1.5.

$$N_2 + O_2 \longrightarrow 2NO \tag{1.5}$$

The rate of formation of NO from N_2 and O_2 was determined as [8]:

$$\frac{d[NO]}{dt} = 9 * 10^{14} * exp(-68180/T) * [N_2] * [O_2]^{0.5} \tag{1.6}$$

The formation of *thermal* NO_x is thus favored by high temperatures and high oxygen contents. Due to the high temperatures in industrial boilers, this type of NO_x is most often the major contributor [1].

Fuel NO_x is formed from the gas-phase oxidation of devolatilised fuel nitrogen. This type of NO_x does not depend on the flame temperature at normal combustion temperatures and is insensitive to the nature of the organic nitrogen compound [1]. A mechanism has been proposed whereby the organic nitrogen compounds form a complex which can be attacked by OH-radicals and NO molecules yielding NO or N_2, respectively. The formation of NO can be depressed in a reducing flame, because the $OH^{\bullet}$ radicals react relatively quickly with hydrogen to form water [1].

Prompt NO_x are formed by the oxidation of HCN to NO in the lean zone of the flame. The HCN intermediate is furnished by the reaction of hydrocarbon fragments with atmospheric nitrogen. The formation of *prompt* NO_x has a weak temperature dependence and is only significant in very fuel-rich flames and at low temperatures.

Figure 1.2 depicts the temperature dependence of the three sources of NO_x for a coal fired furnace. *Fuel* NO_x makes up a small fraction of total NO_x over the

full temperature range. Lowering the combustion temperature can lower the total emissions, since the temperature dependence of the *thermal* NO_x is stronger than that of *prompt* NO_x.

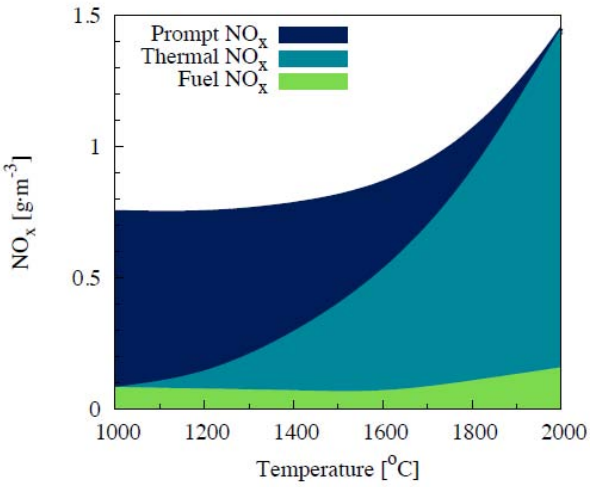

Figure 1.2: Temperature dependence of *thermal* -, *prompt*- and *fuel* NO_x for a coal fired furnace. Adapted from [1]

Chapter 2

NO_x abatement

This chapter gives an overview of the state-of-the art emission control technologies used in stationary sources. These include combustion control measures and post combustion control measures, with the focus being on the latter. Special challenges to the removal of NO_x gases faced in biomass-fired units and waste incineration plants and possible solutions to these challenges are also presented.

There are bascially two kinds of technologies available to limit the NO_x emissions from man-made sources, primary and secondary measures. The primary measures, also called "clean techniques" or "combustion control", consist of a group of combustion control measures that are designed to reduce the formation of NO_x during the combustion process. The secondary measures, also called "clean-up techniques" or "flue gas treatment", consist of post-combustion control measures, i.e. they are designed to destroy NO_x after it has been formed during the combustion process.

2.1 Combustion control measures

Combustion control techniques are the most cost-effective and energy-efficient methods to lower NO_x emissions [9] and have been most successful in the NO_x emission reduction from gas- and oil-fired plants. A subdivision can be made between modifications of operating conditions and modifications of the combustion system. The major objective of combustion control is to decrease the oxygen level at peak temperatures, reduce the peak temperatures and the residence time

in the combustion zone [9]. Reducing the peak temperature and the oxygen level at peak temperature will, according to equation (1.6), reduce the formation of *thermal* NO_x. Reduction of the flame temperature can be achieved by either FGR (Flue gas recirculation) or injection of steam or water. These measures can lower NO_x formation by 20-50 %. Reduction of the oxygen level at peak temperature can be brought about by LEA (Low excess air firing), which causes NO_x formation reductions of 15-20 %. The downside of this method is a reduced flame stability, smoke formation may occur and CO formation from incomplete combustion. In coal-fired power plants, coal-ash slagging and fouling may occur. The measures presented so far are modifications of the operating conditions. More effetive are modifications to the combustion system. One example of these are the so-called low NO_x burners, which can reduce the NO_x formation by 25-60 % [9]. These specially designed burners have an oxygen- or fuel-deficient core flame. The remaining fuel or air to complete the combustion is introduced in a cylindrical zone around the core flame. After the initial combustion has taken place in this mixture, additional oxygen is introduced by a third air stream. In this way, three different zones are formed, one fuel rich, one with a 1:1 ratio and one fuel-deficient zone. This staging leads to reduced *fuel* NO_x formation in coal- and oil-fired burners. In gas-fired burners a reduction of *thermal* NO_x is brought about by reduced peak flame temperatures. Further redutions can be achieved by choosing better low nitrogen containing fuels [9].

2.2 Selective non-catalytic reduction SNCR

The seletive non-catalytic reduction (SNCR) is a conceptually simple process of NO_x emission reduction and is the most widely used non-catalytic technique [10]. A reduction agent, most commonly ammonia or urea, is injected into the upper part of the boiler where the temperature is between 800 and 1200 °C [10], see figure 2.1. The exact temperature window depends on parameters such as flue gas composition, velocity gradients and system geometry [10]. Addition of CH_4 can broaden the temperature window [11]. Reduction levels of up to 50 % can be attained [9]. Below 800 °C, the reduction is too slow and thus leaves ammonia unreacted. Above 1200 °C, oxidiation of ammonia may occur, which results in net NO formation.

The SNCR technology is attractive due to several reasons. Firstly, it is catalyst-free and hence free of associated costs and problems such as catalyst deactivation (e.g. due to arsenic, alkali metals or sintering) and inhibition (e.g. due to fly ash, ammonia sulfate). Secondly, it is easy to install and applicable to all types of stationary-fired equipments and can be combinded with other NO_x emission control technologies such as selective catalytic reduction (SCR). All of this results in low capital and operating costs.

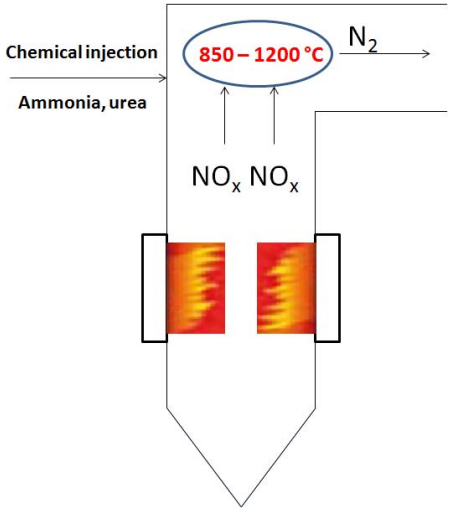

Figure 2.1: Schematic of SNCR process. Adapted from [10].

The main reactions causing NO_x reduction are:

$$6NO + 4NH_3 \longrightarrow 5N_2 + 6H_2O \tag{2.1}$$

$$6NO_2 + 8NH_3 \longrightarrow 7N_2 + 12H_2O \tag{2.2}$$

The major drawbacks of SNCR are a relatively limited removal level (up to 50 % [9]), ammonia slip and ammonium salt formation that can cause plugging and corrosion [9]. SNCR is not desirable in high-dust applications, because of the adsorption of ammonia on fly ash [9]. Due to these reasons, SNCR is sometimes combined with the selective catalytic reduction (SCR), which will be presented in the next chapter.

2.3 Selective catalytic reduction (SCR)

2.3.1 Introduction

In stationary sources, the most widely used technology for NO_x abatement is the selective catalytic reduction (SCR) using ammonia (NH_3) or sometimes urea

as reductants at temperatures between 150 to 450 °C in the presence of a catalyst [12]. The basic chemistry is described by the following equations:

$$4NH_3 + 4NO + O_2 \longrightarrow 4N_2 + 6H_2O \tag{2.3}$$

$$6NH_3 + 8NO_2 \longrightarrow 7N_2 + 12H_2O \tag{2.4}$$

selective or desired reactions

$$4NH_3 + 5O_2 \longrightarrow 4NO + 6H_2O \tag{2.5}$$

$$4NH_3 + 3O_2 \longrightarrow 2N_2 + 6H_2O \tag{2.6}$$

$$2SO_2 + O_2 \longrightarrow 2SO_3 \tag{2.7}$$

non-selective reactions.

The unwanted side reactions are either merely consuming NH_3, or, even worse, producing additional NO_x. Oxidation of SO_2 to SO_3 is unwanted, because the SO_3 can react with NH_3 and H_2O to form $(NH_4)_2SO_4$ and $(NH_4)HSO_4$. Although the formation of $(NH_4)_2SO_4$ is thermodynamically favoured, analysis of condensed salts has shown that it is formed in only limited amounts due to kinetic limitations [8, 14, 15]. The reaction of SO_3 with only H_2O yields H_2SO_4. Both $(NH_4)HSO_4$ and H_2SO_4 are corrosive and cause fouling, plugging and corrosion on e.g. air preheaters [13–15].

$$NH_3 + SO_3 + H_2O \longrightarrow NH_4HSO_4 \tag{2.8}$$

$$SO_3 + H_2O \longrightarrow H_2SO_4 \tag{2.9}$$

Other unwanted side reactions are the formation of the very potent greenhouse gas N_2O and formation of explosive nitrite/nitrate salts at very low temperatures [13].

2.3.2 Placement of SCRunit

The SCR unit containing the catalyst can be placed at three different locations giving rise to the so-called "high dust"-, "low dust"- and "tail-end" (or "clean gas" or "end-of-pipe") configurations, see figure 2.2. Each of the three positions has its advantages and disadvantages and the placement will depend on parameters like the dust level in the flue gas and risk of forming dioxines. In the high dust configuration the SCR unit is placed right behind the boiler. The advantage of this position is that the catalyst bed does not need to be heated and a relatively inexpensive cold electrostatic precipitator (ESP), which is used for dust removal, can be installed. Furthermore, deposition of NH_4HSO_4 on the air pre-heater (APH) which is located after the SCR unit is limited, because it is adsorbed

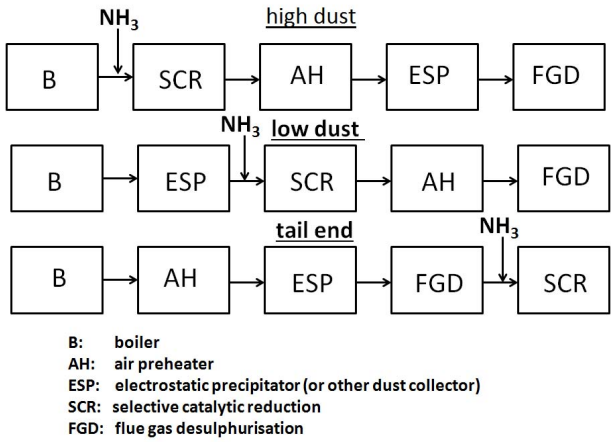

Figure 2.2: Design options for SCR. Adapted from [12].

onto fly ash. The major disadvantage of the high-dust position is a relatively short catalyst lifetime due to high levels of catalyst poisons in the flue gas such as arsenic, potassium, hydrogen chloride etc. [9, 16]. Another disadvantage is that the catalyst monoliths used in the high-dust position can only have a low cell density because of the high particulate levels (1 to 30 g/m^3 [12]) that would otherwise cause plugging. Despite these disadvantages, the high-dust position is the most commonly used one [16]. In the low-dust position, the flue gas has already been cleaned regarding particles right after the boiler. This entails the installation of a relatively expensive hot ESP. After the the hot ESP the flue gas enters the SCR unit without the need for reheating. The obvious advantage of the low dust position is the strongly reduced level of particulates (typically below $0.1g/m^3$ [12]) in the flue gas. This allows the use of monoliths with a higher cell density and can thus lower the space requirement of the SCR unit. Apart from the expensiveness of the hot ESP, the major drawbacks of the low-dust configuration are deposition of NH_4HSO_4 on the APH, which is located right after the SCR unit, and that the catalyst can be inhibited by a layer of very fine particles which have passed the ESP [16]. In the tail-end configuration the SCR unit is placed after the flue-gas-desulphurisation unit (FGD) and just before the smoke stack. Since the flue gas has already passed the ESP and the FGD units, it is almost free of poisons and thus the catalyst lifetime is longer than in the high- and low dust positions. The major disadvantage is the need for reheating the flue gas before it enters the SCR unit. Tail end placement is usually implemented in municipal waste incinerators, where the catalytic removal of NO_x is combined

with catalytic dioxin/furan removal [17,18] and because of a challenging flue gas composition (e.g. high levels of dust, SO_2, lead, zinc, HCl etc.).

2.3.3 Commercial SCR catalysts

There is a myriad of substances active for the selective catalytic reduction of NO with NH_3. However, only few formulations are commercially used. In stationary applications vanadia supported on (anatase) titania and promoted with tungsta (V_2O_5−WO_3−TiO_2) or molybdena (V_2O_5−MoO_3−TiO_2) is usually the catalyst of choice. For high temperature applications in gas fired power plants, metal doped zeolites have been proposed, due to their high de-NO_x activity and thermal stability up to 600 °C, where the vanadia containing catalysts suffer from evaporation of the active phase [19]. In V_2O_5−WO_3−TiO_2 and V_2O_5−MoO_3−TiO_2, vanadia is causing both the SCR activity as well as the oxidation of SO_2 to SO_3. Vanadia is supported on titania, because this results in a higher surface area and higher catalytic activity due to the vanadia-support interactions [20]. Compared to other supports like e.g. Al_2O_3 and ZrO_2, anatase TiO_2 has the advantage that it is only partially and reversibly sulfated, thus avoiding catalyst deactivation [20]. WO_3 and MoO_3 are increasing the SCR activity and selectivity towards N_2 of V_2O_5−TiO_2. Furthermore, WO_3 and MoO_3 are suppressing the formation of SO_3. It should be mentioned that TiO_2-anatase is a metastable titanium dioxide polymorph and tends to convert into the thermodynamically stable rutile form at any temperature and pressure, making V_2O_5−TiO_2 (anatase) an unstable system. Phase transformation of anatase to rutile is favoured by V_2O_5 but hindered by WO_3 and MoO_3, which act as structural promoters [19,21].Phase transformation from anatase to rutile is accompanied by surface area loss and loss in SCR activity [20]. According to several authors, V_2O_5−TiO_2 is more active when promoted with tungsta than when promoted with molybdena, at least in arsenic free atmospheres [20]. In commercial catalysts, the V loading is typically below 1-1.5 wt.% and the WO_3 or MoO_3 loading is close to 6 and 10 wt.%, respectively [19]. Accordingly, the surface coverage fraction of W and Mo are 0.6 - 0.7 and that of V close to 0.2, so that the total surface coverage on titania is just below a monolayer. Depending on the surface coverage and preparation method, three different species of V_2O_5 can be present on the titania support [22]. At loadings far below monolayer coverage, monomeric species dominate. Increasing the V_2O_5 loading results in the formation of dimeric and polymeric species. At loadings above the monolayer coverage, crystalline vanadia will dominate. Figure 2.3 depicts the different vanadia species.

The different vanadia species display very different SCR activity per vanadium atom. Polymeric vanadia species are about 10 times as active as monomeric ones [24], with the N_2O formation increasing at the same time. Monomeric species

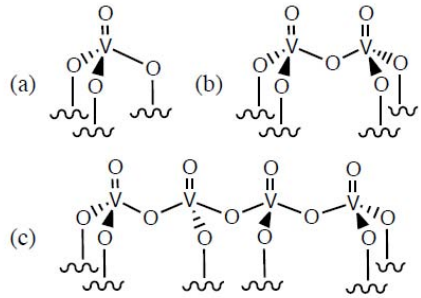

Figure 2.3: Schematic representation of (a) monomeric, (b) dimeric and (c) polymeric species of vanadia. Taken from [23].

form N_2 only. Due to these opposing trends, vanadia loadings just below monolayer coverage are preferable. Kristensen et al. have recently shown that using a sol-gel route affords the accomodation of up to 25 wt.% V_2O_5 on titania without the formation of crystalline vanadia [25]. It has been reported that the SO_2 oxidising ability of this catalyst is not higher than that of an industrial catalyst loaded with only 3 wt.% V_2O_5 and promoted with 7 wt.% WO_3.

An in-depth presentation of the reaction mechanism for vanadium based catalysts is beyond the scope of this chapter. Instead, only the most important facts will be presented, which allow the reader to understand the problems faced in cleaning flue gases in biomass-fired power plants. A compact review of the reaction mechanism was given recently by Kristensen [23]. Nowadays it is widely accepted that the SCR reaction can be desrcribed by an Eley-Rideal mechanism, with ammonia being the species that is adsorbed onto the catalyst surface and NO reacting with it from the gas phase or from a weakly bound state [20, 23, 26, 27]. The majority of NH_3 is adsorbed on vanadyl sites by Brønsted and Lewis acid sites [23], see figure 2.4. Under dry conditions most of the NH_3 adsorbs onto Lewis acid sites. With water in the flue gas, the portion of NH_3 adsorbed onto Brønsted sites can reach 50 % [23]. Figure 2.5 shows the generation of Brønsted acid sites from Lewis acid sites in the presence of water. High alkali metal concentrations in the flue gas can deactivate the vanadia based catalyst, because the alkali metals can react with the vanadyl acid sites, making them unavailable for NH_3 adsorption. This problem is often encountered in power plants firing or co-firing biomass.

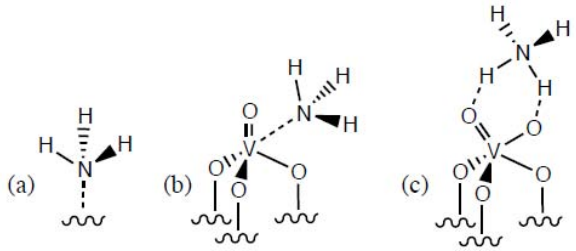

Figure 2.4: NH_3 adsorbed onto different sites: (a) Lewis site of TiO_2 support; (b) Lewis site of vanadyl group; (c) Brønsted site of vanadyl group. Taken from [23].

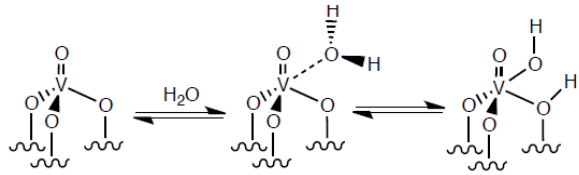

Figure 2.5: Transformation of a Lewis site of V_2O_5/TiO_2 into a Brønsted site in the presence of water. Taken from [23].

Industrially, SCR catalysts are most often used in the form of honeycomb monoliths or metal loaded plates stacked as monoliths with parallel channels [19,23,28]. Monoliths are obtained by extruding the catalyst with some binders and water. Some catalyst manufacturers also support the catalyst on corrugated flexible supports [23]. The use of packed beds is ruled out due to high pressure drops under industrial conditions [28]. The monoliths or plates are assembled into cased modules, which are then placed into the reactor to form catalyst layers. Typically 3-4 layers having a length of one metre each are installed [28]. The linear gas velocity in the reactor is usually 3-5 m/s [28] and the resulting pressure drop is negligible. Monolith catalysts for SCR-DeNOx applications usually work under control of interphase and intraporous mass transfer [28], which means that catalyst development must not only be directed at improving the intrinsic activity but also the pore size distribution of the monolith. The mass transfer limitations are more severe at high temperatures (high- and low-dust positions) than at lower temperatures (tail-end position) [29].

2.4 Biomass applications

Electricity generation using biomass as fuel has increased strongly in the recent past and is projected to grow in the future [33], see figure 2.6. The interest in firing and co-firing biomass is due to its CO_2 neutral image [30] and the fact that it allows the use of existing (coal-fired) power plants entailing only minor retrofiting [32]. However, recently cricital voices have appeared, claiming that the short term CO_2 footprint of biomass is less favourable than that of coal [31]. An in-depth discussion of the environmental impact of biomass-firing is beyond the scope of this work. Here, only the effect on the NO_x aftertreatment unit will be dealt with.

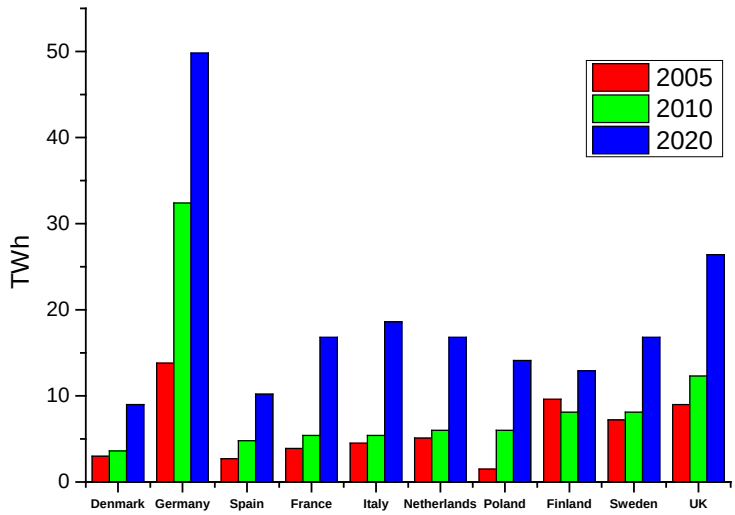

Figure 2.6: Biomass electricity production (TWh) in 2005, 2010 and 2020 in accordance with member state National Renewable Energy Action Plans. Adapted from [19].

From an SCR point of view, the major challenge of burning biomass is the high content of alkali metals, especially potassium, in the biomass, see table 2.1.

Table 2.1: Amounts of Na and K in different fuels on dry basis. MSW (Municipal Solid Waste). Taken from [23].

	Coal ppm		Brown Coal wt.%		MSW wt.%		Wood Chips wt.%		Forrest Residues wt.%		Straw wt.%	
Na	0.015-0.055	[34]	<0.23	[35]	0.16-0.39	[36]	0.04-0.1	[37]	0.01-0.05	[38]	<0.3	[37]
K	0.006-0.06	[34]	<0.085	[35]	**0.11-0.5**	[36]	**0.05-0.4**	[37]	**0.1-0.2**	[38]	**0.2-1.9**	[38]

The high level of potassium in the fuel results in high levels of potassium containing aerosols in the flue gas causing the $V_2O_5{-}WO_3{-}TiO_2$ catalyst to deactivate. Even though coal contains much less alkali metals than biomass does, Chen and Yang [39] reported deactivation of $V_2O_5{-}TiO_2$ due to alkali metals. Chen and Yang have found that the degree of poisoning correlates with the basicity of the metal, following the order: $Cs_2O > Rb_2O > K_2O > Na_2O > Li_2O$. This trend was confirmed at least two times afterwards [40, 41]. In biomass, only potassium and sodium are of real concern, since they constitute around 99 wt.% of the alkali metal content.

Experience at power plants co-firing and firing biomass, especially straw, has shown that the SCR activity declines at an accelerated rate compared to firing fossil fuels only, see figure 2.7. The normal life span of an SCR catalyst is about 3 to 5 years. Several authors have shown that co-firing biomass can lead to substantial deactivation within a couple of months. Strege et al. [42] showed that the SCR activity decreased by 18 % within 1032 h firing a 20 wt.% coal 80 wt.% wood mixture. Extrapolating this rate of deactivation results in 50 % activity loss after 2800 h of operation. Wieck et al. [42] fired 20 wt.% straw together with 80 wt.% coal. They reported that the SCR activity dropped much faster than when firing coal only. In the high-dust position, 2860 h of operation caused 35 % deactivation, whereas in the low-dust position 2350 h caused an activity drop of "only" 15 %. This difference is most probably caused by the ESP filtering out some of the postassium containing particles (e.g. KCl). An average alkali metal ion accumulation rate at a normal biomass-fired power plant of $4.2{*}10^{-2}$ µmol g^{-1} h^{-1} was reported [43].

Both Zheng et al. [45] and Chen et al. [39] showed by NH_3 chemisorption that potassium poisoning is, unsurprisingly, accompanied by reduced NH_3 adsorption onto the catalyst. In addition, Chen et al. [39] claimed that only Brønsted sites were neutralized whereas Lewis sites were unaffected by potassium poisoning. They based this assertion on IR taken with KBr containing pellets. However,

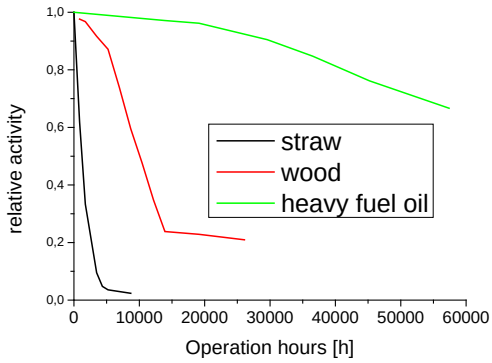

Figure 2.7: Expected deactivation of SCR catalyst for various fuel types. Adapted from [44].

they used the peak at around 1650 cm^{-1} to represent Lewis acid sites, which is a poor choice because it is overlapping with an H_2O [23] peak. Lietti et al. [46] have shown that potassium is reducing the number of both Brønsted and Lewis acid sites. Later, Kamata et al. [47] have reported that Brønsted acid sites are more prone to react with potassium than Lewis acid sites. They derived the concentrations of Lewis and Brønsted sites from dry IR measurements.

Lietti et al. [46], Hangstum et al. [48] and Lewandowska et al.l [49] reported that potassium doping caused decreased reducibility of vanadium sites. Lewandoska et al. [49] also showed, using both Raman spectroscopy and DFT calculations, that potassium is not only interacting with vanadyl sites but also with the titania support forming strong ionic bonds. To the best of the author's knowledge, there are no studies that investigated the effect of the $K-TiO_2$ interaction on the SCR activity.

The mechanism by which potassium deactivates the commercial catalyst is up to this day not fully understood [23]. Especially the $K-V_2O_5$ interaction is subject to controversy. The interested reader is referred to a short overview given by Kristensen [23]. Despite the controversies, there is no doubt that potassium is reducing the number of acid sites on the surface of the catalyst. Most of the strategies to find a more potassium-tolerant catalyst involve increasing the number of acid sites. Here are some of the reported strategies:

Increasing the acidity of the support provides sacrificial acid sites which can react with some of the potassium before it reacts with the active centres [50–52]. Use of sulfated ZrO_2 instead of TiO_2 as support can improve the potassium tolerance somewhat, however, at the expense of the activity before poisoning [52]. Promoting $V_2O_5{-}TiO_2$ with heteropoly acids instead of WO_3 decreases the potassium poisoning strongly, due to a higher number of acid sites [53]. The activity of the fresh catalyst is comparable to that of $V_2O_5{-}WO_3{-}TiO_2$. Promoting $Cu{-}TiO_2$ with heteropoly acids yielded good potassium tolerance [53, 54].

Increasing the V_2O_5 loading is another successful strategy. Kristensen et al. [23, 25] have shown that by using a sol-gel route it is possible to load 20 wt.% V_2O_5 on TiO_2 without forming crystalline vanadia or increasing the SO_2 oxidation rate. The resulting catalyst is about twice as active as an industrial catalyst containing 7 wt. % WO_3 and 3 wt. % V_2O_5 and exhibits excellent potassium tolerance due to the high number of active sites.

Use of metal oxides which possess mainly Lewis acidity like Cu and Fe has proven successful [50–52, 54], since Lewis acidity is reported to be less affected by postassium [47]. Fe ion-exchanged mordernite (a zeolite) and Cu impregnated mordernite have shown excellent potassium tolerance [51]. Impregnating these catalysts with 100 µmol Kg^{-1} reduces their activity at 400 °C by maximum 20 %, when measured in powder form. By comparison, the industrial $V_2O_5{-}WO_3{-}TiO_2$ lost 70 % of its activity. The comparatively weak impact of potassium on catalysts possessing mostly Lewis sites encouraged our institute to venture into hydrocarbon SCR **(HC-SCR)** for biomass-fired applications. This is because many of the catalysts reported to show SCR activity in the presence of hydrocarbons (instead of NH_3) possess mainly Lewis acidity. The first part of this thesis will deal with HC-SCR.

Absorption of NO_x gases into ionic liquids is an emerging technology [55]. It has been reported that some ionic liquids are capable of converting the absorbed NO into HNO_3, which in some locations can be a saleable product.

Placing the SCR unit at the **tail-end** position or **low-dust** positions can decelerate the catalyst poisoning, probably because the dust and SO_2 removal systems lower the concentration of potassium particles. This kind of strategy is probably hard to implement at existing plants equipped with high dust SCR, due to significant retrofitting requirements.

2.5 Waste incineration

The flue-gas treatment at waste incineration plants can be very challenging. The raw off-gas can contain catalyst poisons like e.g. lead, zinc and HCl in high concentrations and high amounts of dust. Placing the catalyst at the-tail end positions alleviates the impact of the aforementioned poisons and dust to a large extent. At waste incinerators, the catalytic removal of NO_x is often combined with catalytic dioxin/furan removal at minimum extra cost [18]. The major drawback of the tail-end position is the need to reheat the flue-gas. When a wet FGD unit is used, the flue gas temperature drops below 100 °C, whereas when using a dry FGD unit the temperature is 140 °C. The second part of this thesis deals with the development of low temperature catalysts to be used at 140 °C, thus removing the need for costly flue-gas reheating.

Chapter 3

Hydrocarbon SCR

This chapter conveys the basics of the selective catalytic reduction using hydrocarbons as reducing agents (**HC-SCR**). The most frequently investigated type of catalyst (Ag/Al_2O_3) as well as the reducing ability of different hydrocarbons including the underlying reaction mechanisms will be presented. Catalyst deactivation by SO_2 will be dealt with.

3.1 Motivation

As described in section 2.4, the most commonly used $V_2O_5{-}WO_3{-}TiO_2$ catalyst is rapidly deactivated when firing biomass. This is because potassium, which biomass contains in large amounts, see table 2.1, reduces the number of acid sites of the catalyst, disabling the adsorption of NH_3. Since the proposed mechanism(s) of HC-SCR [56] are vastly different and involvement of Brønsted acid sites (these seem to be more affected by potassium than Lewis sites [47]) is not mentioned, there was hope that HC-SCR could cope with flue gases rich in potassium.

Some research groups have even reported a beneficial effect of alkali metals on HC-SCR. Rao et al. [57] reported that in the presence of 80 ppm SO_2, the NO conversion over an Ag/Al_2O_3 catalyst using methane (CH_4) as reductant could be increased by doping with alkali metals (K, Na, Cs). They explained the promotional effect by increased NO adsorption and decreased sulfate formation as evidenced by NO - and SO_2-TPD, respectively. Son et al. [58] showed that propene-SCR in the presence of 200 ppm SO_2 over a 2 wt.% Ag/Al_2O_3 catalyst

could be enhanced by adding 0.5 wt.% Cs, escpecially at low temperatures. The promotional effect of Cs was ascribed to enhanced dispersion of silver oxide particles as evidenced by H_2-TPR, TEM and UV-Vis DR. Ukisu et al. [59] promoted Cu/Al_2O_3 at temperatures below 340 °C by adding Cs. The increased activity was ascribed to an increased isocyanate (-NCO) formation which was detected by IR spectroscopy. The authors attribute the increased isocyanate formation to a charge transfer from Cs to Cu.

Apart from a potentially different potassium resistance, HC-SCR has several advantages and disadvantages relative to NH_3-SCR using $V_2O_5{-}WO_3{-}TiO_2$ as catalyst.

advantages

- No NH_3 slip. Most hydrocarbons are less toxic than NH_3.
- No NH_4HSO_4 formation. Useful when operating at low load. Due to increased share of renewables (e.g. wind), incidence of low load operation expected to increase.
- Catalyst most often less toxic than $V_2O_5{-}WO_3{-}TiO_2$.
- Potentially more K resistant.

disadvantages

- Reductants, except for CH_4, usually much more expensive than NH_3.
- Worsening of atom economy and additional CO_2 emissions.
- SCR activities usually lower than NH_3-SCR.
- Not commercially proven in stationary applications.
- Much investigated and relatively active Ag/Al_2O_3 system often prone to SO_2 poisoning.

3.2 Introduction

The research efforts in the field of the selective reduction of NO with hydrocarbons (HC-SCR) are typically directed at the automobile sector. In light of dwindling oil reserves and global warming, more fuel efficient engines operating under lean conditions (excess of oxygen) are desirable [56]. The hitherto used

three-way catalyst for NO_x control is not working effectively in the presence of excess oxygen. Therefore, both industry and academia have conducted much research to find a catalyst that can reduce NO to N_2 using unreacted fuel molecules (hydrocarbons) as reducing agents.

The subject has been extensively reviewed [56, 60–62, 64]. The most effective catalysts are reported to be Pt/Al_2O_3, Cu-exchanged ZSM-5 and Ag/Al_2O_3 [63]. Pt/Al_2O_3 can be ruled out in the present study, due to a narrow operating window, high N_2O formation and its high price. Cu-exchanged ZSM-5 can deactivate because of a combination of Cu sintering and zeolite dealumination. Ag/Al_2O_3 can suffer from coking and poisoning by SO_2 [63].

Since there is a plethora of both possible catalysts (e.g. $metal/Al_2O_3$, metal-zeolites) and reductants (e.g. alkanes, alkenes, oxygenates), there is an almost unmanageable number of catalyst-reductant combinations. Hence it is not possible to present one reaction mechanism, as was done for NH_3-SCR with $V_2O_5{-}WO_3{-}TiO_2$. Therefore, only two very broad reaction mechanisms, namely adsorption-dissociation and oxidation-reduction can be presented, followed by an in-depth discussion of Ag/Al_2O_3.

3.3 General reaction mechanisms

The so-called **adsorption-dissociation** mechanism is usually taken to describe the NO reduction by hydrocarbons over noble metals and Cu-ZSMS-5 [56]. NO is thought to adsorb onto the active metal sites and dissociate into surface adsorbed N(ads) and O(ads) species. The O(ads) reacts with the hyrdrocarbon to give CO_2 and two N(ads) yield N_2. Undissociated NO can combine with N(ads) to give N_2O. The role of the hydrocarbon is to rapidly remove the O(ads) specie and to keep the active sites in a reduced state (e.g. Pt^0, Cu^+) [65], which were reported to be active for NO dissociation.

The **oxidation-reduction** mechanism is used to describe the reaction over supported metal catalysts like e.g. In/Al_2O_3, Sn/Al_2O_3 and Ag/Al_2O_3 [56]. NO is reacting with oxygen to give initial reactive intermediates such as NO_2(ads) and NO_3(ads). At the same time, the hydrocarbon is converted to hydrocarbon oxygenates like e.g. acetate, formate and enolic species. These adsorbed oxygenates can react with the NO_2(ads) and NO_3(ads) to give organo nitrogen species (RNO_2, RONO), which can further hydrolyse to give NCO, CN and NH_3. The hydrolysed species react with NO/NO_2 or surface nitrates to N_2 and CO_2. The oxidation-reduction mechanism is schematically summarised in figure 3.1.

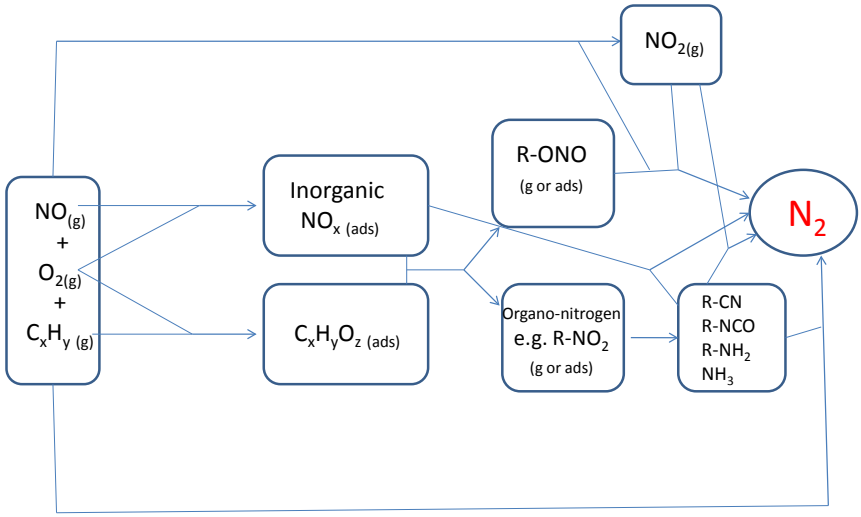

Figure 3.1: General reaction scheme of oxidation-reduction mechanism. Adapted from [56].

The Ag/Al_2O_3-reductant system was comprehensively reviewed by He et al. [64] and to some extent by Lee et al. [66]. Here, emphasis will be placed on the choice of reductant, effect of adding H_2 and H_2O and poisoning by SO_2. Effect of preparation methods and addition of promoters will only be presented briefly.

3.4 Ag/Al_2O_3 - reaction meachanism

Figure 3.2 shows the general mechanism of HC-SCR over Ag/Al_2O_3 for reductants containing two or more carbon atoms as reported by He et al. [64], who based their conclusions mainly on diffuse reflectance infrared fourier transform spectroscopy (DRIFTS) and step response experiments.

First, NO reacts with oxygen to form surface-adsorbed nitrates and nitrites. At the same time, the reductant reacts to form surface adsorbed enolic species or acetates. Formation of acetates is much more suppressed by water than forma-

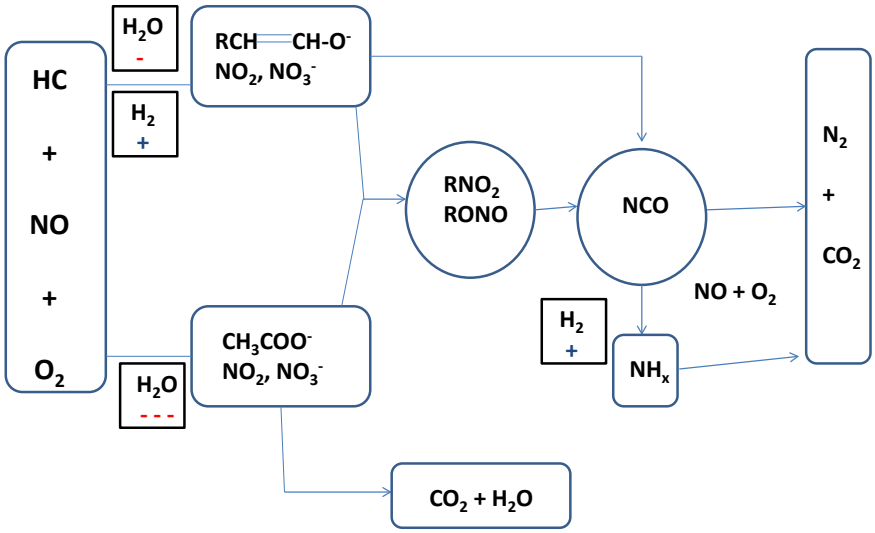

Figure 3.2: Reaction scheme of HC-SCR over Ag/Al_2O_3 according to He et al.. Effects of H_2O and H_2 on formation of species indicatd by + and - in black boxes. Adapted from [64].

tion of enolic species. Hydrogen was reported to enhance the formation of enolic species. Oxygenates, e.g. ethanol, form higher amounts of enolic species than non-oxygenates like propene do. The relative amounts of surface enolic species and acetates are a function of temperature. In the case of ethanol, enolic species dominate between 200 and 400 °C; however, at high temperatures (500 to 600 °C) surface acetates become the dominant species [68]. Reductants with just one carbon atom, e.g. methanol as well as DME, are oxidised to formate species [64, 69] which have a low level of reactivity with nitrates to give isocyanates.

The enolic species can tranform directly to isocyanate (-NCO) species or via organo nitro compounds (RNO_2 and RONO). The acetate species do not show direct transformation to -NCO. Furthermore, they can also decompose to CO_2 and H_2O, hence merely consuming the hydrocarbon.

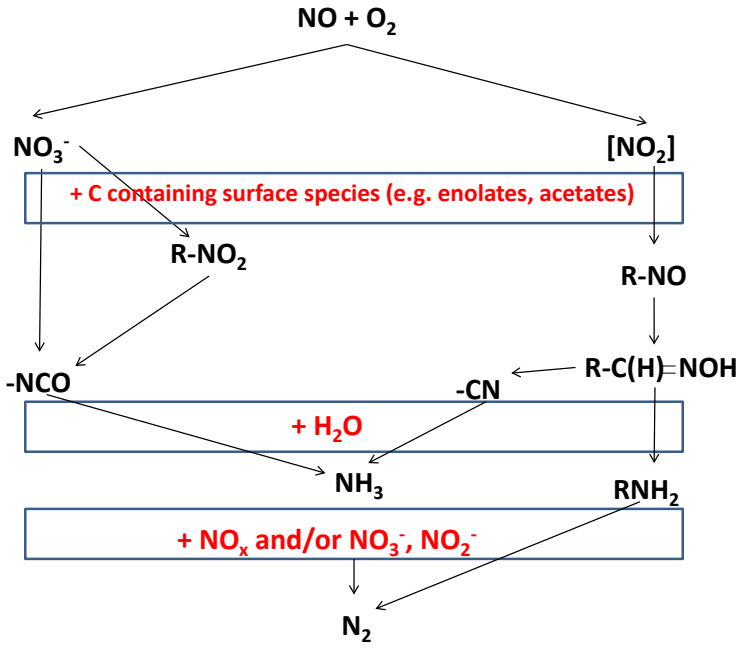

Figure 3.3: Reaction scheme of propene-SCR over Ag/Al_2O_3 including a cyanide pathway as proposed by Tamm et al.. Adapted from [67].

The -NCO species can hydrolyse yielding ammonia, which reacts with gas phase NO or surface nitrates and nitrites to N_2. H_2 increases the formation of ammonia. According to Tamm et al. [67] the -NCO species need to be hydrolysed before reduction of NO can occur whereas He et al. [64] report that the isocyanate can also react directly with NO and oxygen to give N_2.

Tamm et al. [67], who investigated the reaction mechanism of propene-SCR over a 2 wt. % Ag/Al_2O_3 catalyst using gas-phase FTIR, DRIFT and step-response experiments, reported a second reaction pathway involving cyanide (-CN) species in addition to the -NCO pathway published by He [64], see figure 3.3. They reported that the carbon-containing surface species (acetates and enolates) can react with short-lived nitrogen containing surface species or gas phase NO_x to form organo-nitroso compounds (R-NO). These convert to their more stable tautomers, oximes (R−C(H)=NOH). The oximes react mainly with H_2O to give amines (R−NH_2), which in turn can react with gas phase NO_x or surface ni-

trates and nitrites to give N_2. Part of the oximes may also transform to cyanides, which hydrolyse afterwards.

The Ag and Al_2O_3 fulfil different roles in the reaction mechanism. Several studies have shown that Al_2O_3 on its own can convert NO_2 to N_2 very efficiently in the presence of a hydrocarbon [70–73]. Even sulfated Al_2O_3 is able to convert NO_2 to N_2 in the presence of a reductant [71]. Meunier et al. [73] measured the relative mass increase resulting from exposing bare Al_2O_3, 1.2 wt.% Ag/Al_2O_3 and 10 wt.% Ag/Al_2O_3 to a stream of NO and O_2 in He. The mass uptake followed the order: 10 wt.% Ag/Al_2O_3 > 1.2 wt.% Ag/Al_2O_3 > Al_2O_3. The same group has reported [71] that much less NO is oxidised to NO_2 over Ag/Al_2O_3 in the absence of a reductant as is reduced to N_2 in the presence of propene. From this it was concluded that the role of Ag is to promote the oxidation of NO to surface nitrates/nitrites which are transferred to the alumina where they can react with the reductant to N_2. Unlike NO, NO_2 can be transformed to surface nitrates/nitrites directly on the alumina support. In the case of very high Ag loadings (e.g. > 6 wt.%) the alumina only acts as a support and the Ag particles reduce NO via the so-called adsorption-dissocation mechanism with high concentrations of N_2O generated along with N_2 [71]. The Ag is believed to be present in three different forms, namely metallic silver, or cationic silver in the form of (Ag_2O) or isolated Ag^+ ions [74], which can also form clusters ($Ag_n{}^{\delta+}$) [74–76]. The metallic silver is widely believed to catalyse the decomposition-reduction mechanism and is made responsible for the unselective burning of the hydrocarbon at high temperatures [60, 72]. Musi et al. [74] have shown by H_2-TPR and XPS anaylsis that the metallic silver content of unused Ag/Al_2O_3 is not a function of the Ag loading. Around 70 % of the Ag is in metallic form. The content of isolated Ag^+ in freshly prepared samples does increase with increasing Ag loadings in the range of 1 to 3.5 wt.%. Kim et al. [77], on the other hand, have reported that the share of metallic silver on the surface indeed depends on the Ag loading but they did not see a clear correlation. For Ag loadings of 1, 2, 3.8 and 6 wt% surface metal shares of 37, 53, 42 and 50 %, respectively, were determined by UV-vis spectroscopy. H_2-TPR yielded H_2/Ag ratios of 0.23, 0.23, 0.26 and 0.18. There is seemingly no correlation between the UV-vis and H_2-TPR results.

3.5 Effect of reductant

Lee at al. [66] compared the NO conversion over a 2 wt. % Ag/Al_2O_3 catalyst at a space velocity of 50,000 h^{-1} of a wide range of hydrocarbons including alcohols, alkanes, iso-alkanes, alkenes and alkynes at 300, 350 and 400 °C. Table 3.1 summarises their results. The best reductant in this study was clearly ethanol, with NO conversions of around 75 % over the whole temperature range. Second

Table 3.1: NO conversion (%) as function of temperature and reductant. Conditions: NO = 200 ppm, reductant = 1200 ppmC, O_2 = 5 %, H_2O = 5 %. N_2 = balance. Space Velocity = 50,000 h^{-1}. Adapted from [66].

reductant	300 °C	350 °C	400 °C
CH_3OH	30	20	20
C_2H_5OH	75	75	75
C_3H_7OH	37.5	65	72.5
C_2H_2	7.5	35	52.5
C_2H_4	2.5	2.5	22.5
C_3H_6	2.5	5	35
C_3H_8	0	2.5	22.5
n$-C_4H_{10}$	2.5	15	62.5
n$-C_7H_{16}$	7.5	40	47.5
n$-C_8H_{18}$	7.5	37.5	47.5
i$-C_8H_{18}$	2.5	10	25
n$-C_{12}H_{26}$	12.5	32.5	37.5

best was n-propanol, showing lower conversions than ethanol at 300 and 350 °C. The alcohol containing only one carbon atom, methanol, is converting only 20 % over the whole range. Similar results were also reported by He [64]. Out of the short hydrocarbons (C2-C3), the unsaturated ones seem to be more active than C_3H_8. Increasing the chain length of C_nH_{2n+2} is boosting the activity. Compared to n$-C_4H_{10}$, the mid-range straight chained hydrocarbons n$-C_7H_{16}$, n$-C_8H_{18}$ and n$-C_{12}H_{26}$ exhibit higher acitivity at 350 °C. Furthermore, it seems that straight chained mid-range hydrocarbons are more active than their iso forms. Another comparative study was done by Shimizu et al. [78] comparing the activities of ethers ($C_2H_5-O-C_2H_5$, $C_2H_5-O-C_4H_{10}$), alcohols (C_2H_5OH,n$-C_3H_7OH$, 2-C_3H_7OH, t$-C_4H_9OH$ n$-C_4H_{10}OH$), ketones ($(CH_3)_2CO$), esters (ethyl-acetate) and alkenes (C_3H_8) over a 2 wt. % Ag/Al_2O_3 catalyst. In the absence of H_2 they found the following activity sequence: ethers > alcohols > aldehyde > ester > ketone>> C_3H_8, while in the presence of H_2 the order changed to ethers > alcohols $\approx$ C_3H_8 > ester > ketone > aldehyde. See table 3.2 for the NO and hyrdrocarbon conversions at different temperatures. It is worth noting that, irrespective of the presence or absence of hydrogen, alcohols perform best second only to ethers. The use of ethers in power plants might be problematic due to their higher prices. Thus, ethanol seems to be a very promising candidate.

Table 3.2: NO and hydrocarbon conversion of different reductants at 250, 300, 350 and 400 °C. Values for 350 and 400 °C approximated from Fig. 1 in [68]. Conditions: NO = 1000 ppm, reductant = 6,000 ppmC, O_2 = 10 %, H_2O = 3 %, SO_2 = 50 ppm, He = balance. Space Velocity = 19,000 h^{-1}, W/F = 0.12 g s cm^{-3}. Adapted from [78].

reductant	**250 °C**		**300 °C**		**350 °C**	**400 °C**
conversion (%)	NO	HC	NO	HC	NO	NO
Et_2O	28	12	91	49	90	88
ETBE	20	14	72	46	67	69
EtOH	7	14	52	75	68	65
i−Propanol	34	22	58	53	60	62
n−Propanol	17	29	44	68	60	72
t−Butanol	22	2	38	9	65	87
Ethylacetate	5	0	27	44	80	80
Acetone	0	1	9	8	35	55
Propanal	9	10	45	54	67	92
Propane	0	0	0	3	12	45

He et al. [64] investigated the activities of several oxygenates and propene over a 4 wt. % Ag/Al_2O_3 in the absence of SO_2 and the presence of 10 % H_2O at a space velocity of 50,000 h^{-1}. The C1 oxygenates (CH_3-O-CH_3 and CH_3OH) showed maximum NO conversions of only about 20 %. The best performing oxygenates were the C4 (1-C_4H_9OH) and C2 (C_2H_5OH, CH_3CHO), followed by C3 (1-C_3H_7OH, 2-C_3H_7OH, acetone). The activity of propene was only slightly lower than the one of 2-C_3H_7OH. Apart from the C1 oxygenates, all the reductants could convert up to at least 90 % NO.

3.6 Effect of H_2O

He et al. [68] reported that the addition of 10 vol. % H_2O could boost the activity of Ethanol-SCR over a Ag/Al_2O_3 catalyst over the temperature range of 225 to 600 °C, see figure 3.4. At temperatures above 500 °C, the increased NO conversion upon water addition can probably be explained by a reduction in non-selective ethanol burning. It has also been reported that water inhibits the non-selective oxidation of octane [79] and reduces the amount of propene to achieve 50 % NO_x conversion [70].

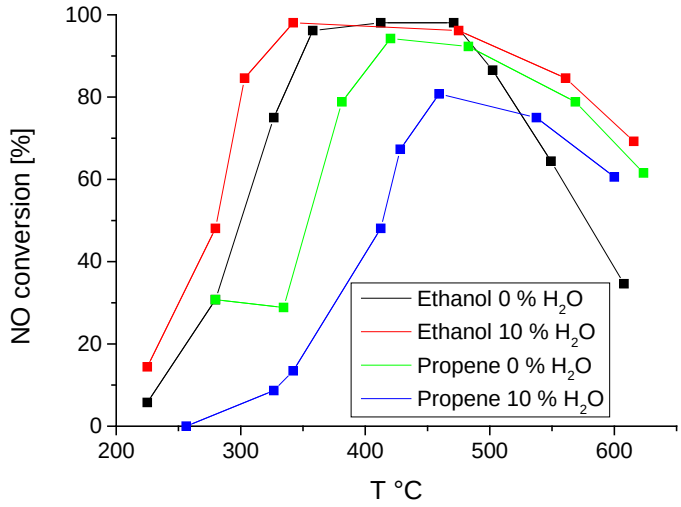

Figure 3.4: Effect of adding 10 vol. % H_2O on Propene and Ethanol-SCR over 4 wt. % Ag/Al_2O_3. Conditions: NO = 800 ppm, Propene = 1714 ppm, Ethanol = 1565 ppm, O_2 = 10 %, N_2 = balance. W/F = 0.018 g s cm^{-3}. Adapted from [68].

On the other hand, the activity of Propene-SCR was reduced by addition of water, especially at low temperatures, see figure 3.4.

The different responses to water were explained by the H_2O favouring the enolic pathway over the "acetate route". Water adsorbed onto the surface of the catalyst heavily suppressed the formation of surface acetate, thus making more sites available for the more reactive enolic species. Since enolic intermediates are more easily formed from ethanol than from propene [64], ethanol-SCR benefits from water addition while propene-SCR is inhibited, especially at low temperatures where water can adsorb more strongly. The effect of water was temporary and reversible. Again, ethanol seems to be a promising candidate.

3.7 Effect of SO_2

This topic has been dealt with in a host of papers. Here a list of some of the recurrent themes:

- Different tolerance for different reductants.
- Deactivation stronger at low temperatures.
- High Ag loadings increase SO_2 tolerance.
- H_2 increases tolerance.
- Activation by SO_2 has also been reported.

He et al. [68] compared the SO_2 tolerance of ethanol, propene, 2-propanol, 1-propanol and 1-butanol at 400 and 450 °C, see table 3.3. Using ethanol, the NO conversion is practically insensitive to the addition of SO_2, though this does not necessarily mean that the activity is not affected. The weak point of this study is that the NO conversions in the absence of SO_2 are very high (around 90 %). The same conversions could perhaps be attained at a substantially higher space velocity. So a poisoning of the catalyst could be masked by measuring at an unnecessarily low space velocity. Nonetheless, the study shows that, also in the presence of moderate SO_2 concentrations, ethanol seems to be the most promising reductant. Shimizu et al. [78] exposed a 3 wt.% Ag/Al_2O_3 catalyst to 50 ppm of SO_2 and 3 % of H_2O at 500 °C and a space velocity of 190,000 h^{-1}. The NO conversion dropped only slightly, from close to 70 to about 60 %, whereas using propene the conversion dropped from about 70 to 20 %, lending further support to both the absolute and relative (to other hydrocarbons) SO_2 tolerance of ethanol-SCR over Ag/Al_2O_3.

The other hydrocarbons fared much worse, especially at 400 °C, see table 3.3. Noteworthy is that at 400 °C, propene, the only non-oxygenate, performed clearly worse than the straight-chained alcohols, converting only 12 % NO. At 450 °C, propene performed second best only to ethanol, converting 74 % of NO. This, however, does not necessarily mean that propene-SCR is less affected by SO_2 at 450 °C, because, as can be seen from tables 3.2 and 3.1 and figure 3.6, the activity of non-oxygenates starts to pick up at higher temperatures relative to most of the oxygenates. Another study by Houel et al. [63] looked at the effect of ageing (350 °C, 68 h, 500 ppm NO, 20 ppm SO_2, 4.5 % H_2O, W/F = 0.06 g s cm^{-3}) on a 2 wt.% Ag/Al_2O_3 using 3000 ppmC n-octane as reductant. The fresh catalyst showed maximum NO conversion of 85 % at 400 °C and close to 60 %

Table 3.3: NO conversions (%) at 400 and 450 °C in the presence and absence of SO_2, using an assortment of reductants and a 4 wt.% Ag/Al_2O_3 catalyst. Conditions: NO = 800 ppm, ethanol = 1565 ppm, Propene = 1714 ppm, 2-propanol = 1043 ppm, 1-propanol = 1043 ppm, 1-butanol = 783 ppm, O_2 = 10%, H_2O = 10%, SO_2 = 0 or 80 ppm, N_2 = balance. W/F = 0.018 g s cm^{-3}. Space Velocity = 50,000 h^{-1}.Values approximated from figure 9 in [64].

	400 °C		**450 °C**	
reductant	fresh	SO_2 exposed	fresh	SO_2 exposed
ethanol	> 95	95	87-90	90
propene	92	12	90	74
2-propanol	> 95	8	90	36
1-propanol	> 95	37	90	49
1-butanol	> 90	43	90	58

at 550 °C. The aged catalyst converted less than 10 % of NO at 400 °C and 55 % at 550 °C, showing that deactivation is more severe at low temperatures and that conversions up to 550 °C are unsatisfactory, despite the low space velocity.

Abe et al. [80] have tested a 4.6 wt.% Ag/Al_2O_3 catalyst in absence and presence of 80 ppm SO_2 and a W/F of only 0.05 g s cm^{-3} at temperatures between 250 and 600 °C (NO = 800 ppm, O_2 = 10 %, ethanol = 1565 ppm, H_2O = 10 %). SO_2 caused a lowering of NO conversions at temperatures below 500 °C, e.g. at 400 °C a drop from 95 % to about 65 %. Practically full ethanol conversion was reached at 400 °C. This suggests that unselective oxidation of ethanol can be caused by sulfur poisoning. The discrepancy between the results of He [64] and Abe [80] might be caused by the fact that the values reported by the latter are part of a temperature profile starting at 250 °C. The poisoning might have happened at temperatures below 400 °C. If this is the case, this might cause problems in power plants prone to operating at low load. A study by Kim et al. [77] seems to confirm that poisoning caused at 275 °C cannot be reversed by heating to 550 °C. They exposed a 3.8 wt.% Ag/Al_2O_3 to 15 ppm SO_2 at 275 °C (Conditions: NO = 400 ppm; ethanol = 640 ppm; simulated diesel = 320 ppmC; O_2 = 6 %; H_2O = 2.5 %; W/F = 0.0429 g s cm^{-3}; SV = 60,000 h^{-1}), which caused the NO_x to N_2 conversion to drop from 60 to 18 %. Post-treatment at 550 °C for 2h could only restore the conversion at 275 °C to about 42 %. This does not prove that the conversion at temperatures above 400 °C would have been compromised by SO_2 exposure at 275 °C, but strongly hints at it because at that temperature SO_2 seems to make changes to the catalyst that cannot be reversed by heating

to 550 °C, which is probably the highest possible temperature of operation, see figure 3.4.

The deactivation due to SO_2 is usually explained by the formation of aluminium and silver sulfates [64, 71, 78], with the silver sulfates decomposing at around 620 °C and the aluminium sulfates at 930 °C [64] after use in Propene-SCR. Abe et al. [80] reported decomposition temperatures of around 427 and 727 °C, respectively, after Ethanol-SCR using a 4.6 wt.% Ag/Al_2O_3 catalyst. The sulfation of the alumina is less problematic, as discussed in section 3.4, sulfated alumina is able to convert NO_2 to N_2 in the presence of a hydrocarbon. Doronkin et al. [81] reported partial regeneration of 2 wt.% Ag/Al_2O_3 after SO_2 exposure in H_2-NH_3-SCR by heating to 670 °C. Based on adsorption energies of SOx (x = 2, 3, 4) on different Ag adsorption sites calculated with DFT they concluded that at 670 °C only "Ag nanoparticles" are freed from sulfur, whereas highly dispersed ${Ag_n}^{\delta+}$ remains sulfated. A drastically different view on SO_2 poisoning was presented by Park et al. [82], who studied 2 and 8 wt.% Ag/Al_2O_3 in Propene-SCR. According to them, decreased activities in the presence of SO_2 are due to the sulfation of alumina and the sulfation of silver, in contrast, has a promotional effect, leading to the following activity series: $Ag_2SO_4 > Ag_2O >> Ag^0$. The 2 and 8 wt.% loaded catalysts were exposed to 30 ppm of SO_2 at 500 °C (NO = 1000 ppm; C_3H_6 = 3000 ppmC; H_2O = 7 %; O_2 0 9 %; SV =30,000 h^{-1}). For the d 8 wt.% sample the N_2 yield increased from 1 to around 28 % upon exposure to SO_2 while at the same time the propene conversion dropped from 100 to around 75 %. After removing SO_2 the N_2 yield dropped and the propene conversion increased. The 2 wt.% catalyst first saw the N_2 yield increase from 54 to 58 % followed by a drop to around 40 %. The propene conversion first saw a rapid drop form 81 to around 77 % while the N_2 yield increased from 54 to 57 %. Then a gradual drop of the propene conversion to around 65 % followed. Preparing a 2 wt.% loaded sample using silver sulfate as precursor, the same N_2 yield profile appeared except for a lack of an initial rise and a starting point of around 75 instead of 54 %. From these results the authors conjectured that an initial sulfation of Ag is enhancing the N_2 yield and reducing unselective oxidation of propene. This is followed by detrimental sulfation of alumina. The authors tried to corroborate their theories with in situ DRIFTS of 2 wt.% Ag/Al_2O_3 in the presence of propene (1000 ppm), NO_2 (1000 ppm) and O_2 (9 %). Very little -NCO adsorbed on silver sites was detected on fresh 2 wt.% Ag/Al_2O_3. Samples that underwent prior SO_2 (30 ppm) exposure generated a much stronger -NCO on Ag sites signal, suggesting an increased NO reduction ability of sulfated silver particles. However, this hardly proves the author's claim that it is the sulfation of alumina that is causing the N_2 yield to decrease. The DRIFTS study is

dodgy in two regards. Firstly, the authors did not explain why they used NO_2 and not NO. It is well known, that sulfated alumina, even without any co-metal, can convert NO_2 to N_2 in the presence of a hydrocarbon [71]. It is imaginable that the -NCO species were actually formed on the sulfated alumina and not the sulfated silver. Secondly, the ratio of C atoms of reductant to NO molecules was only 3 instead of 6 as in most studies, including their own. Maybe the first 1000 ppmC of propene were unselectively combusted by the fresh silver particles and the sulfated silver was no longer able to do that. Though the findings of Park et al. [82] might be interesting, they are of mostly academic interest, because the catalyst that experiences increased N_2 yield in the presence of SO_2 is converting insufficient amounts of NO and is probably also rather expensive due to the high silver loading of 8 wt.%.

The relatively high SO_2 tolerance of Ag/Al_2O_3 in conjunction with ethanol was ascribed to an inhibition of sulfate formation by C2 enolic species evidenced by DRIFTS studies [64] at 400 °C . The authors did not elaborate on which kind of sulfate formation was reduced. Assuming this cleansing effect of ethanol really exists at 400 °C but not at 250 °C, the low NO conversions in the presence of SO_2 as reported by Abe [80] may be reasonable. Shimizu et al. [78] measured SO_2 desorption profiles in HC-TPR (HC: ethanol, Et_2O, propene, He) of 3 wt.% Ag/Al_2O_3 pretreated in $SO_2/H_2O/O_2/H_2/NO/C_3H_8$ for 24 h at 350 °C. The amount of SO_2 desorbed between 200 and 500 °C was larger for the two oxygenates (ethanol, Et_2O) than for propene. The temperatures at which SO_2 desorption begins are: He (350 °C) > C_3H_8 (300 °C) > Et_2O (280 °C) > EtOH (250 °C). The correlation between the sulfate reduction capability and the SO_2 tolerance indicates that the reactivity of the hydrocarbon with sulfates is a key factor for achieving high SO_2 tolerance during HC-SCR.

Several sources claim that adding H_2 increases the SO_2 tolerance of Ag/Al_2O_3 [78, 83, 84]. Shimizu et al. [78] investigated the effect of adding 0.5 vol.% H_2 to Et_2O-SCR and EtOH-SCR over 3 wt.% Ag/Al_2O_3 at 350 °C (Conditions: NO = 1000 ppm; oxygenates = 6000 ppmC; H_2O = 3 %; O_2 : 10 %; SO_2 = 50 ppm; SV = 19,000 h^{-1}; duration = 20 h). The NO conversions dropped from 80 to 55 % in Et_2O-SCR and from 80 to 70 % in H_2-Et_2O-SCR. EtOH-SCR experienced a conversion drop from around 62 to 35 % and H_2-EtOH-SCR from around 90 % to 50 %. In both cases the NO conversion levelled off before the end of the experiment (20 h). The authors did not give reasons for the higher SO_2 tolerance in the pesence of H_2. Besides, at least in the case of ethanol, the conversion data do not really prove that the activity of the H_2-oxygenates-SCR is less affected by SO_2 than oxygenates-SCR, because H_2 also has a promoting effect in the absence of SO_2, see section 3.8. The same group published a more thorough investigation

of H_2−C_3H_8-SCR [83]. The authors have shown by TPR and TPD on sulfated samples that the presence of H_2 helps in removing sulfates strongly adsorbed on silver-containing sites, resulting in gaseous SO_2 or aluminium sulfates. The presence of H_2 is causing partial reduction of Ag^+ ions to $Ag_n{}^{\delta+}$ clusters, even in the presence of SO_2, as shown by UV-vis experiments. Sulfate anions adjacent to partially reduced silver sites are believed to be less stable than those on cationic sites. Increasing the silver loading from 2 to 4 wt.% also leads to more readily decomposable silver sulfates after exposure to SO_2. About 10 times as much SO_2 was desorbed from 4 wt. % than from 2 wt.% Ag/Al_2O_3 after SO_2 exposure. Another study using propane as reductant by Satokawa [84] showed increased tolerance towards 6.4 ppm of SO_2; however, an in-depth study of the poisoning mechanism was not presented.

Apart from high loadings of Ag, use of ethanol, addition of H_2 and operating at high temperatures, one can increase the SO_2 tolerance by modifiying the alumina support [77,85,86]. Li et al. [85] prepared a 5 wt.% $Ag/(Al_2O_3{-}TiO_2)$ (1:1 in mass weight) catalyst by the sol-gel method and used it in propene-SCR in the presence of 100 ppm SO_2 (Conditions: NO = 800 ppm, C_3H_6 = 800 ppm, O_2 = 8 %, SO_2 = 100 ppm, balance = N_2, SV = 18,000 h^{-1}). Compared to the alumina support, the amorphous mixed oxide support causes drastically increased NO conversions at low temperatures, e.g. at 300 °C it converts around 35 % instead of less than 10 %. $Ag/(Al_2O_3{-}TiO_2)$ exhibits maximum NO conversion of around 80 % at 450 °C, while $Ag/(Al_2O_3)$ is peaking at 500 °C with only 60 %. EDS elemental analysis and TPD of SO_2 showed that the sulfur uptake by the mixed oxide was lower than by pure alumina while the aged mixed oxide adsorbed more NOx and released it at higher temperatures indicating formation of strongly adsorbed nitrates instead of nitrites, which was also confirmed by DRIFTS experiments. Jagtap et al. [86] doped alumina with 1 wt. % SiO_2 or TiO_2 for the use in propene-SCR. Both mixed oxides increased the NO conversion in the presence of SO_2 and H_2O (Conditions: NO = 1000 ppm; C_3H_6 = 2000 ppm; H_2O = 5 %; W/F = 0.05 g h L^{-1}). At 350 °C, the NO conversions of Ag/Al_2O_3, Ag/Al−Si and Ag/Al−Ti were 20, 45 and 30 %, respectively. The authors explained the increased SO_2 tolerance of the mixed oxides by their increased acidity resulting in less sulfate formation evidenced by EDAX and FTIR measurements. Another reason given is the fact that sulphates of SiO_2 and TiO_2 are thermally less stable than $Al_2(SO_4)_3$.

The NO conversions in presence of SO_2 also need to be put in perspective. Kristensen et al. [25] have exposed an industrial catalyst containing 3 wt.% V_2O_5 and 7 wt.% WO_3 supported on TiO_2 to 2000 ppm of SO_2 and 2.4 % H_2O at a W/F of 0.00066 g s cm^{-3} at 380 °C using NH_3 as reductant. They reported an NO con-

version of 30 % for the industrial catalyst and 60 % for their home-made 20 wt.% V_2O_5/TiO_2 prepared by a sol-gel method. These conversions are comparable to the ones obtained by using reductants other than ethanol over an Ag/Al_2O_3 catalyst as reported in the study of He [64], see table 3.3. The difference between the two studies is that the catalyst weight used per unit of flow rate is about 27 times higher in the case of the HC-SCR study [64]. This means that the vanadia based catalysts vastly outperform the HC-SCR over Ag/Al_2O_3, at least when hyrdrocarbons other than ethanol are used. A sensible comparison between the NH_3-SCR and ethanol-SCR is not possible, because the NO conversions of 90 % in the case of ethanol-SCR could maybe have been reached using less catalyst. In fairness, we need to admit that there is a weak point in the study of Kristensen [64]. The water content of 2.4 % is unrealistically low. However, it has been reported [87] that the inhibiting effect of H_2O on vanadia containing catalysts at 320 °C is mostly attributable to the first 5 % H_2O. So we can conclude that, at least in the presence of SO_2, HC-SCR using Ag/Al_2O_3 is most probably much less active than NH_3-SCR using vanadia containing catalysts. The only hyrdrocarbon included in the present discussion that might exhibit competitive activities in the presence of SO_2 is ethanol.

3.8 H_2-HC-SCR

A very effective way to enhance the low-temperature activity of HC-SCR over Ag/Al_2O_3 is to add H_2 to the feed-gas, regardless of the reductant being used [64,77,88,90]. Very importantly, the so-called H_2 effect is also present in ethanol-SCR as first reported by Zhang et al. [89]. Ethanol is among the best performing reductants in the presence of H_2O and SO_2, see sections 3.6 and 3.7. Therefore, this section will mostly deal with H_2-ethanol-SCR. Zhang et al. [89] reported over 90 % NO_x conversion in H_2-ethanol-SCR over 4 wt.% Ag/Al_2O_3 at temperatures between 200 and 500 °C (Conditions: NO = 800 ppm; C_2H_5OH = 1565 ppm; O_2 = 10 %; H_2O = 10 %; H_2 = 1 %; W/F = 0.018 g s cm^{-3}; SV = 50,000 h^{-1}). In the absence of H_2, the NO_x conversion at 200 °C is less than 20 % and 90 % conversion is reached at 300 °C. At temperatures above 450 °C, H_2 does not have a promotional but slightly detrimental effect. The authors explained the promotion by H_2 enhancing the formation of enolic species and -NCO. They also assume that H_2 promotes the transformation of -NCO into NHx species, see figure 3.2. A very thorough study on H_2-SCR using mixtures of ethanol and simulated diesel (SD) was published recently by Kim et al. [88]. They divided the effects of H_2 into "morphological", "chemical" and "kinetic" changes. The morphological change comprises the transformation of Ag^+ to metallic Ag^0 and ${Ag_n}^{\delta+}$ clusters as evidenced by UV-vis spectra. This process is relatively slow (timescale of minutes) compared to the response of the activity of HC-SCR to the addition

of H_2, which is almost instantaneous. The "chemical changes" which are a fast process (timescale of seconds) concerning the surface layer and a slow process (timescale of minutes) concerning the bulk phase ultimately lead to the formation of AgO and Ag_2O_3. In AgO, the oxygen metal bonding may be weaker than in Ag_2O, thereby making the oxygen more mobile and reactive, as evidenced by H_2-TPR and O_2-TPD. In Ag_2O_3 a reactive ozonide-like species might be present. The reactive oxygen species in AgO and Ag_2O_3 facilitate the adsorption and oxidation of hydrocarbons and NO, which results in the formation of reactive intermediates such as nitrates and enolic/acetate species. The "chemical change" first involves the oxidation of AgO_x (x = 0 or 0.5) to $Ag(OH)_2$ in the presence of O_2 and H_2 as confirmed by FTIR experiments. $Ag(OH)_2$ decomposes to AgO, which in turn can decompose to AgO_x (x = 0 or 0.5) when H_2 is removed from the stream. AgO can further oxidize to Ag_2O_3. The authors were less clear about the "kinetic changes". They have only concluded that the formation of adsorbed NO_x and enolic/acetate (OHCs) species increases. The ${Ag_n}^{\delta+}$ clusters catalyze the reaction between OHCs and nitrates to form -CN and -NCO, which in turn can generate N_2 when reacting with NO_x and H_2O. For our project only the existence of the "H_2 effect" and the dependence on the hydrogen concentration are of real importance. Most studies [64, 77, 88, 90, 91] used either 0.5 or 1 % H_2. This high level is probably economically unacceptable in stationary applications (e.g. power plants). Injecting 1 % of H_2 and assuming an NO concentration of typically around 500 ppm translates into adding 1.33 tones of H_2 per ton of NO. Satokawa et al. have shown in a series of papers [92, 93] that addition of 455 ppm [92] or 909 ppm [93] of H_2 can drastically enhance the low temperature activity of C_3H_8-SCR over Ag/Al_2O_3. However, in these studies, only 91 ppm of NO and propane were used. To the best of our knowledge, there are no reports on H_2−ethanol−SCR injecting less than 1000 ppm of H_2. In our own H_2−ethanol−SCR studies we have used approximately 500 ppm of H_2.

3.9 Promoters & synthetic methods

Wang et al. [94] have investigated the effect of 0.01 and 0.05 wt.% Pd, Pt and Au on the C_3H_6-SCR activity of 5 wt.% Ag/Al_2O_3. While Au and Pt showed a detrimental effect, Pd has a promotional effect, especially at temperatures below 400 °C. The authors explained this finding by an increased formation of enolic species as evidenced by DRIFTS. A detrimental effect of Au was also reported by Seker et al [95]. Shimizu et al. [91] have sligthly enhanced propene-SCR by doping the alumina support with 5 wt.% of Zn or Mg. Y, P and Na, on the other hand, suppressed the NO conversion. Streker et al. [95] have investigated the effects of the preparation method (sol-gel, co-precipitation and impregnation), silver loading and calcination temperature on the deNOx performance in propene-

SCR. The authors concluded that sol-gel affords higher silver loadings (5 wt. % instead of 3 wt.%) due to a higher surface area resulting in higher NO conversions at low temperatures. Co-precipitation leads to large crystallites of silver and poor activity. Despite this report we refrained from using the sol-gel method, due to the simplicity and high reproducibility of the incipient wetness impregnation method.

3.10 Economic issues with HC-SCR

A general problem of HC-SCR is the high price of hydrocarbons compared to ammonia. In the following, we have compiled the costs of some of the potential reductants as at 21^{st} of July 2011, taken from the ICIS (www.icis.com) homepage. We have assumed that 3 moles of carbon atoms are needed to reduce one mole of NO. Our own experiments using ethanol as reductant suggest that this is a realistic assumption, see figure 4.5. Furthermore, we have assumed that the CO_2 emissions stemming from HC-SCR will be taxed at a rate of 30 €per ton CO_2 in the case of fossil hydrocarbons and that no tax will be levied in the case of bio-ethanol and glycerol. For NH_3 we have assumed use of stoichiometric amounts. Except for methane, all hydrocarbons come at a significantly higher price than NH_3 does. In the case of the most promising reductant, ethanol, the price differential is around a whopping 2000 €or 14900 DKK per ton of NO. Even after the quintupling of the NO_x tax, this is close to 50 % of that tax of 24000 DKK per ton of NO_2 equivalent. The differential between ammonia and ethanol is about 10 times the price of ammonia. According to several sources [97,98], the VWT catalyst cost and the cost of ammonia are roughly equal. This means that the cost differential would allow for catalyst replacement after 3-4 months instead of after 3-4 years. Consequently, the use of ethanol is probably only acceptable if it provides significant advantages over NH_3, e.g. not being at all affected by potassium and in the case of extremely strict NH_3 emission limits.

Table 3.4: Cost of different hydrocarbons as of July 21^{st} 2011, taken from the ICIS (www.icis.com) homepage. CO_2 tax assumed to be 30 €per ton. Calculations based on the assumption that 3ppmC_1 are needed per ppmNO.

reductant	Cost of reductant	mass needed	Cost	CO_2 tax	total cost
	€/ ton	$\text{ton}_{reductant}$ / ton_{NO}	€/ ton_{NO}	€/ ton_{NO}	€/ ton_{NO}
NH_3	315	0.57	180	0	180
Ethanol	1000	2.30	2295	0	2295
Glycerol	470	3.07	1443	0	1443
Methanol	315	3.2	1011	132	1143
Methane	240	1.6	382	132	514
Ethene	1110	1.4	1554	132	1686
Propene	1070	1.4	1498	132	1630

Chapter 4

Ethanol-SCR over Ag/Al_2O_3

4.1 Characterisation

Most of the characterisation results can be found in one of our papers [96]. Increasing the silver loading from 0 to 5 wt.% decreases the surface area only slightly, whereas the number of acid sites as measured by NH_3-TPD tends to increase, though there is no consistent trend. Doping 3 wt.% Ag/Al_2O_3 with increasing amounts of potassium continously reduces the number of acid sites. However, the decrease is sub-stoichiometric, unlike in the case of doped VWT, where the effect is above stoichiometric [53]. The surface area as measured by N_2-BET is only marginally reduced by increasing potassium loadings. In the XRD patterns, only reflections attributable to γ- Al_2O_3 were observed. No reflections attributable to Ag^0, Ag_2O or $AlAgO_2$ were detected. The detection limit of the apparatus is about 5 nm. So, even if there are metallic silver particles, they are well dispersed.

4.2 Ag loading optimisation

Figure 4.1 shows the catalytic acitivity profiles of 1 - 5 wt.% Ag/Al_2O_3 as a function of temperature. Figure 4.2 gives the corresponding ethanol conversion profiles. Increasing the silver loading from 1 to 2 wt.% drastically increases the NO_x and ethanol conversions. 2 wt. % Ag/Al_2O_3 exhibits NO_x conversions

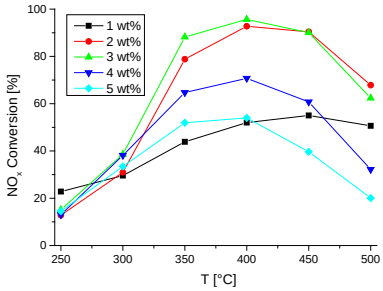

Figure 4.1: NO_x conversion over Ag/Al_2O_3 with varying Ag loadings. W/F = 0.005 g s cm^{-3}.

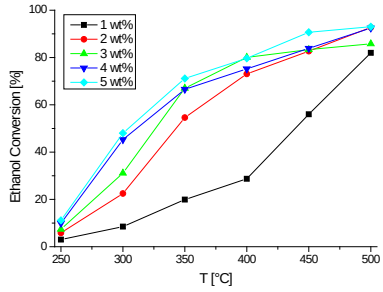

Figure 4.2: Ethanol conversion over Ag/Al_2O_3 with varying Ag loadings. W/F = 0.005 g s cm^{-3}.

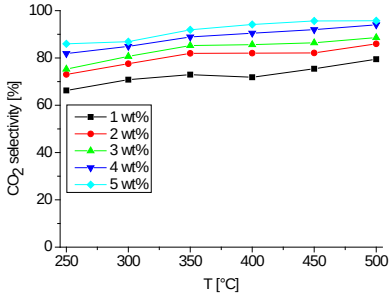

Figure 4.3: $S_{CO_2}(T)$ over Ag/Al_2O_3 with varying Ag loadings. W/F = 0.005 g s cm^{-3}.

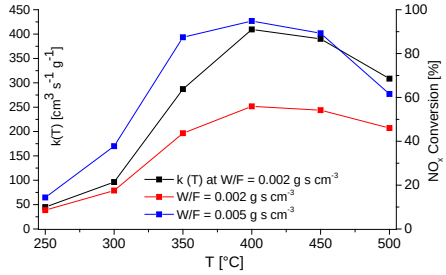

Figure 4.4: NO_x conversion over 3 wt.%Ag/Al_2O_3 and first-order rate constant k(T) at varying W/F.

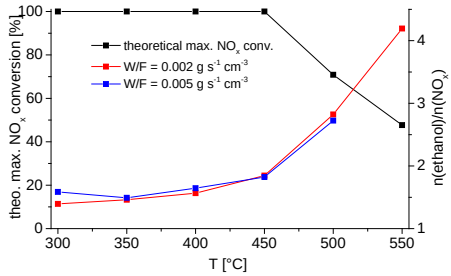

Figure 4.5: Moles of ethanol consumed per mole of NO_x reduced at W/F of 0.005 and 0.002 g s cm^{-3} and theoretical max. NO_x conversion.

higher than 80 % between 350 and 450 °C; however, at 500 °C the conversion was only 68 %. Further increasing the Ag loading to 3 wt.% makes little difference regarding both the ethanol and NO_x conversion. Silver loadings of 4 and 5 wt.% show ethanol conversion profiles similar to the one of 3 wt.%. However, the NO_x conversion profiles at temperatures above 300 °C differ significantly in that the catalysts with 4 and 5 wt.% silver exhibit maximum conversions at 400 °C of only 71 and 54 %, respectively. Apparently, increasing the silver loading beyond 3 wt.% only boosts the unselective oxidation of ethanol. Note that there is no formation of N_2O for any of the catalysts in the given temperature range. Figure 4.3 shows the corresponding $S_{CO_2}(T)$. Increasing the Ag loading from 1 to 5 wt.% is gradually increasing the $S_{CO_2}(T)$ whereas increasing the temperature only has a slightly increasing effect.

Since the NO_x conversions reached almost 100 %, it is not possible to use these data to calculate first-order rate constants with equation A.11. Therefore, the optimum 3 wt.% Ag/Al_2O_3 catalyst was retested, keeping the flow rate at 3 NL/min but reducing the catalyst weight from 250 mg to 100 mg resulting in a W/F of 0.002 g s cm^{-3}. These conditions were also used for testing the potassium poisoned catalysts. Figure 4.4 shows the NO_x conversions at W/F of 0.005 and 0.002 g s cm^{-3}, the latter allowing for the calculation of first order rate constants k(T). Separate experiments have shown that the NO_x reduction in ethanol-SCR is zero order with respect to ethanol and first-order with respect to NO up to an NO concentration of 500 ppm. 3 wt.% Ag/Al_2O_3 reaches maximum first-order rate constants of around 400 cm^3 s^{-1} g^{-1} at 400 and 450 °C. The NO_x conversions at these temperatures are not limited by unselective ethanol oxidation, since testing at lower space velocity yields values over 90 %, see figure 4.1. However, the k(T)

at 500 °C of 309 cm^3 s^{-1} g^{-1} could not be reproduced at a W/F of 0.005 g s cm^{-3}, where it was caculated to be only 195 cm^3 s^{-1} g^{-1}. On the other hand, k(T) values at 300 °C are practically insensitive to the change in W/F and close to 100 cm^3 s^{-1} g^{-1} . The industrial reference VWT catalyst [53] exhibits k(T) values of around 420, 900 and 900 cm^3 s^{-1} g^{-1} at 300, 400 and 450 °C, respectively. Because of the low activity of 3 wt.% Ag/Al_2O_3 at 300 °C it is doubtful that operation within the usual temperature window of 300 to 400 °C is feasible. Moving the SCR unit closer to the burner in order to increase the temperature might entail significant retrofitting. Furthermore, it seems doubtful if operation above 450 °C is possible, due to unselective oxidation of ethanol. The study of He et al. [68], see figure 3.4, suggests that it should be possible to extend the temperature window up to 550 °C without letting the NO_x conversion decrease below 85 % when using 10 % H_2O in the gas stream, which is a more realistic concentration anyway. Similar results were presented by Abe et al. [80]. The ratio of ethanol to NO [68, 80] was practically the same as the one used in our study. However, He et al. [68] have reported that even in the absence of water, more than 80 % can be converted at 500 °C and more than 60 % at 550 °C. We have calculated the number of moles of ethanol consumed per number of moles of converted NO_x at W/F values of 0.005 and 0.002 g s cm^{-3}, see figure 4.5. The amount of ethanol consumed per reduced NO_x is remarkably insensitive to the W/F value. Therefore, we have calculated the theoretical maximum NO_x conversion at full ethanol conversion, assuming inlet concentrations of 500 ppm NO and 1000 ppm ethanol, see figure 4.5. According to our calculations, only around 71 and 48 % NO_x can be converted at 500 and 550 °C, respectively. The only apparent difference in the catalyst preparation method is the fact that He et al. have dried the freshly impregnated samples in a rotary evaporator under reduced pressure. We have refrained from using this method because we doubt its scalability. The fact that He et al. loaded 4 instead of 3 wt. % Ag and used 600 instead of 550 °C as calcination temperature can most likely not explain their higher NO conversions at high temperatures.

In summary, the 3 wt.% Ag/Al_2O_3 can convert at least 90 % NO_x at temperatures of up to 450 °C in the presence of 2 % H_2O and an ethanol to NO molar ratio of two. The corresponding first-order rate constant of around 400 cm^3 s^{-1} g^{-1} is about 55 % lower than the maximum activity of the industrial VWT catalyst. Above 450 °C ethanol-SCR over our 3 wt.% Ag/Al_2O_3 catalyst suffers from unselective oxidation of ethanol. Results of other groups suggest that using the same ethanol to NO molar ratio, it should be possible to attain at least 85 % conversion up to 550 °C in the presence of 10 % H_2O. The selectivity towards CO_2 increases with the Ag loading and depends only weakly on the temperature.

4.3 Effect of H_2

Figure 4.6 shows the NO_x and ethanol conversions as well as the corresponding selectivity towards CO_2 as a function of the H_2 concentration ranging from 0 to 1400 ppm over a 3 wt.% Ag/Al_2O_3 catalyst at 400 °C. Figure 4.7 gives the corresponding rate constants and moles of converted ethanol per mole of converted NO_x. Adding 500 ppm of H_2 causes the NO_x conversion to increase from 55.9 to 65.7 % and the corresponding rate constants to increase from 409 to 535 cm^3 s^{-1} g^{-1}. Further increasing the hyrdrogen concentration to up to 1400 ppm does not boost the activity. The ethanol conversion increases in line with the NO_x conversion, keeping the molar ratio of ethanol consumed per NO_x at around 1.6. The selectivity towards CO_2 is unaffected by H_2 addition. Further H_2 additions were done with 500 ppm.

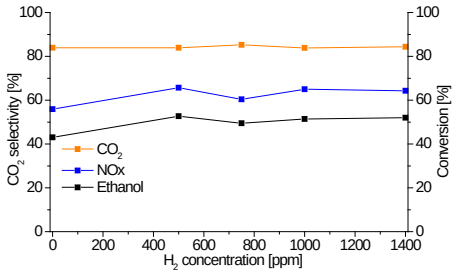

Figure 4.6: NO_x and ethanol conversions and selectivity towards CO_2 at 400 °C over 3 wt.% Ag/Al_2O_3 at various H_2 concentrations. W/F = 0.002 g s cm^{-3}.

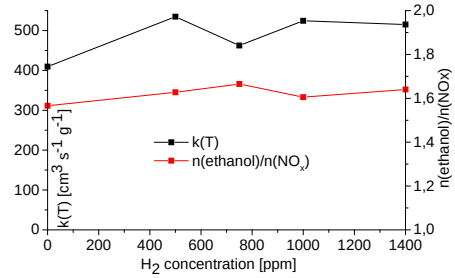

Figure 4.7: Moles of ethanol consumed per mole of NO_x reduced and k(T) at 400 °C over 3 wt.% Ag/Al_2O_3 at various H_2 concentrations. W/F = 0.002 g s cm^{-3}.

4.4 Potassium poisoning

Figure 4.8 and figure 4.9 show the NO_x and ethanol conversions over 3 wt.% Ag/Al_2O_3 with different K loadings as functions of temperature. The NO_x con-

versions are heavily suppressed by increasing K loadings, whereas the ethanol conversions are relatively unaffected. This results in very high molar ratios of consumed ethanol to converted NO_x, see figure 4.11. So poisoning by potassium is a twofold problem in that not only the SCR activity per gram of catalyst decreases but also the potential total NOx conversion, irrespective of the space velocity being used. One way to partially alleviate the latter problem could be a staged ethanol injection, e.g. before each catalyst layer. The selectivity towards CO_2 is enhanced by increasing potassium loadings, see figure 4.10. In that sense, potassium has the same effect as increasing the Ag loading. Figure 4.12 shows the first-order rate constants as functions of temperature and potassium loading and figure 4.13 gives the relative (to unpoisoned catalyst) first-order rate constants of ethanol-SCR using 3 wt.% Ag/Al_2O_3 and NH_3-SCR over the industrial VWT catalyst. Though the ethanol-SCR is somewhat less affected by potassium this does not mean that higher absolute activities are obtained in the presence of potassium, since the VWT catalyst exhibits roughly double the activity in the fresh state.

Adding 500 ppm of H_2 leaves the ethanol conversion over K/Ag = 0.5 practically untouched and the NO_x conversion even decreases slightly, see figures 4.14 and 4.15.

Since doping 3 wt.% Ag/Al_2O_3 with lithium (Li/Ag = 1.0) promoted propene-SCR (see section 5.2), and pre-adsorbed lithium might make adsorption sites unavailable to potassium due to its chemical similarity, its influence on the ethanol-SCR performance was tested, see figures 4.16 and 4.17. As no significant promotional effect in ethanol-SCR could be ascertained and the side-blocking strategy proved to be largely ineffective in propene-SCR, we did not go down this route any further.

4.5 SO_2 poisoning

3 wt.% Ag/Al_2O_3 was exposed to increasing concentrations of SO_2 ranging from 25 to 150 ppm at 400 °C, see figure 4.18, which shows the NO_x and ethanol conversions at steady state. Introducing 25 ppm of SO_2 causes the NO_x conversion to drop from 55.9 to 26.0 %, which corresponds to a 63 % drop in the first order rate constant. Further increases in the SO_2 concentration lead to more gradual decreases in the NO_x conversion, reaching 15.6 % at 150 ppm SO_2. The ethanol conversion decreases roughly in line with the NO_x conversion. The $S_{CO_2}(T)$ seems to decrease with increasing SO_2 content; however, the near zero value at 150 ppm SO_2 needs to be taken with a pinch of salt, since the corresponding CO and CO_2

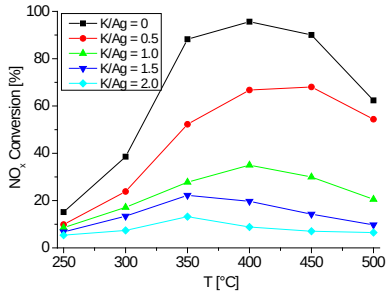

Figure 4.8: NO_x conversion over 3 wt.% Ag/Al_2O_3 poisoned with varying K/Ag molar ratios. W/F = 0.005 g s cm^{-3}.

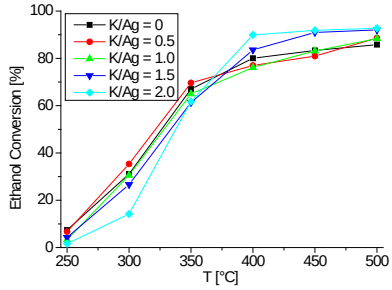

Figure 4.9: Ethanol conversion over 3 wt.% Ag/Al_2O_3 poisoned with varying K/Ag molar ratios. W/F = 0.005 g s cm^{-3}.

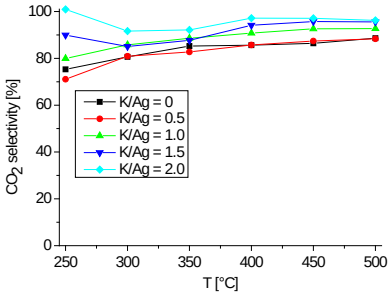

Figure 4.10: S_{CO_2}(T) over 3 wt.% Ag/Al_2O_3 poisoned with varying K/Ag molar ratios. W/F = 0.005 g s cm^{-3}.

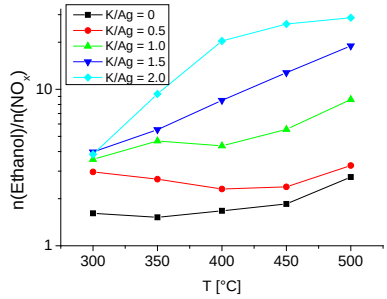

Figure 4.11: Moles of ethanol consumed per mole of NO_x reduced over 3 wt.% Ag/Al_2O_3. W/F = 0.005 g s cm^{-3} and 0.002 g s cm^{-3} for K/Ag = 0.

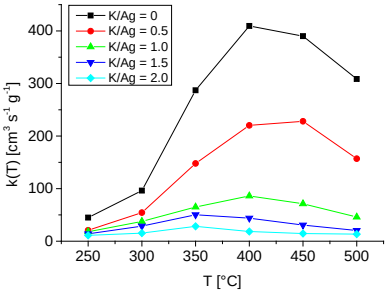

Figure 4.12: First order rate constants k(T) over 3 wt.% Ag/Al_2O_3 poisoned with varying K/Ag molar ratios. W/F = 0.005 g s cm^{-3} and 0.002 g s cm^{-3} for K/Ag = 0.

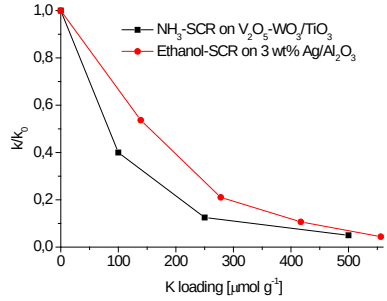

Figure 4.13: Relative activities of NH_3-SCR and ethanol-SCR as function of K loading at 400 °C.

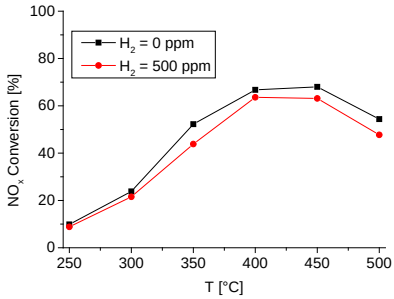

Figure 4.14: NO_x conversion over 3 wt.% Ag/Al_2O_3 poisoned with K/Ag = 0.5 in the presence and absence of 500 ppm H_2. W/F = 0.005 g s cm^{-3}.

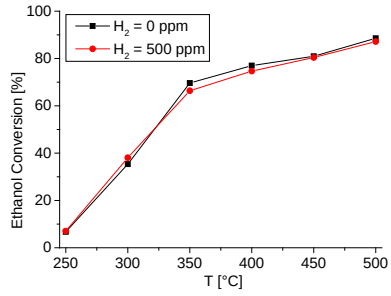

Figure 4.15: Ethanol conversion over 3 wt.% Ag/Al_2O_3 poisoned with K/Ag = 0.5 in the presence and absence of 500 ppm H_2. W/F = 0.005 g s cm^{-3}.

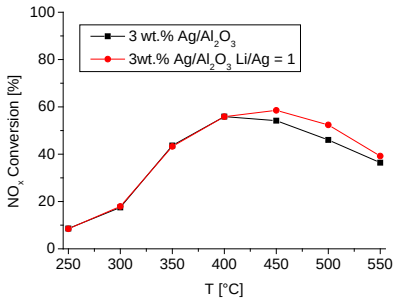

Figure 4.16: NO_x conversion over 3 wt.% Ag/Al_2O_3 doped with Li/Ag = 1.0. W/F = 0.002 g s cm^{-3}.

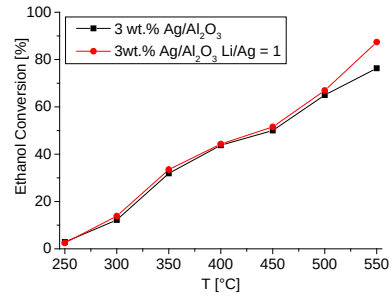

Figure 4.17: Ethanol conversion over 3 wt.% Ag/Al_2O_3 doped with Li/Ag = 1.0. W/F = 0.002 g s cm^{-3}.

concentrations are very low. Though the SO_2 tolerance might be higher at higher temperatures (e.g. 500 °C), we did not repeat the experiment at those temperatures, because the catalyst probably needs to be operational at around 400 °C. This is because the temperature difference between full and low load is approximately 100 °C and the maximum temperature that allows for close to full NO_x conversion is around 500 °C, see section 4.2 and [68, 80].

The combined effect of 500 ppm H_2 and 60 ppm SO_2 was investigated, see figures 4.19 and 4.20. The addition of 500 ppm H_2 boosted the NO_x and ethanol conversions only slightly over the full temperature range of 250 to 550 °C. The absence of a significant activity enhancement at temperatures below 350 °C as reported in the literature [88, 89] prevents the extension of the temperature window towards lower values. Furthermore, the hydrogen concentration in the present study does not seem to lessen the impact of SO_2.

The impact of SO_2 on H_2-ethanol-SCR over potassium poisoned (K/Ag = 0.5) 3 wt.% Ag/Al_2O_3 was investigated, see figures 4.21 and 4.22. Like in the case of potassium-free catalyst, addition of 60 ppm of SO_2 appreciably suppresses both the NO_x and ethanol conversions between 250 and 450 °C. At 500 °C, the conversions in presence of SO_2 are roughly on par with those in the absence of SO_2, resulting in a maximum first order rate constants of a meagre 160 $cm^3\ s^{-1}\ g^{-1}$. The decreased deactivating effect of SO_2 at higher temperatures is in congruence with most literature reports (e.g. [80]).

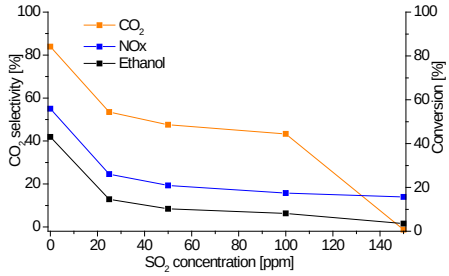

Figure 4.18: NO_x and ethanol conversions and $S_{CO_2}(T)$ as a function of SO_2 content at 400 °C. W/F = 0.002 g s cm^{-3}.

The effect of doping the alumina support with 5 mol% Ti on the SO_2 resis-

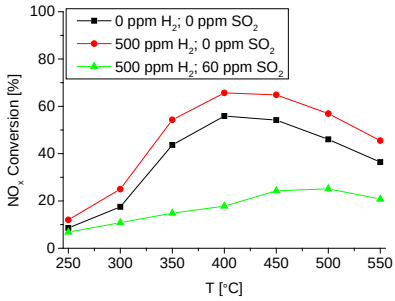

Figure 4.19: Effects of 500 ppm H_2 and 60 ppm SO_2 on the NO_x conversion over 3 wt.% Ag/Al_2O_3. W/F = 0.002 g s cm^{-3}.

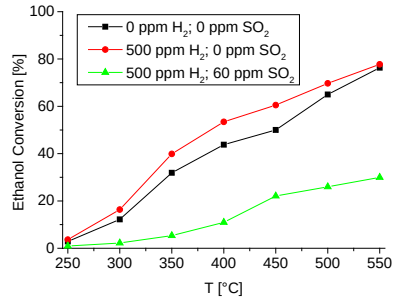

Figure 4.20: Effects of 500 ppm H_2 and 60 ppm SO_2 on the ethanol conversion over 3 wt.% Ag/Al_2O_3. W/F = 0.002 g s cm^{-3}.

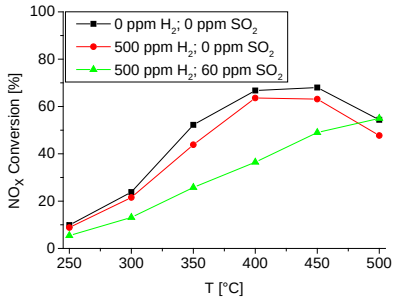

Figure 4.21: Effects of 500 ppm H_2 and 60 ppm SO_2 on the NO_x conversion over 3 wt.% Ag/Al_2O_3 poisoned with K/Ag = 0.5. W/F = 0.005 g s cm^{-3}.

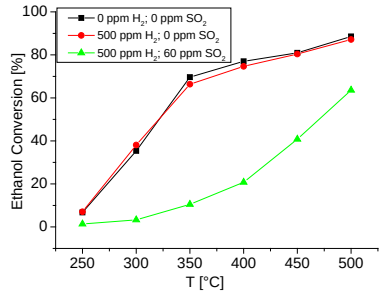

Figure 4.22: Effects of 500 ppm H_2 and 60 ppm SO_2 on the ethanol conversion over 3 wt.% Ag/Al_2O_3 poisoned with K/Ag = 0.5. W/F = 0.005 g s cm^{-3}.

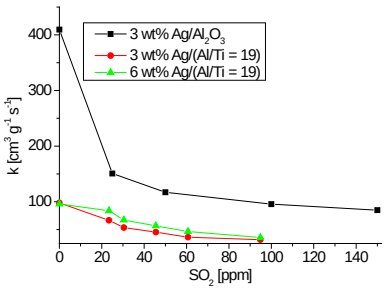

Figure 4.23: Effect of SO_2 on the first order rate constant over 3 and 6 wt.% $Ag/(Al_2O_3{-}TiO_2)$ (5 mol% Ti) and 3 wt.% Ag/Al_2O_3. W/F = 0.005 g s cm^{-3}. for $Al_2O_3{-}TiO_2$ and 0.002 g s cm^{-3} for Al_2O_3 support.

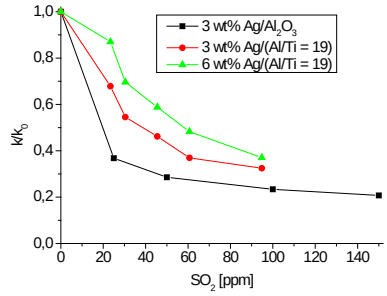

Figure 4.24: Effect of SO_2 on the relative activity (k/k0) over 3 and 6 wt.% $Ag/(Al_2O_3{-}TiO_2)$ (5 mol% Ti) and 3 wt.% Ag/Al_2O_3. W/F = 0.005 g s cm^{-3}. for $Al_2O_3{-}TiO_2$ and 0.002 g s cm^{-3} for Al_2O_3 support.

tivity was tested, see figures 4.23 and 4.24. Though doping with Ti enhances the SO_2 tolerance, concentrations as low as 60 ppm can still knock off 50 % of the initial activity. Note that unselective oxidation of ethanol was not a much bigger problem than in the case of the pure alumina support. Because of the unimpressing SO_2 tolerance enhancement we have desisted from optimising the Ti content.

4.6 Conclusion: ethanol-SCR over Ag/Al_2O_3

Ethanol-SCR over 3 wt.% Ag/Al_2O_3 can reach activities of around 400 cm^3 s^{-1} g^{-1} at 400 °C, which is about half of the activity of NH_3-SCR over the industrial VWT catalyst. Poisoning by potassium decreases NO_x conversions while not affecting the ethanol conversions, meaning that the maximum attainable NO_x conversion at a given ethanol/NO_x molar ratio is strongly reduced, irrespective of the space velocity. H_2 at concentrations of up to 1400 ppm has only a mildly promoting effect and does not significantly enhance the SO_2 or potassium tolerance. SO_2 levels as low as 25 ppm reduce the catalyst activity by more than 50 % at 400 °C. Doping the alumina support with Ti enhances the SO_2 tolerance only insufficiently. As potassium seems to be as much a problem in ethanol-SCR as it is in NH_3-SCR and SO_2 is causing additional headaches, and taking the high

cost of ethanol into account, we have decided to cease working on ethanol-SCR.

Chapter 5

Propene-SCR over Ag/Al_2O_3

5.1 Ag loading optimisation

Figures 5.1 and 5.2 show the NO and propene conversion, respectively, of 1-4 wt.% Ag as functions of temperature. 1 wt.% reaches maximum NO conversion at around 550 °C of a meagre 18 %, because propene is insufficiently activated. 2 wt.% converts propene to a much bigger extent, e.g. 64 and 100 % at 500 and 550 °C, respectively. This results in max. NO conversions of around 80 % at 525 to 550 °C and 74 % at 500 °C. This translates to first-order rate constants of around 67 $cm^3\ s^{-1}\ g^{-1}$ at 500 °C and 80 $cm^3\ s^{-1}\ g^{-1}$ at 525 - 550 °C, which is about one order of magnitude lower than the activity of NH_3-SCR at 400 °C using the industrial VWT catalyst. Up to 525 °C it is unlikely that the same NO conversions could have been obtained at a lower space velocity, since the propene conversion was safely below 100 %. Increasing the silver loading to 3 wt.% does not enhance the NO conversion, not even at the lower end of the temperature range. However, the propene conversion increases, e.g. 88 % conversion are reached at 500 instead of 525 °C. Despite these results, we have opted to use 3 wt.% Ag/Al_2O_3 for the poisoning study, because of its potentially higher SO_2 tolerance and to ensure better comparability with the results of ethanol-SCR. Silver loading of 4 wt.% exhibits maximum NO conversion of only 61 % at 500 °C. Unselective oxidation of propene is, unsurprisingly, a bigger problem at higher silver loadings. The selectivity towards CO_2 is increasing with increasing silver loadings as was already observed with ethanol-SCR, see figure 4.3 in section 4.2.

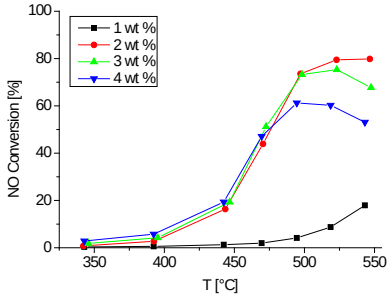

Figure 5.1: NO conversion over Ag/Al_2O_3 with varying Ag loadings. W/F = 0.02 g s cm^{-3}.

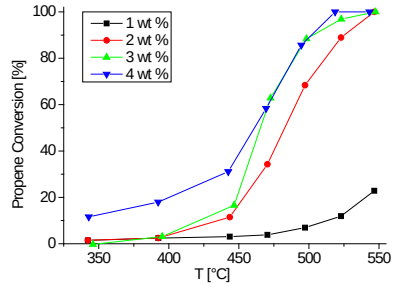

Figure 5.2: Propene conversion over Ag/Al_2O_3 with varying Ag loadings. W/F = 0.02 g s cm^{-3}.

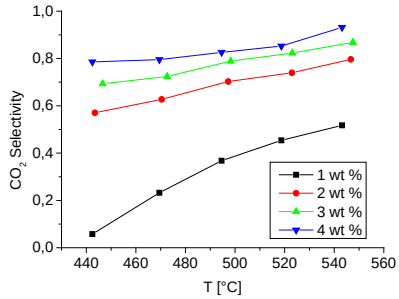

Figure 5.3: S_{CO_2} over Ag/Al_2O_3 with varying Ag loadings. W/F = 0.02 g s cm^{-3}.

5.2 Poisoning with alkali & alkali earth metals

Figures 5.4 and 5.5 show the NO and propene conversion of 3 wt.% Ag/Al_2O_3 doped with different alkali and alkali earth metals at a one-to-one molar ratio corresponding to concentrations of 278 µmol g^{-1}. The degree of poisoning correlates with the basicity of the dopant just as ascertained for NH_3-SCR over $V_2O_5-TiO_2$ by Chen at al. [39]. Lithium, the metal with the lowest basicity, promotes the NO conversion slightly at temperatures above 500 °C, while not increasing the propene conversion. The metals which are most detrimental to the NO conversion, sodium, caesium and, most importantly, potassium, do not cause a significant reduction in propene conversion. This leads to high ratios of consumed propene to converted NO, see figure 5.6, and is ultimately limiting the maximum attainable NO conversion. Note that, even in the case of undoped Ag and Li doped Ag, about 2 moles of propene are consumed per mole of reduced NO, making the cost of propene-SCR as listed in table 3.4 an underestimate. The selectivity towards CO_2 is enhanced by the dopants, see figure 5.7, as was already observed for potassium doped catalysts in ethanol-SCR, see section 4.4.

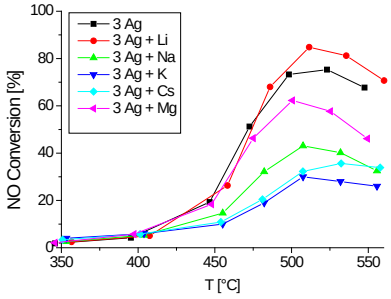

Figure 5.4: NO conversion over 3 wt.% Ag/Al_2O_3 doped with different metals at metal/Ag = 1 loadings. W/F = 0.02 g s cm^{-3}.

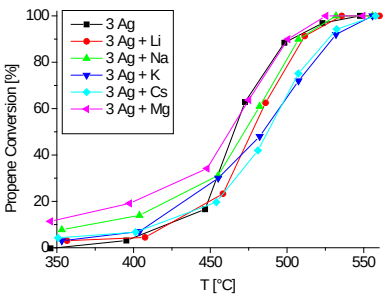

Figure 5.5: Propene conversion over 3 wt.% Ag/Al_2O_3 doped with different metals at metal/Ag = 1 loadings. W/F = 0.02 g s cm^{-3}.

In the next step, the effect of different potassium loadings was investigated, see figure 5.8. The poisoning effects of sodium, potassium and caesium extend all the way to 556 µmol g^{-1}. It turns out that propene-SCR over 3 wt.% Ag/Al_2O_3 at its optimum temperature is as much affected as ethanol-SCR using the same catalyst, see figure 5.9, and offers only a marginal advantage over NH_3-SCR on a relative basis. Considering the vastly different activities at zero potassium

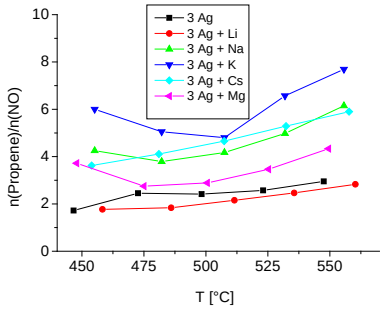

Figure 5.6: Moles of propene converted per mole of NO reduced over 3 wt.% Ag/Al_2O_3 doped with different metals at metal/Ag = 1 loadings. W/F = 0.02 g s cm^{-3}.

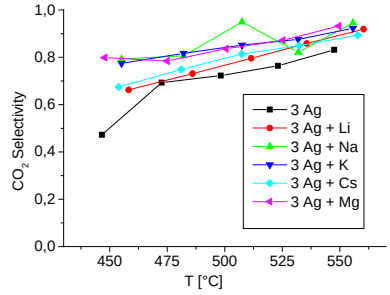

Figure 5.7: $S_{CO_2}(T)$ over 3 wt.% Ag/Al_2O_3 doped with different metals at metal/Ag = 1 loadings. W/F = 0.02 g s cm^{-3}.

loading, this is of academic interest at most.

Since doping 3 wt.% Ag/Al_2O_3 with Li had a slighlty promotional effect without increasing the propene conversion one possible strategy to improve the potassium tolerance could be to dope the catalyst with lithium. Due to its chemical similarity to potassium, it might bind to the same sites and thus make them unavailable to potassium. First, 3 wt.% Ag/Al_2O_3 was doped with Li at a Li/Ag ratio of one (278 µmol g^{-1}) followed by poisoning with potassium at different concentrations. Figure 5.10 shows that this side-blocking strategy is only effective at comparatively low potassium loadings of up to 139 µmol g^{-1}. At higher potassium loadings, lithium has no effect at all on the NO conversion.

5.3 TiO_2-Al_2O_3 support

Alumina-titania mixed oxides with varying Ti contents were prepared, because they might be more SO_2 tolerant as reported in [85] and due to their high surface areas also more potassium resistant. Figure 5.11 shows the BET surface areas as determined by N_2 physisorption measurements. We decided to proceed with an Al/Ti ratio of 19, corresponding to 5 mol % Ti, because it has the highest surface area. Figures 5.12 and 5.13 show the NO and propene conversions over the mixed oxide loaded with 3, 4.5 and 6 wt.% Ag. The sample loaded with 3 wt.% reaches maximum NO conversion of about 75 % at 500 to 525 °C, which is close to the value of 3 wt.% Ag/Al_2O_3, see figure 5.1. The NO conversion

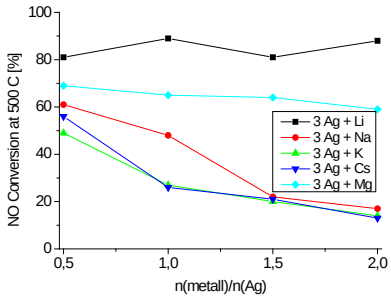

Figure 5.8: NO conversion over 3 wt.% Ag/Al_2O_3 doped with different metals at various metal/Ag loadings at 500 °C. W/F = 0.02 g s cm^{-3}.

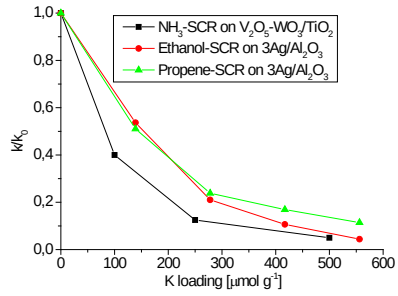

Figure 5.9: Relative activities of NH_3-SCR and ethanol-SCR at 400 °C and propene-SCR at 500 °C as functions of the K loading.

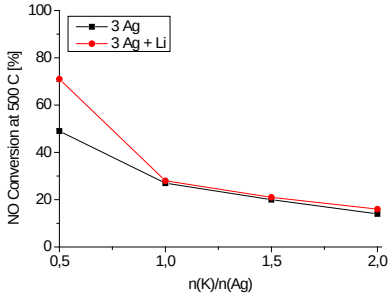

Figure 5.10: NO conversion over 3 wt.% Ag/Al_2O_3 doped with Li/Ag = 1 and different K loadings at 500 °C. W/F = 0.02 g s cm^{-3}.

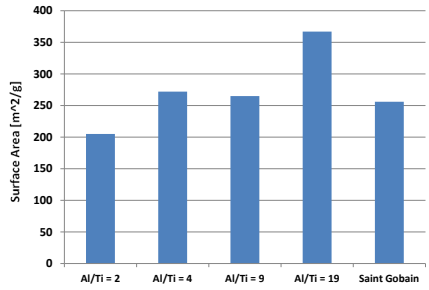

Figure 5.11: BET surface areas of Al-Ti mixed oxides as a function of elemental composition.

over the mixed oxide supported catalysts is much less sensitive to the Ag loading than when using pure Al_2O_3 as support. The higher surface area of the mixed oxide alone cannot account for the lowered sensitivity. The Ag concentrations on 3 wt.% Ag/Al_2O_3 and the 4.3 wt.% loaded mixed oxide are identical (1.09 µmol g^{-1}) and the ones of 4 wt.% Ag/Al_2O_3 (1.48 µmol g^{-1}) and 6 wt.% loaded mixed oxide (1.51 µmol g^{-1}) are very close to each other. Yet, in the case of the alumina supported catalyst this increase in Ag loading is accompanied by a decrease of the maximum NO conversion from 74 to 60 %, whereas the activity of the mixed oxide based catalyst is unaffected. The incorporation of Ti into the support might stifle the formation of big Ag clusters that favour the unselective oxidation of propene.

3 wt.% $Ag/(Al_2O_3{-}TiO_2)$ (Al/Ti =19) was loaded with various amounts of potassium, see figures 5.14 and 5.15. The deactivation is relatively mild compared to the 3 wt.% Ag/Al_2O_3 case, see figures 5.4 and 5.8. Noteworthy is the fact that there is no turning point in the NO conversion temperature profiles of the two catalysts with the higher K loadings of 278 and 417 µmol g^{-1}. At 550 °C they are almost as active as the unpoisoned catalyst. The fact that the potassium concentration on a per area basis is lower in the mixed oxide case cannot explain the increased potassium tolerance. The loading of 417 µmol g^{-1} in the mixed oxide case corresponds to 1.136 µmol m^{-2}, very close to the value of (K/Ag) = 1 in the case of pure alumina support (1.086 µmol m^{-2}). Yet the conversions differ vastly at 550 °C, being 53% in the mixed oxide case versus less than 30 % in the 3 wt.% Ag/Al_2O_3 case.

Last, the effect of 278 µmol g^{-1} potassium on 3 wt.% Ag/Al_2O_3, 3 and 6 wt.% $Ag/(TiO_2{-}Al_2O_3)$(Al/Ti = 19) was compared as shown by figures 5.16 and 5.17. The mixed oxide based catalysts were more potassium tolerant; however, especially at temperatures above 500 °C, the one loaded with 6 wt.% Ag was almost as much affected as 3 wt.% Ag/Al_2O_3. So the relatively high activity of potassium poisoned 3 wt.% loaded mixed oxide might not only stem from a relatively low potassium concentration per unit of surface area but also from a lower Ag loading on a surface area basis. It is imaginable that a charge transfer from potassium to ${Ag_n}^{\delta+}$ clusters occurs, reducing the charge of the latter und thus making them more metal like. In this regard, potassium would have a similar effect as increasing the Ag loading beyond the optimum level. This could explain the fact that the drastically reduced NO conversion upon potassium poisoning is not matched by a similar drop in propene (or ethanol) conversion. The fact that both doping with potassium and other alkali metals (figure 5.7) and increasing silver loadings (figure 5.3) lead to increased S_{CO_2} is lending support to this theory. Unfortunately, we could not investigate the oxidation state of the silver

species because the machine used for conducting H_2-TPR experiments was not operational at the time of this study and we were not able to run UV-vis spectra on the specimens.

Avgouropoulos et al. [99] have reported a promotional effect of sodium and potassium on the complete oxidation of ethanol over Pt/Al_2O_3. The authors explained the activity increase by a reduced amount of surface adsorbed acetic acid. This could either come from a suppression of the oxidation of acetaldehyde to acetic acid, or from a faster oxidation of acetic acid after its formation. The latter could explain why K doped Ag/Al_2O_3 converts as much hydrocarbons as undoped Ag/Al_2O_3 but much less NO to N_2.

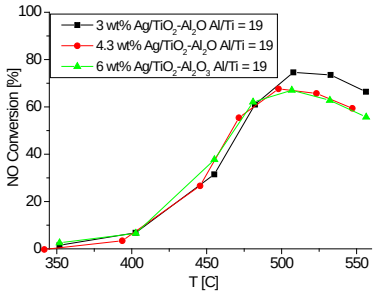

Figure 5.12: NO conversion over $Ag/(Al_2O_3{-}TiO_2)$ (Al/Ti =19) with varying Ag loadings. W/F = 0.02 g s cm^{-3}.

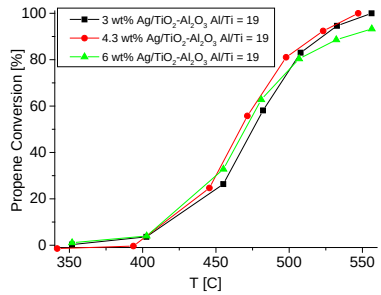

Figure 5.13: Propene conversion over $Ag/(Al_2O_3{-}TiO_2)$ (Al/Ti =19) with varying Ag loadings. W/F = 0.02 g s cm^{-3}.

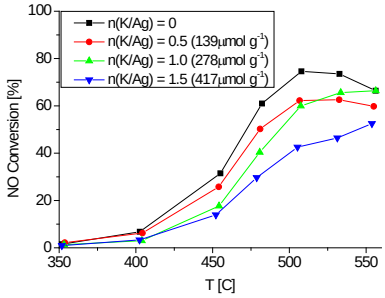

Figure 5.14: NO conversion over 3 wt.% $Ag/(Al_2O_3{-}TiO_2)$ (Al/Ti =19) with varying K loadings. W/F = 0.02 g s cm^{-3}.

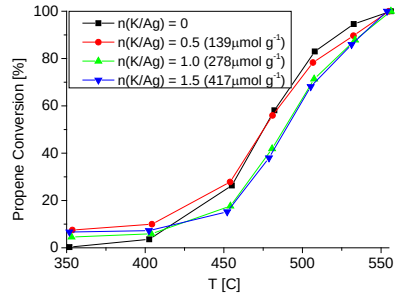

Figure 5.15: Propene conversion over 3 wt.% $Ag/(Al_2O_3{-}TiO_2)$ (Al/Ti =19) with varying K loadings. W/F = 0.02 g s cm^{-3}.

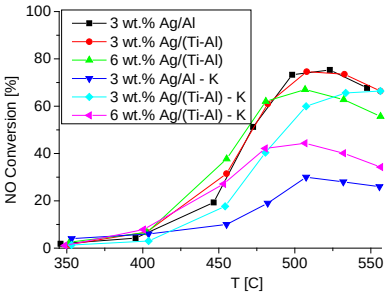

Figure 5.16: NO conversion over various catalysts doped with 279 µmol g^{-1} K. W/F = 0.02 g s cm^{-3}.

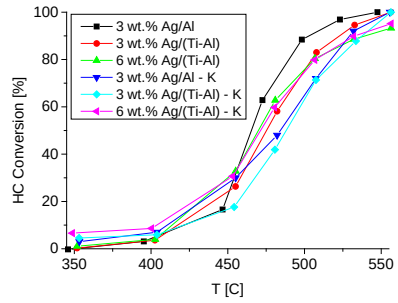

Figure 5.17: Propene conversion over various catalysts doped with 279 µmol g^{-1} K. W/F = 0.02 g s cm^{-3}.

5.4 Conclusion: Propene-SCR over Ag/Al_2O_3

Propene-SCR over Ag/Al_2O_3, in the absence of potassium, SO_2 and H_2 exhibits maximum activities which are about one order of magnitude lower than those of NH_3-SCR over the industrial VWT catalyst. Potassium poisoning is as severe as in the case of ethanol-SCR over Ag/Al_2O_3 and only marginally milder than in the NH_3-SCR case. Potassium poisoning is accomponied by unselective oxidation of propene, reducing the maximum attainable NO conversion drastically. Doping the alumina support with 5 mol.% Ti considerably reduces the potassium poisoning, especially at temperatures above 500 °C, and is potentially enhancing the SO_2 tolerance. In the absence of H_2 the SCR temperature window would have to be between 450 and 550 °C and would therefore require retrofitting at existing plants. Whether H_2 at economically justifiable levels could expand the temperature window is questionable.

Since the high cost of propene and strong SO_2 poisoning cause additional problems, we decided to stop working on propene-SCR. Instead, we have started to work on low temperature NH_3-SCR.

Chapter 6

Low-temperature NH_3-SCR

6.1 Motivation & foreword

Placing the SCR unit at the tail-end position has several advantages and can also help to solve the alkali poisoning problem experienced when firing biomass. Wieck et al. [42] have reported that deactivation of the SCR catalyst during biomass co-firing is much slower at the low-dust position than it is at the high-dust position. This is probably due to the ESP filtering out much of the potassium particles. One can expect that the desulphurization unit will further reduce the potassium content. Tail-end placement of the SCR unit is commonly used in waste incineration units due to the very challenging flue gas, see section 2.5. Over the last two years we have collaborated with an engineering company from the flue gas cleaning sector with the aim to develop a catalyst that can be used at 140 °C, the typical exit temperature of dry FGD units. The work culminated in a patent application, due to which most of the results need to be presented in a disguised form. The interested reader can look forward to up to 4 publications in peer-reviewed journals.

6.2 Introduction

The potential benefits of low temperature SCR have sparked research activity over the past decade. The subject was reviewed several times, see e.g. [100–102]. Currently, the most active industrially used solution is probably the so-called "Shell DENOX System" (SDS) [102, 103], which consists of a V/Ti type catalyst and a lateral flow reactor (LFR). The LFR is essentially made up of numerous shallow slabs of catalysts. The design ensures a low pressure drop (2 - 50 mbar) and ease of catalyst loading and unloading. The SDS has been installed at a

number of plants, including refinery heaters, ethylene crackers, nitric acid plants, catalyst factories and waste incineration units [97].

Furthermore, a number of transition metals like Fe, V, Cr, Cu, Co and Mn as well as some rare earth metals (Ce, La) have been intensively studied [100, 101] and references therein. Broadly speaking, there are four types of LT-SCR catalysts: single metal oxides, mixed metal oxides, supported metal oxides and zeolite based catalysts. As in the case of HC-SCR, the major poisons/inhibitors are SO_2 and H_2O. Water mostly acts as an inhibitor, though it can in some cases also reduce the activity irreversibly. All catalysts can be affected reversibly by ammonium sulfate salt formation. Fe and Cu based catalysts stand out in that they are much less irreversibly poisoned by SO_2 than most other transition metals are, attested by the fact that zeolite based catalysts are on the verge of commercialization in mobile applications.

This chapter will shortly introduce the four types of catalysts, followed by the effects of SO_2 and H_2O.

6.3 Single metal oxides

The most prominent single oxide for low temperature NH_3-SCR is probably MnOx [101, 104–107]. Chen et al. [106] compared MnOx and FeOx prepared by the citric acid method (dissolution of the metal precursor in water with an equivalent molar amount of citric acid followed by drying and calcination). FeOx converted less than 15 % between 80 and 220 °C (Conditions: [NO] = [NH_3] = 1000 ppm; [O_2] = 3 % ; SV = 30000 h^{-1}). MnOx, on the other hand, converted 43 %, 53 % and 85 % of NO at 80, 100 and 120 °C, respectively, and kept above 95 % conversion up to 220 °C. Chen et al. [105] compared the activities of MnOx and CrOx which had been prepared by the citric acid method. (Conditions: [NO] = [NH_3] = 1000 ppm; [O_2] = 3 %; SV = 30000 h^{-1}). MnOx converted more than 80 % NO at temperatures above 120 °C. CrOx, on the other hand, converted less than 50 % NO at temperatures of up to 180 °C and only reached 70 % conversion at 200 °C.

Some authors have explained the superior activity of MnOx by its ability to convert NO to NO_2. Hua et al [107], who compared the activities of unsupported MnOx and CeOx, which had been prepared by a precipitation method and calcined at 400 °C, measured NO to NO_2 conversions at 150 °C (Conditions: [NO] = 500 ppm; [O_2] = 3 %; W/F = 0.06 g s cm^{-3}) of 55 % and 7 %, respectively. Li et al [104] who compared the activities of unsupported MnOx, CoOx, CeOx and LaOx, which were prepared by a precipitation method and calcined at 400

°C, measured NO to NO_2 conversions at 150 °C (Conditions: [NO] = 500 ppm; $[O_2]$ = 3 %; W/F = 0.045 g s cm^{-3}) of 50 %, 43 %, 8 % and 6 %, respectively. Qi et al [108] compared the oxidizing ability of MnOx and CeOx prepared by the citric acid method (Conditions: [NO] = 1000 ppm; $[O_2]$ = 2 %; W/F = 0.002 g s cm^{-3}). At 150 °C, MnOx converted 7 % NO to NO_2, whereas CeOx hardly converted about 2 %.

The activity of MnOx depends strongly on its composition (oxidation state), crystallinity and preparation method. The following manganese oxides are known: MnO, Mn_3O_4, Mn_2O_3, MnO_2, Mn_5O_8 and Mn_2O_7. Several authors have reported that MnO_2 is the most active phase [109–112]. Singoredjo et al. [113], on the other hand, have reported that Mn_2O_3 is more active than MnO_2, at least when supported on Al_2O_3. Kapteijn et al. [111] came up with the following order of activity for unsupported MnOx: $MnO_2 > Mn_5O_8 > Mn_2O_3 > Mn_3O_4$. However, in terms of N_2 selectivity, MnO_2 performs worse. According to the same study, the order of the N_2 selectivity is: $Mn_2O_3 > MnO_2 \approx Mn_5O_8 > Mn_3O_4$. All oxides have in common that the N_2 selectivity decreases with increasing temperature. Tang et al [114] compared the SCR activities and N_2O formation over α Mn_2O_3 and β MnO_2 (Conditions: [NO] = $[NH_3]$ = 680 ppm; $[O_2]$ = 3 %; T = 150 °C; W/F = 0.04 g s cm^{-1}). NO conversions of 43.6 and 86.1 % and N_2O selectivities of 8.8 and 30.0 % were reported for α Mn_2O_3 and β MnO_2, respectively. H_2-TPR showed that the Mn-O bonds in β MnO_2 are weaker than in α Mn_2O_3. Therefore, β MnO_2 can more easily cleave N-H bonds of the adsorbed NH_3, which in turn can form both N_2 via adsorbed NHx and N_2O via adsorbed N. The strong formation of N_2O, which is a very potent greenhouse gas, is of concern. However, it is well known that the N_2O formation is dampened in the presence of water [25]. Since the water content at the tail-end positon is between 15 and 20 %, we were not too concerned about N_2O and thus did not measure it during the screening stage.

Tang et al. [115] studied the influence of different methods of preparation on the crystallinity and activity. They used rheological phase reaction (RP), low temperature solid phase reaction (SP), co-precipitation (CP) and the citric acid method (CA). Use of the citric acid method yielded mostly crystalline Mn_2O_3, which was significantly less active in the reduction of NO compared to the mostly amorphous substances afforded by the other methods of preparation. Also Kang et al. [112], who prepared MnOx with a precipitation method using different bases, reported that the less crystalline catalysts showed higher SCR activity. Hua et al. [116] synthesised hollandite MnO_2 (HMO), starting from $MnSO_4 \cdot H_2O$ and $(NH_4)_2S_2O_8$, using a refluxing route. Treating the same starting materials hydrothermally yielded β MnO_2. In the absence of H_2O, HMO converted more than 90 % NO in the temperature range of 100 to 300 °C (Conditions: [NO] =

$[NH_3]$ = 500 ppm; $[O_2]$ = 3 %; W/F = 0.03 g s cm^{-3}) . β MnO_2, on the other hand, only converted 10, 20 and 70 % NO at 100, 150 and 200 °C, respectively. In the presence of 10 % H_2O, HMO exhibited NO conversions of 10, 40 and 70 % at 100, 150 and 200 °C, whereas β MnO_2 only converted about 5, 8 and 10 % NO at those temperatures. The high activity of hollandite catalysts was ascribed to the relatively high surface area (70.6 vs. 14.4 m^2 g^{-1}), good NH_3 adsorption ability as well as a high electronegativity of the lattice oxygen in hollandite, which should favour the cleavage of N-H bonds in adsorbed NH_3, thus accelerating the SCR process [117]. The different responses of the two catalysts to water will be discussed in more detail in section 6.7.

6.4 Mixed metal oxides

Most mixed oxides reported to be SCR active contain Mn. This is probably because MnOx on its own is probably the most active single oxide, see section 6.3. Qi et al. [108] prepared highly active MnOx - CeOx mixed oxides by using three different methods, namely impregnation, co-precipitaton and the citric acid method. The most active catalyst contains 30 mol % Mn and is prepared by the citric acid method and calcined at 650 °C. It converts 54, 75 and 87 % at 100, 120 and 150 °C, respectively (Conditions: [NO] = $[NH_3]$ = 1000 ppm; $[O_2]$ = 2 %; W/F = 0.06 g s cm^{-3}). Since the reaction is first-order with respect to NO and zero order with respect to NH_3, first-order rate constants of 40.5, 76.2 and 120.7 cm^3 s^{-1} g^{-1} could be reported for the above-mentioned temperatures. The activity at 150 °C is about as high as the activity of the industrial VWT catalyst when measured at 250 - 270 °C [25]. However, in the presence of H_2O and SO_2, the rosy picture deteriorates, see sections 6.7 and 6.8. The authors explained the high activity of the mixed oxide with an increased rate of NO to NO_2 oxidation as compared to the single oxides. Casapu et al. [118] investigated the effect of doping MnCeOx with Nb, W, Zr and Fe (molar ratio of Mn:Dopant:Ce = 23:23:54). Between 150 and 200 °C, only Nb promoted the deNOx activity slightly and drastically reduced the N_2O formation. The activities of MnCe and MnNbCe at 150 °C and in the presence of 5 % H_2O roughly matched the one of a VWT reference catalyst at 200 °C. Along the way, the authors also reported MnCe and MnNbCe to be highly sensitive to SO_2, see section 6.8. Chang et al. [119] doped Mn(0.4)Ce with 10 molar % Sn and reported a slight promotional effect in the absence of H_2O and SO_2, which was explained by an increased number of surface acid sites, reducibility of MnOx at lower temperatures, an increase in surface area and loss of crystallinity. The Sn doped catalyst vastly outperforms the undoped one at 110 °C in the presence of 12 % H_2O and 100 ppm SO_2 (65 vs 20 % NO conversion), see also section 6.8. Li et al. [104] boosted the NO to NO_2 oxidation at 150 °C from 50 % (MnOx) to 80 % by adding Ce and Co.

Chen et al. [106] prepared MnFeOx by co-precipitation, solid reaction and the citric acid method, with the last mentioned method yielding the most active catalysts. The most active catalyst, Fe(0.4)MnOx, converts 90 and 95 % NO at 80 and 100 °C, respectively, and above 95 % up to 220 °C (Conditions:[NO] = 1000 ppm; $[O_2]$ = 3 %; W/F = 0.1884 g s cm^{-3}). MnOx only converted about 42, 65 and 90 % at 80, 100 and 120 °C, respectively. The higher activity of the mixed oxide was explained by an increase in surface area (54.9 vs.22.9 m^2 g^{-1}), the partial formation of a $Fe_3Mn_3O_8$ phase alongside MnOx and reducibility of Mn at lower temperatures. Doping with iron also increases the rate of NO to NO_2 transformation. The $Fe_3Mn_3O_8$ phase was claimed to be relatively SO_2 tolerant.

The effect of doping MnOx with Cr [105] was investigated by Chen et al. by using the citric acid route for preparation. Cr(0.4)MnOx converts 46, 78 and 98 % NO at 80, 100 and 120 °C, respectively, and above 95 % at up to 220 °C (Conditions:[NO] = 1000 ppm; $[O_2]$ = 3 %; W/F = 0.2233 g s cm^{-3}). MnOx only converts about 35, 55 and 80 % at 80, 100 and 120 °C, respectively. The enhanced activity of the mixed oxide compared to MnOx was ascribed to an increase in surface area, reducibility of MnOx at lower temperatures and an increased rate of NO to NO_2 transformation.

Kang et al. [120] investigated the effect of Cu doping using a co-precipitation technique. They succeeded in extending the temperature window of near-full conversion of NO to above 200 °C. Since the activity testing was done at too low a space velocity, no conclusion concerning the effect of Cu on the activity at temperatures below 200 °C could be drawn. Amorphous MnOx phases were reported to be present in Cu doped catalysts as evidenced by XRD.

6.5 Supported single metal oxides

According to Li et al. [101], the major role of the support is to provide a huge surface area and to prevent formation of big crystalline particles. Since MnOx is probably the most active single oxide and most of the highly active mixed oxides contain Mn, supported formulations containing this metal were extensively studied. Several support materials have been tested, with TiO_2 probably being the most investigated and active one as reported by Smirniotis et al. [121], who compared several TiO_2 materials with SiO_2 and γ-Al_2O_3. It is noteworthy that they reported 20 wt.% Mn/(rutile) to be as active as 20 wt.% Mn/(anatase) at 100 and 120 °C.

Up to now, most Mn/(TiO_2) catalysts have been prepared by using the impregna-

tion technique [101,123]. Li et al. [122] studied the effects of Mn precursors with 20 wt.% manganese loading. At temperatures of up to 200 °C, the Mn-acetate derived catalyst was more active than the Mn-nitrate based one, e.g. at 100 and 150 °C the former converted 70 and almost 100 % NO, whereas the latter only converted 30 and 85 % (Conditions:[NO] = [NH_3] = 1000 ppm; [O_2] = 3 %; W/F = 0.1 g s cm^{-3}). Interestingly, the more active catalyst possesses a lower surface area (42.42 m^2 g^{-1}) than the nitrate derived one (69.82 m^2 g^{-1}). The XRD pattern of the nitrate based catalyst shows MnO_2 reflections. The acetate based catalyst, on the other hand, shows very weak Mn_2O_3 reflections, implying that most of the MnOx is in an amorphous state. The lack of a clear step in the TG curve lends support to this assumption. XPS analysis confirmed that the acetate based catalyst contains mostly Mn^{+3} species whereas the nitrate based one contains Mn^{+4} and some un-decomposed manganese nitrate. Furthermore, XPS has revealed that the Mn/Ti ratio on the surface is much higher in the acetate case, suggesting that the MnOx phase is more dispersed. Pena et al. [109] have reported that nitrate based 5 wt.% Mn/TiO_2 is more active than the acetate based one. The contradiction with the results of the Li group [122] can probably be explained by the different Mn loadings. The higher dispersion of Mn that comes along with the use of the acetate precursor as evidenced by XPS is probably more beneficial at high Mn loadings. Smirniotis et al. [121] observed mostly amorphous MnOx by XRD in their nitrate derived 20 wt.% Mn/(TiO_2) but confirmed the presence of MnO_2 by XPS. Qi et al. [124] reported the appearance of Mn_2O_3 reflections in the XRD patterns of acetate derived Mn/(TiO_2) at Mn loadings of 20 wt.% and above. According to their study, loading increases beyond 10 wt.% Mn do neither increase nor decrease the NO conversions at temperatures between 80 and 180 °C; however, the N_2O formation increases.

Some authors claim that the activity of MnOx/TiO_2 can be enhanced by using the sol-gel method of preparation [123,126,127]. Wu et al. [123,125] reported that the activity at 150 °C of sol-gel prepared and Mn-nitrate derived Mn/TiO_2 peaked at a molar Mn/Ti ratio of 0.4, a much higher value than the 10 wt.% Mn reported in an earlier study using the impregnation method [124]. XRD patterns of the sol-gel prepared catalysts show strongly reduced anatase reflections indicating that TiO_2 and MnOx strongly interact. Reflections due to MnO_2 appear starting from Mn/Ti molar ratios of 0.4, the value of maximum NO conversion. The orders of reaction with respect to [NO] and [NH_3] were determined to be one and zero, respectively, allowing for the calculation of first-order rate constants. At 150 °C and in the absence of H_2O a rate constant of 116 cm^3 g^{-1} s^{-1} was determined for the optimum catalyst, which is very close to the value measured for Mn−CeOx prepared by the citric acid method [108]. The apparent activation energy was reported to be 38 kJ/mol. Jiang et al. [126] reported the Mn/Ti

ratio of 0.4 to be the optimum one for sol-gel, impregnation and co-precipitation prepared catalysts with the sol-gel prepared one being only slightly more active than the impregnated one. For the sol-gel sample, XPS revealed a higher Mn concentration on the surface and XRD strong Mn-TiO_2 interactions as well as a lack of crystalline MnOx. Kim et al. [127] reported drastic differences in activity between impregnation and sol-gel derived samples. At 150 °C, the optimum sol-gel sample (30 wt.% Mn/TiO_2) converts about 53.5 % NO whereas the optimum impregnation sample (13 wt.% Mn/TiO_2) only converts about 10 % of NO (Conditions: [NO] = [NH_3] = 500 ppm; [O_2] = 5 %; [H_2O] = 10 %; SV = 100,000 h^{-1}). The explanations for the higher activity are the same as given in the other studies [123, 126] (strong Mn−TiO_2 interactions, absence of crystalline MnOx), but also include increased surface area. Our own results [128] comparing $Mn_{0.6}Fe_{0.4}/TiO_2$ (metal/Ti = 0.62) did not show much of a difference between sol-gel and impregnation, both in terms of activity and surface properties like NH_3-TPD profile and surface area as well as similar XRD patterns.

Also Al_2O_3 can be used as support for MnOx [113, 121], albeit resulting in activities and N_2 selectivities that are reported to be lower than when using TiO_2 [121]. Mn(acetate) results in higher activities and lower N_2 yields than Mn(nitrate) [113].

6.6 Supported mixed metal oxides

Supported MnOx catalysts can be greatly enhanced by doping with another transition- or rare-earth metal just like in the case of unsupported MnOx, see section 6.4. The dopant usually causes the MnOx to be in an amorphous state and increases the rate of oxidation of NO to NO_2.

Wu et al. [125] have studied the effect of doping different transition metals (Fe, Cu, Ni, Cr) (M/Ti = 0.1) to sol-gel prepared, Mn-nitrate based MnOx/TiO_2 (Mn/Ti = 0.4 or 0.6). Each dopant has a promotional effect at both Mn/Ti ratios. The temperatures needed to achieve 90 % NO conversion were lowered from 420 K in the undoped Mn/Ti = 0.4 case to 360, 385, 370 and 390 K by doping with Fe, Cu, Ni and Cr, respectively (Conditions: [NO] = [NH_3] = 1000 ppm; [O_2] = 3 %; [H_2O] = 10 %; F = 2000 cm^3 min^{-1}, V_{cat} = 4 mL). In the Mn/Ti = 0.6 case the temperature at 90 % NO conversion was lowered from 450 K to about 370, 415, 380 and 415 K by doping with Fe, Cu, Ni and Cr, respectively. This study suggests that the most promising dopant is iron. The promotional effect of all the transitional metals was ascribed to the suppression of crystalline MnO_2. Fe seems to be most effective at this because the XRD pattern of Fe(0.1)Mn(0.4)/TiO_2 does not show any reflections assignable to any

crystalline MnOx species. Doping of $Mn(0.4)/TiO_2$ with Fe also boosts the surface area from 75.3 to 112.6 $m^2\ g^{-1}$. Also Kim et al. [127] reported an enhancing effect of Fe. Doping sol-gel prepared 22 wt.% Mn/TiO_2 with 11 wt.% Fe increased the NO conversion at 150 °C from about 43 to 60 % (Conditions: [NO] = [NH_3] = 500 ppm; [O_2] = 5 %; [H_2O] = 10 %; SV = 100,000 h^{-1}). Fe also promoted 13 wt.% Mn/TiO_2 prepared by impregnation, albeit not so strongly. Qi et al. [124] doped Mn-acetate derived 10 wt.% Mn/TiO_2 prepared by impregnation with 5, 10 and 15 wt.% Fe and reported the strongest activity enhancement when using 10 wt.% Fe. The undoped catalyst needs to be tested at 180 °C to reach NO conversions of above 90 %; this conversion is already attained at 120 °C by the 10 wt.% Fe - 10 wt.% Mn/TiO_2 catalyst (Conditions: [NO] = [NH_3] = 1000 ppm; [O_2] = 2 %; W/F = 0.15 g s cm^{-3}). Fe suppressed the formation of crystalline Mn_2O_3; however, it did not increase the surface area. Furthermore, Fe was reported to reduce the N_2O formation.

Ni is another promising dopant for $MnOx/TiO_2$ [110, 125, 129], second only to Fe, according to the comparative study of Wu et al. [125]. Thirupathi et al. [110] doped Mn-nitrate based 5 wt.% Mn/TiO_2 with different Ni/Mn loadings using impregnation. The optimum catalyst loaded with an Ni/Mn = 0.4 ratio is not only more active than the parent Mn/TiO_2 but also possesses a markedly improved thermal stability. After 6h of operation at 200 °C (Conditions: [NO] = [NH_3] = 400 ppm; [O_2] = 2 %; W/F = 0.04286 g s cm^{-3}) the optimum Ni doped catalyst maintained its initial (1h of operation) NO conversion of more than 98 %. The un-doped catalyst, on the other hand, witnessed a decrease in NO conversion from 87.5 % to about 73 %. Presence of Ni also increased the N_2 selectivity from about 66 to nearly 100 %. The authors explained the higher activity by an improved reducibility of MnOx and a higher concentration of Mn^{+4}, as evidenced by XPS. No crystalline MnOx was detected by XRD, explaining the high N_2 selectivity. NH_3-TPD revealed an increased number of Lewis acid sites upon Ni doping.

Because of the good performance of unsupported MnOx - CeOx [108, 118] an obvious choice is to dope Mn/TiO_2 with Ce. Unfortunately, at the time of the experimentation we partially overlooked the promising reports on $MnCe/TiO_2$ [130–135] and $MnCe/Al_2O_3$ [135]. In supported formulations Ce is present at much lower concentrations than in unsupported $Mn_{0.3}Ce_{0.7}$, making the former more economically viable. Wu et al. [133] doped their optimum, sol-gel prepared catalyst [123] (Mn/Ti = 0.4) and found the activity maximum at a Ce/Ti ratio of 0.07 corresponding to a stochiometry of $Mn_{0.851}Ce_{0.149}$. Zhongyi et al. [131] prepared $MnCe/TiO_2$ (Mn/Ti = 0.4) with a co-precipitation procedure and reported an optimum Ce/Ti ratio of 0.075, corresponding to a stochiometry of

$Mn_{0.842}Ce_{0.158}$. In the study of Wu et al. [133], the addition of Ce reduces the temperature needed to attain 90 % NO conversion from 140 to 90 °C (Conditions: [NO] = [NH_3] = 1000 ppm; [O_2] = 3 %; [H_2O] = 3 %; SV = 40,000 h^{-1}) . In the study of Zhongyi et al. [131], the best Ce containing catalyst reached 90 % at about 110 °C. The undoped MnOx/TiO_2 only converted about 70 % NO at 180 °C (Conditions: [NO] = [NH_3] = 600 ppm; [O_2] = 3 %; [H_2O] = 3 %; SV = 40,000 h^{-1}). Boxiong et al. [134] doped 8 wt.% Mn/TiO_2−PILC (pillared interlayed clay) with Ce and found the optimum at 2 wt.%. The activity enhancement was only moderate, e.g. at 160 °C the NO conversion increased from about 40 to 55 %. Most studies [133, 134] relate the promotional effect of Ce to the creation of Lewis acid sites, enhanced reducibility of Mn, an increased amount of chemisorbed oxygen as evidenced by XPS results and the suppression of crystalline MnOx phases. Wu et al. [133] also reported an increase in surface area. Another paper by Boxiong et al. [136] compared the activities of sol-gel prepared $Fe_{0.33}Mn_{0.67}/TiO_2$, $Mn_{0.4}Ce_{0.6}/TiO_2$, and $Fe_{0.167}Mn_{0.33}Ce_{0.5}/TiO_2$, all having a Mn/Ti ratio of 0.2, and measured NO conversions at 140 °C of about 60, 70 and 82 %, respectively (Conditions: [NO] = [NH_3] = 600 ppm; [O_2] = 3 %; SV = 50,000 h^{-1}). Fe doping has apparently only a moderate promotional effect, which was explained by an increase in both surface area and NH_3 adsorption capacity as well as an increase in dispersion of Mn and Ce and an increase in chemisorbed O_2 which might be responsible for the increased NO to NO_2 transformation. The reader should note that the Fe/Ti ratio had been optimised in the range of 0.05 to 0.2. However, both the Mn/Ti ratio and the Ce/Mn ratio are far from the optimal values of 0.4 [123, 125] and about 0.175 [131], respectively. The Ce/Mn ratio is more akin to the optimal one in the unsupported $Mn_{0.3}Ce_{0.7}$ [108, 118]. Therefore, it is hard to say if Fe doping could not have a more pronounced effect on MnCe/TiO_2 or maybe also on unsupported MnCeOx. Fe doping of the latter was tested by us, yet without bearing fruits. Lastly, it is worthy of mention that $Mn_{0.851}Ce_{0.149}/TiO_2$ is more active than $Mn_{0.851}Ce_{0.149}/Al_2O_3$ at up to about 150 °C; however, at higher temperatures the reverse is true [135].

6.7 Effect of H_2O

The effect of H_2O on the deNOx activity at temperatures below 200 °C can be dramatic, see table 6.1, and is usually explained by the competitive adsorption of H_2O and NH_3 [116, 118, 134, 136], meaning that the adverse effect of H_2O is "only" a reversible inhibition. Competitive adsorption between H_2O and NO, evidenced by an increase in reaction order with respect to NO at 150 °C from 0.79 (dry) to 1.07 (wet), was also listed as one of the reasons for inhibition [137]. Some reports also mention that the deactivating effect of H_2O has an irreversible component [116, 137]. This is due to the transformation of Lewis into Brønsted

acid sites caused by the dissociative adsorption of H_2O. This tranformation can be reverted by heating to 500 °C [137], a fact that is more of academic interest because when operating at below 200 °C the Lewis acid sites will again transform to Brønsted ones. Kijlstra et al. [137] ruled out sintering of MnOx on 15 wt.% Mn/Al_2O_3, which would be caused by the hydrolysis of Mn-O-Al bonds, due to the fact that water exposure does not lead to a higher degree of crystallinity. The activity data for $Mn_{0.3}Ce_{0.7}$ [118] clearly show that the inhibiting/deactivating effect of H_2O is stronger at lower temperatures, e.g. the ratios of k_{no-H_2O}/k_{H_2O} at 100, 150 and 200 °C are 16, 4.7 and 2.9, respectively.

Since most of the promissing catalysts contain manganese, it is of interest to look at the impact of H_2O on MnOx. This was done by Hu et al. [116], who compared the water tolerance of HMO-MnO_2 and β-MnO_2. In the presence of 10 % H_2O the HMO-MnO_2 clearly outperforms β-MnO_2, see table 6.1. The reported NO conversions do not necessarily allow the conclusion that water has a relatively bigger impact on β-MnO_2 because the conversions over HMO-MnO_2 in the absence of H_2O were clearly above 90 %. Based on NH_3-TPD results the authors reported that HMO-MnO_2 is much better than β-MnO_2 at retaining NH_4^+ in the presence of H_2O. Both catalysts do not desorb NH_3 in the presence of H_2O, which can be explained by the transformation of Lewis into Brønsted acid sites. This report gives some hope that it is possible to enhance the water tolerance of MnOx based catalysts. The effect of low H_2O concentrations on Mn/Al_2O_3 was reported to be stronger in the case of low Mn loadings [137], which makes synthesis routes allowing for higher Mn loadings more attractive than the commonly used impregnation method.

Some reports also claim that H_2O only has a marginal impact on the catalytic activity. For example, Qi et al. [108] reported that the NO conversion over the citric acid prepared $Mn_{0.3}Ce_{0.7}$ at 120 °C only decreased by 2 %, from 100 to 98 %. The fact that the conversion drops by only 2 % does not mean that water does not have an inhibiting effect because the initial conversion of 100 % could have been reached at a higher space velocity. Nonetheless, calculating conservative first order rate constants (see equation A.11) using fractional conversions of 0.98, 0.95 and 0.90 yields values of 32.6, 25.0 and 19.2 $cm^3\ g^{-1}\ s^{-1}$, respectively. The first order rate constant at 120 °C in the absence of H_2O was reported to be 76.2 $cm^3\ g^{-1}\ s^{-1}$ measured at an NO conversion of 75 % [108]. This means that the activity reduction upon addition of 19 % H_2O is between 43 and 75 % assuming NO conversions in the presence of H_2O of 98 and 90 %, respectively. These data are in some conflict with those of Casapu et al. [118], who reported activity reductions of 94 and 78 % at 100 and 150 °C, respectively, using only a moderate H_2O concentration of 5 %. Note that the use of first order rate con-

stants is justified in this case because the reaction was ascertained to be first order with respect to NO and zero order with respect to NH_3.

The impact of 20 % H_2O on our in-house catalyst is tremendous. At 140 °C the NO conversion decreases from above 90 % to 16.2 %, which is close to the one over the VWT reference catalyst tested at 170 °C under otherwise identical conditions. Assuming first order kinetics, this corresponds to an activity reduction of at least 90 %.

The last entry in table 6.1 is used as the benchmark in our study. A quick look at table 6.1 reveals that basically all of the catalysts are far from reaching the benchmark activity at 140 - 150 °C, even though they were tested at relatively moderate H_2O concentrations of up to 11 %.

In summary, H_2O is reported to have a much bigger impact on most catalysts at temperatures below 200 °C than it has on the traditional VWT catalyst at temperatures above 200 °C. The deactivation is mostly caused by reversible adsorption of water and partly by the transformation of Lewis into Brønsted acid sites. At temperatures of 140 to 150 °C all of the reviewed catalysts including our in-house solution failed to deliver the activity stipulated by our collaborator even though they were often tested at water concentrations far below 20 %, a level often encountered at the tail-end position.

Table 6.1: Effect of H_2O on NO conversions at temperatures of up to 200 °C. Note that first-order rate constants were calculated assuming the reduction of NO is first order with respect to [NO] and zero order with respect to [NH_3]. This assumption might not always hold true.

catalyst	reference	T (°C)	[H_2O] (vol. %)	$X_{NO-no-H_2O}$ (%)	X_{NO-H_2O} (%)	k_{no-H_2O} ($cm^3\ g^{-1}\ s^{-1}$)	k_{H_2O} ($cm^3\ g^{-1}\ s^{-1}$)
HMO-MnO_2	[116]	100	10	> 90	10	> 76.8	3.6
HMO-MnO_2	[116]	150	10	> 90	40	> 76.8	17.0
HMO-MnO_2	[116]	200	10	> 90	70	> 76.8	40.1
β-MnO_2	[116]	100	10	10	2	3.5	0.7
β-MnO_2	[116]	150	10	22	3	8.3	1.0
β-MnO_2	[116]	200	10	70	10	40.1	3.5
$Mn_{0.3}Ce_{0.7}$	[118]	100	5	n.g.	n.g.	16	1.0
$Mn_{0.3}Ce_{0.7}$	[118]	150	5	n.g.	n.g.	179	38
$Mn_{0.3}Ce_{0.7}$	[118]	200	5	n.g.	n.g.	357	125
$Mn_{0.3}Ce_{0.7}$	[108]	120	19	100	98	-	32.6
CuMnOx	[120]	120	11	> 90	65	n.g.	n.g.
20 %FeMn/TiO_2	[120]	150	2.5	100	92	-	8.4
20 %FeMn/TiO_2	[120]	150	6	100	87	-	6.8
20 %FeMn/TiO_2	[120]	150	15	100	82	-	5.7
8 %Mn/TiO_2−PILC	[134]	160	3	57	52	8.4	7.3
FeMnCe/TiO_2	[136]	140	3	83	72	17.7	12.7
MnCoCe	[104]	150	15	80	65	35.8	23.6
$Mn_{0.4}Ce_{0.6}$/TiO_2	[136]	140	3	71	55	12.4	8.0
in-house	-	140	20	> 90	16.2	> 38.4	3.7
in-house	-	150	20	> 90	30.6	> 38.4	7.6
in-house	-	160	20	> 90	55.6	> 38.4	16.9
ind. VWT ref.	-	170	20	54.0	17.3	12.9	4.0
ind. VWT ref.	-	**220**	**20**	-	**≈ 90**	-	**≈ 38.0**

6.8 Effect of SO_2

SO_2 is at least as much of concern as H_2O to most of the reported low temperature catalysts. The deactivation can be caused by $(NH_4)_2SO_4$ and $(NH_4)HSO_4$ covering the active sites or, more seriously, by the formation of metal sulfates, most prominently manganese sulfates. The former mode of deactivation can be reverted by heating the catalyst bed to about 350 °C and can also occur when operating the traditional VWT catalyst at low temperatures. The formation of metal sulfates is generally much more troublesome since they are often very thermally stable and water soluble, excluding heating and water washing as modes of regeneration.

Table 6.2 provides a summary of some of the reported SO_2 exposure data. Generally SO_2 causes strong deactivation both in the presence and absence of H_2O. The reader might not straightforwardly be able to put the SO_2 loading (μ mol SO_2/g_{cat}) into context. For this reason we have obtained some real life data from a tail-end SCR unit in a waste incineration plant [98]. Using these data plus making some educated guesses regarding the density of the catalyst, we determined the average SO_2 exposure to be 0.317 μmol $SO_2/(g_{cat}$ * h * $ppm_{SO_2})$. See appendix B.1 for the detailed calculations. This means that an average SO_2 exposure of 1000 μmol SO_2/g_{cat} will be reached after 315, 63 and 32 h of operation assuming SO_2 concentrations of 10, 50 and 100 ppm, respectively. These values suggest that at least in terms of the amount of SO_2 per gram of catalyst most of the studies are not unrealistically harsh. On the contrary, some studies have shown that low SO_2 loadings administered at low SO_2 concentrations can lead to strong deactivation, see e.g. MnFE-spinel [139]. It is important to note that strong deactivation also occurs in the combined presence of high water content and low temperature, see MnCoCe [104] and MnOx [115]. The data set is unfortunately too small to subject it to statistical analysis, e.g. multiple linear regression analysis, which could shed some light onto the influence of the testing conditions like e.g. temperature, water- and SO_2 concentration. The influence of catalyst composition and preparation on the SO_2 tolerance as well as the influence of temperature during testing were reported in various papers and will be discussed below.

Table 6.2: Effect of SO_2 on NO conversions. Note that first order rate constants were calculated assuming the reduction of NO is first order with respect to [NO] and zero order with respect to [NH_3]. This assumption might not always hold true.

catalyst	ref.	$[H_2O]$ (%)	T (°C)	$[SO_2]$ (ppm)	δ t (min)	n_{SO_2} /m_{cat} (μmol SO_2/g_{cat})	$X_{NO-no-SO_2}$ (%)	X_{NO-SO_2} (%)	k_{SO_2} ($cm^3g^{-1}s^{-1}$)
MnCoCe	[104]	0	150	150	360	482	80	60	20.4
MnCoCe	[104]	15	150	150	360	482	65	23	5.8
$Mn_{0.6}Fe_{0.4}$	[106]	0	120	100	270	341	99	93	14.1
$Mn_{0.6}Fe_{0.4}$	[106]	5	120	100	270	341	90	88	11.3
$Mn_{0.3}Ce_{0.7}$	[108]	5	120	100	225	502	100	95	25.0
MnOx	[115]	10	80	100	270	723	92	73	13.1
$Mn_{0.3}Ce_{0.7}$	[118]	5	250	50	270	5000	70	21	32.6
MnNbCe	[118]	5	250	50	270	5000	92	21	32.6
MnCe	[119]	12	110	100	480	1071	-	25	2.4
MnSnCe	[119]	12	110	100	480	1071	-	65	8.7
Mn/TiO_2	[124]	2.5	150	100	300	268	-	58	2.9
MnFe	[124]	2.5	150	100	300	268	-	90	7.7
Ce(0.6)Ti	[130]	0	300	200	480	-	100	75	-
MnCeTi	[131]	3	120	700	950	-	92	34	-
MnCeTi	[135]	3	200	100	390	1045	93	30	3.6
MnCeTi	[136]	3	180	100	300	804	80	50	6.9
MnFeCeTi	[136]	3	180	100	300	804	92	85	19.0
MnFeCeTi	[140]	8	180	100	90	717	84	62	28.8
MnFe-spinel	[141]	5	?	50	100	44	100	60	3.1
$CuSO_4Ce/Ti$	[142]	10	220	350	320	-	89	20	-
$CuSO_4Ce/TiSi$	[142]	10	220	350	320	-	93	90	-
$CuSO_4Ce/TiSi$	[142]	10	220	350	3900	-	93	37	-
MnFeCe/Ti-i	[139]	10	240	300	150	-	88	50	-
MnFeCe/Ti-sg	[139]	10	240	300	150	-	92	81	-
Mn/Ti	[143]	3	150	100	400	-	92	30	-
MnCe/Ti	[143]	3	150	100	400	-	100	84	-
in-house	-	8	160	10	1285	1941	69	17.5	10.9

Jin et al. [132] studied the influence of temperature on SO_2 poisoning by subjecting $MnCe/TiO_2$ to a SO_2 containing simulated flue gas at different temperatures (100 - 200 °C) at a fixed space velocity (Conditions: [NO] = [NH_3] = 800 ppm; [SO_2] = 100 ppm; [H_2O] = 3 %; SV = 40000 h^{-1}). In the absence of SO_2 the reaction conditions afforded near 100 % NO conversion in the full temperature range. Upon addition of SO_2 the NO conversions decreased at different rates. The time needed for the NO conversion to drop to 60 % was about 175, 225, 375, 500 and 610 min at 200, 180, 150, 120 and 100 °C, respectively. This result is surprising in light that several publications [131, 134] report monotonically increasing NO conversions in the temperature range of 100 - 200 °C in the absence of SO_2. Therefore, the data of Jin et al. [132] strongly suggest that SO_2 deactivates $MnCe/TiO_2$ more rapidly at higher temperatures. Furthermore, the authors investigated regeneration by water washing. After washing, the catalysts previously exposed at 200, 180, 150, 120 and 100 °C reached NO conversions at 150 °C of roughly 73, 82, 92, 95 and 99 %, respectively. NH_3-TPD revealed a loss of acid sites in the region of 430 to 770 °C after SO_2 exposure, with the loss being more pronounced in the high temperature exposure cases. Coupled with DRIFTS experiments in the presence of NH_3, the authors concluded that at high temperatures (200 °C) SO_2 sulfates the metals of the catalyst and thus transforms Lewis into Brønsted acid sites whereas at low temperatures (100 °C) the deactivation is mostly caused by NH_4HSO_4 and $(NH_4)_2SO_3$, which can be easily washed away with water. The presented activity data suggest that some metal sulfate formation should take place at 150 °C, close to the target temperature stipulated by our collaborators. Jiang et al. [144] confirmed the formation of metal sulfates on $MnFe/TiO_2$ at 150 °C. This is worrisome, because manganese sulfates are reported to be very thermally stable [131, 138]. Furthermore, in case of simultaneous formation of metal- and ammonium sulfates and sulfites water washing would potentially also wash the manganse sulfates away (leaching). Even the exclusive formation of ammonium sulfates and sulfites is not as unproplematic as Jin et al. might suggest because water washing would probably interrupt the operation of the SCR unit. Our own study [128] showed that a mesoporous $MnFe/TiO_2$ catalyst was seriously inhibited by a $(NH_4)_2SO_4$ loading of only 250 $\mu mol/g_{cat}$, a level that is probably rapidly reached at an average SO_2 exposure at a concentration of 10 ppm of about 3.17 μmol $SO_2/(g_{cat} * h)$. Heating to 400 °C in an inert gas flow does not cause any regeneration, confirming the results of Zhongyi et al. [131], who reported heating to 400 °C to be the worst mode of regeneration and conjectured that the decomposition of the ammonium sulfates and sulfites furnished SO_3, which in turn could react with the catalyst surface to form metal sulfates.

The study of Jiang et al. [144] reached slightly different conclusions on the mode

of SO_2 poisoning, especially concerning the role of Brønsted and Lewis acid sites. At 150 °C their $MnFe/TiO_2$ catalyst experienced an NO conversion drop from 100 % to about about 80 % within 30 minutes after introduction of 200 ppm SO_2. After this initial steep activity loss, the NO conversion dropped much more slowly and reached 65 % after about 4 h. The steep activity loss was explained by the formation of metal surface sulfates and the ensuing gradual decline by the deposition of ammonium sulfates. DRIFT experiments revealed that the presence of SO_2 does not reduce the amount of coordinated NH_3 and greatly increases the amount of NH_4^+, suggesting that the number of Lewis sites does not decrease and the number of Brønsted sites increases. However, the NO adsorption decreases in the presence of SO_2. The authors thus concluded that SO_2 strongly suppresses the Langmuir-Hinshelwood pathway. In an earlier paper [145] the same group reported that a not to be neglected part of NO is reduced over $MnFe/TiO_2$ via the Langmuir-Hinshelwood pathway. The possible importance of the Langmuir-Hinshelwood pathway at low temperatures was also reported for MnFe-spinel catalysts [141]. Indeed, some papers reported partial [104, 106, 140, 142] or even full [108, 115] reestablishment of the NO conversion after removal of SO_2, while others [118, 130, 131, 136] reported no positive effect, see table 6.3. It is noteworthy that regeneration by removal of SO_2 from the gas stream was also reported in the presence of H_2O (up to 10 %) and at temperatures of up to 220 °C, conditions under which the NO adsorption [137, 146] and the contribution of the Langmuir-Hinshelwood pathway [145] are reported to be weak.

Yu et al. [139] investigated the effect of the preparation method (impregnation and sol-gel) on the SO_2 tolerance of $MnFeCe/TiO_2$ at 240 °C (Conditions: [NO] = 600 ppm; $[NH_3]$ = 480 ppm; $[O_2]$ = 2 %; $[H_2O]$ = 10 %; $[SO_2]$ = 300 ppm). During the 2.5 h of exposure, the NO conversion over the catalyst prepared by impregnation decreased continuously from 88 to about 50 %. The sol-gel derived catalyst on the other hand experienced only a conversion drop from about 92 to 81 % during the first hour after which a plateau was reached. Long-term exposure of 60 h confirmed that this high level of activity could be maintained. Due to a lack of a Mn^{2+} signal in the XPS spectra of the spent catalysts, the authors rejected the possibility of manganese sulfate ($MnSO_4$) formation and ascribed the deactivation to ammonium sulfates blocking the active sites. The higher SO_2 tolerance of the mesoporous, sol-gel prepared catalyst could thus be explained with purely morphological reasons. The weight loss in TG experiments of sol-gel derived catalyst samples exposed to SO_2 for 16 and 60 h was practically the same, indicating that the deposition and decomposition of ammonium sulfates is in equilibrium. The initial loss of activity can therefore be explained by the attainment of the mentioned equilibrium and not by metal sulfate formation, as was done in other studies [132, 144]. However, the authors did not consider the possibility of the formation of $(NH_4)_2Mn_2(SO_4)_3$, which could explain the absence

Table 6.3: Effect of removal of SO_2 on the NO conversion.

catalyst	ref.	$[H_2O]$ (%)	T (°C)	$X_{NO-no-SO_2}$ (%)	X_{NO-SO_2} (%)	$X_{after-SO_2-removal}$ (%)
MnCoCe	[104]	0	150	80	60	67
$Mn_{0.6}Fe_{0.4}$	[106]	0	120	99	93	97
MnFeCeTi	[140]	8	180	84	62	75
$CuSO_4Ce/TiSi$	[142]	10	220	93	37	65
MnOx	[115]	10	80	92	73	92
MnOx	[115]	0	80	100	92	98
$Mn_{0.3}Ce_{0.7}$	[108]	2.5	120	100	95	100
$Mn_{0.3}Ce_{0.7}$	[118]	5	250	70	21	21
MnNbCe	[118]	5	250	92	21	21
MnCeTi	[131]	3	120	92	34	34
MnCeTi	[136]	3	180	80	50	53
MnCeTi	[136]	3	180	92	85	86

of Mn^{2+} in the XPS data of Yu et al. [139]. Nagaishi et al. [147] reported MnO_2 to react with $(NH_4)_2SO_4$ to give $(NH_4)_2Mn_2(SO_4)_3$ at 220 °C in a TG experiment using a heating rate of 10 °C min^{-1}.

The catalyst composition can also have an influence on the SO_2 tolerance and some examples will be given here. Wu et al. [143] observed increased SO_2 tolerance of Mn/TiO_2 during the first 400 min of exposure by doping it with Ce (Conditions: $[NO] = [NH_3] = 1000$ ppm; $[O_2] = 3$ %; $[H_2O] = 3$ %; $[SO_2] = 100$ ppm; T = 150 °C; SV = 40000 h^{-1}). XPS analysis of the spent catalysts showed a much higher surface sulfur concentration on Mn/TiO_2 (3.8 atomic %) than on $MnCe/TiO_2$ (1.0 atomic %) and a shift of the main peak of Mn towards higher energies indicative of Mn sulfate formation in the case of Mn/TiO_2. Doping $MnCe/TiO_2$ with Sn was reported to suppress the formation of manganese sulfates and promoted the formation of cerium sulfates resulting in an enhanced SO_2 tolerance [119]. Sulfation of pure CeO_2 was reported to enhance the activity greatly at 200 °C [148] by increasing the amount of chemisorbed O_2 and the number of acid sites. Tong et al. [142], on the other hand, reported drastic activity loss upon sulfation of Ce in $CuSO_4Ce/TiSi$. In the case of TiO_2 supported catalysts, doping the support with Si can suppress the oxidation of SO_2 to SO_3 and thus milden the effect of SO_2 [142].

In summary, SO_2 acts as a strong poison on manganese containing catalysts, both by the formation of manganese sulfates and ammonium sulfates and sulfites which cover the active sites. The ammonium compounds can be removed by water washing, however, not by heating because this will lead to manganese sulfates. The formation of manganese sulfates can neither be reverted by heating to 350 °C because of their thermal stability nor by water washing because it would lead to leaching of Mn. Some authors [118,138] reached the conclusion that Mn based catalysts should only be used for SO_2 free flue gases.

6.9 Vanadia based solutions

Since most of the Mn containing catalysts are severely deactivated by SO_2, V_2O_5 based solutions should not be ignored altogether. Lately, Gao et al. [149] reported that the activity of 1 wt.% V - 10 wt.% -W/TiO_2 at 200 °C can be markedly improved by addition of 3 wt.% Fe. The enhancement was ascribed to an increased concentration of surface oxygen which in turn increased the NO to NO_2 conversion. Kristensen et al. [25] reported sol-gel synthesis of 20 wt.% V_2O_5/TiO_2 which is about 2.5 times as active as the commercial reference but did not investigate the low temperature region. It is conceivable that incorporation of Fe into the sol-gel prepared catalyst can further boost its activity at temperatures below 200 °C. Furthermore, to the best of our knowledge, we were the first to prepare a VWTi catalyst by the deposition precipitation method.

Chapter 7

Low-temperature NH_3-SCR catalyst screening

Mixed oxides, supported oxides and supported mixed oxides were prepared by impregnation, citric-acid, co-precipitation, and sol-gel methods, see table 7.1 for details. Some catalysts investigated during the screening stage cannot be reported due to a concurrent patent application.

Table 7.1: Summary of preparation details of catalyst tested during the screening phase. Stoichiometry of supported catalysts expressed as metal to support metal ratio and as wt. % in the case of zeolite based systems. Abrreviations: CA = citric acid method; CP = co-precipitation method; IMP = impregnation; SG = sol-gel; H = hydrothermal; S = secret.

catalyst	ref.	method	support	drying T	calcination T
				[°C]	[°C]
4 wt.% Cu/BEA		IMP	BEA (Si/Al) =	100	400
$FeTiO_4$		CP	-		450
$Mn_{0.3}Ce_{0.7}$	[108]	CA	-	120	550-750
$Mn_{0.25}Ce_{0.75}$	[108]	CA	-	120	650
$Mn_{0.325}Ce_{0.675}$	[108]	CA	-	120	650
$Mn_{0.35}Ce_{0.65}$	[108]	CA	-	120	650
$Mn_{0.285}Fe_{0.05}Ce_{0.665}$	[108]	CA	-	120	650
$Mn_{0.27}Fe_{0.10}Ce_{0.63}$	[108]	CA	-	120	650
$Mn_{0.255}Fe_{0.15}Ce_{0.595}$	[108]	CA	-	120	650
$Mn_{0.6}Fe_{0.4}$	[106]	CA	-	120	500
$Mn_{0.6}Co_{0.4}$	-	CA	-	120	500
$Mn_{0.6}Cr_{0.4}$	-	CA	-	120	500
$Mn_{0.6}Fe_{0.3}Co_{0.1}$	-	CA	-	120	500
$Mn_{0.6}Fe_{0.3}$ $Cr_{0.1}$	-	CA	-	120	500
$Mn_{0.6}Fe_{0.3}Ce_{0.1}$	-	CA	-	120	500
$Mn_{0.6}Fe_{0.35}Ce_{0.05}$	-	CA	-	120	500
$Mn_{0.57}Fe_{0.38}Ce_{0.05}$	-	CA	-	120	500
$Mn_{0.51}Fe_{0.34}Ce_{0.15}$	-	CA	-	120	500
$Mn(0.363)/TiO_2$	-	IMP	DT-51	120	500
$Mn(0.371)Fe(0.248)/TiO_2$	-	IMP	G5	120	500
$Mn(0.371)Fe(0.248)/TiO_2$	[128]	SG	$Ti(OC_4H_9)_4$-based	105	450
$Mn(0.371)Fe(0.248)/TiO_2$	[128]	H	$Ti(OC_4H_9)_4$-based	105	450
$Mn(0.371)Fe(0.248)/TiO_2$	[128]	CA	G5	100	500
$Mn(0.371)Fe(0.248)/TiO_2$	-	CA	G5	120	500
$Mn(0.371)Fe(0.248)Ce(0.026)/TiO_2$	-	CA	G5	120	500
$Mn(0.371)Fe(0.248)Ce(0.044)/TiO_2$	-	CA	G5	120	500

7.1 Binary mixed oxides - overview

Figure 7.1 shows the NO conversions over binary mixed oxides all containing Mn and one other transition metal, all prepared by the citric acid method. The oxides containing Ce and Fe are clearly more active than those containing Co and Cr. At 150 °C, $Mn_{0.3}Ce_{0.7}$ is clearly the most active binary mixed oxide tested, converting 55 % of NO, while $Mn_{0.6}Fe_{0.4}$ only converts about 33 %. In the presence of only 2.3 % H_2O, both catalysts are at least as active as the commercial VWT catalyst at 220 °C. However, as described in section 6.7, high contents of water cause more inhibition at low temperatures than they do at higher ones. Therefore, the activity data do not at all suggest that the Ce and Fe containing mixed oxides would meet the benchmark at a H_2O concentration of 20 %.

At 300 °C, $Mn_{0.3}Ce_{0.7}$ and $Mn_{0.6}Fe_{0.4}$ maintain NO conversions of 81 and 92 %, respectively, meaning that they would also show significant activity during short periods of reheating.

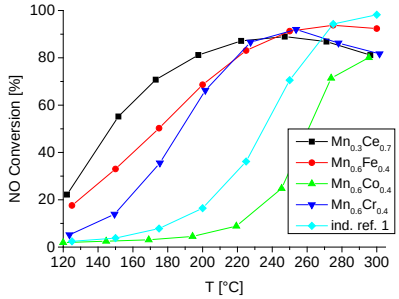

Figure 7.1: NO conversion over binary oxides. W/F = 0.01 g s cm^{-3}.

The reader might wonder why the $Mn_{0.6}Cr_{0.4}$ catalyst only converts about 5 % NO at 125 °C while $Mn_{0.5}Cr_{0.5}$ was reported to convert close to 100 % at 120 °C [105]. The discrepancy can be explained by the fact that Chen et al. [105] used a W/F ratio which is about 22 times higher than the one used in our study, and no H_2O at all.

The comparison between Ce and Fe containing oxides with Cr and Co containing ones might not be exactly fair because the compositions of $Mn_{0.3}Ce_{0.7}$ [108] and $Mn_{0.6}Fe_{0.4}$ [106] had been optimised elsewhere. Nonetheless, at 150 °C, which

is about the target temperature, the activity differential is so pronounced that we concluded that further efforts should be directed mostly at mixed oxides containing Mn in conjunction with Fe and Ce. Another reason against Co and Cr is their high toxicity.

7.2 Mn_xCe_{1-x}

Since $Mn_{0.3}Ce_{0.7}$ was by far the most active binary oxide at 150 °C, we tried to further optimise its composition and preparation method. As Qi et al. [108] used rather big step sizes in the optimisation of the calcination temperature and the Mn content, we expected there to be further optimization potentials. Furthermore, the study of Boxiong et al. [136] made us try to enhance the Mn_xCe_{1-x} by adding small amounts of Fe.

First, we made sure that the $Mn_{0.3}Ce_{0.7}$ prepared by us using the previously optimised synthesis method [108] is as active as reported in the literature [108, 118] and that the reaction is first-order with respect to NO, making the use of equation A.11 permissible, see figure 7.2. Since the values calculated with equation A.11 are practically insensitive to the W/F ratio, we can be confident that use of equation A.11 is sensible.
At 150 °C, the first-order rate constant is about 80 $cm^3\ g^{-1}\ s^{-1}$, in between the value reported in presence of 5 % H_2O (38 $cm^3\ g^{-1}\ s^{-1}$) [118] and the one reported in absence of H_2O (121 $cm^3\ g^{-1}\ s^{-1}$).

Next, the Mn content in Mn_xCe_{1-x} was optimised using steps of just 2.5 mol. % from 25 to 35 mol. %. Qi et al. [108] used steps of 10 mol. % and reported $Mn_{0.2}Ce_{0.8}$ to be significantly less active than $Mn_{0.3}Ce_{0.7}$. Our data show that $Mn_{0.3}Ce_{0.7}$ is indeed the optimum composition, see figure 7.3. The syntheses of $Mn_{0.325}Ce_{0.675}$ and $Mn_{0.35}Ce_{0.65}$ were repeated to make sure that the activity bump at 32.5 mol. % Mn really exists. Increasing the Mn molar content beyond 35 % was not attempted because $Mn_{0.4}Ce_{0.6}$ was reported to be less active than $Mn_{0.3}Ce_{0.7}$.

Addition of Fe at concentrations of up to 15 mol. % was investigated, keeping the molar ratio Mn to Ce at the level of $Mn_{0.3}Ce_{0.7}$, see figure 7.4. Iron loadings up to 10 mol. % have little effect on the activity, whereas 15 mol. % causes an activity drop of about 40 %.

Lastly, the effect of the calcination temperature was studied in the range from 550 to 750 °C using steps of only 25 °C. Qi et al. [108] only used 650, 500 and

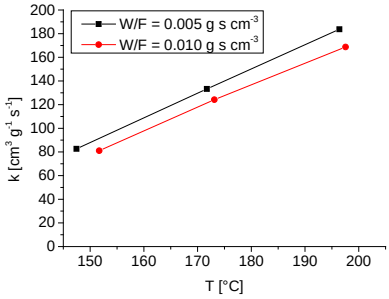

Figure 7.2: First-order rate constants over $Mn_{0.3}Ce_{0.7}$ at different W/F values..

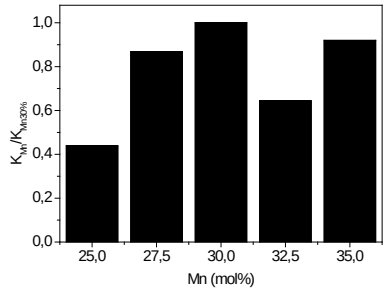

Figure 7.3: Relative first-order rate constants at 150 °C of Mn_xCe_{1-x} calcined at 650 °C

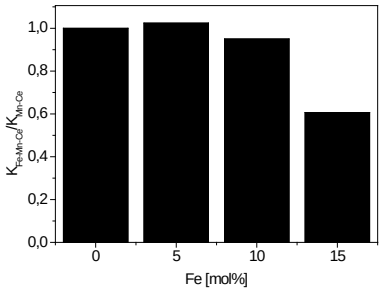

Figure 7.4: Relative first-order rate constants at 150 °C of $Fe_zMn_xCe_{1-x-z}$ (x/(1-x-z) = 0.429) calcined at 650 °C

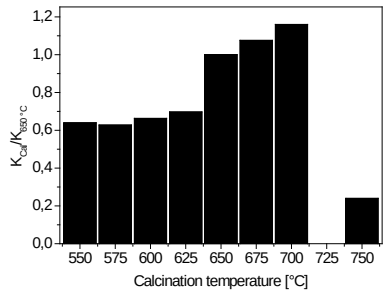

Figure 7.5: Relative first-order rate constants at 150 °C of $Mn_{0.3}Ce_{0.7}$ calcined at different temperatures

750 °C, with the latter two temperatures yielding significantly lower activities. Our own data suggest that the activity is relatively insensitive to the calcination temperature up to about 625 °C and about 40 % lower than when 650 °C is used. Raising the calcination temperature to 700 °C increases the activity by about 20 %. 750 °C, on the other hand, is definitely too high a calcination temperature, as reported earlier [108].

In summary, it seems that the previously reported [108] optimum method of preparation did not leave big optimisation potentials. The beneficial effect of Fe [136] might be restricted to supported MnCe, where it causes, among other things, an increased dispersion of Mn and Ce. We decided to leave it at the sequential optimisation attempt (Mn content followed by Fe content and calcination temperature) and did not embark on a global optimisation, partly due to the relatively high price of Ce and because we found a synthesis method that affords supported catalysts at least as active as $Mn_{0.3}Ce_{0.7}$, using metal precursors cheaper than cerium nitrate.

7.3 Ternary mixed oxides

Most of the ternary oxides tested by us have their origin in $Mn_{0.6}Fe_{0.4}$, which turned out to be the second most active binary oxide in our comparative study, see fig 7.1, and Co, Cr or Ce as the third metal.

Figure 7.6 shows the effect of replacing 5 and 10 mol.% Fe in $Mn_{0.6}Fe_{0.4}$ by Ce and the effect of adding 5 and 15 mol.% Ce to MnFe keeping the molar Mn/Fe ratio at 1.5. All catalysts were prepared by the citric acid method and calcined at 500 °C. $Mn_{0.3}Ce_{0.7}$ prepared by the citric acid method and calcined at 650 °C as well as a commercial VWT catalyst are included as references.

Figure 7.6 shows that adding small amounts of Ce can clearly ameliorate $Mn_{0.6}Fe_{0.4}$ at temperatures of up to 175 °C. The enhancement seems to be more effective when fixing the Mn content to 60 mol. % than when fixing the Mn/Fe ratio to 1.5. At about 150 °C, both $Mn_{0.6}Fe_{0.3}$ $Ce_{0.1}$ and $Mn_{0.51}Fe_{0.34}Ce_{0.15}$ convert about 47 % of NO, roughly halfway between $Mn_{0.6}Fe_{0.4}$ (33 %) and $Mn_{0.3}Ce_{0.7}$ (55 %). It is quite conceivable that small, further increases in the Ce content coupled with an optimisation of the Mn/Fe ratio and of the calcination temperature could have yielded a catalyst as active as $Mn_{0.3}Ce_{0.7}$, coming at a much lower cost due to a lower Ce content. However, since we discovered a method to prepare highly active, supported and Ce free catalysts we did not pursue the optimisation of MnFeCe catalysts.

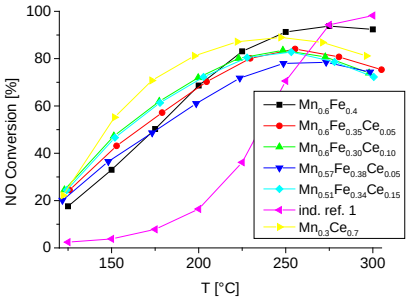

Figure 7.6: Effect of adding Ce to MnFe on NO conversions. W/F = 0.01 g s cm^{-3}.

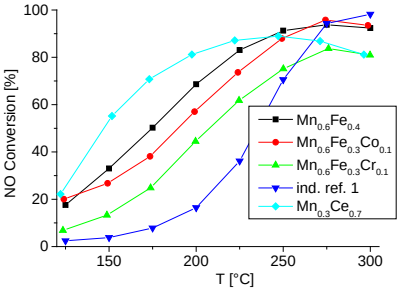

Figure 7.7: Effect of adding Co and Cr to MnFe on NO conversions. W/F = 0.01 g s cm^{-3}.

Figure 7.7 shows that substituting 10 mol.% Fe in $Mn_{0.6}Fe_{0.4}$ by Co and Cr has a detrimental effect on the activity throughout the whole temperature range, especially in the case of Cr. This reflects the order of activity of the Mn-X mixed oxides as presented in figure 7.1.

7.4 Supported catalysts

Since some comparative studies [22, 135] reported TiO_2 to be the best support for Mn containing catalysts our efforts were mostly directed at this material and its mixed oxides to a much lesser extent.

Because of the relatively high activity of $Mn_{0.6}Fe_{0.4}$ and reports on high activity of Mn_xFe_y/TiO_2 [21, 124, 127] it was an obvious choice to compare the activity of $Mn_{0.6}Fe_{0.4}/TiO_2$ to that of $Mn_{0.3}Ce_{0.7}$, the most active catalyst so far. Figure 7.8 shows the loading effect on the NO conversion. All catalysts were prepared by the citric acid method. The activity of the supported formulations reach that of the pure $Mn_{0.6}Fe_{0.4}$ at dopant to Ti ratio of about 0.43 but do not increase further at higher dopant to Ti ratios. The comparison between supported and unsupported $Mn_{0.6}Fe_{0.4}$ is not exactly fair because in the latter case the Mn to Fe ratio was not optimised. Addition of small amounts of Ce (Ce/Ti =0.031 and 0.053) to $Mn_{0.6}Fe_{0.4}(0.619)/TiO_2$ causes the activity to drop. This is in contradiction to the reported enhancing effect of Ce on TiO_2 supported Mn

catalysts [130, 131, 133, 134].

Mn(0.371)Fe(0.245)/TiO_2(G5) was prepared by both the citric method and by conventional impregnation. The former yielded only marginally higher NO conversions (data not shown).

Preparation of mesoporous $Mn_{0.6}Fe_{0.4}/TiO_2$ by a hydrothermal method [128] greatly enhanced the pore size distribution to make the catalyst less susceptible to ammonium sulphates but did not increase its activity. Replacing 10 mol.% of Ti by Si to suppress the oxidation of SO_2 [142] drastically decreases the activity. Applying the hydrothermal method to support $Mn_{0.3}Ce_{0.7}$ onto TiO_2 resulted in even less attractive activities. Reducing the Ce content [131, 147] might have yielded higher activities. Because of the elaborateness of the preparation, our collaborators ended this project in favour of the secret method which will be presented in chapter 8.

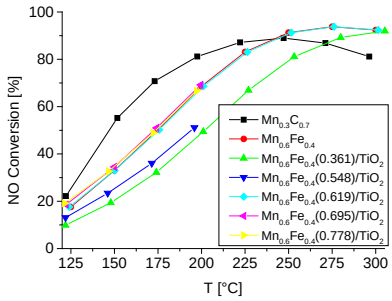

Figure 7.8: Effect of dopant loading on activity over $Mn_{0.6}Fe_{0.4}/TiO_2$ (G5). W/F = 0.01 g s cm^{-3}.

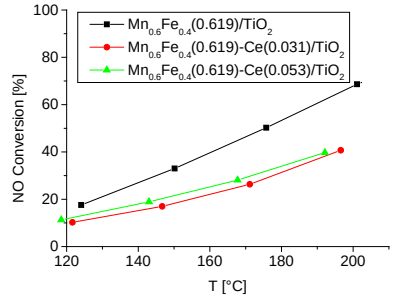

Figure 7.9: Effect of adding Ce to $Mn_{0.6}Fe_{0.4}(0.619)/TiO_2$ (G5). W/F = 0.01 g s cm^{-3}.

Chapter 8

AB/C and AB/D prepared by method S

8.1 Motivation & foreword

Due to the above-mentioned concurrent patent application very limited information on the composition of the catalyst and the method of preparation can be given. A series of A(a)B(b)/C and A(a)B(b)/D catalysts were prepared, characterised and tested for SCR activity.

1. **A and B**
   Transition metal dopants
   Expected to be present in oxidic form after calcination

2. **C and D**
   Support materials
   Metal oxides

3. **a and b**
   a: molar ratio of A to C or D.
   b: molar ratio of B to C or D.

4. **Suffixes**
   suffix S: catalyst prepared by S method.
   suffix IMP: catalyst prepared by wet impregnation.

   a and b are not the actual molar ratios but can be calculated as follows: Once the patent issues are solved the reader can get the values of x_i, y_i

and z_i enabling the calculation of the actual molar ratios of A and B to the support metals C and D with equations 8.1 and 8.2, which give the relation between the reported and the real molar ratios. The values of x_i, y_i and z_i were chosen so that a(reported) and b(reported) are monotonically increasing with increasing a(real) and b(real), respectively.

$$a(reported) = x_1 * (a(real))^2 + y_1 * a(real) + z_1 \quad (8.1)$$

$$b(reported) = x_2 * (b(real))^2 + y_2 * b(real) + z_2 \quad (8.2)$$

8.2 AB/C

8.2.1 Activity optimisation of AB/C

The activity optimisation using method of preparation S consisted of sequential optimisation of the total metal loading (sum of a(real) and b(real)) at a fixed a(real) to b(real) ratio followed by optimisation of the a(real) to b(real) ratio at a practically fixed total metal loading.

Figure 8.1 shows the activity of catalysts prepared by the S method as a function of metal loading, keeping the a(real) to b(real) ratio fixed and figure 8.2 an equivalent optimisation using conventional wet impregnation.

Comparison of figures 8.1 and 8.2 reveals the clear superiority of method S over the conventional impregnation method. The best performing catalyst, prepared by the S method, A(1.823)B(0.189)/C-S, converts about 70 % of NO at 150 °C. Even $Mn_{0.3}Ce_{0.7}$, the most active catalyst tested so far, converts only 55 % of NO at that temperature. The most active IMP prepared catalyst, A(1.981)B(0.269)/C-IMP only converts around 30 % of NO at 150 °C and needs to be tested at 200 °C to convert 70 %. Also the minimum temperature to reach 90 % conversion is with 250 °C about 50 °C higher in the optimum IMP case than it is in the optimum S case. H_2-TPR experiments permitted the determination of the average oxidation states of A and B, thus making the calculation of the metal contents possible. A(1.823)B(0.189)/C-S contains only 22.7 wt. % dopants (A and B combined) while A(1.981)B(0.269)/C-IMP contains 31.0 wt. %, adding to the attractiveness of the S method.

Next, attempts were made to further increase the activity of A(a)B(b)/C-S by varying the ratio of a(real) to b(real) at a practically fixed total metal loading,

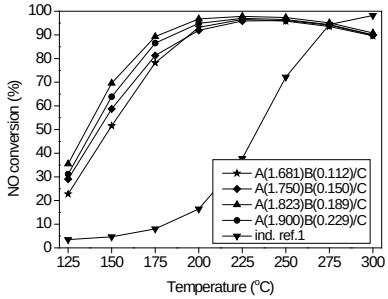

Figure 8.1: Effect of metal loading on A(a)B(b)/C-S. W/F = 0.01 g s cm^{-3}.

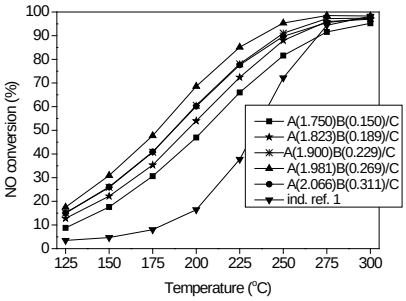

Figure 8.2: Effect of metal loading on A(a)B(b)/C prepared by the IMP method. W/F = 0.01 g s cm^{-3}.

see figure 8.3. Apparently, A(1.823)B(0.189)/C-S was already the optimum composition. Some papers on supported AB catalysts also reported stoichiometries close to our optimum one.

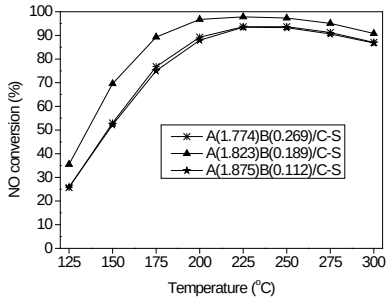

Figure 8.3: Effect of a(real) to b(real) ratio on activity of A(a)B(b)/C-S. W/F = 0.01 g s cm^{-3}.

8.2.2 Characterisation of AB/C

Various methods of characterisation were used to try to explain the superior activity of the A(a)B(b)/C-S over the A(a)B(b)/C-IMP catalysts. Not all of the characterisation results can be disclosed at the moment because some might give too strong a hint at the real composition of the catalysts.

- **XRD**
  The XRD pattern of A(1.981)B(0.269)/C-IMP showed some reflections assignable to AO_x, while the one of A(1.823)B(0.189)/C-S only contains reflections assignable to the support material C. This means that the S-prepared catalyst only contains amorphous AO_x and BO_x or that the size of the crystals is below the detection limit of around 5 nm. Superior SCR activity of amorphous transition metal oxides over the corresponding crystalline phases was also reported elsewhere [112, 115].

- **N_2-physisorption**
  Figure 8.4 shows the cumulative BJH surface areas as a function of the pore width of A(1.823)B(0.189)/C-S, A(1.981)B(0.269)/C-IMP and C. The surface area of the S-prepared catalyst is about 37 % higher than that of the IMP-prepared one. This difference can certainly help to explain the superior activty of the S-prepared catalyst; however, it can most probably not be the sole reason for an NO conversion increase from 30 to 70 % at 150 °C. Furthermore, it is worrisome that a considerable part of the surface area of A(1.823)B(0.189)/C-S is located in small pores, eg. 30 % in pores smaller than 5 nm. This can cause diffusion limitations in shaped (monolith) catalysts and increased loss of surface area upon extrusion because the binder, typically a clay, might plug the micro pores, see chapter 9.

- **NH_3-TPD**
  Figure 8.5 shows NH_3-TPD of A(1.823)B(0.189)/C-S and A(1.981)B(0.269)/C-IMP. The S-prepared catalyst differs from the IMP-prepared one in that it possesses about 84 % more surface acid sites and a very pronounced high temperature (425 to 525 °C) desorption peak.

- **H_2-TPR**

Figure 8.6 shows the H_2-TPR profiles of the most active catalysts prepared by the IMP and the S method. Both profiles have in common that they consist of two reduction peaks. There are two basic differences. Compared to the IMP-prepared sample, the high-temperature reduction peak of the S-prepared sample is shifted from 400 to about 370 °C. The low-temperature reduction peak at around 250 °C is markedly higher, although both the A and the B loadings are lower, indicating that a higher portion of the metal atoms is present in a high oxidation state in the S-prepared case. The average oxidation state of A was determind to be about 0.27 higher in A(1.823)B(0.189)/C-S than in A(1.981)B(0.269)/C-IMP.

- **TGA**

  Figure 8.7 shows the TG curves of AB/C-S and AB/C-IMP. AB/C-IMP shows continuous weight loss up to 600 °C totalling only about 3 wt. % while AB/C-S loses more than 5 wt. % and exhibits two steps at around 425 and 525 °C. This is an unexpected result because the XRD pattern of the AB/C-IMP sample showed some reflections due to crystalline AO_x. Continuous weight loss was reported for supported amorphous MnOx [122] while the supported crystalline form exhibits more of a step function and loses more weight. Assuming that these results are transferable to other metal oxides on any support one could reach the conclusion that AB/C-S is more crystalline than AB/C-IMP. This is quite possible if all of the oxide crystallites in AB/C-S are smaller than 5 nm, the detection limit of our XRD results. Another possible explanation for the higher weight loss of AB/C-S is its higher content of chemisorbed oxygen (about 3.8 wt. % difference) as determined by XPS.

- **XPS**

  Only the XPS spectra of O 1s may be shown, because the spectra of the metal constituents of A, B and C might disclose their identity. Figure 8.8 shows the O 1s spectra of A(1.823)B(0.189)/C-S and A(1.981)B(0.269)/C-IMP. Both spectra consist of two peaks, a major one at about 530.2 keV and a minor one at about 532.0 keV. The former peak (O_β) can be assigned to lattice oxygen and the latter peak (O_α) to chemisorbed surface oxygen. Use of the S method yields an O_α % concentration of 50.1 % of the total oxygen while the IMP method only yields 31.3 %. The beneficial influence of high concentrations of chemisorbed oxygen on the low-temperature SCR reaction has been reported before [133,134,136] and is explained by an increased rate of NO to NO_2 oxidation [136]. Furthermore, the ratio of a(real)/b(real) is about 24 % lower in A(1.823)B(0.189)/C-S than in A(1.981)B(0.269)/C-IMP. In other words, the use of the S method leads to a higher relative surface concentration of dopant B.

- **NO conversion in absence of NH_3**
  Strictly speaking, this is not a method of characterisation, however, it still adds to the understanding of why the S-prepared catalyst is highly active. The favourable influence of a high rate of NO to NO_2 oxidation was reported several times before e.g. [105–108]. The reaction conditions were as follows: [NO] = 1000 ppm; [O_2] = 4 %; [NH_3] = [H_2O] = 0. w_{cat} = 0.1 g (180 - 300 μ m); F= 150 cm^3 min^{-1}; T = 150 °C; W/F of 0.04 g s cm^{-3}. Since we had no NO_2 gas bottle at the time of the experimentation, we cannot report the amount of NO_2 formed. However, the N_2O formation was monitored and determined to be zero. Therefore, it can be assumed that most of the converted NO is transformed into NO_2. A(1.823)B(0.189)/C-S converts about 11 % of NO while A(1.981)B(0.269)/C-IMP only converts around 4.5 %. These values reflect the difference in O_α concentration as measured by XPS.

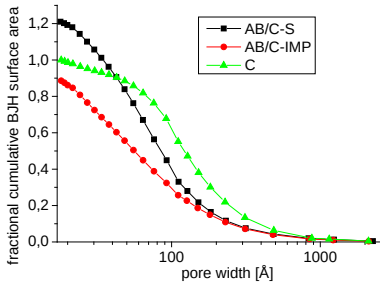

Figure 8.4: Cumulative BJH (adsorption branch) surface areas as function of the pore width. Values are normalised to total surface area of C

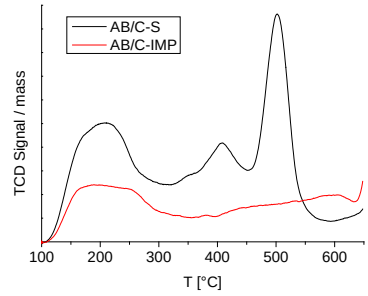

Figure 8.5: NH_3-TPD profiles of AB/C prepared by S and IMP.

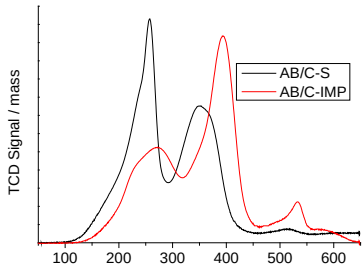

Figure 8.6: H_2-TPR profiles of A(1.823)B(0.189)/C-S and A(1.981)B(0.269)/C-IMP.

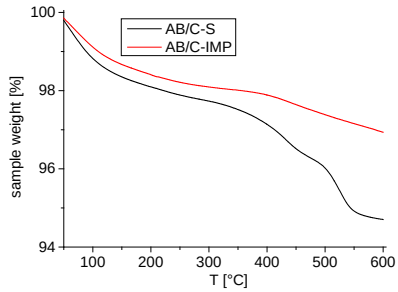

Figure 8.7: TG profiles of AB/C prepared by S and IMP. Heating rate = 10 °C min^{-1}; atmosphere = N_2.

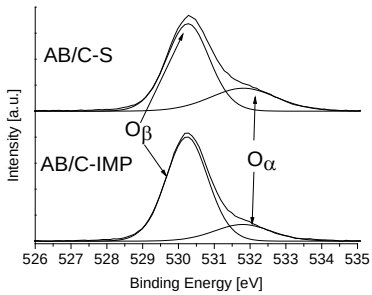

Figure 8.8: O 1s XPS spectra of AB/C-S and AB/C-IMP.

8.3 AB/D

The phenomenal success of the secret method S in enhancing the SCR activity of AB/C made us try to use it in conjunction with another support material, D. One of the main drivers of the AB/D investigation was the hope to enhance the H_2O tolerance, see chapter 10. The change of support material from C to D did not require changes to the method of preparation.

8.3.1 Activity optimisation of AB/D

As in the case of AB/C-S, the optimisation of the metal loading, keeping the ratio of a(real) to b(real) constant, preceeded the optimisation of the a(real) to b(real) ratio at practically constant total metal loading.

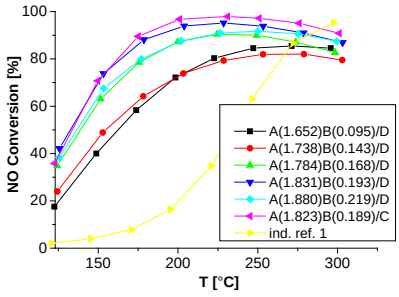

Figure 8.9: Effect of metal loading on the activity of A(a)B(b)/D-S. W/F = 0.01 g s cm^{-3}.

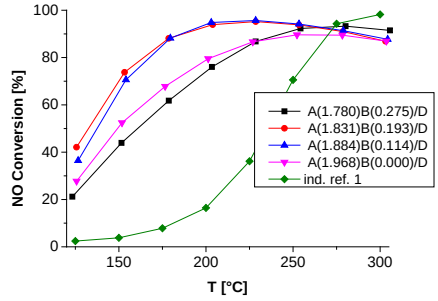

Figure 8.10: Effect of a(real) to b(real) ratio on the activity of A(a)B(b)/D-S. W/F = 0.01 g s cm^{-3}.

Figure 8.9 shows the NO conversion profiles as a function of temperature of the AB/D-S catalysts with varying metal loadings and also contains the optimum AB/C-S catalyst as reference. The NO conversion profiles of the optimum AB/C-S and AB/D-S catalysts are practically identical. However, A(1.831)B(0.193)/D-S contains 25.4 wt.% dopants, while A(1.823)B(0.189)/C-S contains only 18.4 wt.%, making the C-supported catalyst more active on a per gram of dopant basis. Figure 8.11 shows the NO conversion profiles of A(1.831)B(0.193)/D-S and A(1.831)B(0.193)/D-IMP. Note that the composition of the IMP-prepared cata-

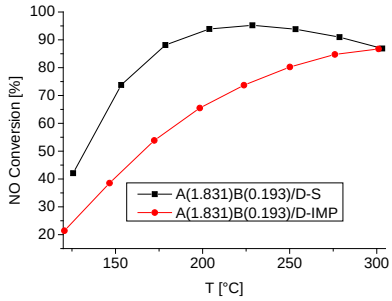

Figure 8.11: Comparison of NO conversions over A(1.831)B(0.193)/D prepared by S and IMP. W/F = 0.01 g s cm^{-3}.

lyst was not optimised. The use of the S method affords much higher conversions, e.g. the IMP-prepared sample needs to be tested at about 225 °C to exhibit the same activity as the S-prepared sample does at 154 °C.

8.3.2 Characterisation of AB/D

- **XRD**
  As in the case of AB/C, A(1.831)B(0.193)/D-S shows only reflections assignable to the support D, meaning AOx and BOx are present in an amorphous form or as crystals below the detection limit of about 5 nm. A(1.831)B(0.193)/D-S showed some reflections assignable to AOx phases.

- **N_2-physisorption**
  The BET surface area of A(1.831)B(0.193)/D-S is about 10 % higher than the one of A(1.831)B(0.193)/D-IMP, thus hardly explaining the difference in activities.

- **NH_3-TPD**
  Figure 8.12 shows the NH_3-TPD profiles of A(1.831)B(0.193)/D-S and the corresponding IMP-prepared catalyst. As in the case of AB/C, the S-prepared sample gives a higher TCD signal over the full temperature range, with the difference being especially pronounced in the region of 425 to 575 °C. Overall, the S-prepared catalyst possesses 67 % more surface acid sites than the IMP-prepared one.

- **H_2-TPR**
  Figure 8.13 shows the H_2-TPR profiles of A(1.831)B(0.193)/D-S and the

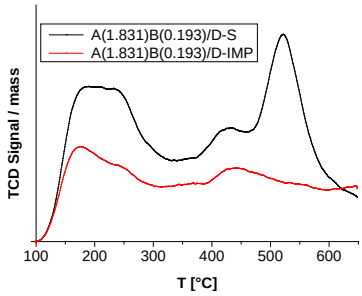

Figure 8.12: NH_3-TPD profiles of AB/D prepared by S and IMP.

corresponding IMP-prepared catalyst. Both samples exhibit an H_2 consumption profile consisting of two peaks. The high temperature peak of the S-prepared sample appears at about 350 °C, which is about 25 °C lower than for the IMP-prepared sample. The low-temperature peak is definetely bigger in the S-prepared case while the high-temperature peaks are of similar size. The average oxidation state of A was determined to be about 0.22 higher in A(1.831)B(0.193)/D-S than in A(1.831)B(0.193)/D-IMP.

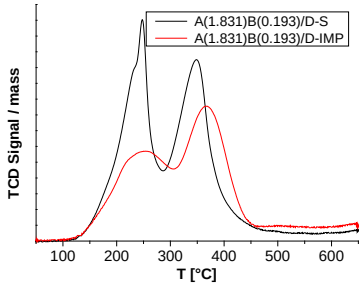

Figure 8.13: H_2-TPR profiles of AB/D prepared by S and IMP.

8.4 Conclusion: AB/C & AB/D

Loading the transition metals A and B onto the support materials C and D using method S results in catalsyts much more active than the impregnation prepared

ones. Furthermore, the metal content can be lowered. The activity enhancement can be explained by an increased number of surface acid sites, increased surface area, reducibility of the metal oxides at lower temperature, reduced crystallinity or formation of sub 5 nm crystals and an increased share of chemisorbed surface oxygen. The last factor could make the catalyst also interesting for the removal of organic volatile compounds (VOC). Since support material C affords the same activity at lower AB loadings than D does, further efforts were directed at AB/C-S.

Chapter 9

Shaping (extrusion) of AB/C

As mentioned in section 2.3.3, deNO$_x$ catalysts need to be shaped into monoliths to be used on an industrial scale because the pressure drop over the catalyst would otherwise be too high [28]. Most of the work related to the shaping of the optimised AB/C-S catalyst was undertaken at CSIC [1] in Madrid.

There are many demands to the binders, here a list of some of the most important ones.

- **Extrudability**
  Very importantly, the binder - catalyst mixture needs to be extrudable, meaning it must be able to exit the extruder and must not collapse afterwards. Not every clay - catalyst combination is extrudable. Sometimes the addition of rheological agents can help to increase the extrudability. In our case, glass fibres were used. To the best of my knowledge, it is very hard to predict the extrudability of a given mixture. Using 20 mL plastic syringes as extruders can help to get a feeling of the extrudability. However, extrusions on a larger scale can both be easier and more difficult than the manual ones.

- **Mechanical stability**
  As a matter of course the extrudates need to have sufficient mechanical stability (breaking strength). The mechanical strength depends strongly on the binder - catalyst combination and can be enhanced by e.g. rein-

[1] Instituto de Catálisis y Petroleoquímica, Consejo Superior de Investigaciones Científicas

forcement with glass fibres. As in the case of extrudability, the mechanical stability can be investigated by preparing syringe extrudates.

- **Activity**
  The catalytic activity of the resulting monolith is another very important parameter and can differ massively from the one of the pure catalyst, see e.g. [150]. Kristensen [23], on the other hand, reported conformation of a V_2O_5/TiO_2 catalyst using sepiolit as binder without any loss in activity. Deactivation can be caused by dilution, surface coverage by binder, pore plugging by binder (reduced surface area) and by chemical poisoning by binder constituents like alkali metals.

- **Pore size distribution**
  The pore size distribution of the monolith is another important parameter determining the effective activity in an actual SCR-plant. A high fraction of micro-porosity is not desirable because it can lead to diffusion limitations [28] and can increase the rate of pore plugging by ammonium sulfates [14]. The porosity can be enhanced by adding pore generating agents to the paste.

9.1 Mechanical strength

Figure 9.1 shows the breaking strength of syringe extrudates containing 30 wt.% binders as a function of the sepiolite - bentonite composition. Both sepiolite and bentonite have recently been successfully used in the conformation of SCR catalysts [23, 150]. Increasing the sepiolite content at the expense of the bentonite content is clearly decreasing the mechanical strength. Adding 1 wt.% of glass fibres slightly enhances the mechanical strength throughout the full range of binder composition. Since the glass fibres also ameliorate the rheological properties, further extrusions all included them. All mixtures are easily extrudable.

Since most of the strength seems to originate from the bentonite component, mixtures of AB/C-S - bentonite which were calcined at 400 and 450 °C were investigated, see figure 9.2. The breaking strength increases over the full range of bentonite content from 15 to 30 wt.%. With increasing bentonite content the extrusions become easier. Increasing the calcination temperature from 400 to 450 °C does not have a strong effect on the strength. However, the activity of the pure AB/C-S is adversely affected by calcination temperatures higher than 400 °C. Therefore, 400 °C was chosen for further syringe- and large scale extrusions. Comparing the breaking strenghts of extrudates containing 15 and 20 wt.% bentonite in figure 9.2 with the corresponding values in figure 9.1 reveals

that sepiolite seemingly does not contribute much to the strength.

Figure 9.3 shows the breaking strength of syringe extrudates containing 40 wt.% clays (bentonite, sepiolite, celite), reinforced with 1 wt.% glass fibres and calcined at 400 °C. Apparently, celite does not add any strength to the extrudate. The extrudate containing both 20 wt.% bentonite and 20 wt.% celite is weaker than the one only containing 20 wt.% bentonite, see figure 9.2. A mixture containing equal parts of bentonite, celite and sepiolite is not significantly more stable than 15 wt.% bentonite on its own. A mixture containing both 20 wt.% bentonite and sepiolite is about as strong as 20 wt.% bentonite on its own, see figure 9.2. Note also that the mixture containing 20 and 10 wt.% bentonite and sepiolite, respectively, is stronger than the one containing 20 wt.% of both clays. This, however, does not necessarily permit the conclusion that addition of 20 wt% sepiolite to 20 wt.% bentonite weakens the extrudates compared to adding just 10 wt% sepiolite because the level of uncertainty in the strength measurements is high.

Extrudates containing 20 wt.% starch combined with either 10 wt.% sepiolite or bentonite were prepared, however, their breaking strenghts were not tested because they seemed to be rather weak and their activity was very low. The same applies to the corresponding extrudates containing P_{123} instead of starch. Extrudates containing various amounts of Montmorillonit K10 were prepared but not stength tested but they seemed rather week and more difficult to extrude than the corresponding bentonite samples.

The mechanic strength data permit the conclusion that use of at least some bentonite is indispensable and that glass fibres should be added to increase the strength and extrudability.

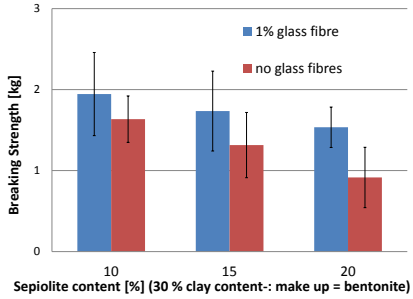

Figure 9.1: Mechanical strength of AB/C-S extrudates with bentonite and sepiolite as binders (30 wt.% in total), optionally reinforced with 1 wt.% glass fibres and calcined at 400 °C

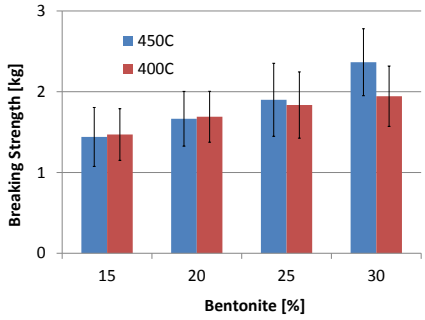

Figure 9.2: Mechanical strength of AB/C-S extrudates with bentonite reinforced with 1 wt.% glass fibres and calcined at 400 and 450 °C

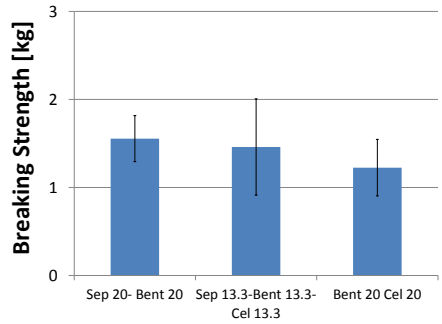

Figure 9.3: Mechanical strength of AB/C-S extrudates calcined at 400 °C using mixtures of bentonite-sepiolite and celite totalling 40 wt.% as binders and reinforced with 1 wt.% glass fibres.

9.2 Activity of syringe extrudates

Table 9.1 gives the NO conversions measured at 150 °C of AB/C-S syringe extrudates. The first line corresponds to the pure AB/C-S catalyst. Addition of the strongly binding clay bentonite comes, as regards activity, at a high price reflected by a drop in NO conversion from 70 to 20.9 %. Using 0.1 molar HNO_3 for the paste preparation does not reduce the level of deactivation. The sepiolite and Montmorillonit-K10 containing catalysts fare much better, both converting about 46 % of NO. Interestingly, the catalyst that contains both 20 % bentonite and 20 % sepiolite is not less active than the one containing only 20 % bentonite and the resulting extrudate is not much less stable according to figures 9.2 and 9.3. Addition of sepiolite to AB/C-S - bentonite mixtures increases the acitivty on a per gram of AB/C-S basis probably by counteracting the deactivating effect of bentonite. The strength data shown in figure 9.1 suggest that a decrease in the bentonite loading should be permissible, potentially greatly enhancing the activity. A binder combination of 15 wt.% Montmorillonit-K10 and 10 wt.% bentonite is not much less active than the one that only contains 20 wt.% Montmorillonit-K10. The use of starch and P_{123} results in rather inactive extrudates. Coupled with their low breaking strength these extrudates are probably not worthy of further investigation.

The reader should note that the activity data presented in table 9.1 was not available in the current form when the binders for the machine-extruded monoliths were selected. The home-made NO_x measuring system, which was available on site furnished spurious data. In the case of the bentonite containing extrudates the measured activities were significantly higher, probably due to some issues with the flow rate. Therefore, breaking strength and extrudability considerations were most influential in the clay selection.

9.3 Characterisation of selected syringe extrudates

The main point of this section is to investigate why bentonite reduces the activity so strongly compared to sepiolite and especially Montmorillonit-K10.

- **Mercury intrusion porosimetry (MIP)**

  One of the more seasoned extrusion experts at CSIC was afraid of bentonite plugging meso pores because he had observed this in C-bentonite extrudates. Therefore, syringe extrudates containing 15, 20 and 25 wt.%

Table 9.1: NO conversions of AB/C-S syringe extrudates at 150 °C. Testing conditions: [NO] = [NH_3] = 1000 ppm; [O_2] = 4 %; [O_2] = 2.3 %; W/F = 0.01 g s cm^{-3} (180 - 300 μm).

binder1		binder 2		NO conversion
	[wt.%]		[wt.%]	[%]
-	-	-	-	70
bentonite	20	-	-	20.9
bentonite	20	-	-	20.9 (a)
Mont-K10	20	-	-	45.5
sepiolite	20	-	-	46.7
bentonite	20	sepiolite	20	21.8
Mont-K10	15	bentonite	10	41.7
sepiolite	10	P_{123}	20	28.8
sepiolite	10	P_{123}	20	28.8
bentonite	10	P_{123}	20	20.5
sepiolite	10	starch	20	19.7
bentonite	10	starch	20	14.4

(a) paste prepared with 0.2 mol L^{-1} HNO_3.

bentonite were characterised by mercury intrusion porosimetry, see figures 9.4 and 9.5. The scale of the axis of ordinates was removed so that the reader can draw no conclusions on the identity of AB/C-S. However; the reader can be assured that the total intrusion volume is similar to the one of an industrial reference catalyst. Increasing the bentonite content from 15 to 25 wt.% comes at the cost of some macroporosity, however, the amount of mesoporosity is practically untouched. The slight variations might be due to different pressures applied during the extrusion. The data give an indication that plugging of pores by bentonite is probably not the major cause of deactivation. This, however, is not a guarantee for the machine-extruded monolith to have the same favourable pore size distribution since the pressure during extrusion is higher.

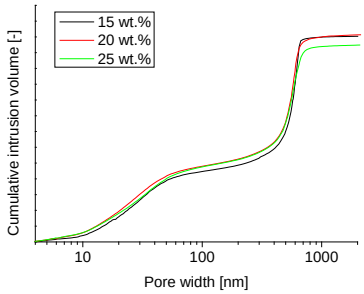

Figure 9.4: Cumulative pore-size distribution determined by MIP of syringe extrudates of AB/C-S using different amounts of bentonite as binder.

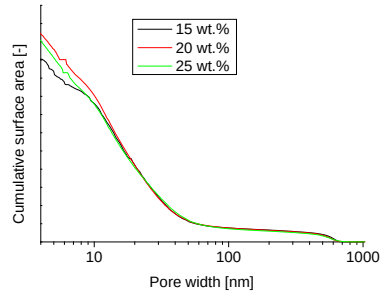

Figure 9.5: Cumulative surface area distribution determined by MIP of syringe extrudates of AB/C-S using different amounts of bentonite as binder.

- **NH_3-TPD**

  The NH_3-TPD profiles reveal that all clays reduce the number of acid sites in the temperature region of up to about 250 °C with bentonite having the strongest impact. The Montmorillonit-K10 and sepiolite containing samples show higher signals in the temperature region of 250 to 450 °C than the AB/C-S while the bentonite containing sample shows a similar profile. The lower activity of the bentonite containing extrudate can in part be explained by its slightly lower acidity in the temperature region of 100 to 450 °C.

- **H_2-TPR**

  Figure 9.7 reveals that the presence of clays has an adverse effect on the reducibility of the active phase. This could be due to clay material covering the surface of AB/C-S as is also suggested by electrophoretic mobility. A similar effect was observed after SO_2 exposure of AB/C-S , see section 10.2. Bentonite and Montmorillonit-K10 cause almost exactly the same shift in reduction temperature; thus H_2-TPR cannot explain the difference in deactivation caused by these two clays.

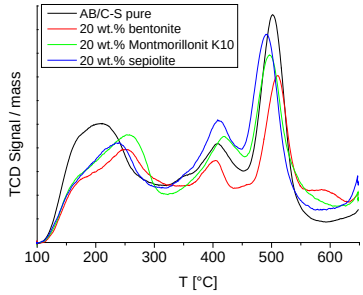

Figure 9.6: NH_3-TPD profiles of syringe extrudates of AB/C-S and pure AB/C-S.

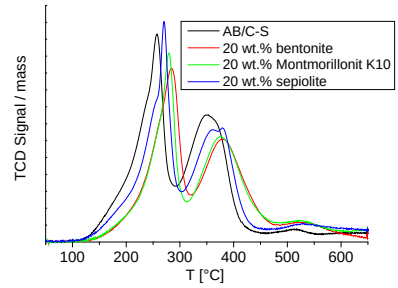

Figure 9.7: H_2-TPR profiles of syringe extrudates of AB/C-S and pure AB/C-S.

- **Electrophoretic mobility**

  The fractional surface coverage of bentonite in the syringe extrudate containing 20 wt. % of it was determined by measuring the zero point charge of the extrudate and the isoelectric points of its components (AB/C-S and bentonite). Bentonite covers about 68 % of the surface even though it only accounts for 20 wt.%. This result nicely reflects the strong loss in activity.

- **Scanning electron microscopy (SEM)**

  Secondary electron images of bentonite, Montmorillonit-K10 and the corresponding 20 wt.% syringe extrudates were taken to assess to what extent the binders are dominating the topography. Unexpectedly, the surfaces of the extrudates resemble very much AB/C-S and not the respective clay component, which was suggested by the electrophoretic mobility measurements. XPS surface analysis could have helped to solve the conundrum and will be peformed shortly.

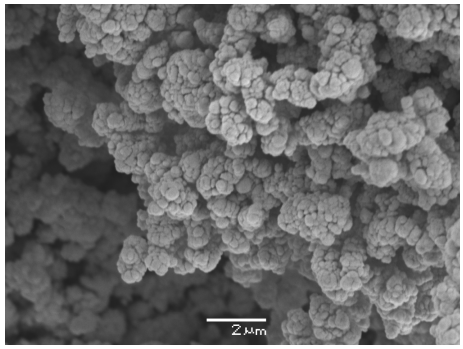

Figure 9.8: Secondary electron image of AB/C-S.

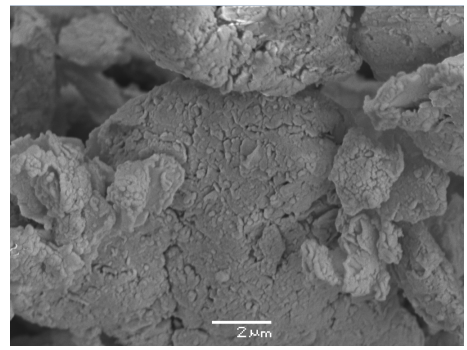

Figure 9.9: Secondary electron image of bentonite.

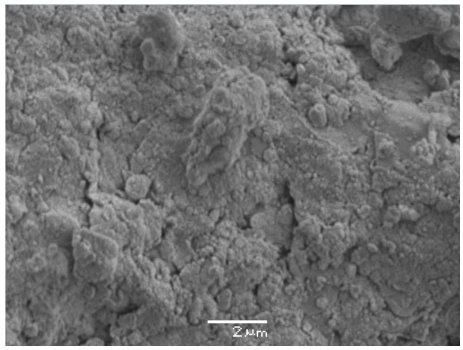

Figure 9.10: Secondary electron image of Montmorillonit-K10.

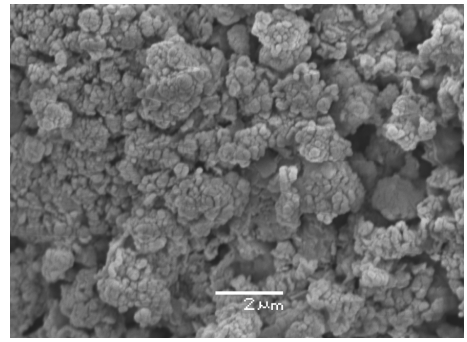

Figure 9.11: Secondary electron image of syringe extrudate of AB/C-S with 20 wt.% bentonite.

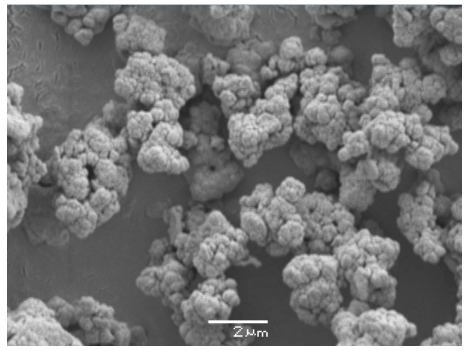

Figure 9.12: Secondary electron image of syringe extrudate of AB/C-S with 20 wt.% Montmorillonit-K10.

- **Raman spectroscopy**

  Raman spectra of AB/C-S and the corresponding 20 wt.% bentonite and Montmorillonit-K10 syringe extrudates were taken. The spectra of the extrudates only differ from the one of AB/C-S in that some additional peaks assignable to the clay components appear and therefore do not help in understanding the different deactivation strengths.

9.4 Large scale extrudates

Two machine extruded monoliths were prepared, one containing 20 wt.% bentonite and 1 wt.% glass fibres (M1) and the other one 12.5 wt.% bentonite, 10 wt.% Montmorillonit-K10 and 1 wt.% glass fibres (M2). In the latter case a mixture containing 10 wt.% of both clays was envisaged, however, the bentonite content had to be increased due to extrudability issues.

Figure 9.13 shows the NO conversions of M1 and M2 as a function of temperature at a water content of 2.3 %. M2 is more active than M1 throughout the full temperature range, which was expected because the Montmorillonit-K10 containing syringe extrudates are more active than the one containing only bentonite. See also figure 10.4 for a comparison in the presence of 20 % H_2O. Figure 9.14 shows the NH_3-TPD profiles of the pure phase, the two machine extrudates and the syringe extruded equivalent of M1. As in the case of the syringe extrudates, M1 and M2 possess significantly fewer acid sites in the temperature region of 100 to 350 °C. At higher temperatuers, especially at around 500 °C, the difference is much less pronounced although the active AB/C-S phase is diluted with clay material which on its own possesses very few acid sites. The desorption profiles of M1 and M2 hardly differ in spite of the clear activity difference, so the deactivation cannot solely stem from a decreased NH_3 adsorption ability. The H_2-TPR profiles of M1 and M2 differ from the one of pure AB/C-S in that both reduction peaks are shifted towards higher temperatures, see figure 9.15 as was observed when examining the syringe extrudates. Decreased reducibility of ABO_x could help to explain the lower activity of the extrudates. However, the reduction peaks of the more active extrudate M2 appear at higher temperatures than those of M1. The pore volumes of M1 and M2 were determined with N_2-physisorption and Hg intrusion porosimetry, see figure 9.16. For pores up to 10 nm in diameter, the N_2-physisorption data were used. Both extrudates exhibit very similar pore-size distributions. Unlike in the case of syringe extrudates (figure 9.5), no plateau is reached at a pore size of about 1000 nm. This is probably due to the fact that in the case of M1 and M2 the MIP measurements were performed on crushed samples. Figure 9.17 shows the cumulative BJH surface area (adsorption branch) of M1 and M2 as a function of the pore size. Compared to the parent AB/C-S sample, both M1 and M2 have less surface area in pores smaller than approximately 6 nm. However, the differences are only about 15 and 22 % for M1 and M2, respectively, hardly explaining the activity losses upon extrusion.

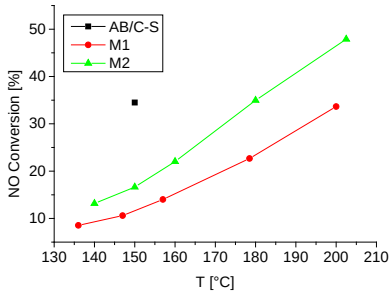

Figure 9.13: NO Conversion over M1 and M2. W/F = 0.005 g s cm^{-3}

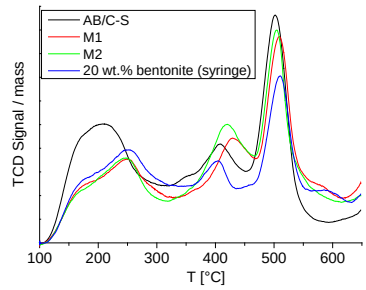

Figure 9.14: NH_3-TPD profiles of machine extrudates of AB/C-S and pure AB/C-S.

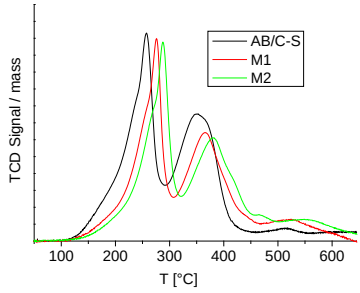

Figure 9.15: H_2-TPD profiles of machine extrudates of AB/C-S and pure AB/C-S.

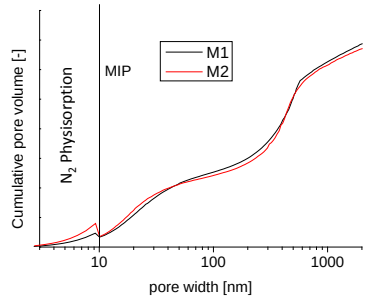

Figure 9.16: Pore volume of machine extrudates of AB/C-S determined by MIP and N_2-physisorption.

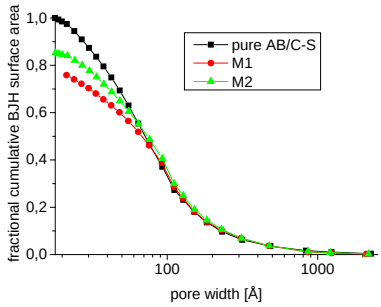

Figure 9.17: Fractional cumulative BJH surface area (adsorption branch) of machine extrudates of AB/C-S and pure AB/C-S as a function of pore size.

9.5 Conclusion: Shaping of AB/C-S

The conformation of AB/C-S is a challenging task. Out of the binders which were investigated, only bentonite added sufficient strength to be used on its own. Sepiolite and Montmorillonit-K10 can only be used in mixtures with bentonite, where they reduce the strength but also the deactivating effect of bentonite. Starch and P_{123} as binders resulted in weak extrudates and low activity. Addition of 1 wt.% glass fibres enhanced the extrudability of bentonite containing mixtures and increased the breaking strength. The high deactivating strength of bentonite can probably be explained by reduced surface acidity of AB/C-S due to the alkaline nature of bentonite. Another explanation could be a disproportionately high surface coverage by bentonite as zeta potential and H_2-TPR measurements suggest. For demonstration purposes and to study the deactivation by e.g. SO_2 in a pilot plant, the machine extrudates M1 and M2 are probably good enough. However, if AB/C-S should be commercialised the extrusion process has to be greatly improved to retain more of the activity.

Chapter 10

H_2O and SO_2 exposure of AB/C and AB/D

The tolerance towards H_2O concentrations of up to 20 % and SO_2 is of utmost importance. Sections 6.7 and 6.8 have shown that both substances can have dramatic effects on the low temperature activity.

10.1 H_2O exposure

The ability of a catalyst to operate at water contents of up to 20 % is of critical importance. The optimised AB/C-S and AB/D-S catalysts were tested in the presence of 20 % H_2O and benchmarked against a VWT sample originating from a commercial tail-end monolith. As in the measurements using only 2.3 % H_2O, optimized AB/C-S and AB/D-S perform essentially equally well, see figure 10.1. Substitution of the support C by D has apparantly no influence on the H_2O tolerance. At the target temperature of 140 - 150 °C, our home-made catalysts definitely do not meet the benchmark and need to be tested at around 170 to 180 °C to do so. Figure 10.2 shows the effect of 10 and 20 % H_2O on the NO conversion over the optimized AB/C-S catalyst. The profiles clearly show that the inhibiting/deactivating effect of H_2O extends clearly beyond 10 % of H_2O. In presence of only 10 % H_2O, the benchmark conversion of around 35 % is reached somewhere between 140 and 160 °C. At 150 °C, Hu et al. [116] observed 40 % NO conversion over their supposedly highly H_2O tolerant HMO-MnO_2 catalyst. However, they used a W/F ratio of 0.03 instead of 0.012 g s cm^{-3}, which demonstrates the clear superiority of our catalyst.

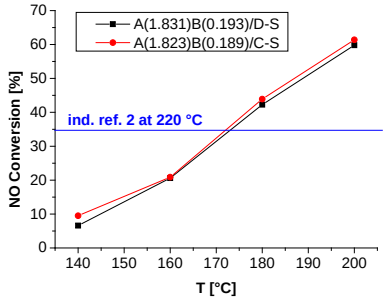

Figure 10.1: Activity of optimised AB/C-S and AB/D-S in presence of 20 % H_2O. W/F = 0.012 g s cm^{-3}.

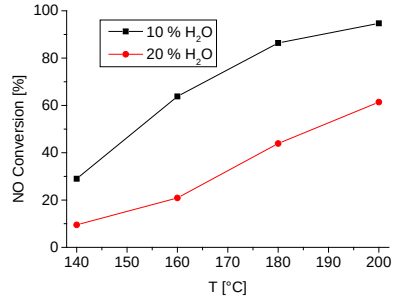

Figure 10.2: Activity of optimised AB/C-S in presence of 10 and 20 % H_2O. W/F = 0.012 g s cm^{-3}.

A meaningful comparison of the activities of the VWT reference catalyst at 220 °C and our catalysts at lower temperatures is difficult, since the presence of a first order reaction with respect to NO is not granted over the full temperature range. Therefore, the amount of reference catalyst to obtain about 90 % NO conversion at 220 °C at a flow rate of 500 mL min^{-1} and in the presence of 20 % H_2O was determined, see figure 10.3, and turned out to be 400 mg.

Figure 10.4 shows the conversion profiles of the optimised AB/C-S, the two machine extrudates M1 and M2 as well as a syringe extrudate of 20 wt.%V_2O_5/TiO_2 with 20 wt.% sepiolite at the adjusted W/F value. At 180 °C, the pure AB/C-S almost meets the benchmark of 90 % NO conversion; however, at 150 °C it only converts 30 %. The machine extrudates M1 and M2 fare even worse, with the former being barely more active than the commerical VWT reference catalyst in the temperature range of 170 to 200 °C and the latter just meeting the benchmark at 200 °C. This reflects the activity of the syringe and machine extrudates measured in the presence of 2.3 % H_2O. So the presence of bentonite and Montmorillonit-K10 seems not to enhance the H_2O tolerance of AB/C-S. It is noteworthy that the syringe extrudate of the 20 wt.%V_2O_5/TiO_2 catalyst is almost as active as the M2 extrudate and, since it is based on vanadia, most probably has the clear advantage of being SO_2 tolerant.

The spent AB/C-S catalyst was characterized with XRD, NH_3-TPD and H_2-

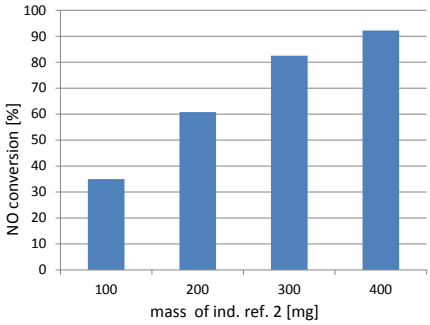

Figure 10.3: NO conversion of commercial VWT catalyst using different m_{cat} at 220 °C, 20 % H_2O and 500 mL min^{-1}.

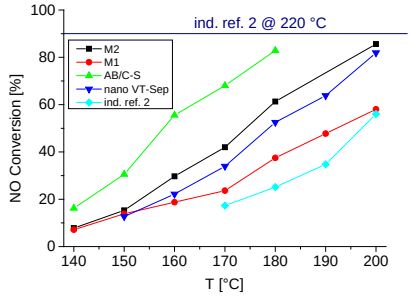

Figure 10.4: Activities of various conformed catalysts in presence of 20 % H_2O. W/F = 0.048 g s cm^{-3}.
.

TPR. The XRD patterns of the fresh and spent catalysts do not differ. This means that H_2O is probably not cleaving A-O-C or B-O-C bonds which could result in crystalline AO_x or BO_x [137]. The NH_3-TPD profiles, see figure 10.5, reveal that upon H_2O exposure the catalyst gains acidity in the temperature region of 150 to 350 °C, which comes at the cost of the stronger acid sites. This could be explained by a transformation of Lewis into Brønsted acid sites, as reported earlier [116, 137]. The H_2-TPR profiles reveal that water exposure causes the reduction peaks to shift to slightly higher temperatures, see figure 10.6, giving another cause for the activity reducing effect of H_2O.

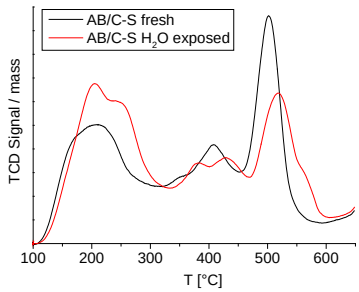

Figure 10.5: NH_3-TPD of fresh and H_2O-exposed AB/C-S.

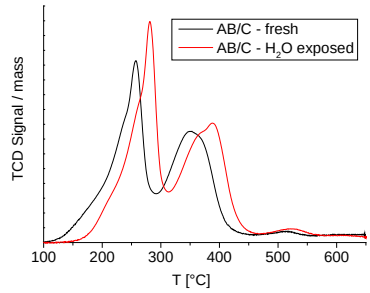

Figure 10.6: H_2-TPR of fresh and H_2O-exposed AB/C-S.

10.2 SO_2 exposure & regeneration

AB/C-S was exposed to a simulated flue gas at 160 °C containing 10 ppm SO_2 and 8 % H_2O at a W/F value of 0.0177 s cm^{-3}. In the absence of SO_2, the NO conversion was 69 %. After 1285 min of SO_2 exposure the conversion dropped to 17.5 % and did not recover after removal of SO_2 from the gas stream. This behaviour was reported several times before [118,130,131,136] and shows that it is most probably not competetive adsorption between SO_2 and NO and/or NH_3 that is causing the strong deactivation.

The spent catalyst was characterized with XRD, TG, N_2-physisorption, XPS, NH_3-TPD, H_2-TPR and FTIR. Regeneration was attempted with water washing, organic base washing, heating to 400 °C and H_2-treatment. For the sake of simplicity, only NO conversions at 150 °C in the presence of 2.3 % H_2O were measured. Fresh, deactivated, heat treated, water washed and base washed samples convert about 60, 10 ,10, 30 and 47 % of NO at a W/F ratio of 0.01 g s cm^{-3}. The reader should note that the base treated sample after drying at around 100 °C only converts about 26 % and needs to be heated to 400 °C for about 1h to reach 47 % conversion. This is probably due to some organic fragments covering the surface.

- **XRD**

The XRD pattern of the SO_2 exposed catalyst shows clear reflections assignable to a sulfate containing A compound in addition to the reflections of the support C. Water and base washing (pH 9) removes these reflections, however, heating to 400 °C and H_2(1%)-treatment at 150 °C are ineffective. This means that not just ammonium sulfates are formed but also metal sulphates which are much harder to remove because of their higher thermal stability and water solubility, excluding heating and water washing as modes of regeneration.

- **FTIR**

Figure 10.7 shows the FTIR spectra of fresh, SO_2 exposed and water washed AB/C-S as well as a A-sulfate reference compound. The SO_2 exposed sample and the A-sulfate reference compound exhibit an absorption band at around 1120 cm^{-1}, which can be assigned to sulfate groups. After washing with water this band disappears and is not present in fresh AB/C-S. Figure 10.8 shows that heat treatment at 400 °C and exposure to 1 % H_2 at 350 °C are ineffective in removing the sulfate groups. Only washing with water and organic base solution at pH 9 are effective.

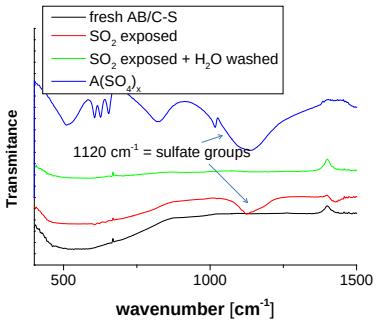

Figure 10.7: FTIR spectra of fresh-, SO_2-exposed and regenerated AB/C-S and A($(SO_4)_4$) reference.

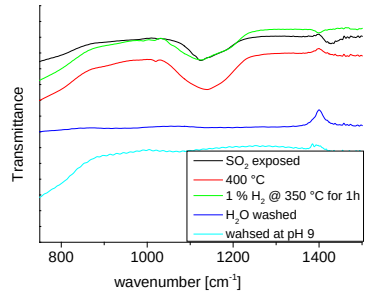

Figure 10.8: FTIR spectra of fresh-, SO_2-exposed and regenerated AB/C-S.

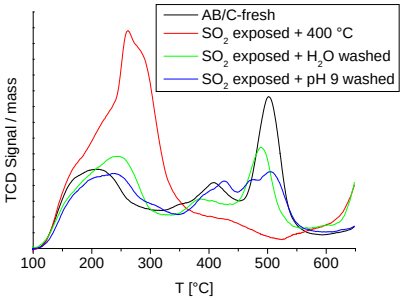

Figure 10.9: NH_3-TPD of fresh-, SO_2-exposed and regenerated AB/C-S.

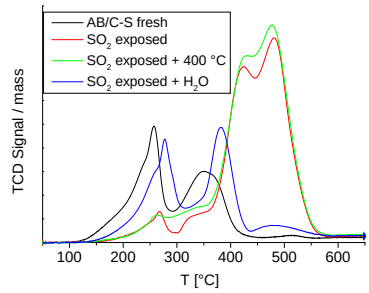

Figure 10.10: H_2-TPR of fresh-, SO_2-exposed and regenerated AB/C-S.

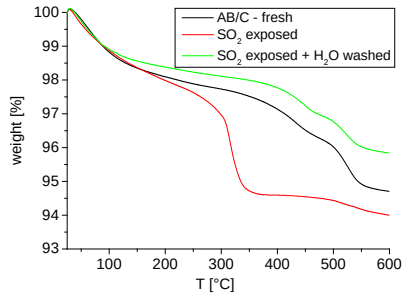

Figure 10.11: TGA of fresh, SO_2 exposed and H_2O washed samples.

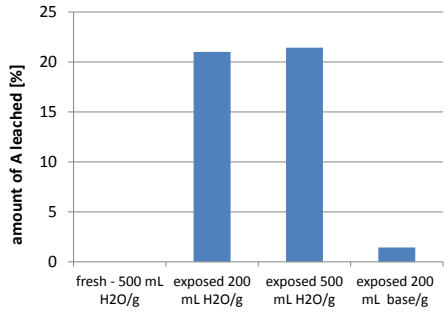

Figure 10.12: Amount of A leached by washing with water and base (pH = 9).

- **NH_3-TPD**

Figure 10.9 shows the NH_3-TPD profiles of the fresh, SO_2 exposed, heated (400 °C), water washed and base washed AB/C-S. SO_2 exposure creates acid sites in the temperature range of 150 to 350 °C, which are probably Brønsted type (sulphate groups). However, in the temperature range between 350 and 600 °C the number of acid sites is strongly diminished, probably by the transformation of strong Lewis sites into weaker Brønsted ones upon sulfation [144]. Water washing removes most of the added acid sites in the range of 150 to 350 °C but only partially reestablishes the lost sites in the range of 350 to 600 °C. The former observation is consistent with the formation of water soluble metal sulfates and the later one could also be explained by the fact that not only SO_2 but also H_2O was present in the flue gas, see section 10.1. Washing with an organic base of pH 9 had a similar effect, however, some more acid sites in the region of up to 350 °C were retained and fewer sites were reestablished in the high-temperature region.

- **H_2-TPR**

Figure 10.10 shows the H_2-TPR profiles of the fresh, SO_2 exposed, heated (400 °C) and water washed AB/C-S. The reduction of the sulphated sample occurs at much higher temperatures compared to the fresh one, probably due to sulphates hindering the reduction process as reported elsewhere [138]. The heated sample behaves practically like the poisoned one. Water washing reestablishes the initial reduction pattern to a big extent, however, both peaks are shifted to higher temperatures, helping to explain; why the initial activity is only partially recovered.

- **N_2-physisorption**

SO_2 exposure causes the BET surface area to decrease by 46 % and water washing recovers it to about 84 % of the fresh sample. If the poisoning was only due to ammonium sulphates one would expect the surface area to fully recover. So the BET results support the theory that SO_2 has a more pronounced effect on the surface than just covering it with ammonium sulphates.

- **TGA**

Figure 10.11 shows the TG profiles of fresh, exposed and water washed AB/C-S. The exposed sample shows a weight loss of about 2.3 wt.% between 300 and 350 °C which can probably be ascribed to the decomposition of $(NH_4)HSO_4$. This weight loss is neither present in the fresh nor in the washed sample, which look very much the same except for the fact that the washed sample shows slightly lower weight loss.

- **XPS**

The sulphur content was determined to be about 2 atomic %. The relative share of chemisorbed oxygen did not decrease. No more information can be given due to the patent issue.

- **Leaching of A - FAA spectroscopy**

The decanted washing liquids were analyzed with FAA spectroscopy to determine the leached amount of A, see figure 10.12. The water washed samples loses more than one fifth of the A metal, irrespective of the amount of water used. The fresh catalyst does not lose any A, demonstrating that the A in the washing liquid is really due to SO_2 exposure. Washing at a pH of 9 greatly reduces the amount of leaching.

10.3 N_2O formation

The N_2O formation over M2 at 200 °C in the presence of 10 % H_2O was below 10 ppm, at a NO inlet concentration of 606 ppm and a NO conversion of more than 90 %. As expected, the formation of N_2O is not a problem in the presence of high water concentrations and therefore needs no further investigation.

10.4 Conclusion: H_2O & SO_2 poisoning

At temperatures below 200 °C, both H_2O and SO_2 dramatically reduce the catalytic activity over AB/C-S. The activity reducing effect of H_2O extends beyond contents of 10 %. In the presence of 20 % H_2O, pure AB/C-S converts only about 30 % of NO; meeting the benchmark under the testing conditions requires an NO conversion of about 90 %. This level of activity is almost reached at 180 °C, which is, according to our collaborators, unacceptably high to be implemented in waste incineration units. Water acts not only as an inhibitor but also has a lasting effect on AB/C-S. Water exposure creates acid sites, which are probably of

Brønsted nature, while the number of the strong acid sites, which are probably of Lewis nature, is reduced. The reducibilty of AB is adversely affected. Substituting the support C with D does not enhance the water tolerance. SO_2 deactivates AB/C-S dramatically even when administered at just 10 ppm and 160 °C. The cause of deactivation is at least in part due to the formation of thermally stable and water soluble A-sulfates, excluding heating and water washing as modes of regeneration. Use of an organic base at pH 9 instead of water strongly reduces leaching of A and reestablishes the catalytic activity to a large extent after heat treatment at 400 °C. However, frequent base washing might be too interruptive to be implemented on an industrial scale. Because SO_2 seems to be an insurmountable obstacle to the implementation of AB/C-S in SCR units handling off-gases containing even very low amounts of SO_2, we decided to investigate alternative, vanadia based catalysts. Due to the very high content of chemisorbed oxygen in AB/C-S, it should be tested for VOC abatement.

Chapter 11

$V^{-}Fe/TiO_2$-SG & $V^{-}W/TiO_2$ - DP

11.1 $V^{-}Fe/TiO_2$-SG

Because of the strong activity enhancement brought about by doping VW/TiO_2 with Fe [149], we investigated the effect of Fe on sol-gel prepared V_2O_5/TiO_2 [25]. Addition of Fe was achieved by impregnating the calcined $V(0.17)/TiO_2$ with iron nitrate (pc), impregnating the dried $V(0.17)/TiO_2$ with iron nitrate, followed by calcination (npc) or by adding the iron precursor during the gel formation (sg). The molar ratio of Fe to Ti is 0.029, making the total dopant loading 0.199, which is slightly below the optimum one of V/TiO_2 of 0.22. The calcined catalysts were characterised with N_2-physisorption, NH_3-TPD and XRD. Syringe extrudates containing 20wt.% sepiolite as binder were used for the activity measurements. Kristensen [23] has recently shown that syringe extrudates of $V(0.22)/TiO_2$ containing 20 wt.% sepiolite are as active as the parent catalyst. We made the same observation on $V(0.17)Fe(0.029)/TiO_2$-npc.

The fractionated syringe extrudates were tested in the presence of 20 % H_2O, under the same conditions as used in the benchmarking study in section 10.1, see figure 11.1. None of the iron containing catalysts is as active as $V(0.22)/TiO_2$. The npc sample is about as active as the iron free $V(0.17)/TiO_2$, while the sg and especially the pc sample are less active at 190 and 200 °C. Figure 11.2 shows the NH_3-TPD profiles of the sepiolite free samples and table 11.1 gives the number of acid sites, BET surface areas and TiO_2 particle sizes. The most active

Fe containing sample, V(0.17)Fe(0.029)/TiO_2-npc, possesses the highest number of acid sites, highest surface area and smallest particle size. This explains why V(0.17)Fe(0.029)/TiO_2-npc is more active than the corresponding pc and sg samples. Even though addition of iron to V(0.17)/TiO_2 increases its surface area by 32 % and the number of acid sites by 21 %, there is no increase in activity. The formation of crystalline phases upon Fe addtion is unlikely, because XRD patterns do not exhibit reflections other than those assignable to anatase TiO_2, see figure 11.3. XPS analysis could give valuable information on the bonding and dispersion situations of V and Fe and will probably be conducted as part of a future in-depth study, which will also include the effect of different iron and vanadia loadings as well as the effect of other metals like e.g. tungsten.

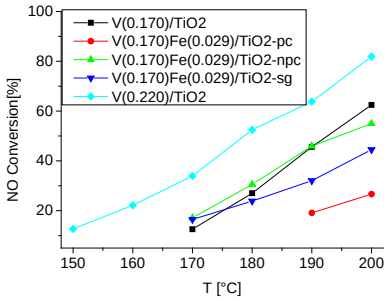

Figure 11.1: NO convesions over VFe/TiO_2 in the presence of 20 % H_2O. Samples derived from syringe extrudates containing 20 wt.% sepiolite. W/F = 0.012 g s^{-1} cm^{-3} .

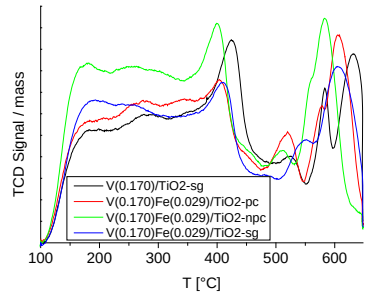

Figure 11.2: NH_3-TPD profiles of VFe/TiO_2 (sepiolite free).

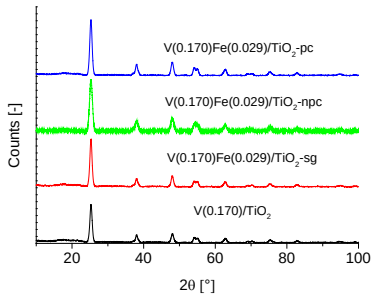

Figure 11.3: XRD patterns of sepiolite free VFe/TiO_2.

Table 11.1: Properties of VFe/TiO_2. Number of acid sites was obtained by peak integration from 100 to 650 °C. Particle size was calculated with the Scherrer equation using the peak at $2\theta = 25.3$ °.

catalyst	desorbed NH_3 [μmol g^{-1}]	BET surface area [m^2g^{-1}]	particle size [nm]
V(0.17)/TiO_2	1523	126	13.5
V(0.17)Fe(0.029)/TiO_2-sg	1548	148	13.6
V(0.17)Fe(0.029)/TiO_2-npc	1848	166	10.8
V(0.17)Fe(0.029)/TiO_2-pc	1526	117	13.1

11.2 V–W/TiO_2-DP

The activity of 3 wt.% V_2O_5 - 10 wt.% WO_3/TiO_2 can be increased by about 30 % by using the deposition precipitation method with ammonium carbamate as precipitating agent instead of the commonly used impregnation method [151]. The activity enhancement is constant throughout the temperature range of 200 to 450 °C and is ascribed to the altered acidic and redox properties of vanadium. Combining the use of the deposition precipitation method with the addition of another metal like e.g. iron [149] might give even better results. This study showed that there is still some potential to be reaped in vanadium based SCR catalysts.

Chapter 12

Conclusion & Outlook

The objective of this thesis has been to investigate alternative catalysts and technologies which are able to handle the challenging off-gases of biomass- and waste-fired units.

The first part of this work dealt with the potassium tolerance of ethanol- and propene-SCR using Ag/Al_2O_3 as catalyst and was targeted only at the biomass-firing. The hope that HC-SCR is less sensitive to potassium has been in vain. The $deNO_x$ activity over 3 wt.% Ag/Al_2O_3 used in ethanol-SCR is practically as much reduced as in the NH_3-SCR case over the traditional VWT catalyst. Furthermore, poisoning with potassium leads to unselective oxidation of the hydrocarbons instead of NO reduction. This means, that no matter how low the space velocity in the SCR unit, only a low NO conversion can be obtained. HC-SCR has two more major drawbacks. First, the relatively active Ag/Al_2O_3 catalyst system is very sensitive to SO_2, even at concentrations as low as 20 ppm. Second, the price of the reductant furnishing the highest activity, ethanol, is about 10 times as high as the price of ammonia, making the cost differential between the two reductants a multiple of the catalyst cost. Due to these three reasons, unselective reductant oxidation, SO_2 sensitivity and high cost of hydrocarbons, we conclude that ethanol-SCR is unfit for biomass-fired power plants.

The advantage of the tail-end position is the cleanliness of the flue-gas, the major drawback is the need for re-heating the flue gas from the outlet-temperature of the flue gas desulfurization unit to about 200 - 250 °C. Our tasks was to develop a catalyst to be at least as active as the commercial VWT one is at 220 °C in the presence of 20 % H_2O. We tested a number of manganese based catalyst and a secret binary-, supported transition metal catalyst. At a water concentration

of 10 %, the latter meets the benchmark at 150 °C; however, high water concentrations (20 %) lead to strong inhibition and deactivation resulting in the need to operate at about 180 °C in order to reach the benchmark.

SO_2 exposure at 160 °C resulted in strong deactivation by the formation of metal sulfates. The only method of regeneration that yielded encouraging results was base washing which, however, might be hard to implement under industrial conditions.

Two stable monoliths have been successfully produced by extrusion using bentonite and Montmorillonit-K10 as binders. Glass fibres added strength and made the extrusion process easier. Much of the SCR activity was lost upon extrusion, probably due to loss of acid sites and by the clay materials covering the surface of the catalyst material. The knowledge created regarding the shaping might also be of use to applications other than SCR.

We conclude that the catalyst can probably only be used in SO_2 free applications e.g. nitric acid plants. If used at low temperature and high water concentrations, the catalyst needs to be made more hydrophobic by e.g. coating with polymers. Furthermore, the catalyst might have some potential in the removal of volatile organic compounds (VOC) due to its high level of chemisorbed surface oxygen. Preliminary tests are under planning.

Future research on low-temperature deNO_x should not ignore vanadia based catalysts, because of their high SO_2 tolerance. The preparation of VWT using the deposition precipitation method showed that this class of catalysts still has some optimisation potential.

Bibliography

[1] Bosch, H.; Janssen, F. Catal. Today (1988), 2, 369 - 379

[2] Roy,S;Hedge, M; Madras, G. Appl. Energy (2009), 86, 2283 - 2297

[3] Health Aspects of Air Pollution with Particulate Matter, Ozone and Nitrogen Dioxide, WHO, (January 2003) page 30

[4] Ann M. Middlebrook and Margaret A. Tolbert; " STRATOSPHERIC OZONE DEPLETION" (2000); UNIVERSITY SCIENCE BOOKS; SAUSALITO, CALIFORNIA

[5] Unece EB. Protocol to abate acidification, eutrophication and ground-level ozone, 30 November, 1999

[6] Finansministeriet. Aftaler om finansloven 20 November, 2012

[7] Zhao, B; Wang, S; Xu, J; Fu, K; Hao,J; He,K; Cofala,J; Amann, M., Atmos. Chem. Phys. Discuss. (2013), 13, 16047 - 16112

[8] Ando, Jumpei; "NOx Abatement for Stationary Sources in Japan"; (1979); EPA - 600/7 - 79 - 205 EPA Contract No. 68 - 02 - 2161

[9] Bosch, H.; Janssen, F.; Catal. Today (1988), 2, 381 - 401

[10] Tayyeb Javed, M.; Irfan, N.; Gibbs, B.M., J. Environ. Manage. (2007), 83, 251 - 289

[11] Bae, S. W.,Roh S. A.; Kim, S. D. Chemosphere (2006), 65, 170 - 175

[12] Heck, R.M. Catal. Today (1999), 53, 519 - 523

[13] Parvulesco, V; Grange, P.; Delmon, B., Catal. Today (1998), 46, 233 - 316

[14] Joakim Reimer Thgersen, Hans Jensen-Holm, "Limitations in reduced load SCR operation" (2012); VGB PowerTech Tätigkeitsbericht

[15] Burke, J.M. et al., "Ammonium Sulfate and Bisulfate Formation in Air Preheaters" (1982); EPA - 600/S7 - 82 - 025a

[16] Jansen, F.; Meijer, R., Catal Today (1993), 16, 157 - 185

[17] Hans-Ulrich Hartenstein and Anthony Licata "MODERN TECHNOLOGIES TO REDUCE EMISSIONS OF DIOXINS AND FURANS FROM WASTE INCINERATION" (page 99),Babcock Borsig Power, DB Riley Worcester, MA

[18] Goemans M.; Clarysse P.; Johannes J.; De Clercq P.; Lenaerts S.; Matthys K.; Boels K. Chemosphere (2003), 50, 489 - 497

[19] Forzatti, P. Appl. Catal. A (2001), 222, 221 - 236

[20] Busca, G.; Lietti, L; Ramis, G; Berti, F., Appl. Catal. B (1998), 18, 1 - 36

[21] Lietti, L.; Nova, I.; Ramis, G.; DallAcqua, L.; Busca, G.; Giamello, E.; Forzatti, P.; Bregani, F., J. Catal. (1999), 187, 419 - 435

[22] Bulushev, D.A.; Kiwi-Minsker, L.; Zaikovskii,V.I.; Renken, A., J. Catal. (2000), 193, 145 - 153

[23] Steffen Buus Kristensen "deNO_x catalysts for biomass combustion" (2013); DTU Department of Chemistry, Kgs. Lyngby Denmark

[24] Went, G.T.; Leu, L.J.; Rosin, R. R.; Bell, A. T. J. Catal. (1992), 134, 492 - 505

[25] Kristensen, S.B.; Kunov-Kruse, A.J.; Riisager, A.; Rasmussen, S.B.; Fehrmann, R. J. Catal (2011), 284, 60 - 67

[26] Dumesic, J.A.;Topse, N.;Topse, H.; Chen, Y.; Slabiak, T. J. Catal. (1996), 163, 40 9- 417

[27] Inomata, M.; Miyamoto, A.; Murakami, Y. J. Catal (1980), 62, 14, 0- 148

[28] Tranconi, E.; Beretta, A. Catal. Today (1999), 249, 249 - 258

[29] Ruggeri, M.P.; Nova, I.; Tronconi, E. J. Chem. Eng. (2012), 207, 57 - 65

[30] Jeswani, H.K.; Gujba, H.; Ayapagic, A., Waste Biomass Valor (2011),2, 33 - 42

[31] "Wood: The fuel of the future: Environmental lunacy in Europe"; (2013, April 6th). The Economist.

[32] Hansson, J.; Berndes, G.; Johnsson, F.; Kjärstad, J., Energy Policy (2009) 37, 1444 - 1455

[33] "Biomass 2020: Opportunities, Challenges and Solutions" (October 2011), Union of the Electricity IndustryEURELECTRIC, Boulevard de lImpratrice, 66 bote 2, 1000 Brussels, Belgium

[34] Gottwald, U.; Monkhouse, P.; Wulgaris, N.; Bonn, B., Fuel Process. Technol. (2002), 75, 215 - 226

[35] Oleschko, H.; Schimroczyk, A.; Lippert, H. Mller, M., Fuel (2007), 86, 2275 - 2282

[36] Wiles, C. C., J. Hazard. Mater. (1996), 47, 325 - 344

[37] Zheng, Y.; Jensen, A.D.; Johnsson. J.E., Appl. Catal. B (2005), 60, 253 - 264

[38] Kling, Å.; Andersson, C.; Myringer, Å.; Eskilsson, D.; Järås, S.G., Appl. Catal. B (2007), 69, 240 - 251

[39] Chen, J.; Yang, R.T.; J., Catal. Today (1999), 125, 411 - 420

[40] Calatayud, M.; Minot, C., J. Phys. Chem. C (2007), 111, 6411 - 6417

[41] Martiin, C.; Martin, I.; del Moral, C.; Rives,V., J. Catal. (1994), 146, 415 - 421

[42] Wieck-Hansen, K.; Overgaard, P.; Larsen, O. Biomass Bioenergy (2000), 19, 39 - 47

[43] Huang, Z.; Gu, X.; Wen, W.; Hu, P.; Makkee, M.; Lin, H.; Kapteijn, F.; Tang, X., Angew. Chem. Int. Ed. (2013), 52, 660 - 664

[44] Jensen-Holm et al. Power-Gen Europe (2009) Haldor Topse

[45] Zheng, Y.; Jensen, A.D.; Johnsson. J.E., Ind. Eng. Chem. Res. (2004), 43, 941 - 947

[46] Lietti, L.; Foryatti, P.; Ramis, G.; Busca, G.; Bregani, F.; Appl. Catal. B (1993), 3, 13 - 35

[47] Kamata H.; Takahashi K.; Odenbrand C.U.I., J. Mol. Catal. A (1999), 139, 189

[48] van Hengstum, A.J.; Pranger, J.; van Ommen, J.G.; Gellings, P. J., Appl. Catal. (1984), 11, 317 - 330

[49] Lewandowska, A.E.; Clatayud, M.; Lozano-Diz, E.; Minot, C.; Banarez, M.A., Catal. Today (2008), 139, 209 - 213

[50] Kustov, A.; Rasmussen, S.; Fehrmann, R.; Simonsen, P. Appl., Catal. B (2007), 76, 9 - 14

[51] Due-Hansen, J.; Kustov, A.L.; Rasmussen, S.B., Appl. Catal. B (2006), 66, 161 - 167

[52] Putluru, S.S.R; Kristensen, S.B.; Duehansen, J; Riisager, A., Catal. Today (2012), 184, 192 - 196

[53] Putluru, S.S.R; Jensen, A.D.; Riisager, A.; Fehrmann, R., Catal. Sci. Technol. (2011), 1, 631 - 637

[54] Putluru, S.S.R.; Mossin, S.; Riisager, A; Ferhmann, R., Catal. Today (2001), 176, 292

[55] Thomassen, P.; Kunov-Kruse, A.J.; Mossin, S.; Kolding, H.; Kegns, S.; Riisager, A.; Ferhmann, R. ECS Transactions (2012), 50 (11), 433 - 442

[56] Liu Z.; I.S. Woo, Catalysis Reviews (2006), 48, 43 - 89

[57] Rao, K.N.; Ha, H.P., Appl. Catal. A (2012), 433, 162 - 169

[58] Son, I.H.; Kim, M.C.; Koh, H.L.; Kim, K.L., Catal. Lett. (2001), 75, 191 - 197

[59] Ukisu, Y.; Sato S.; Muramatsu G.; Yoshida K., Catal. Lett. (1992), 16, 11 - 16

[60] Burch, R.; Breen, J.P.; Meunier, F.C., Appl. Catal. B (2002), 39, 283 - 303

[61] Akama, H.; Matsushita, K., Catal. Surv. Jpn. (1999), 3, 139

[62] Gilot, P.; Guyon, M.; Stanmore, B.R., Fuel (1997), 76, 507

[63] Houel, V.; James, J.; Millington, P.; Pollington, S.; Poulston, S.; Rajaram, R.; Torbati, R., J. Catal. (2005), 230, 150 157

[64] He, H.; Zhang, X.; Wu, Q.; Zang, C.; Yu, Y., (Catal Surv Asia 2008), 12, 38 - 55

[65] Fritz, A.; Pitchon, V., Appl. Catal. B (1997), 13, 1 - 25

[66] Lee, J.;Song, S.; Chun. K.W., Ind. Eng. Chem. Res. (2010), 49, 3553 - 3560

[67] Tamm, S.; Ingelsten, H.H.; Palmqvist A.E.C., J. Catal. (2008), 255, 304 - 312

[68] He, H.; Yu, Y., Catal. Today (2005), 100, 37 - 47

[69] Hong, H.E.; Yunbo, Y.; Qiang W., Chin. J. Catal. (2006), 27, 993 - 998.

[70] Meunier, F.C.; Ukropec, R.; Stapleton, C.; Ross, J.R.H., Appl. Catal. B (2001), 30, 163 - 172

[71] Meunier, F.C.; Ross, J.R.H., Appl. Catal. B (2000), 24, 23 - 32

[72] Bethke, K.A.; Kung, H.H., J. Catal. (1997), 172, 93 - 102

[73] Meunier, F.C.; Breen, J.P.; Zuzaniuk, V.; Olsson, M.; Ross, J. R. H., J. Catal. (1999), 187, 493 - 505

[74] Musi, A.; Massiani, P.; Brouri, D.; Trichard, J.M.; Da Costa, P., Catal. Lett. (2009), 128, 25 - 30

[75] Breen, J.P.; Burch, R.; Hardacre, C.; Hill, C.J., Phys. Chem. B (2005), 109, 4805-4807

[76] Sazama P.; Capek L.; Drobn H.; Sobalk Z.; Dedecek J.; Arve K.; Wichterlová B., J. Catal. (2005), 232, 302 - 317

[77] Kim, M.K.; Kim, P.S.; Baik, J.H.; Nam, I.; Cho, B.K.; Oh, S.H., Appl. Catal. B (2011), 105, 1 - 14

[78] Shimizu, K.I.; Tsuzuki, M.; Satsuma, A., Appl. Catal. B: Environmental (2007), 71, 80 - 84

[79] Shimizu, K.; Sastuma, A.; Tadashi, H., Appl. Catal. B (2000), 25, 239 - 247

[80] Abe, A.; Aoyama, N.; Sumiya, S.; Yoshida, K., Catal. Lett. (1998), 51, 5 - 9

[81] Doronkin, E.D.; Khan, T.S.; Bligaard, T.; Forgel, S., Appl. Catal. B (2012), 117, 49 - 58

[82] Park, P.W.; Boyer, C.L., Appl. Catal. B (2005),59, 27 - 34

[83] Shimizu, K.; Higashimata, T.; Tsuzuki, M.; Sastuma, A., J. Catal. (2006), 239, 117 - 124

[84] Satokawa, S.; Shibata, J.; Shimizu, K.; Satsuma, A.; Hattori, T., Appl. Catal. B. (2003), 42, 179 - 186

[85] Li. J.; Zhu, Y.; Ke, R.; Hao, J., Appl. Catal. B (2008), 80, 202 - 213

[86] Jagtap, N.; Umbarkar, S.B.; Miquel, P.; Granger, P.; Dongare, M.K., Appl. Catal. B (2009), 90, 416 - 425

[87] Svachula, J.; Ferlazzo, N.; Forzatti, P.; Tronconi, E., Ind. Eng. Chem. Res. 1993,32, 1053 - 1060

[88] Kim, P.S.; Kim, M.K.; Cho, B.K.; Nam, I., Oh, S.H., J. Catal. (2013), 301, 65 - 76

[89] Zhang, X.; He, H.; Ma, Z., Catal. Comm. (2007), 8, 187 - 192

[90] Eränen, K.; Klingstedt, F.; Arve, K.; Lindfors, L.; Murzin, D.Y., J. Catal. (2004), 227, 328

[91] Shimizu K.; Hashimoto M.; Shibata, J.; Hattori, T.; Satsuma, A., Catal. Today (2007), 126, 266 - 271

[92] Satokawa, S.; Shibata, J.; Shimizu, K.; Satsuma, A.; Hattori, T.; Kojima, T., Chem. Eng. Sc. (2007), 62, 5335 - 5337

[93] Satokawa, S.; Shibata, J.; Shimizu, K.; Satsuma, A.; Hattori, T., Appl. Catal. B (2003), 42, 179 - 186

[94] Wang, J.; He, H.; Feng, Q.; Yu, Y.; Yoshida, K.; Catal. Today (2004) 93, 783 - 789

[95] Seker, E.; Cavataio, J.; Gulari, E.; Lorpongpaibon, P.; Osuwan, S., Appl. Catal. A (1999),183, 121 - 134

[96] Schill, L.; Putluru, S.S.R.; Jacobsen, C.F.; Hansen, C.H.; Fehrmann, R.; Jensen, A.D., Appl. Catal. B (2012), 127, 323 - 329

[97] Maaskant, O.L.; Miggelbrink, M., "A Catalytic System for NO_x and Dioxin Removal, applications, performance and costs", Conference on Nox/NO2 control techniques, 21/22 March 2001, Paris.

[98] Hatton, J.; Bulionnis, P.; "A case study of the selective catalytic reducution (SCR) system at the Algonquin power energy-from-waste facility", NAWTEC16 (2008)

[99] Avgouropoulos, G.; Oikonomopoulos, E.; Kanistras, D.; Ioannides, T., Appl. Catal. B (2006), 65, 62 - 69

[100] Fu, M.; Li, C.; Lu, P.; Qu, L.; Zhang, M.; Zhou, Y.,; Yua, M.; Fange, Y., Catal. Sci. Technol. (2014), 4, 14 - 25

[101] Li, J.; Changa, H.; Maa, L.; Haoa, J.; Yangb, R.T., Catal. Today (2011), 175, 147 - 156

[102] Feng, Y.S.; Liu, S.G.; Chen, C.W.; Zhao, H.Y.; Xu, Y.S., Applied Mechanics and Materials (2013), 320, 629 - 638

[103] van der Grift, C.J.G.; Woldhuis, A.F.; Maaskant, O.L.,Catalysis Today (1996), 27, 23 - 27

[104] Li, K.; Tang, X.; Yi, H.; Ning, P.; Kang, D.; Wang, C., Chem. Eng. J. (2012), 192, 99 - 104

[105] Chen, Z.; Yang, Q.; Li, H.; Li, X.; Wang, L.; Tsang, S.C, J. Catal. (2010), 276, 56 - 65

[106] Chen, Z.; Wang, F.; Li, H.; Yang, Q.; Wang, L.; Li, X., Ind. Eng. Chem. Res. (2012), 51, 202 - 212

[107] Hua, L.; Xiaolong, T.; Honghong, Yi.; Lili, Y.; J. Rare Earth (2010), 28, 64 - 68

[108] Qi, G.; Yang, R.T., J. Catal. (2003), 217, 434 - 441

[109] Pea, D.A.; Uphade, B.S.; Smirniotis, P.G., J. Catal, (2004), 221, 421.

[110] Thirupathi, B.; Smirniotis, P.G., J. Catal, (2012), 288, 74

[111] Kapteljn, F.; Smgoredjo, L.; Andremli, A., Appl. Catal. B (1994), 3, 173 - 169

[112] Kang, M.; Park, E.D.; Kim, J.M.; Yie, J.E., Appl. Catal. A (2007), 327, 261 - 269

[113] Singoredjo, L.; Korver, R.; Kapteijn, F.; Mouhjn, J., Appl. Catal. B (1992), 1, 297- 316

[114] Tang, X.F.; Li, J.H.; Sun, L.A.; Hao, J.M., Appl. Catal. B (2010), 99, 156.

[115] Tang, X.; Hao, J.; Xu, W.; Li, J., Catal. Comm. (2007), 8, 329 - 334

[116] Hua, P.; Huanga, Z.; Huab, W.; Gua, X.; Tanga, X., Applied Catalysis A (2012), 437 438, 139 - 148

[117] Wang, C.; Sun, L.; Cao, Q.; Hu, B.; Huang, Z.; Tang, X., Appl. Catal. B (2011), 101, 598 - 605

[118] Casapu, M.; Krcher, O.; Elsener, M., Appl. Catal. B (2009), 88, 413 - 419

[119] Chang, H.; Li, J.; Chen, X.; Ma, L.; Yang, S.; Schwank J.W.; Hao, J., Catal. Comm. (2012), 27, 54 - 57

[120] Kang, M.; Park, E.D.; Kim, J.M; Yie, J.E., Catal. Today (2006), 111, 236 - 241

[121] Smirniotis,P.G.; Sreekanth, P.M.;Pena, P.A.; Jenkins, R.G., Ind. Eng. Chem. Res. (2006), 45, 6436 - 6443

[122] Li, J.; Chen, J.; Ke, R.; Luo, C.; Hao, J., Catal. Commun. (2007), 8, 1896.

[123] Wu, Z.; Jiang, B.; Liu, Y.; Zhao, W.; Guan, B., Journal of Hazard. Mater. (2007), 145, 488 - 494

[124] Qi, G.; Yang, R.T., Appl. Catal. B (2003), 44, 217 - 225

[125] Z. Wu, B. Jiang, Y. Liu, Appl. Catal. B, 79 (2008), 347

[126] Jiang, B.; Liu, Y.; Wu, Z., Journal of Hazard. Mater. (2009), 162, 1249 - 1254

[127] Kima, Y.J.; Kwona, H.J.; Nama, I.S.; Choungb, J.W.; Kil, J.K.; Kimb, H.J.; Chac, M.S.; Yeoc, G.K., Catal. Today (2010), 151, 244 - 250

[128] Schill, L.; Putluru, S.S.R.; Fehrmann, R.; Jensen, A.D., Catal. Lett. (2014), 144, 395 - 402

[129] Wana, Y.; Zhaoa, W.; Tanga, Y.; Li, L.; Wanga, H.; Cuia, Y.; Gua, J.; Li, Y.; Shi, J., Appl. Catal. B (2014), 148, 114 - 122

[130] Gao, X.; Jiang, Y.; Zhong, Y.; Luo, Z.; Cen, K., Journal of Hazard. Mater. (2010), 174, 734 - 739

[131] hongyi, S.; Yufeng, H.; Jianming, X.; Xiaoming, W.;Weiping, L., J. RARE EARTH (2012), 30, 676 - 682

[132] Jin, R.; Liu, Y.; Wu, Z.; Wang, H.; Gu, T., Catal. Today (2010), 153, 84 - 89

[133] Wu, Z.; Jin, R.; Liu, Y.; Wang,. H.; Catal. Commun. (2008), 9, 2217 - 2220

[134] Boxiong, S.; Yan, Y.; Hongqing, M.; Ting, L.,Chin. J. Catal. (2011), 32, 1803 - 1811

[135] Jin, R.; Liu, Y.; Wu, Z.; Wang, H.; Gu, T., Chemospere (2010), 78, 1160 - 1166

[136] Shen, B.; Liu, T.; Zhao, N.; Yang, X.; Deng, L., J. Environ. Sci. (2010), 22, 1447 - 1454

[137] Kijlstra, W.S.; Daamen, J.C.M.L.; van de Graaf, J.M.; van der Linden, B.; Poels, E.K.; Bliek, A., Appl. Catal. B (1996), 7, 337 - 357

[138] Kijlstra, W.S.; Biervliet, M.; Poels, E.K.; Bliek, A., Appl. Catal. B (1998), 16, 327 - 337

[139] Yu, J.; Guo, F.; Wanga, Y.; Zhu, J.; Liu, Y.; Su, F.; Gao, S.; Xu, G.; Appl. Catal. (2010), 95, 160 - 168

[140] Lee, S.M.; Park, K.H.; Hong, S.C., Chem. Eng. J. (2012), 195, 323 - 331

[141] Yang, S.; Wanga, C.; Li, J.; Yanb,N.; Maa, L.; Chang, H., Appl. Catal. B (2011), 110, 71 - 80

[142] Tong, H.; Dai, J.; He, Y.; Tong, Z., Environ. Technol. (2011), 32, 891 - 900

[143] Wu, Z.; Jin, R.; Wang, H.; Liu, Y.,Catal. Commun. (2009), 10, 935 - 939

[144] Jiang, B.Q.; Wu, Z.B.; Liu, Y.; Lee, S.C.; Ho, W.K., J. Phys. Chem. C (2010), 114, 4961 - 4965

[145] W U, Z.; J I A N G, Q.; L I U, Y.; W A N G, H.; J I N, R., Environ. Sci. Technol. (2007), 41, 5812 - 5817

[146] Li, Y.; Batavio, P.J.; Armor, J.N., J. Catal. (1993), 142, 561 - 571

[147] Nagaishi, T.; Ishiyarna, S.; Matsumoto, M.; Yoshinaga, S., J. Therm. Anal. (1984), 29, 121 - 129

[148] Gu, T.; Liu, Y.; Weng, X.; Wang, H.; Wu, Z., Catal. Commun. (2010), 12, 310 - 313

[149] Gao, R.; Zhang, D.; Liu,X.; Shi, L.; Maitarad,P.; Li, H.; Zhangb, J.; and Caob, W., Catal. Sci. Technol. (2013), 3, 191

[150] Søren B. Rasmussen, Johannes Due-Hansen, MalcolmYatesa, Mirza Villaroelc, F. Javier Gil Llambíasc, Rasmus Fehrmannb, Pedro Ávilaa. "Pore design of pelletised $VO_X/ZrO_2{-}SO_4$/Sepiolite composite catalysts" 10^{th} International Symposium Scientific Bases for the Preparation of Heterogeneous Catalysts

[151] Putluru, S.S.R.; Schill, L.; Gardini, D.; Mossin, S.; Wagner, J.B.; Jensen, A.D.; Fehrmann, R., J. Mater. Sci. (2014), 49, 2705 - 2713

[152] Casper Funk Jacobsen and Christian Houmann Hansen." Development of alkali resistant $DeNO_x$ catalysts, based on hydrocarbons as reductants." (June 2011) Technical University of Denmark,CHEC Research Centre

Appendices

Appendix A

Experimental

A.1 Catalyst preparation

A.1.1 HC-SCR

- **Ag/Al_2O_3**
  Ag/Al_2O_3 with Ag loadings of 1-5 wt.% were prepared by incipient wetness impregnation with aqueous $AgNO_3$ (Sigma-Aldrich, 99 %) solution using γ-Al_2O_3 (Saint-Gobain, 256 m^2g^{-1}) as support (fraction: 180-300 μm). The catalysts were oven dried at 120 °C for 2 h and then calcined for 5 h at 550 °C.

- **$K-Ag/Al_2O_3$**
  The 3 wt. % Ag/Al_2O_3 catalyst was poisoned by impregnating it with aqueous KNO_3 (SigmaAldrich, 99.99%) solutions to yield K concentrations of 139, 278, 417 and 556 μmol/g corresponding to K/Ag molar ratios of 0.5, 1.0, 1.5 and 2.0. The poisoned catalysts were also dried at 120 °C for 2 h and then calcined for 5 h at 550 °C.

- **$Al_2O_3-TiO_2$**
  $Al_2O_3-TiO_2$ mixed oxides were synthesized by dissolving applicable amounts of titanium isopropoxide (Sigma-Aldrich, 97 %) and aluminium isopropoxide (Sigma-Aldrich, 98 %) in 2-propanol followed by precipitation using 2.25 molar HNO_3. The solvent was removed under reduced pressure. The mixed oxides were oven dried at 120 °C for 2 h and then calcined for 5 h at 600 °C.

A.1.2 Low-temperature NH_3-SCR catalyst screening

- **Citric acid method (CA)**
  Appropriate amounts of metal precursors and support material (if used) were placed in a beaker and dissolved in water yielding a 1 molar solution. Citric acid ($C_6H_8O_7$, 99 %, Aldrich) was added (1 mol L^{-1}). The mixture was dried on a hot plate at 100 °C and further oven dried for 4 h followed by calcination in air for 3 h at 500 °C.

- **Impregnation (IMP)**
  The same as citric acid method, however, leaving citric acid out.

- **Hydrothermal (H)**
  The metal precursors were dissolved in acetic acid aqeous solution (20 vol.%) at room-temperature under vigorous stirring. Titanium ($Ti(OC_4H_9)_4$, 98 %, Aldrich) butoxide was added dropwise under vigorous stirring. The mixed solution was sealed and kept stirring for 4 h to obtain solution A. In a separate beaker, block copolymer P_{123} (Mav = 5800, Aldrich) was dessolved in ethanol (CH_3CH_2OH, 99.8 %, Aldrich) to yield solution B. Solution B was added dropwise to solution A. The resulting solution was sealed and further stirred for 24 h at room temperature. The solution was then transferred into a Teflon sealed container which was then heated in an oven at 120 °C for 0 (no hydrothermal treatment), 12, 14 and 24 h. After the hydrothermal step the precipitate, if formed, was collected and dried over night in air at 100 °C. The as-prepared samples were finally calcined at 450 °C for 4 h. For more details, see [128].

- **Sol-Gel (SG)**
  The same as hydrothermal (H), however, omitting the hydrothermal step.

- **VWT-industrial reference catalyst 1**

  A commercial V_2O_5-WO_3/TiO_2 monolith with a V_2O_5 loading of 3 wt.% and WO_3 of 7 wt.% on anatase TiO_2 was used as a reference material. The monolith consists of a corrugated SiO_2 fibre framework loaded with the active material. The monolith was crushed and the active material separated from the SiO_2 fibres. The catalyst powder was pressed at 2 tons and fractionated to a particle size of 180 - 300 μm.

Table A.1: List of metal precursors used in screening study.

metal	**metal precursor**	**purity**	**supplier**
Ce	$Ce(NO_3)_3$	99 %	Sigma-Aldrich
Fe	$Fe(NO_3)_3 \cdot (H_2O)_9$	98 %	Sigma-Aldrich
Co	$Co(NO_3)_2 \cdot (H_2O)_6$	98 %	Riedel-de Haen
Cr	$Cr(NO_3)_3 \cdot (H_2O)_9$	98 %	Sigma-Aldrich
Mn	$Mn(acetate)_2$ * $(H_2O)_4$	99.9 %	Sigma - Aldrich

A.1.3 AB/C & AB/D

Absolutely no information will be given due to a concurrent patent application. The reader should look forward to publications in peer reviewed journals.

A.1.4 Shaping (extrusion) of AB/C

The binders tested in this study are sepiolite (Pansil 100, Tolsa, 60 %), bentonite (Tolsa, > 95 %), montmorillonit-K10 (Aldrich) and to a lesser extent celite (diatomaceous earth), starch and P_{123} (Mav = 5800, Aldrich). Glass fibres cut into pieces of approximately 3 - 5 mm were also used as reinforcement- and rheological agents. The mass of the clay ingredients needed to reach a specific clay content in the final extrudate was adjusted for the loss upon heating to 150 °C which was determined on a daily basis.

The most practical binder or binder combination had to be found. For this purpose small-scale extrusions were carried out using a 20 mL syringe with an orifice diameter of 2 mm. The binder and glass fibres, if used, were thoroughly mixed with the AB/C-S catalyst followed by addition of water to give an extrudable paste. The extrudates were dried over night at room temperature followed by drying at 110 °C for 5 h. Calcination was carried out at 400 or 450 °C for 4 h using a temperature ramp of 97 °C h^{-1}. The calcined extrudates were broken down in to cylindrically shaped pieces sized 5 ± 0.5 mm which were used to measure the breaking strength as depicted by figure A.1. Ten pieces per extrudate were measured to allow for the calculation of mean and standard deviation. The results need to be taken with a pinch of salt since the standard deviations are high.

Some of the samples were characterized using NH_3-TPD, H_2-TPR and mercury intrusion porosimetry (MIP).

Two large scale extrusions (≈ 1.5 kg) were performed using a mechanical

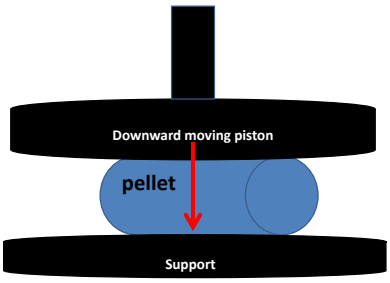

Figure A.1: Depiction of breaking strength experiment

extruder, see figure A.2, resulting in monoliths with the following dimensions: pitch = 6.10 mm; wall thickness = 1.49 mm; geometric surface area = 495 m^2 m^{-3}, see figure A.3. The monolith were abbreviated with M1 and M2. The composition of M1 is: 20 wt.% bentonite; 1 wt.% glass fibres; 79 wt.% AB/C-S. The composition of M2 is: 12.5 wt.% bentonite; 10 wt.% Montmorillonit K10; 1 wt.% glass fibres; 76.5 wt.% AB/C-S.

Figure A.2: Mechanical extruder used for large scale extrusions at CSIC in Madrid.

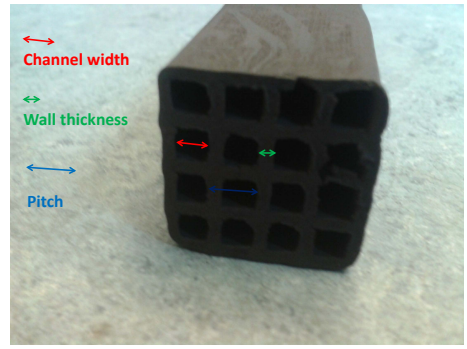

Figure A.3: Product of mechanical extrusion.

A.1.5 H_2O and SO_2 exposure of AB/C and ab/d

- **VWT-industrial reference catalyst 2**

  A commercial V_2O_5-WO_3/TiO_2 monolith (extruded form) with unknown composition was crushed and fractionated to a particle size of 180 - 300 μm. The monolith had a pitch of 4 mm and a wall thickness of 1 mm. The density of the monolith was about 0.512 g cm^{-3}.

- **Regeneration of SO_2 exposed catalyst**

  Regeneration by washing was attempted by placing 100 mg of spent catalyst into a beaker. Addition of 5 mL of washing liquid (H_2O or organic base at pH 9) followed by decanting was repeated 4 or 10 times to yield ratios of 200 and 500 mL g^{-1}, respectively. *Regeneration with H_2* practically consisted of performing a H_2-TPR experiment with a heating rate of 10 °C min^{-1} to 350 °C and a dwelling time of 1h at that temperature. *Regeneration by heating* was performed in the flow set-up shown in figure A.6 at 400 °C and a flow rate of 300 mL min^{-1} of air.

A.1.6 V−Fe/TiO_2-SG & V−W/TiO_2-DP

- **V−Fe/TiO_2-SG**

  V−Fe/TiO_2-SG catalysts were prepared using a modified recipe reported in [23] used for making 20 wt. % V_2O_5/TiO_2. The molar ratios of V/Ti and Fe/Ti are 0.1697 and 0.0287, respectively. The iron precursor, $Fe(NO_3)_3 \cdot (H_2O)_9$ (98 %, Aldrich) was added in three ways, giving rise to VFe/TiO_2-sg, VFe/TiO_2-npc and VFe/TiO_2-pc.

  In a typical VFe/TiO_2-sg preparation yielding approximately 1.5 g of catalyst, a wet solution consisting of 0.1043 g of iron precursor and 0.489 g of NH_4Cl (99.0%, Aldrich) was added to a 0 °C solution comprising 0.501 of vanadium ethoxide (home-made), 4.25 g of Ti isopropoxide (97%, Aldrich) and 0.025 g of H_2SO_4 in 25 g of absolute ethanol. The sol-gel is aged at room temperature for 4 h followed by transferal to a petridish and dried in a ventilated oven at 80 ° for 4 days. Once a day, the powder is ground to a fine powder. Calcination took place in a static oven at 400 °C for 2 h using a temperature ramp of 33 °C h^{-1}.

  The preparations of VFe/TiO_2-npc and VFe/TiO_2-pc differ from the one of VFe/TiO_2-sg in that the Fe precursor is added after the calcination and the drying step, respectively. For activity measurement purposes, extrudates

containing 20 wt.% sepiolite as binder were prepared as described in section A.1.4. Characterisation was carried out using the binder-free samples.

- **V−W/TiO_2-DP**

  A series of catalysts was prepared using the incipient wetness impregnation (IMP) and the deposition precipitation method (DP). The supports used for this study are TiO_2 (DT-51 from Cristal Global with a sulphur content of 1.25 wt%, surface area of 87 m^2 g^{-1}) and 10 wt% WO_3/TiO_2 (surface area of 75 m^2 g^{-1}), which was prepared by impregnating the former with ammonium metatungstate (Fluka, 99 %) followed by drying and calcination at 550 °C for 5 h.

A.2 Characterisation

A.2.1 X-ray powder diffraction (XRPD)

X-ray powder diffraction (XRPD) measurements were performed on a Huber G670 powder diffractometer using CuK_α radiation within a 2θ range of 2 to 100° in steps of 0.02 °.

A.2.2 N_2-physisorption

BET and BJH surface areas and pore size distributions of the samples (100 mg of catalyst) were determined from nitrogen physisorption measurements at liquid nitrogen temperature with a Micromeritics ASAP 2010 instrument.

A.2.3 NH_3-TPD

NH_3-TPD experiments were conducted on a Micromeritics Autochem-II instrument. In a typical TPD experiment, 100 mg of dried sample was placed in a quartz tube and pretreated in flowing He at 100 °C for 1 h. Then the sample was treated with anhydrous NH_3 gas (Air Liquide, 5% NH_3 in He). After NH_3 adsorption, the sample was flushed with He (50 ml/min) for 60 min at 100 °C. Finally, the TPD operation was carried out by heating the sample from 100 to 500 °C (10 °C/min) under a flow of He (50 ml/min).

A.2.4 SEM-EDX

The distribution of silver and potassium in Ag/Al_2O_3 was investigated by using SEM-EDX on a LEO 440 microscope. The samples were prepared using an MT-990 rotary microtome. Before analysis, the samples were covered with

a very thin carbon film to become conductive. To compare the different spectra and samples, both carbon and oxygen were excluded from the analysis and the amount of other elements was recalculated on a carbon and oxygen free basis.

AB/C-S and some of its extrudates were analysed on a JEOL JSM-5900 scanning electron microscope using a secondary electron detector to study their topography. The samples were first gold coated using a Thermo Polaron SC 7620 sputter coater (3 times 3 minutes, 6.5 nm min^{-1}). An accelerating voltage of 5 keV, working distance of 11 mm and a magnification of 8000 were used.

A.2.5 H_2-TPR

H_2-TPR studies were conducted on a Micromeritics Autochem-II instrument. In a typical experiment, 50-100 mg of oven-dried sample was placed in one arm of a U-shaped quartz tube on quartz wool. Prior to TPR, the catalyst sample was pretreated by flushing 5% H_2 and balance Ar (Air Liquide) at 50 °C for 30 min. After pretreatment, TPR analysis was carried out in a reducing mixture (50 ml/min) consisting of 5% H2 and balance Ar (Air Liquide) from 50 to 650 °C (10 °C/min). The hydrogen concentration in the effluent stream was monitored by a thermal conductivity detector (TCD) and the H_2 consumption values were calculated from calibration experiments.

A.2.6 Mercury Intrusion Porosimetry (MIP)

Samples were dried at 150 °C over night. A CE Instruments Pascal 140/240 porosimeter was used.

A.2.7 Thermo Gravimetric Analysis (TGA)

TGA measurements were conducted on a Mettler Toledo TGA/DSC 1 SF instrument. About 25 mg of sample were placed in 70 μL alumina crucibles and heated from room temperature up to 600°C with a heating rate of 10 °C/min under a N_2 flow of 20 mL/min.

A.2.8 Electrophoretic mobility

The zero point charges (ZPC) of the composite materials were determined by measuring the zeta potential[1] as a function of the solution pH. The experiments were carried out on a Malvern Zetasizer Nano ZS. Samples of fine powder were suspended in premade pH solutions all containing 10^{-3} molar KCl. The pH

[1] difference in potential between dispersed particle and medium

solutions were based on KOH and HCl. The sample concentration was about 0.2 mg mL^{-1}. Just before inserting the cuvette containing the suspended powder into the Zetasizer, thorough agitation was achieved by using a pipette. The surface coverages of components A and B (X_A, X_B) can be obtained from the isoelectric points of the components ($(IEP)_A$, $(IEP)_B$) and the zero point charge (ZPC) of the mixture (extrudate) by solving the following set of equations:

$$X_A + X_B = 1 \tag{A.1}$$

$$ZPC = X_A * (IEP)_A + X_B * (IEP)_B \tag{A.2}$$

A.2.9 Fourier transform infrared spectroscopy (FTIR)

FTIR spectra of the samples were recorded on a Perkin Elmer 1710 spectrometer at ambient conditions in KBr discs.

A.2.10 X-ray photoelectron spectra (XPS)

XPS was acquired with a ThermoScientific system at room temperature using Al K_{alpha} radiation (1484.6 eV). AB/C-S and AB/C-IMP were analysed at four points and the average was taken.

A.2.11 Flame atomic absorption spectrometry (FAA)

FAA spectra of solutions containing metal A were taken on a Perkim Elmer AAnalyst 200 machine.

A.2.12 Raman spectroscopy

Raman spectra were acquired with a single-monochromator Renishaw System 1000 equipped with a cooled CCD detector (- 73 °C) and an Edge filter. The samples were excited with the 514 nm Ar^+ line Spectra Physics ; power 19 mW and 1 mW on the sample; the spectral resolution was ca. 3 cm^{-1}, and spectra acquisition consisted of 10 accumulations of 30 s.

A.3 Activity measurements

A.3.1 Ethanol-SCR

The SCR activity measurements were carried out at atmospheric pressure in a fixed-bed reactor loaded with 100 - 250 mg of fractionised (180 – 300 μm) catalyst at a flow rate of 3 NL/min (at room temperature). The inlet concentrations

were: NO = 500 ppm, ethanol = 1000 ppm, H_2 = 0 - 500 ppm, SO_2 = 0 - 150 ppm, H_2O = 2 % and O_2 = 5 % with N_2 as balance gas. During the experiments the temperature was increased stepwise from 250 to 550 °C while the NO and NO_2 concentrations were continuously monitored by UVvis (Eco Physics CLD 700 EL) analyser. The CO and CO_2 concentrations were continuously monitored by a Rosemount NGA 2000 analyser and the N_2O with a Varian Micro GC CP-4900 using a PORAPLOT Q column. The activity was measured after attaining steady state and care was taken not to reach 100% conversion to allow calculation of first-order rate constants. The ethanol concentration could not be measured directly, because ethanol was condensed out directly after the reactor, due to possible cross-sensitivity problems in the NO_x analyzer. The ethanol conversion was estimated from the CO and CO_2 outlet concentrations. This may underestimate the true ethanol conversion due to the formation of intermediate oxidation products.

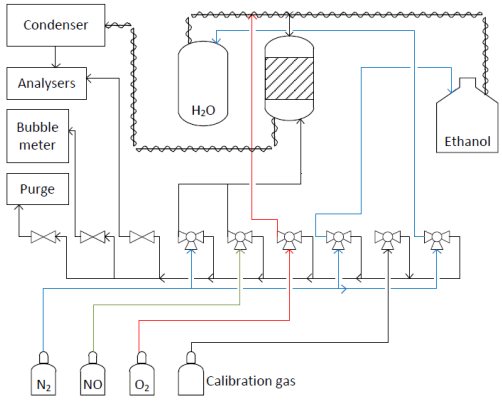

Figure A.4: Schematic drawing of the flow set-up used for ethanol-SCR catalytic activity measurements. Taken from [152]

The following equations have been used to calculate:

- NO_x concentration ($[NO_x]$)

$$[\mathrm{NOx}] = [NO] + [\mathrm{NO_2}] \tag{A.3}$$

- NO_x conversion (X_{NOx})

$$X_{\mathrm{NOx}}(T) = 1 - \frac{[\mathrm{NOx}(T)]}{[\mathrm{NOx}(background)]} \tag{A.4}$$

- Ethanol conversion ($X_{C_2H_5OH}(T)$)

$$X_{\mathrm{C_2H_5OH}}(T) = \frac{[CO](T) + [\mathrm{CO_2}](T)}{2 * [\mathrm{C_2H_5OH}](inlet)} \tag{A.5}$$

- Pseudo first order rate constant (k(T))

$$k(T) = -\frac{F}{w} ln(1 - X(T)) \tag{A.6}$$

with F and w being the volumetric flow rate and the catalyst weight, respectively. A derivation of equation A.11 is given in e.g. [23].

- CO_2 selectivity ($S_{CO_2}(T)$)

$$S_{\mathrm{CO_2}}(T) = \frac{[\mathrm{CO_2}(T)]}{[\mathrm{CO_2}(T)] + [\mathrm{CO}(T)]} \tag{A.7}$$

It is assumed that CO and CO_2 are the only products from the ethanol conversion. Since there are probably other, undetected products, equation A.7 is an upper limit to the CO_2 selectivity.

- Theoretical maximum NO_x conversion ($X_{theo.\ max.\ NOx}$)

$$X_{\mathrm{theo \cdot max \cdot NOx}}(T) = \frac{X_{\mathrm{NOx}}(T)}{X_{\mathrm{C_2H_5OH}}(T)} * \frac{[\mathrm{C_2H_5OH}](inlet)}{[\mathrm{NOx}](inlet)} \tag{A.8}$$

Equation A.8 is based on the assumption that the moles of converted ethanol per moles of converted NOx are not a function of the respective conversions up to 100 % NOx conversion. The results presented in figure 4.5 suggest that this is a reasonable assumption.

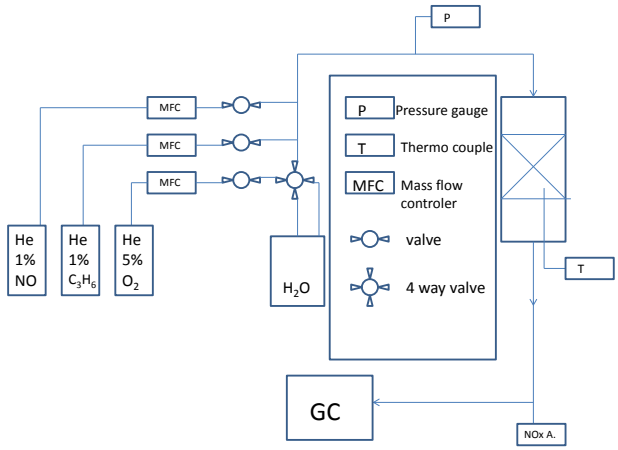

Figure A.5: Schematic drawing of the flow set-up used for propene-SCR catalytic activity measurements.

A.3.2 Propene-SCR

The SCR activity measurements were carried out at atmospheric pressure in a fixed-bed reactor loaded with 100 mg of fractionised (180 – 300 μm) catalyst at a flow rate of 300 mL/min (at room temperature), resulting in a W/F = 0.02 g s cm^{-3}. The inlet concentrations were: NO = 1000 ppm, propene = 2000 ppm, H_2O = 2.3 % and O_2 = 4 % with He as balance gas. During the experiments the temperature was increased stepwise from 250 to 550 °C while the NO concentration was continuously monitored by a Thermo Electron Model 17C chemiluminescence NH_3−NOx gas analyser. The product stream was analysed by an online GC (HP6890A) equipped with a TCD for CO_2 - and an FID for propene concentration determination. The concentrations were obtained with calibration experiments. The activity was measured after attaining steady state and care was taken not to reach 100% NO conversion to allow calculation of first order-rate constants.

The following equations were used to calculate:

- NO conversion (X_{NO})

$$X_{\mathrm{NO}}(T) = 1 - \frac{[\mathrm{NO}(T)]}{[\mathrm{NO}(background)]} \tag{A.9}$$

- Propene conversion ($X_{C_3H_6}$(T))

$$X_{C_3H_6}(T) = 1 - \frac{[C_3H_6(T)]}{[C_3H_6(background)]} \tag{A.10}$$

- Pseudo first order- rate constant (k(T))

$$k(T) = -\frac{F}{w} ln(1 - X(T)) \tag{A.11}$$

  with F and w being the volumetric flow rate and the catalyst weight, respectively. A derivation of equation A.11 is given in e.g. [23].

- CO_2 selectivity (S_{CO_2}(T))

$$S_{CO_2}(T) = \frac{[CO_2(T)]}{3 * X_{C_3H_6}(T) * [C_3H_6(background)]} \tag{A.12}$$

Note that both $X_{C_3H_6}$(T) and S_{CO_2}(T) are, unlike in the case of ethanol-SCR, directly determined.

A.3.3 LT-SCR catalyst screening

The activity measurements during the screening stage were conducted using the set-up depicted in figure A.6, which is the same as used for the propene-SCR measurements. The SCR activity measurements were carried out at atmospheric pressure in a fixed-bed reactor loaded with 50 mg of fractionised (180 – 300 μm) catalyst at a flow rate of 300 mL/min (at room temperature), resulting in a W/F = 0.01 g s cm^{-3}. The inlet concentrations were: NO = 1000 ppm, NH_3 = 1000 ppm, H_2O = 2.3 % and O_2 = 4 % with He as balance gas. During the experiments the temperature was increased from 125 to 300 °C in steps of 25 °C, while the NO concentration was continuously monitored by a Thermo Electron Model 17C chemiluminescence NH_3−NOx gas analyser. The use of only 2.3 % water was chosen for the sake of simplicity to allow for a high throughput. This was by hindsight a mistake. The use of 20 % H_2O during the screening stage would have made us aware of the real challenges of this project.

A.3.4 Shaping (extrusion) of AB/C

See section A.3.3. No dedicated SCR test rig was available on site (CSIC). Attempts were made to measure the activities of the syringe extrudates using a home-made rig with a mass spectrometer for quantification of the NO concentration. However, it turned out that the system delivered spurious activity data.

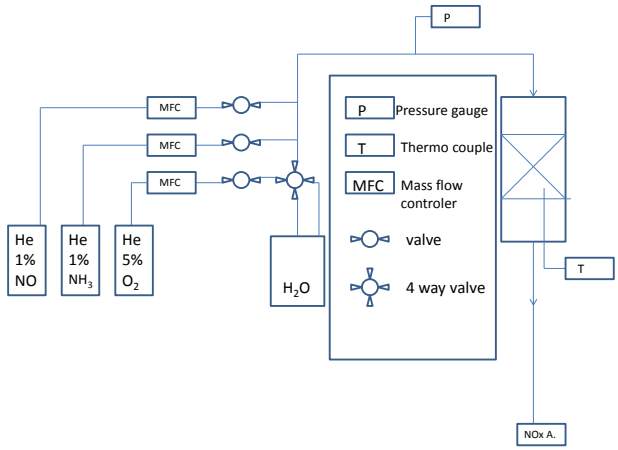

Figure A.6: Schematic drawing of the flow set-up used for low-temperature NH_3-SCR catalyst screening catalytic activity measurements.

Therefore, only activity data obtained at DTU are presented here. Activities of both syringe- and machine extrudates were measured in powder form. The conformed catalysts were crushed and sieved to a fraction of 180 to 300 μm.

A.3.5 H_2O and SO_2 exposure of AB/C and AB/D

H_2O exposure (10 to 20 %) was conducted on a set-up shown in figure A.7, which is basically the same as the one used for the LT-NH_3-SCR screening experiments A.3.3. There are two basic differences. H_2O is not added by bubbling a gas through a water reservoir but by using a pump. To prevent condensation, the lines up to the furnace need to be heated with heating tape due to the higher H_2O contents. The inflexible metal tubing downstream of the furnace was replaced by circa 2 metres of flexible teflon tubing. This was done because at the time of the experimentation no condensor was available.

In a typical experiment, 100 to 400 mg of fractionated catalyst (180 – 300 μm) were loaded into the reactor, heated to the maximum temperature of the (typically 200 °C) followed by exposure to the dry gas mixture for about 30 minutes for catalyst activation. Then 0.0804 g min^{-1} of H_2O were added to the gas stream, resulting in total flow rates between 500 and 1000 mL min^{-1} and water concentrations of 20 to 10 %. At this stage, the teflon tubing located downstream

of the reactor is connected to the venting system in order not to expose the NO_x analyzers to high concentrations of H_2O. After about 45 minutes of H_2O exposure the teflon tubing was briefly removed and the condensed water blown out with compressed air followed by connecting the (dry) tubing to the reactor and the analysers. NO concentrations were measured for about 5-10 minutes. During this time the teflon tubing acted as a condenser. The experiments proved to be reproducible and an empty reactor experiment yielded close to 0 % NO conversion. Usually, the procedure was repeated at each temperature in order to ensure that a steady state had been reached. The teflon tubing was removed from the NO_x analysers after each measurement period and reconnected to the venting system. The temperature was lowered in steps of 10 or 20 °C. The procedure outlined above was repeated at each temperature. With a H_2O concentration of 10 %, the conditions were as follows: [NO] = 720 ppm; [NH_3] = 770 ppm; [O_2] = 15.0 %. With a H_2O concentration of 20 %, the conditions were as follows: [NO] = 720 ppm; [NH_3] = 780 ppm; [O_2] = 12.8 %.

N_2O formation was measured with a Shimadzu GC-14B equipped with a PORAPLOT Q column connected to a TCD detector.

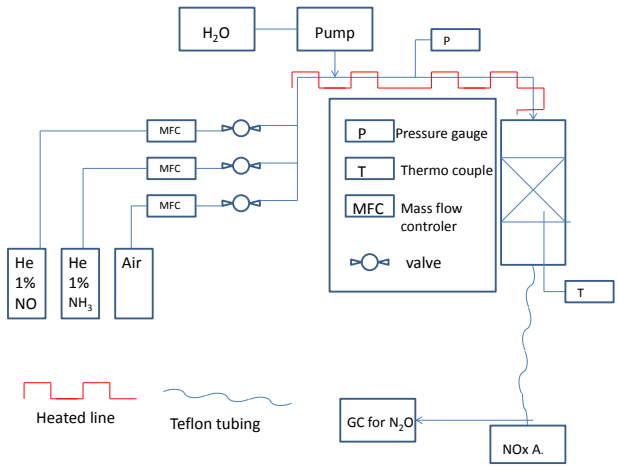

Figure A.7: Schematic drawing of the flow set-up used for H_2O exposure experiments

SO_2 exposure was conducted on a the set-up shown in figure A.4. Instead of Ethanol, NH_3 was pumped from a gas cylinder and H_2O was added using a pump.1.33 g of optimsed AB/C-S (180 – 300 μm) was exposed at 160 °C to a

flow of 4500 mL/min with the following composition: [NO] = 606 ppm ; [NH_3] = 744 ppm ; [O_2] = 11.3 % ; [H_2O] = 8 %; [SO_2] = 10 ppm; N_2 = make up gas. First, the NO conversion in absence of SO_2 was measured after attaining steady state. Then, the catalyst was exposed to SO_2 for 1280 min followed by removal of SO_2 for 1 h. Unfortunately, the activity data went missing. So only the initial (in absence of SO_2) NO conversion as well as the NO conversions after 1280 min of exposure and after SO_2 removal can be reported.

A.3.6 V−Fe/TiO_2-SG & V−W/TiO_2-DP

For V−Fe/TiO_2-SG see A.3.5. Catalysts were exposed to 20 vol.% H_2O using a flow rate of 500 mLmin^{-1} and 400 mg of catalyst resulting in a W/F value of 0.048 g s cm^{-3}. For V−W/TiO_2-DP, see A.3.3.

Appendix B

Calculations

B.1 Calculation of SO_2 exposure at tail-end position

Table B.1: Operational data from the Algonquin Power Energy-From-Waste Facility [98]

property	**abbreviation**	**value**	**unit**
catalyst volume	V_{cat}	32.08	m^3
gas velocity	v_{gas}	3.93	m s^{-1}
gas velocity in channel	v_{gas-ch}	5.6	m s^{-1}
Pre SCR average NO_x	$[NO_{x-0}]$	233	ppm
NO_x removal efficiency	R_{-eff}	68	%
Mass of NO_x removed	R-mass-NO_2	227	tonnes per year
molar mass of NO_2	m-NO2	46	g mol^{-1}
desnity of monolith	d_{cat}	1.17 (estimate)	g cm^{-3}

Basically we want to know how many moles of flue gas pass by one gram of catalyst per unit of time. For this purpose we used data from the Algonquin Power Energy-From-Waste Facility [98]. Table gives the data availalbe from source [98].

First, the volume number of moles of NO_x removed per year are calculated with equation B.1.

$$n_{NO_x} = \frac{R_{mass-NO_2}}{m_{NO_2}} = \frac{227 tonnes/a}{4.6 * 10^{-5} tonnes/mol} = 4934 * 10^6 moles/a \tag{B.1}$$

Then the mass of the catalyst is calculated, see B.2.

$$m_{cat} = V_{cat} * d_{cat} * (1 - \frac{v_{gas}}{v_{ch}}) m_{cat} = 32 m^3 * 1.17 * 10^6 g m^{-3} * (1 - \frac{3.93 m s^{-1}}{5.60 m s^{-1}}) = 1.12 * 10^7 g \tag{B.2}$$

With this the number of SO_2 molecules per gram per year per ppm of SO_2 can be calculated $N_{SO_2/g}$.

$$n_{SO_2/g} = \frac{n_{NO_x}}{R_{eff} * [NO_{x-0}]} * \frac{1}{m_{cat}} = \frac{4.934 * 10^6 moles/a}{0.68 * 233 ppm} * \frac{1}{2.63 * 10^7 g} = 2.79 * 10^{-3} \frac{moles}{g * a * ppm_{SO2}} \quad \text{(B.3)}$$

which ist the same as **0.317 μmol $\mathbf{SO_2}$/($\mathbf{g}_{cat}$ * h * $\mathbf{ppm_{SO_2}}$)**.

Appendix C

Articles

1. **Ethanol-selective catalytic reduction of NO by Ag/Al_2O_3 catalysts: Activity and deactivation by alkali salts**

   Schill, L.; Putluru, S.S.R; Jacobsen, J.F.; Hansen, C.H.; Fehrmann, R.; Jensen, A.J., Appl. Catal. B (2012), 127, 323-329

2. **Low-Temperature NH_3-SCR of NO on Mesoporous $Mn_{0.6}Fe_{0.4}/TiO_2$ Prepared by a Hydrothermal Method**

   Schill, L.; Putluru, S.S.R.; Fehrmann, R.; Jensen, A.J., Catal. Lett. (2014), 144, 395 - 402

3. **Superior $DeNO_x$ activity of $V_2O_5{-}WO_3/TiO_2$ catalysts prepared by deposition-precipitation method**

   Putluru, S.S.R.; Schill, L.; Gardini, D.; Mossin, S.; Wagner, J.B.; Jensen, A.J.; Fehrmann, R., J. Mater. Sci. (2014), 49, 2705-2713

Applied Catalysis B: Environmental 127 (2012) 323–329

Contents lists available at SciVerse ScienceDirect

Applied Catalysis B: Environmental

journal homepage: www.elsevier.com/locate/apcatb

Ethanol-selective catalytic reduction of NO by Ag/Al_2O_3 catalysts: Activity and deactivation by alkali salts

Leonhard Schill[a,b], Siva Sankar Reddy Putluru[a,b], Casper Funk Jacobsen[a,b], Christian Houmann Hansen[a,b], Rasmus Fehrmann[b], Anker Degn Jensen[a,*]

[a] Combustion and Harmful Emission Control Research Centre, Department of Chemical and Biochemical Engineering, Building 229, Technical University of Denmark, DK-2800 Kgs. Lyngby, Denmark
[b] Centre for Catalysis and Sustainable Chemistry, Department of Chemistry, Building 207, Technical University of Denmark, DK-2800 Kgs. Lyngby, Denmark

ARTICLE INFO

Article history:
Received 29 June 2012
Received in revised form 6 August 2012
Accepted 28 August 2012
Available online 4 September 2012

Keywords:
SCR of NO with ethanol
Ag/Al_2O_3
Potassium poisoning

ABSTRACT

Ag/Al_2O_3 catalysts with and without potassium doping were prepared by incipient wetness impregnation and characterized by N_2 physisorption, XRPD, NH_3-TPD and SEM. The influence of the Ag content from 1 to 5 wt.% was investigated for the selective catalytic reduction (SCR) of NO with ethanol. The 3 wt.% Ag/Al_2O_3 catalyst was found to be the most active and CO_2 selective over a wide temperature window (300–500 °C). Addition of 500 ppm of H_2 has a mild promotional effect on the activity while SO_2 has a strong negative influence on the SCR activity. Furthermore, the Ag/Al_2O_3 ethanol-SCR catalyst deactivated significantly by the addition of potassium although it was more resistant than the conventional V_2O_5 based NH_3-SCR catalyst, which deactivated more at lower potassium loading. The higher potassium resistivity of the Ag/Al_2O_3 catalysts seems to be due to differences in reaction mechanism of Ag/Al_2O_3 ethanol-SCR catalyst compared to the conventional NH_3-SCR catalyst. The still low potassium resistance, in combination with the high sensitivity to SO_2, seems not to make these catalysts a real option for biomass fired boilers.

1. Introduction

The selective catalytic reduction (SCR) of nitrogen oxides is an important process in the avoidance of harmful emissions from stationary and mobile sources [1–6]. The process is currently being used extensively to reduce NO_x from stationary sources with NH_3-SCR (especially power plants) with increasing attention for reduction of NO_x from automotive vehicles by hydrocarbon based SCR (HC-SCR) and NH_3-SCR processes.

The selective catalytic reduction by ammonia is currently the most widespread method for the cleanup of NO_x in flue gases from stationary sources by using V_2O_5–WO_3/TiO_2 catalysts. However, there are some drawbacks in terms of toxicity of vanadium, catalyst deterioration, NH_3-slip, ash odor and ammonia sulfate formation. There is therefore a desire to develop new catalysts operating in a wider temperature range and it is attractive to substitute ammonia by another reductant because of the dangers of storage, leakage, transport of liquid ammonia and ammonia sulfate formation on the catalyst which leads to poor performance [7–10]. These drawbacks can be overcome with hydrocarbon reductants using a suitable catalyst. The selective catalytic reduction of NO with hydrocarbons has been studied thoroughly in the last years as a possible competitor for the commercial NH_3-SCR process [5,11].

Since the discovery of the HC-SCR technology, various types of catalysts have been reported, such as ion-exchanged zeolites [5,7,11], supported precious metals [5,11], and metal oxide-based catalysts [12–15]. All the above mentioned catalysts have their advantages and disadvantages for practical use. Metal oxide-based catalysts show high stability and moderate tolerance to SO_2 and water vapor and in this context, Ag/γ-Al_2O_3 catalysts have been proposed. However, the development of an industrial HC-SCR technology has not yet been possible and the most significant reason is that no suitable catalytic system has been found exhibiting high selectivity to N_2 and CO_2, wide operational temperature performance, and high tolerance of SO_2 [5,7,11].

Several studies indicate that Ag/Al_2O_3 is a promising catalyst, showing a high efficiency in NO_x reduction with hydrocarbons in excess oxygen [12–15]. Applied in stationary sources the cost and availability of the reductant is very important. Recently Lee et al. [13] investigated Ag/Al_2O_3 catalyst with a wide variety of hydrocarbon reductants ranging from C_2 to C_{12} chain length. Among all the reductants ethanol showed the highest NO reduction activity in a wide temperature range. Shimizu et al. [14] found the following order for the NO_x conversion by different hydrocarbons: ethers > alcohols > aldehydes > esters > ketones $\gg C_3H_8$.

* Corresponding author. Tel.: +45 45252841; fax: +45 45882258.
E-mail address: aj@kt.dtu.dk (A.D. Jensen).

0926-3373/$ – see front matter © 2012 Elsevier B.V. All rights reserved.
http://dx.doi.org/10.1016/j.apcatb.2012.08.035

Biomass residues such as straw and wood are increasingly used as fuels and co-fuels at stationary sources such as power plants [16,17]. One of the major problems arising from the use of biomass is the deactivation of the V_2O_5–WO_3/TiO_2 based SCR catalyst by alkali metals, especially potassium, which the biomass contains in relatively large amounts [17]. Potassium deactivates the V_2O_5–WO_3/TiO_2 SCR catalyst by irreversibly binding to the V—OH Brønsted acidic sites, which are responsible for the ammonia adsorption, thus decreasing both their number and activity in NO reduction [18,19]. So far, the strategies to make the NH_3-SCR catalyst more alkali resistant have been: Adding sacrificial acidic sites (e.g. sulphated zirconia); increasing initial activity by using high loading of nano V_2O_5 on high surface TiO_2; using other active species (e.g. Cu/Zeolites) [20].

Another approach concerns development of deNO_x catalysts functioning by a different mechanism that may be non- or less alkali sensitive. It is known from the literature that the HC-SCR mechanism involve activation of NO and the hydrocarbon by coordination to the Lewis acid sites of the active metal oxides distributed on the carrier surface, thus not involving the Brønsted sites mentioned above being active in the NH_3-SCR. Therefore, catalysts functioning with hydrocarbons as reductants in SCR of NO_x may possibly be less sensitive to potassium salts in the flue gas, displaying a longer lifetime in biomass fired power plants. Typically, HC-SCR mechanisms are classified into two categories. One is the adsorption/dissociation mechanism (noble metal and Cu-zeolite catalysts) and the second one is the oxidation-reduction mechanism (metal oxide catalysts such as Ag/Al_2O_3, Sn/Al_2O_3 and In/Al_2O_3) [5]. This mechanistic advantage compared to NH_3-SCR would potentially increase the potassium resistance of the HC-SCR catalyst. The postulated reaction mechanism of ethanol-SCR using the Ag/Al_2O_3 catalyst apparently involves formation of both adsorbed nitrates (via NO oxidation by O_2) and enolic/acetate species (via the partial oxidation of ethanol). Further reaction between the nitrates and enolic/acetate species then leads to the formation of —NCO, which reacts with NO + O_2 and nitrates to yield N_2 [5,15]. Since ethanol-SCR is also comparatively active by HC-SCR standards, this combination of reductant and catalyst could be a potential substitute for NH_3-SCR using the V_2O_5–WO_3/TiO_2 catalyst at power stations firing biomass.

The catalysts used for the SCR process should be highly selective, particularly with respect to SO_2 oxidation. SO_2 levels can be decreased when firing with biomass since they contain relatively less sulphur compared to coal. The effect of SO_2 on various catalysts was examined by Okazaki et al. [21] concluding that the deactivation is a function of catalyst and reductant. Abe et al. [22] noted that silver sulfate decomposes at a lower temperature (427 °C) than aluminum sulfate (727 °C). Catalysts tested in their studies maintained their activity in the presence of SO_2 at higher temperatures (>427 °C) but tend to be inactive at temperatures lower than this.

In the present work, we report the influence of alkali and sulphur on the performance of Ag/Al_2O_3 SCR catalyst using ethanol as a reductant for biomass fired SCR application without compromising the activity, selectivity and also most importantly working within the desired SCR operating temperature region.

2. Experimental

2.1. Catalyst preparation and characterization

Ag/Al_2O_3 (Ag = 1–5 wt %) catalysts were prepared by incipient wetness impregnation of 180–300 μm γ-Al_2O_3 (Saint-Gobain, 256 m^2/g) particles with aqueous $AgNO_3$ (Sigma–Aldrich 99.0%) solutions. The catalysts were dried at 120 °C for 2 h and then calcined for 5 h at 550 °C. The 3 wt % Ag/Al_2O_3 catalyst was poisoned by impregnating it with aqueous KNO_3 (Sigma–Aldrich, 99.99%) solutions to yield K concentrations of 139, 278, 417 and 556 μmol/g corresponding to K/Ag molar ratios of 0.5, 1.0, 1.5 and 2.0. The poisoned catalysts were also dried at 120 °C for 2 h and then calcined for 5 h at 550 °C.

X-ray powder diffraction (XRPD) measurements were performed on a Huber G670 powder diffractometer using CuK_α radiation within a 2θ range of 2–100° in steps of 0.02°. BET surface areas of the samples (100 mg of catalyst) were determined from nitrogen physisorption measurements at liquid nitrogen temperature with a Micromeritics ASAP 2010 instrument.

NH_3-TPD experiments were conducted on a Micromeritics Autochem-II instrument. In a typical TPD experiment, 100 mg of dried sample was placed in a quartz tube and pretreated in flowing He at 500 °C for 2 h. Then, the temperature was lowered to 100 °C and the sample was treated with anhydrous NH_3 gas (Air Liquide, 5% NH_3 in He). After NH_3 adsorption, the sample was flushed with He (50 ml/min) for 100 min at 100 °C. Finally, the TPD operation was carried out by heating the sample from 100 to 500 °C (10 °C/min) under a flow of He (50 ml/min).

The distribution of silver and potassium in the catalysts was investigated by using SEM-EDX on a LEO 440 microscope. The samples were prepared using an MT-990 rotary microtome. Before analysis, the samples were covered with a very thin carbon film to become conductive. To compare the different spectra and samples, both carbon and oxygen were excluded from the analysis and the amount of other elements was recalculated on a carbon and oxygen free basis.

2.2. Catalytic activity measurements

The SCR activity measurements were carried out at atmospheric pressure in a fixed-bed reactor loaded with 100–250 mg of fractionized (180–300 μm) catalyst at a flow rate of 3 NL/min (at room temperature). The inlet concentrations were: NO = 500 ppm, ethanol = 1000 ppm, H_2 = 0–500 ppm, SO_2 = 0–150 ppm, H_2O = 2% and O_2 = 5% with N_2 as balance gas. During the experiments the temperature was increased stepwise from 250 to 550 °C while the NO and NO_2 concentrations were continuously monitored by UV–vis (Eco Physics CLD 700 EL) analyzer. The CO and CO_2 concentrations were continuously monitored by a Rosemount NGA 2000 analyser and the N_2O with a Varian Micro GC CP-4900 using a PORAPLOT Q column. The activity was measured after attaining steady state (1 h) and care was taken not to reach 100% conversion to allow calculation of rate constants. Fresh and poisoned catalysts are compared by change in relative activity (%) of the corresponding catalysts. The ethanol concentration could not be measured directly, because ethanol was condensed out directly after the reactor, due to possible cross-sensitivity problems in the NO_x analyzer. The ethanol conversion was estimated from the CO and CO_2 outlet concentrations. This may underestimate the true ethanol conversion due to the formation of intermediate oxidation products.

3. Results and discussion

The results of N_2-BET surface area and weight percentage of Ag are shown in Table 1. The bare support has higher surface area than the Ag/Al_2O_3 and potassium poisoned catalysts. With an increase in metal loading to Al_2O_3, a gradual decrease in surface area is noted. The X-ray powder diffraction (XRPD) patterns of Ag/Al_2O_3 catalysts are shown in Fig. 1. The presence of a dominating γ-Al_2O_3 phase was observed in all catalysts. No peaks attributable to Ag^0, Ag_2O, or $AlAgO_2$ phases were observed. This shows a good dispersion of the silver on the support. The detection limit of the XRPD apparatus is around 5 nm, and so any silver particles would be below this size.

Table 1
Physico-chemical properties of Ag/Al_2O_3 catalysts.

Catalyst	Ag (wt.%)	K/Ag (mol/mol)	Surface area (m^2/g)	Acidity (μmol/g)
γ-Al_2O_3	–	–	256	484
1 wt.% Ag/Al_2O_3	1.0	–	255	547
2 wt.% Ag/Al_2O_3	2.0	–	254	570
3 wt.% Ag/Al_2O_3	3.0	–	252	607
4 wt.% Ag/Al_2O_3	4.0	–	248	549
5 wt.% Ag/Al_2O_3	5.0	–	243	517
K/Ag – 0.5	3.0	0.5	250	478
K/Ag – 1.0	3.0	1.0	235	436
K/Ag – 1.5	3.0	1.5	231	365
K/Ag – 2.0	3.0	2.0	229	269

Fig. 2 shows the catalytic activity profiles of 1–5 wt.% Ag/Al_2O_3 catalysts as a function of reaction temperature. Fig. 2a shows that a gradual increase in Ag loading enhanced the NO conversion which reaches a maximum at 3 wt.% Ag while further increase of Ag loading leads to a gradual decrease of NO conversion. At the low temperature range below 300 °C, the catalysts exhibited low activity and appreciable activity was only observed between 350 and 500 °C. These results are similar to those reported in the literature with temperature window ranging from 300 to 500 °C for 2–3 wt.% Ag/Al_2O_3 catalysts [12,13,23]. The highest NO conversions were observed at silver loadings of 2 and 3 wt.% Ag/Al_2O_3, both at 400 °C. An optimum content at 3 wt.% Ag in the catalyst was observed with a maximum NO conversion of 96% at 400 °C. Note that there is no formation of N_2O for all the catalysts in the given temperature range. The Ag loading of 2 wt.% has been widely accepted as the optimal Ag content for the HC-SCR technology [5]. However, the optimum Ag content of the Ag/Al_2O_3 catalyst seems to vary depending on the catalyst preparation method (affect the Ag oxidation state and particle size), support surface area and type of reductant employed [5,7,23]. Fig. 2b and c shows the ethanol conversion and CO_2 selectivity profiles of 1–5 wt.% Ag/Al_2O_3 catalysts as a function of reaction temperature. With increasing Ag content from 1 to 5 wt.% the ethanol conversion and CO_2 selectivity increases steadily. 3 wt.% Ag is mild in ethanol conversion and maintained above 80% CO_2 selectivity. The 3 wt.% Ag/Al_2O_3 catalyst was chosen for further experiments, because of higher NO conversions at lower temperatures (300–350 °C), mild ethanol conversion and slightly lower CO emissions. Generally, higher silver loading leads to high hydrocarbon conversion [5,24]. The optimum ethanol-SCR activity of the 3 wt.% Ag/Al_2O_3 catalyst can be partly explained

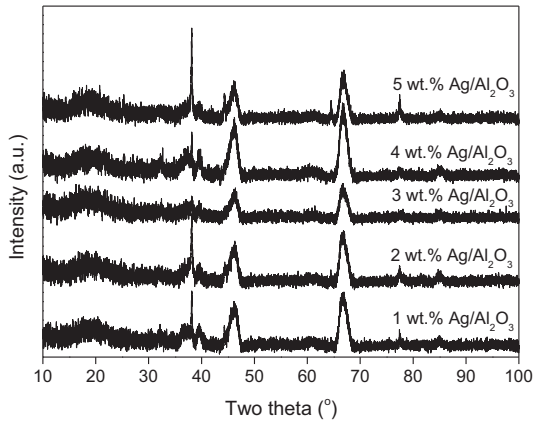

Fig. 1. XRPD patterns of 1–5 wt.% Ag/Al_2O_3 catalysts.

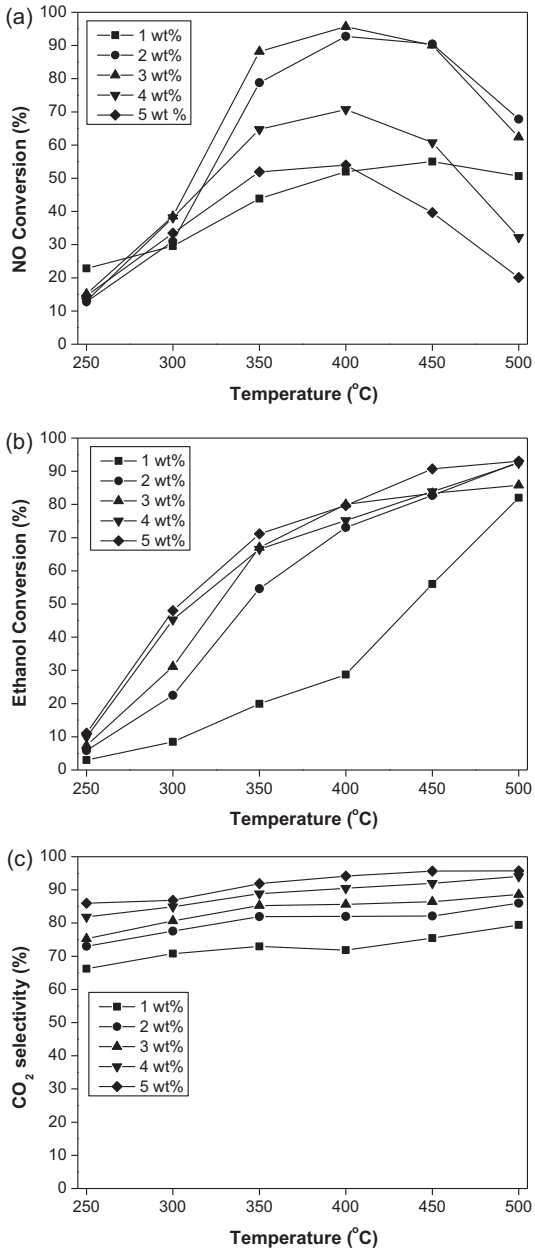

Fig. 2. NO conversion (a), ethanol conversion (b) and CO_2 selectivity (c) for 1–5 wt.% Ag/Al_2O_3 catalysts. Reaction conditions: SV = 720,000 N ml/(g h); 500 ppm NO, 1000 ppm ethanol, 5% O_2, 2% H_2O, balance N_2.

by the physico-chemical properties of the catalysts displayed in Table 1. The 3 wt.% Ag/Al_2O_3 catalyst was found to be the most acidic among all catalysts and the attained surface area close to the Al_2O_3 support.

Fig. 3 shows the influence of H_2 on ethanol-SCR activity of the 3 wt.% Ag/Al_2O_3 catalyst at 400 °C. H_2 has proven to enhance the conversion of NO and reductants [7,14,25,26]. One of the reasons for the enhanced activity of H_2 is attributed to the favored

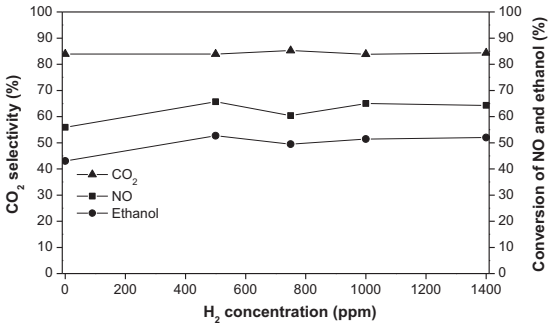

Fig. 3. NO conversion, ethanol conversion and CO_2 selectivity as a function of H_2 concentration at 400 °C on 3 wt.% Ag/Al_2O_3 catalyst. Reaction conditions: SV = 1,800,000 N ml/(g h); 500 ppm NO, 1000 ppm ethanol, 0–1400 ppm H_2, 5% O_2, 2% H_2O, balance N_2.

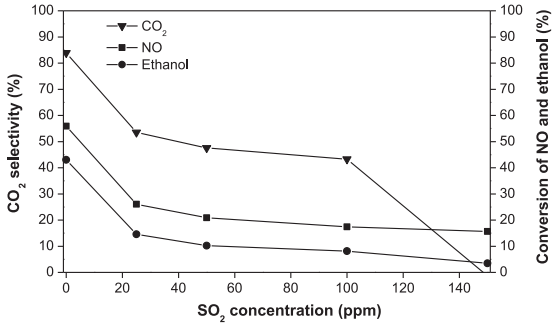

Fig. 4. NO conversion, ethanol conversion and CO_2 selectivity as a function of SO_2 concentration at 400 °C on 3 wt.% Ag/Al_2O_3 catalyst. Reaction conditions: SV = 1,800,000 N ml/(g h); 500 ppm NO, 1000 ppm ethanol, 0–150 ppm SO_2, 5% O_2, 2% H_2O, balance N_2.

formation of important species such as acetate and NCO species, whose formation is viewed as the rate-determining step in the absence of H_2 [25–27]. Shimizu et al. [14] have tested the effect of 0.5 vol.% H_2 on various hydrocarbon reductants over wide ranges of temperatures and found that the NO conversion is enhanced at lower temperatures. To monitor the changes in conversion levels the conversion was decreased by increasing the space velocity from 720,000 to 1,800,000 N ml/(g h). The addition of 500 ppm of H_2 to the ethanol leads to an increase in NO conversion from 56% to 66% and the ethanol conversion is also increased from 43% to 51%. Further increase in H_2 does not have a significant impact on the conversion levels. The ethanol conversion values (calculated from the CO and CO_2 concentrations) are relatively lower than the NO conversion at low reaction temperatures (Fig. 2). It indicates that NO is reduced while the ethanol is oxidized to intermediate products [27], as reported in the literature where acetaldehyde formation is observed between 100 and 300 °C on a 3 wt.% Ag/Al_2O_3 catalyst [28]. Further, an increase in acetaldehyde formation was also observed in the presence of H_2. The CO_2 selectivity is not much affected by the presence of H_2. Most of the previous investigations were done at comparatively high H_2 concentrations (0.2–1 vol.%) [7,14,25]. However, high H_2 concentrations may have less practical applications in industrial power plants due to cost and safety issues. The present results show that 500 ppm of H_2 is sufficient to promote the ethanol-SCR activity and more attractive for industrial purpose.

The influence of SO_2 in concentrations of 25, 50, 100 and 150 ppm, at 400 °C is shown in Fig. 4. The catalytic performance of the 3 wt.% Ag/Al_2O_3 catalyst is very strongly affected by the presence of SO_2 in the flue gas. The results show that a large drop in conversion, from 56% to 26%, happened from 0 to 25 ppm of SO_2. A further increase to 50 ppm of SO_2 still reduced the conversion, down to 21% but as the concentration was further increased to 100 and 150 ppm the slope flattens out to 17% and 16%, respectively. It should be noted that the ethanol conversion decreases by about the same factor as the NO conversion. This indicates that SO_2 merely decreases the number of active sites but does not alter the reaction mechanism. The CO_2 selectivity, however, decreases drastically with increasing SO_2 concentration up to 150 ppm indicating a change in a part of the mechanism. He et al. [15] have studied the influence of 80 ppm of SO_2 on the NO_x conversion for various hydrocarbon reductants using a 4 wt.% Ag/Al_2O_3 catalyst. Ethanol showed a much higher resistance towards SO_2 (NO conversion changed from 98% to 93% only) than other reductants at 50,000 h^{-1} GHSV. In the present investigation the severe deactivation of 25 ppm SO_2 (NO conversion changed from 56% to 26%) is observed at a high space velocity of 1,800,000 N ml/(g h). The poisoning mechanism by SO_2 could be that SO_2 reacts with oxides on the catalyst surface to form stable sulfates (silver sulfate and aluminum sulfate) under reaction conditions. The formation of stable sulfate species results in a reduced number of sites for chemisorption of NO [5,22]. Since flue gases from purely biomass-fired boilers may contain up to 100 ppm of SO_2, increasing the SO_2 tolerance of alumina based catalysts will be of utmost importance.

3 wt.% Ag/Al_2O_3 catalyst was investigated under the influence of 500 ppm of H_2 and 60 ppm SO_2 gases (Fig. 5). It was observed that the addition of 500 ppm of H_2 enhanced the overall conversion of NO and the conversion pattern was similar to that of the pure ethanol-SCR. At low temperatures the NO conversions of the pure catalyst were low and the addition of hydrogen showed positive effect, though still at a low degrees of conversion. At the optimum temperature of 400 °C, the degree of conversion was shifted from 56% to 66% under the influence of 500 ppm of H_2. When introducing SO_2 into the H_2–ethanol–SCR system, a dramatic loss of activity was observed. The maximum conversion was reached at a relatively high reaction temperature (500 °C) and maximum conversion of NO dropped from 66 to 25%. Overall, presence of 500 ppm of H_2 gas slightly promotes the ethanol-SCR and 60 ppm of SO_2 gas deactivates the catalyst even in the presence of H_2.

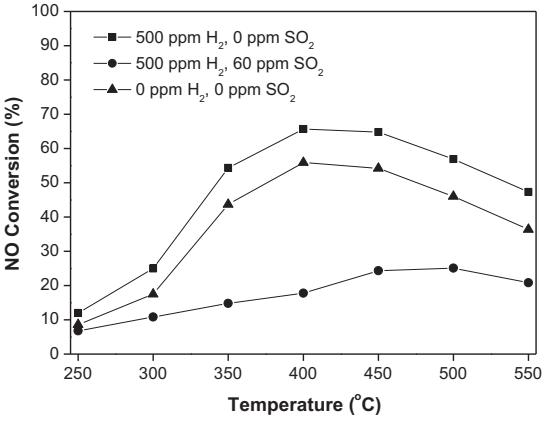

Fig. 5. Effect of H_2 and SO_2 on 3 wt.% Ag/Al_2O_3. Reaction conditions: SV = 1,800,000 N ml/(g h); 500 ppm NO, 1000 ppm ethanol, 0–500 ppm H_2, 0–60 ppm SO_2, 5% O_2, 2% H_2O, balance N_2.

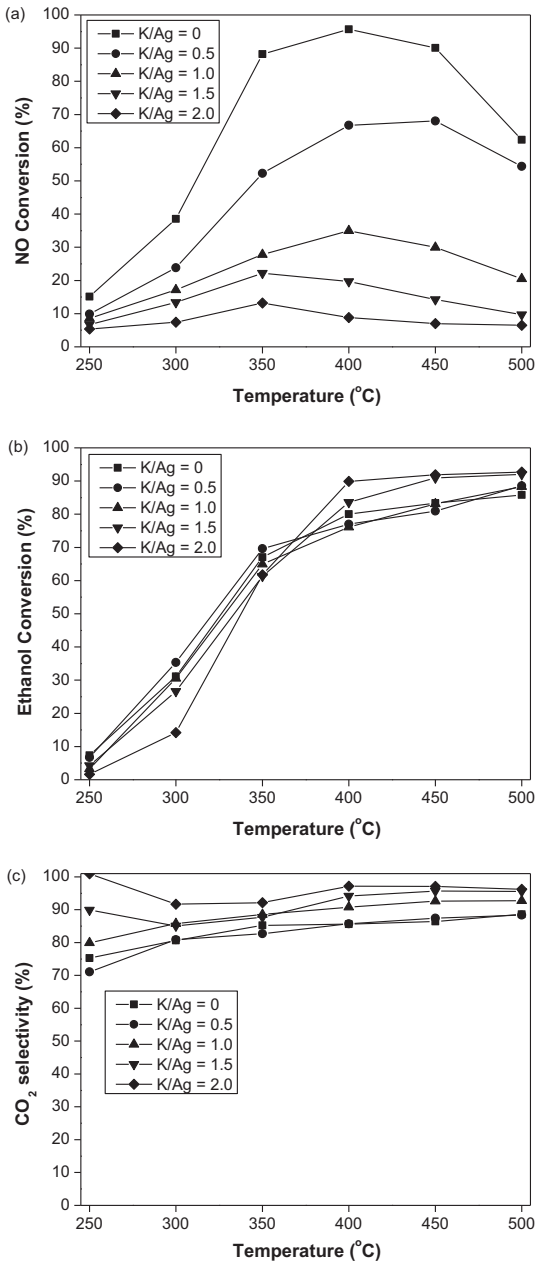

Fig. 6. NO conversion (a), ethanol conversion (b) and CO_2 selectivity (c) for potassium poisoned 3 wt.% Ag/Al_2O_3 catalysts. Reaction conditions: SV = 720,000 N ml/(g h); 500 ppm NO, 1000 ppm ethanol, 5% O_2, 2% H_2O, balance N_2.

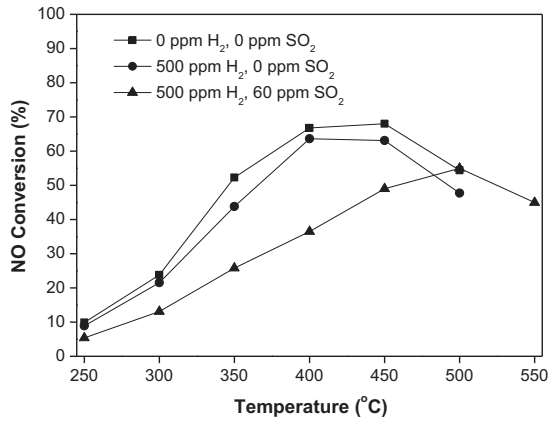

Fig. 7. Effect of H_2 and SO_2 on potassium poisoned 3 wt.% Ag/Al_2O_3 catalyst (K/Ag – 0.5). Reaction conditions: SV = 720,000 N ml/(g h); 500 ppm NO, 1000 ppm ethanol, 0–500 ppm H_2, 0–60 ppm SO_2, 5% O_2, 2% H_2O, balance N_2.

Deactivation of 1 wt.% V_2O_5–7 wt.% WO_3/TiO_2 catalyst at a biomass fired power plant showed an average concentration of K/V (mol/mol) up to 2 [18]. In the present investigation the potassium concentration was also studied up to K/Ag (mol/mol) concentration of 2. Doping the optimum 3 wt.% Ag/Al_2O_3 catalyst with potassium (K/Ag = 0.5–2.0) resulted in a gradual decrease in NO conversion (Fig. 6). The results show that a molar ratio of K/Ag = 0.5, decreased the maximum NO conversion from 96% to 67%. Further addition of potassium to a molar ratio of K/Ag = 1.0 decreased the maximum NO conversion to 35%. At the molar ratios of K/Ag = 1.5 and 2.0 the catalysts were almost completely deactivated, exhibiting maximum NO conversions of 22 and 13%, respectively. Fig. 6 also shows the ethanol conversion and CO_2 selectivity profiles of potassium poisoned Ag/Al_2O_3 catalysts as a function of reaction temperature. Compared to the potassium free 3 wt.% Ag/Al_2O_3 catalyst, K/Ag = 0.5 and 1.0 catalysts showed slightly increased or almost similar ethanol conversions below 350 °C and lower conversions above 350 °C while the conversion for the K/Ag = 1.5 and 2.0 catalysts showed the opposite trend. Regarding CO_2 selectivity, the catalysts showed higher CO_2 selectivity compared to 3 wt.% Ag/Al_2O_3 except for the K/Ag = 0.5 catalyst throughout the temperature window. 1 wt.% potassium on 2 wt.% Ag/Al_2O_3 catalyst also showed deactivation effect for SCR of NO with C_3H_6 [29].

The potassium doped 3 wt.% Ag/Al_2O_3 catalyst (K/Ag = 0.5) was further investigated under the influence of 500 ppm of H_2 and 60 ppm SO_2 gases (Fig. 7). The maximum conversion of K/Ag = 0.5 catalyst was determined to 68% at 450 °C, under normal ethanol-SCR conditions. Upon addition of 500 ppm hydrogen, the conversion profile followed the same pattern, however the conversion was slightly lower, i.e. 63% at 450 °C. Thus hydrogen addition seems to have no positive influence on the conversion of for the poisoned catalyst. When introducing SO_2 to the H_2-ethanol-SCR system, the conversion profile of the catalyst switched to higher temperatures reaching maximum NO conversion of 55% at 500 °C. Overall, there is no promotional effect of H_2 on poisoned K/Ag catalyst and SO_2 further decreases the NO conversion, probably by conversion of the Al_2O_3 carrier to $Al_2(SO_4)_3$.

The surface of the catalysts was investigated on a scale of 1 μm through scanning electron microscopy (SEM). Fresh and potassium poisoned Ag/Al_2O_3 catalysts were analyzed using SEM and the images are shown in Fig. 8. It was observed that the surface particles vary in shape and size depending on the Ag content. The 1 wt.% Ag/Al_2O_3 catalyst image is assumed to resemble the pure alumina surface, due to the low silver concentration on the surface. When increasing the silver content to 3 wt.%, the particles are found to be smaller and evenly distributed on the surface. By further increase of the silver content to 5 wt.% uneven particle sizes are observed with a rough surface. Furthermore, agglomeration of silver oxide is more common at the highest weight percentage resulting in larger particles. Potassium poisoned 3 wt.% Ag/Al_2O_3 catalyst (K/Ag = 1)

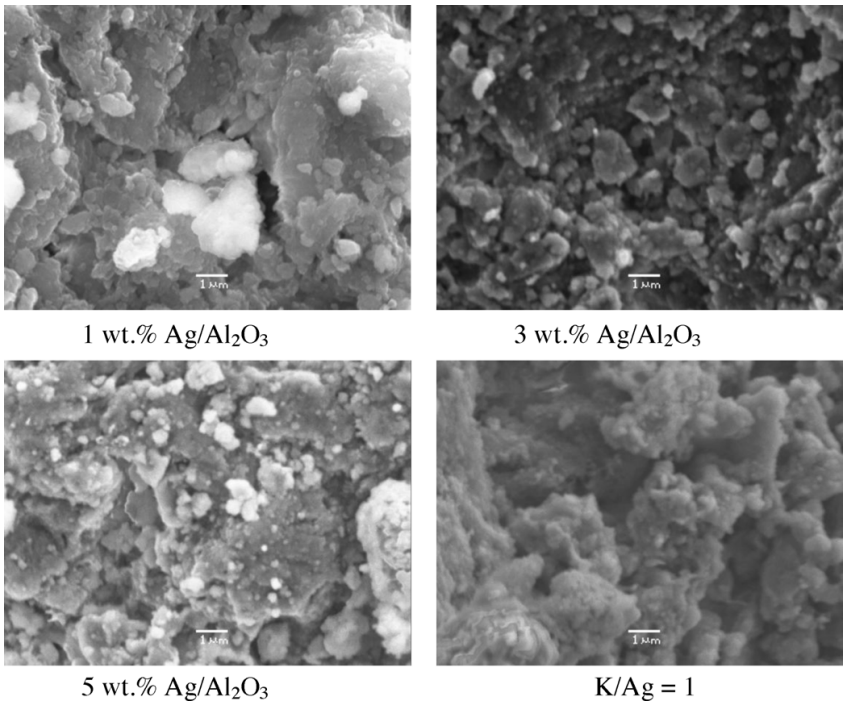

Fig. 8. SEM images of fresh and potassium poisoned Ag/Al_2O_3 catalysts.

showed rough surface with uneven particles, possibly caused by masking by the potassium on the catalyst surface.

The activity of a vanadia based NH_3-SCR catalyst (3 wt.% V_2O_5–7 wt.% WO_3/TiO_2) and ethanol-SCR catalysts was calculated in terms of a first order (in NO) rate constant at 400 °C for different potassium loadings and the results are shown in Fig. 9 as the relative activity (k/k_0). The ethanol-SCR catalyst showed higher relative activity compared to the NH_3-SCR catalyst even at elevated potassium loadings. Table 1 shows the acidity of the potassium poisoned 3 wt.% Ag/Al_2O_3 catalysts. The K/Ag – 0.5 catalyst showed almost stoichiometric acidity loss after doping with 139 μmol/g of potassium. However, the NH_3-SCR catalyst showed above stoichiometric (≈5 times) acidity loss after doping with 100 μmol/g of potassium [30]. Such a change in relative activity and acidity between the both processes reveal that potassium deactivation is milder on ethanol-SCR catalyst compared to NH_3-SCR catalyst, possibly due to the difference in reaction mechanism as discussed above.

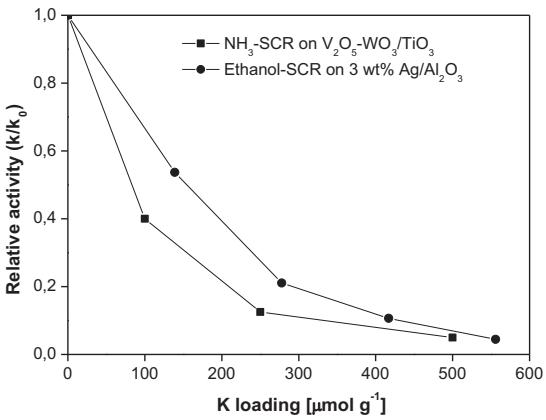

Fig. 9. Relative activity of 3 wt.% V_2O_5–WO_3/TiO_2 catalyst and 3 wt.% Ag/Al_2O_3 catalyst at various potassium concentrations at 400 °C. k, k_0 represent first order rate constants ($cm^3/g\,s$) of potassium poisoned and fresh catalysts, respectively.

4. Conclusions

In summary, Ag/Al_2O_3 catalysts are highly active and CO_2 selective in the ethanol-SCR of NO. Ag/Al_2O_3 catalysts exhibited higher resistance to alkali poisoning compared to the NH_3-SCR catalyst. 500 ppm of H_2 has a mild promotional effect while SO_2 is severely deactivating the Ag/Al_2O_3 catalyst. The potassium doped catalysts did not exhibit any promotional effect by H_2 which instead slightly decreased the NO conversion. Overall, the presently investigated Ag/Al_2O_3 catalysts do not seem robust enough to be a real option for SCR on biomass fired boilers.

Acknowledgments

This work is financially supported by Energinet.dk through the PSO project 10521.

References

[1] H. Bosch, F.J.J.G. Janssen, Catal. Today 2 (1988) 369.
[2] G. Busca, L. Lietti, G. Ramis, F. Berti, Appl. Catal. B 1 (1998) 18.
[3] P. Forzatti, L. Lietti, Heterog. Chem. Rev. 3 (1996) 33.
[4] S. Brandenberger, O. Kröcher, A. Tissler, R. Althoff, Catal. Rev. 50 (2008) 492.
[5] Z. Liu, S.I. Woo, Catal. Rev. 48 (2006) 43.

[6] M. Klimczak, P. Kern, T. Heinzelmann, M. Lucas, P. Claus, Appl. Catal. B 95 (2010) 39.
[7] S. Roy, M.S. Hegde, G. Madras, Appl. Energy 86 (2009) 2283.
[8] H. Gutberlet, B. Schallert, Catal. Today 16 (1993) 207.
[9] L. Valanidou, C. Theologides, A.A. Zorpas, P.G. Savva, C.N. Costa, Appl. Catal. B 107 (2011) 164.
[10] G. Busca, L. Lietti, G. Ramis, F. Berti, Appl. Catal. B 18 (1998) 1.
[11] V.I. Parvulescu, P. Grange, B. Delmon, Catal. Today 46 (1998) 233.
[12] T. Miyadera, Appl. Catal. B 2 (1993) 199.
[13] J. Lee, S. Song, K.M. Chun, Ind. Eng. Chem. Res. 49 (2010) 3553.
[14] K. Shimizu, M. Tsuzuki, A. Satsuma, Appl. Catal. B 71 (2007) 80.
[15] H. He, X. Zhang, Q. Wu, C. Zhang, Y. Yu, Catal. Surv. Asia 12 (2008) 38.
[16] B. Sander, Biomass Bioenergy 12 (3) (1997) 177.
[17] Y. Zheng, P.A. Jensen, A.D. Jensen, B. Sander, H. Junker, Fuel 86 (2007) 1008.
[18] Y. Zheng, A.D. Jensen, J.E. Johnsson, J.R. Thøgersen, Appl. Catal. B 83 (2008) 186.
[19] J. Due-Hansen, S. Boghosian, A. Kustov, P. Fristrup, G. Tsilomelekis, K. Ståhl, C.H. Christensen, R. Fehrmann, J. Catal. 251 (2007) 459.
[20] S.S.R. Putluru, S.B. Kristensen, J. Due-Hansen, A. Riisager, R. Fehrmann, Catal. Today 184 (2012) 192.
[21] N. Okazaki, S. Osada, A. Tada, Appl. Surf. Sci. 121/122 (1997) 396.
[22] A. Abe, N. Aoyama, S. Sumiya, N. Kakuta, K. Yoshida, Catal. Lett. 51 (1998) 5.
[23] A. Musi, P. Massiani, D. Brouri, J.M. Trichard, P. Da Costa, Catal. Lett. 128 (2009) 25.
[24] K.A. Bethke, H.H. Kung, J. Catal. 172 (1997) 93.
[25] X. Zhang, H. He, Z. Ma, Catal. Commun. 8 (2007) 187.
[26] S. Satokawa, J. Shibata, K. Shimizu, A. Satsuma, T. Hattori, Appl. Catal. B 42 (2003) 179.
[27] A. Westermann, B. Azambre, Catal. Today 176 (2011) 441.
[28] R. da Silva, R. Cataluña, A. Martinez-Arias, Catal. Today 143 (2009) 242.
[29] I.H. Son, M.C. Kim, H.L. Koh, K.L. Kim, Catal. Lett. 75 (2001) 191.
[30] S.S.R. Putluru, A.D. Jensen, A. Riisager, R. Fehrmann, Catal. Sci. Technol. 1 (2011) 631.

Catal Lett (2014) 144:395–402
DOI 10.1007/s10562-013-1176-2

Low-Temperature NH_3–SCR of NO on Mesoporous $Mn_{0.6}Fe_{0.4}/TiO_2$ Prepared by a Hydrothermal Method

Leonhard Schill · Siva Sankar Reddy Putluru · Rasmus Fehrmann · Anker Degn Jensen

Received: 3 July 2013 / Accepted: 26 November 2013 / Published online: 11 December 2013

Abstract Mesoporous 30 wt% $Mn_{0.6}Fe_{0.4}/TiO_2$ has been prepared by a novel hydrothermal method using a structure directing agent and characterized by N_2 adsorption, SEM, XRD, EDX, H_2-TPR and the catalytic activity for the selective catalytic reduction (SCR) of NO by ammonia was measured under power plant flue gas conditions. Compared to 30 wt% $Mn_{0.6}Fe_{0.4}/TiO_2$ prepared by impregnation, the average pore size was significantly increased. The method of preparation has only a small effect on the catalytic activity at temperatures between 125 and 300 °C. The hydrothermal preparation method leads to a somewhat higher $(NH_4)_2SO_4$ tolerance at 150 °C compared to the impregnation preparation method. Regeneration of the $(NH_4)_2SO_4$ loaded samples by heating to 400 °C was not possible whereas water washing yielded better regeneration. The catalysts are significantly more active than a commercial VWT SCR catalyst at temperatures up to 200 °C, but do not match the activity of the latter at the higher temperatures typically encountered at the high dust position in power plants.

Keywords Low temperature NH_3 SCR · Mesoporous TiO_2 · Mn–Fe · Sol–gel · Hydrothermal

L. Schill · S. S. R. Putluru · R. Fehrmann (✉)
Centre for Catalysis and Sustainable Chemistry, Department of Chemistry, Technical University of Denmark, Building 207, 2800 Kgs. Lyngby, Denmark
e-mail: rf@kemi.dtu.dk

L. Schill · S. S. R. Putluru · A. D. Jensen
Combustion and Harmful Emission Control Research Centre, Department of Chemical and Biochemical Engineering, Technical University of Denmark, Building 229, 2800 Kgs. Lyngby, Denmark

1 Introduction

Over the last 10 years a large number of publications on low-temperature SCR of NO_x have appeared in the open literature. Many of the investigated catalysts contain transition metals, with Mn being the most prominent one. One of the major drawbacks of Mn containing catalysts is their low SO_2 tolerance [1, 2]. Jin et al. [2] have performed an in depth study of the effect of SO_2 on MnCe/TiO_2 and found that when exposed at low temperatures the catalyst is mainly deactivated by pore plugging caused by $(NH_4)_2SO_4$ and $(NH_4)HSO_4$ whereas, at higher temperatures, metal sulfate formation takes place. The former mode of deactivation proved to be reversible. The ammonia sulfates could be removed by either water washing or heating [2, 3], with water washing recovering more of the initial activity [3]. Zhongyi et al. [3] have hypothesized that upon heating to 400 °C $(NH_4)_2SO_4$ decomposes with SO_3 being one of the products which in turn might form metal sulfates with the Mn and Fe species of the catalyst. This would explain the lower effectiveness of regeneration by heating compared to water-washing. One way of retarding the deactivation caused by pore plugging is to employ mesoporous Mn–Fe–Ce/TiO_2 catalysts as suggested by Yu et al. [4] using a sol–gel route in conjunction with a structure directing agent (SDA). Liu et al. [5] have reported that mesoporous titania can be synthesized by a hydrothermal method under weak acid conditions employing an SDA. Kim et al. [6] have reported high activity of sol–gel prepared Mn–Fe/TiO_2 (22 wt% Mn, 11 wt% Fe) in a wide temperature window. At a space velocity of 100,000 h^{-1} they measured 60 % NO conversion at 150 °C and above 80 % NO conversion between 175 and 300 °C. The promoting effect of Fe was ascribed to an increased dispersion of Mn on TiO_2 [6].

In the present study we have synthesized 30 wt% $Mn_{0.6}Fe_{0.4}/TiO_2$ using a hydrothermal method. The duration of the hydrothermal treatment was varied between 0 and 24 h. The surface area and average pore size were measured by N_2 adsorption. The NH_3–SCR activities of the mesoporous $Mn_{0.6}Fe_{0.4}/TiO_2$ catalysts were measured between 125 and 300 °C in steps of 25 °C and compared with a 30 wt% $Mn_{0.6}Fe_{0.4}/TiO_2$ prepared by the citric acid method (impregnation) and also with a commercial VWT (3 wt% V_2O_5–7 wt% WO_3/TiO_2) catalyst. The $(NH_4)_2SO_4$ tolerance at 150 °C of a catalyst prepared by impregnation and one prepared by the hydrothermal method was investigated by impregnating these catalysts with $(NH_4)_2SO_4$ followed by drying at 150 °C. Regeneration of these catalysts by heating to 400 °C and by water washing was also tested.

2 Experimental

2.1 Catalyst Preparation

2.1.1 Citric Acid Method

30 wt% $Mn_{0.6}Fe_{0.4}/TiO_2$ was prepared by the citric acid method [7] and is denoted as MnFe/TiO_2-i. Appropriate amounts of manganese(II) acetate tetrahydrate [$(CH_3COO)_2Mn \times 4\ H_2O$, 99.9 %, Aldrich)], Iron(III) nitrate nonahydrate [$Fe(NO_3)_3 \times 9\ H_2O$, 98 %, Aldrich] and TiO_2 (G5, with surface area 356 $m^2\ g^{-1}$) were placed in a beaker and dissolved in water yielding a 1 molar solution. Citric acid ($C_6H_8O_7$, 99 %, Aldrich) was added (1 mol L^{-1}). The mixture was dried on a hot plate at 100 °C and further oven dried at 105 °C for 4 h followed by calcination in air for 3 h at 500 °C.

2.1.2 Hydrothermal Method

30 wt% $Mn_{0.6}Fe_{0.4}/TiO_2$ was prepared using a modified version of the recipe for mesoporous TiO_2 reported elsewhere [5] and is denoted as MnFe/TiO_2-h-xh with x being the duration of the hydrothermal treatment in hours. In a typical preparation, 1.338 g of manganese(II) acetate tetrahydrate [$(CH_3COO)_2Mn \times 4H_2O$, 99.9 %, Aldrich] and 1.470 g of iron(III) nitrate nonahydrate [$Fe(NO_3)_3 \times 9H_2O$, 98 %, Aldrich] were dissolved in 30 mL acetic acid aqueous solution (20 vol%) at room-temperature under vigorous stirring. To this solution 5 g titanium butoxide [$Ti(OC_4H_9)_4$, 98 %, Aldrich] were added dropwise under vigorous stirring. The mixed solution was sealed and kept stirring for 4 h to obtain solution A. In a separate beaker, 3 g of block copolymer P_{123} [$HO(CH_2CH_2O)_{20}(CH_2CH(CH_3)O)_{70}(CH_2CH_2O)_{20}H$ (Mav = 5800, Aldrich)] were dissolved in 20 mL absolute ethanol (CH_3CH_2OH, 99.8 %, Aldrich) to yield solution B. Solution B was added dropwise to solution A. The resulting solution was sealed and further stirred for 24 h at room temperature. The solution was then transferred into a Teflon sealed container which was then heated in an oven at 120 °C for 0 (no hydrothermal treatment), 12, 14 and 24 h. After the hydrothermal step the precipitate, if formed, was collected and dried over night in air at 100 °C. The as-prepared samples were finally calcined at 450 °C for 4 h. In addition to the MnFe/TiO_2-h-xh samples, one bare titania sample was prepared as described in [5] with 48 h of hydrothermal treatment and is denoted as TiO_2-h-48 h.

2.1.3 $(NH_4)_2SO_4$ Poisoning

MnFe/TiO_2-h-24 h and MnFe/TiO_2-h were impregnated with aqueous $(NH_4)_2SO_4$ solutions to give loadings of 125 and 250 μmol g^{-1} followed by over-night drying at 150 °C.

2.2 Catalytic Activity Measurement

The SCR activity measurements were carried out at atmospheric pressure in a fixed-bed reactor loaded with 50 mg of fractionized (180–300 μm) catalyst mixed with 50 mg of SiO_2 (180–300 μm) at a flow rate of 290 mL min^{-1}. The inlet concentrations were: NO = 1,000 ppm, NH_3 = 1,000 ppm, O_2 = 4 % and H_2O = 2.3 % with He as balance gas. The NO concentration was continuously monitored by a Thermo Electron Model 17C chemiluminescent NH_3–NO_x gas analyzer. The activity data were collected when the reaction reached steady state after 20 min at each temperature.

In the case of the $(NH_4)_2SO_4$ loaded samples we only measured the activity at 150 °C. We also attempted to regenerate the samples loaded with 250 μmol g^{-1} of $(NH_4)_2SO_4$ by heating them for 1 h to 400 °C in a flow of He followed by cooling to 150 °C and activity measurement at that temperature. Both samples loaded with $(NH_4)_2SO_4$ were water washed with around 50 mL deionized water per 0.1 g of poisoned catalyst followed by drying at 150 °C and activity measurement at that temperature.

2.3 Catalyst Characterization

BJH and BET surface areas and pore sizes were determined from nitrogen physisorption measurements on about 100 mg sample at liquid nitrogen temperature with a Micromeritics ASAP 2020 instrument. The samples were heated to 200 °C for 1 h prior to the measurement. SEM-EDX was performed on a LEO 440 microscope. The samples were prepared using an MT-990 rotary microtome.

Before analysis, the samples were covered with a very thin carbon film to become conductive. X-ray powder diffraction (XRPD) measurements were performed on Huber G670 powder diffractometer using CuK_α radiation within a 2θ range of 2°–100° in the steps of 0.02°. H_2-TPR studies were conducted on a Micromeritics Autochem-II instrument. In a typical experiment, 100 mg of oven-dried sample was placed in one arm of a U-shaped quartz sample tube on a quartz wool plug. TPR analysis was carried out in a reducing mixture (50 mL/min) consisting of 4 % H_2 and balance Ar (Air Liquide) from 50 to 600 °C (10 °C/min). The hydrogen concentration in the effluent stream was monitored by a thermal conductivity detector (TCD) and the H_2 consumption values were calculated from calibration experiments. NH_3–TPD experiments were conducted on a Micromeritics Autochem-II instrument. In a typical TPD experiment, 50–100 mg of dried sample was placed in a quartz tube and pretreated in flowing He at 100 °C for 1 h. Then the sample was treated with anhydrous NH_3 gas (Air Liquide, 5 % NH_3 in He). After NH_3 adsorption, the sample was flushed with He (50 ml/min) for 60 min at 100 °C. Finally, the TPD operation was carried out by heating the sample from 100 to 650 °C (10 °C/min) under a flow of He (50 ml/min).

3 Results and Discussion

Using the hydrothermal method it turned out that 12 h of hydrothermal treatment at 120 °C was insufficient to form a precipitate. Therefore, MnFe/TiO_2-h-12 h was discarded in the following discussion. Table 1 presents the textural properties of the different catalysts and TiO_2-h-48 h. The textural properties of TiO_2-h-48 h matched those reported in [5] sufficiently well, e.g. Liu et al. [5] reported a BET surface area of 116 $m^2\ g^{-1}$ while we could measure one of 126 $m^2\ g^{-1}$. The surface areas of the MnFe containing catalysts are larger when using a SDA as compared to the sample prepared by impregnation, though the differences are not very pronounced. Subjecting the gel to hydrothermal treatment does not necessarily increase the surface area. The surface area of the hydrothermally prepared (pure) titania is similar to that of the hydrothermally prepared MnFe/TiO_2 samples.

The mean pore width of MnFe/TiO_2-i (100 Å) is, surprisingly, larger than that of MnFe/TiO_2-h-0 h (85 Å). This, however, can be explained by the existence of inter particle spaces, as will be discussed below. Subjecting the SDA containing gel to hydrothermal conditions clearly increases the mean pore size, with 24 h of duration (160 Å) yielding similarly large pores than after 14 h of duration (147 Å). The bare titania, TiO_2-h-48 h, exhibits a slightly smaller average pore size (126 Å) than the MnFe/TiO_2 prepared by the hydrothermal method. This, however, can again be explained by the presence of inter particle spaces. The pore volumes of MnFe/TiO_2-i and MnFe/TiO_2-h-0 h are practically identical. Apparently, using a SDA without hydrothermal treatment does not increase the pore volume. Applying hydrothermal treatment increases the pore volume significantly, with no big difference between 14 and 24 h of duration. These two catalysts have slightly larger pore volumes than TiO_2-h-48 h, which again can be explained by the presence of inter particle spaces.

Figure 1 shows the nitrogen adsorption/desorption isotherms. For the bare TiO_2, according to the IUPAC classification [8], we see a type IV curve with a H1 hysteresis loop, indicating that the sample has ordered cylindrical pore geometry with a high degree of pore size uniformity. This was also observed by Liu et al. [5]. The hysteresis loop is generally ascribed to the condensation of N_2 in mesopores. The two hydrothermally prepared catalysts (MnFe/TiO_2-h-14 h and MnFe/TiO_2-h-24 h) show type IV curves, however, with H3 hysteresis loops, often associated with aggregates of plate-like particles giving rise to slit-

Table 1 Texture parameters of the MnFe/TiO_2 catalysts and the bare TiO_2

Catalyst	BET surface area (m^2g^{-1})[a]	BJH surface area (m^2g^{-1})[b]	Mean pore size (Å)[c]	Pore volume ($cm^3\ g^{-1}$)[d]	Pore volume ($cm^3\ g^{-1}$)[e]
MnFe/TiO_2-i	110	115	100	0.288	0.217
MnFe/TiO_2-h-0 h	126	139	85	0.295	0.279
MnFe/TiO_2-h-14 h	142	145	147	0.533	0.445
MnFe/TiO_2-h-24 h	125	127	160	0.508	0.431
TiO_2-h-48 h	126	137	126	0.432	0.426

[a] Calculated from the linear part of the BET plot

[b] Calculated from BJH Adsorption

[c] BJH adsorption average pore width

[d] BJH adsorption cumulative volume of pores

[e] BJH adsorption cumulative volume of pores excluding pores >500 Å

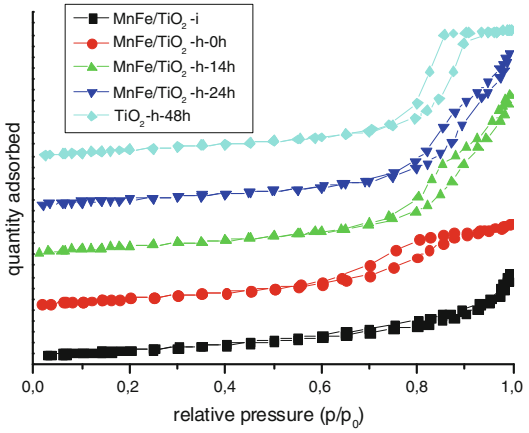

Fig. 1 Adsorption/desorption isotherm of the $MnFe/TiO_2$ catalysts and the bare TiO_2

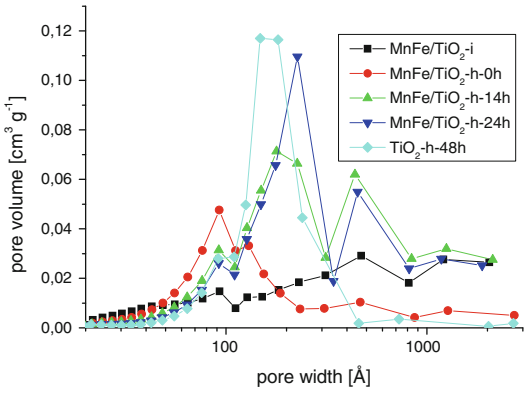

Fig. 2 BJH pore width distribution (from adsorption branch) of the $MnFe/TiO_2$ catalysts and the bare TiO_2

shaped pores. $MnFe/TiO_2$-h-0 h exhibits a similar curve, however, shifted to lower partial pressures, indicating smaller pores. The curve of $MnFe/TiO_2$-i has a H4 hysteresis loop often associated with narrow slit-like pores. The hysteresis in this case is much less pronounced, indicating a relatively non-mesoporous structure [8].

Figure 2 shows the BJH pore width distribution. TiO_2-h-48 h has a mono-modal distribution centered at 160 Å and very little nitrogen is adsorbed in "pores" larger than 500 Å. Table 1 gives the pore volumes including and excluding the contributions from "pores" larger than 500 Å. $MnFe/TiO_2$-h-14 h and $MnFe/TiO_2$-h-24 h both show a bi-modal distribution with the major peaks at 180 and 230 Å, respectively. Both distributions have a minor peak at around 450 Å and continue to adsorb nitrogen into "pores" up to 2,000 Å in width. These "pores" or

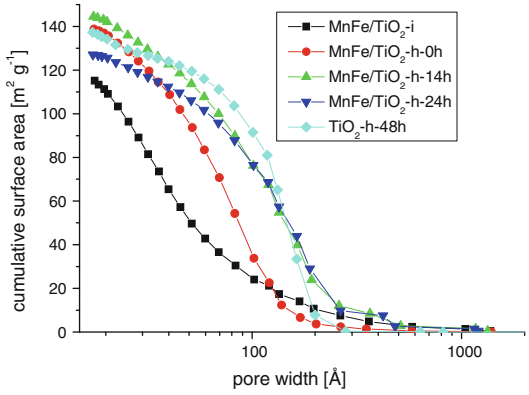

Fig. 3 Cumulative surface area as function of the BJH pore width (from adsorption branch) of the $MnFe/TiO_2$ catalysts and the bare TiO_2

interparticle voids are the reason why $MnFe/TiO_2$-h-14 h and $MnFe/TiO_2$-h-24 h have larger pore volumes and average pore sizes than TiO_2-h-48 h. $MnFe/TiO_2$-h-0 h exhibits a mono-modal distribution centered at 90 Å and very little adsorption into "pores" larger than 500 Å. Hydrothermal treatment apparently causes a shift to larger pores and creation of inter particle spaces. $MnFe/TiO_2$-i does not show a clear distribution. Note the presence of inter particle voids and a relatively large nitrogen uptake into pores smaller than 50 Å. Adsorption into pores sized 60–200 Å is much smaller than in the case of the sol–gel/hydrothermally prepared catalysts.

Figures 3 and 4 show the cumulative BJH surface area and fraction of surface area as a function of the minimum width of the pores they are located in. The cumulative surface area of $MnFe/TiO_2$-i shows a relatively constant increase when decreasing the pore size. The samples prepared with a SDA show a more edge-like increase, especially when treated hydrothermally for long periods of time. Most noticeably, the fraction of surface area located in small pores was significantly reduced, e.g. the fraction in pores smaller than 80 Å could be reduced from 73 to 29 % when applying 24 h of hydrothermal treatment compared to the impregnated sample. Therefore, we can expect deactivation due to pore plugging by $(NH_4)_2SO_4$ and $(NH_4)HSO_4$ to be less pronounced.

Figure 5 shows the NO conversion profiles of our catalysts and that of an industrial reference catalyst (3 wt% V_2O_5–7 wt% WO_3/TiO_2). Over the whole temperature range (125–300 °C), the 30 wt% $Mn_{0.6}Fe_{0.4}/TiO_2$ catalysts perform essentially equally well, irrespective of the method of preparation. This is somewhat in conflict with the findings of Kim et al. [6] who reported that sol–gel prepared Mn/TiO_2 outperforms Mn/TiO_2 prepared by impregnation.

Comparing the activities of our catalysts to those of the Kim group is not possible, since the water contents in the feed are too different (2.3 vs. 10 vol% H_2O). The industrial reference catalyst is essentially inactive up to 200 °C and approaches the activity of the 30 wt% $Mn_{0.6}Fe_{0.4}/TiO_2$ catalysts only at 250 °C. Activity parity of 30 wt% $Mn_{0.6}Fe_{0.4}/TiO_2$ prepared by impregnation and the hydrothermal method might be explained by the fact that N_2-adsorption (BET surface area), SEM, NH_3–TPD, EDX and XRD all yield similar results (see below).

Figure 6 shows the conversions of MnFe/TiO_2-h-24 h and MnFe/TiO_2-i at 150 °C as a function of the $(NH_4)_2SO_4$ loading. MnFe/TiO_2-h-24 h (fresh: 36 % conversion) retains more of its activity after poisoning. At 125 μmol g^{-1} it retains 25 % conversion and at 250 μmol g^{-1} 16 %. MnFe/TiO_2-i (fresh: 39 % conversion) only shows 20 and 11 % conversions at those loadings, respectively. Using the hydrothermal preparation method which imparts the catalyst a mesoporous structure seems to lower the deactivation by pore plugging. However, in the case of the samples loaded with 250 μmol g^{-1} regeneration by heating to 400 °C was not effective (Fig. 7). The conversions decreased even further, reaching 12 % in the case of MnFe/TiO_2-h-24 h and 8 % in the case of MnFe/TiO_2-i. This might be due to the formation of metal sulfates [3]. Water washing proved much more effective, especially in the case of the hydrothermally prepared catalyst. MnFe/TiO_2-i and MnFe/TiO_2-h-24 h reached conversions of 22 and 31 %, respectively. This is in line with earlier reports [3].

SEM analysis (Fig. 8) could not discriminate between MnFe/TiO_2-i and MnFe/TiO_2-h-24 h. Loading these two catalysts with 125 μmol g^{-1} of $(NH_4)_2SO_4$ did not lead to visible changes in the SEM images. XRD analysis (Fig. 9) shows anatase and MnO_2 phases for both MnFe/TiO_2-i and MnFe/TiO_2-h-24 h. The TiO_2 particle sizes were

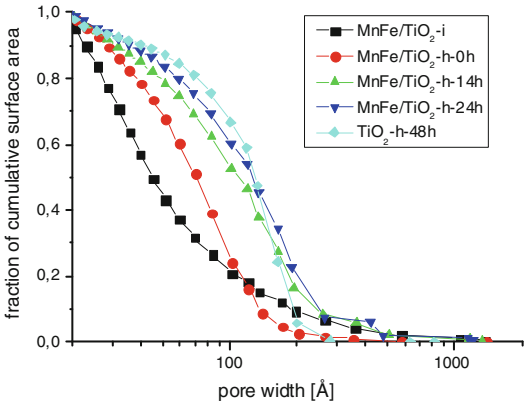

Fig. 4 Relative cumulative surface area as function of the BJH pore width (from adsorption branch) of the MnFe/TiO_2 catalysts and the bare TiO_2

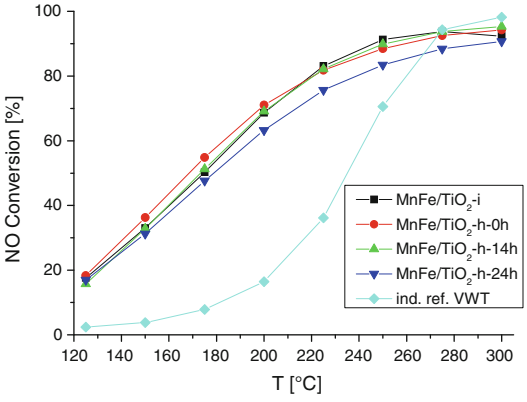

Fig. 5 NO conversions ([NO] = [NH_3]: 1,000 ppm; O_2: 4 %; H_2O: 2.3 %; total flow: 290 mL min^{-1}; catalyst weight: 0.05 g

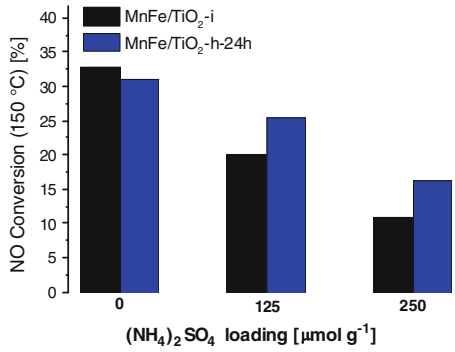

Fig. 6 NO conversions of MnFe/TiO_2-i and MnFe/TiO_2-h-24 h at 150 °C as function of the $(NH_4)_2SO_4$ loading

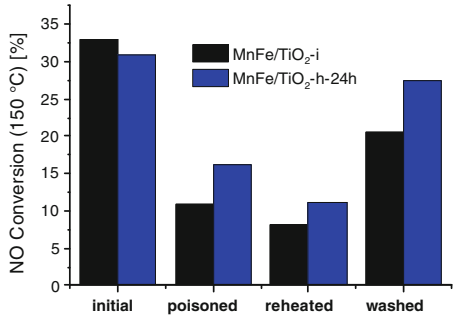

Fig. 7 NO conversions of MnFe/TiO_2-i and MnFe/TiO_2-h-24 h at 150 °C loaded with 250 μmol g^{-1} of $(NH_4)_2SO_4$ and regenerated at 400 °C for 1 h or by water washing

determined by Scherrer's equation using the peak at $\theta = 25.3°$, yielding 110 and 87 Å for MnFe/TiO_2-i and MnFe/TiO_2-h-24 h, respectively. Using the hydrothermal method of preparation does not shift the anatase peaks, indicating that Mn and Fe are not necessarily incorporated into the TiO_2 framework. The atomic compositions were determined with EDX. For the catalyst prepared by impregnation we found a composition of 25 wt% $Mn_{0.56}Fe_{0.44}$/TiO_2-i and 24 wt% $Mn_{0.61}Fe_{0.39}$/TiO_2-h-24 h for the hydrothermally prepared sample. The metal loadings are in both cases lower than the theoretical 30 wt%. This can be explained by the fact that in the final catalyst, Mn and Fe are not present in metallic but oxide form. The relative amounts of Mn and Fe are close to the theoretical $Mn_{0.6}Fe_{0.4}$.

De-convoluted H_2-TPR spectra of MnFe/TiO_2-i and MnFe/TiO_2-h-24 h are shown in Fig. 10 and the peak sizes are summarized in Table 2. Like in the case of unsupported $Mn_{0.6}Fe_{0.4}$ [7] the TPR patterns are difficult to interpret due to the presence of both Mn and Fe ions. The pattern of MnFe/TiO_2-i very much resembles the pattern of 20 wt% Mn/TiO_2 reported by Park et al. [9]. Adopting their peak assignments, the peak at 269 °C may be associated with surface bridged oxygen atoms, such as Mn–O–TiO_2, the peak at 368 °C may be associated with reduction of surface

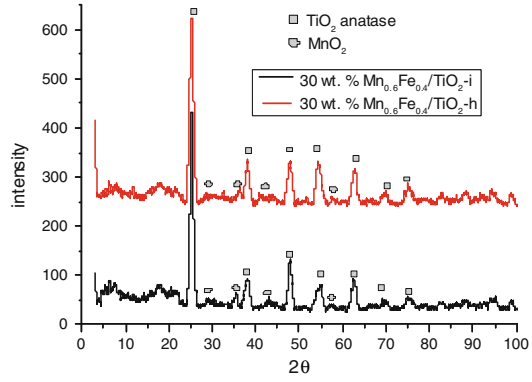

Fig. 9 XRD patterns of of MnFe/TiO_2-i and MnFe/TiO_2-h-24 h

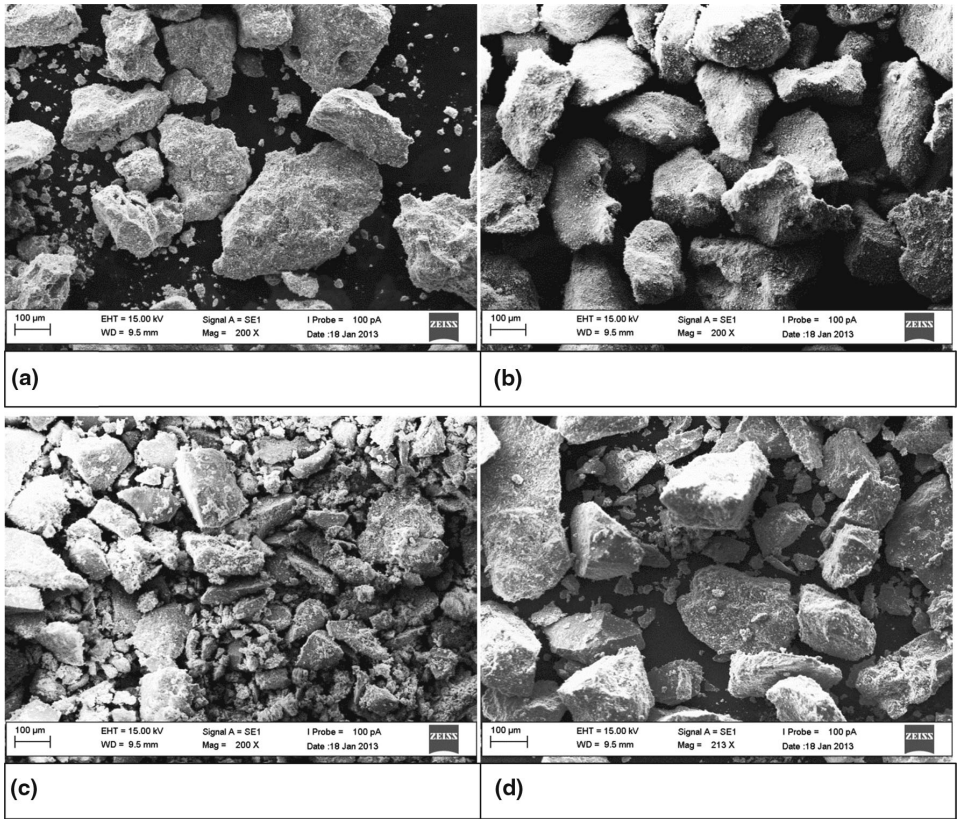

Fig. 8 SEM images of fresh and $(NH_4)_2SO_4$ loaded samples. **a** MnFe/TiO_2-i fresh, **b** MnFe/TiO_2-i poisoned, **c** MnFe/TiO_2-h-24 h fresh and **d** MnFe/TiO_2-h-24 h poisoned

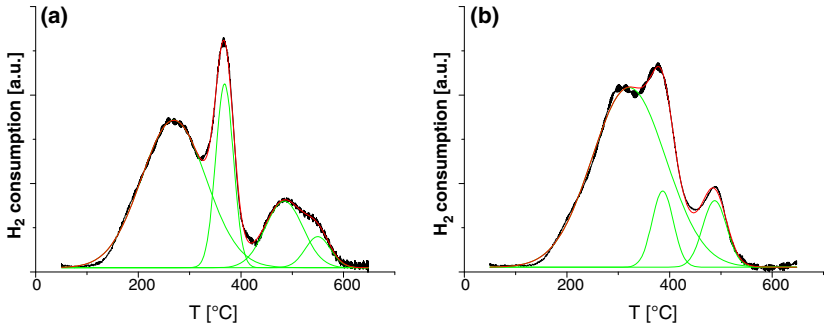

Fig. 10 H_2–TPR of **a** MnFe/TiO_2-i and **b** MnFe/TiO_2-h-24 h

Table 2 Peak areas of de-convoluted H_2–TPR of MnFe/TiO_2-i and MnFe/TiO_2-h-24 h

MnFe/TiO_2-i		MnFe/TiO_2-h-24 h	
T (°C)	Peak area (μmol H_2 g^{-1})	T (°C)	Peak area (μmol H_2 g^{-1})
269	2,221	321	2,172
368	759	387	264
484	583	488	262
550	182	–	–
Total	3,745	Total	2,699

MnO_2 to Mn_2O_3, the peak at 484 °C may be associated with reduction of surface Mn_2O_3 to Mn_3O_4 and the peak at 550 °C may be associated with reduction of surface Mn_3O_4 to MnO. The pattern of MnFe/TiO_2-h-24 h consists of only 3 peaks. The first peak which might be associated with surface bridged oxygen atoms, such as Mn–O–TiO_2, is located at a significantly higher temperature (321 °C). This might suggest that the interaction of Mn with the TiO_2 differs between the two catalysts. However, size-wise the first peak of the two samples does not differ much. The peaks that might be assigned to the reduction of surface MnO_2 to Mn_2O_3 and Mn_2O_3 to Mn_3O_4 are located at similar temperatures as in the MnFe/TiO_2-i case, however, are very much smaller. The peak at 550 °C is missing altogether (up to 650 °C). One might conclude that the surface Mn oxides are harder to reduce in the MnFe/TiO_2-h-24 h case.

In addition we have made H_2-TPR measurements on 5 wt% Fe/TiO_2 (not shown) and found one peak at approximately 350 °C, possibly due to the reduction of Fe_2O_3 to Fe. Accordingly, the second peak may also be assigned in this way.

Figure 11 shows NH_3–TPD of MnFe/TiO_2-i and MnFe/TiO_2-h-24 h. MnFe/TiO_2-i and MnFe/TiO_2-h-24 h desorbed 1,039 and 1,327 μmol NH_3 g^{-1} of substance, respectively. The slightly higher number of surface acid sites of MnFe/TiO_2-i is more pronounced in the high

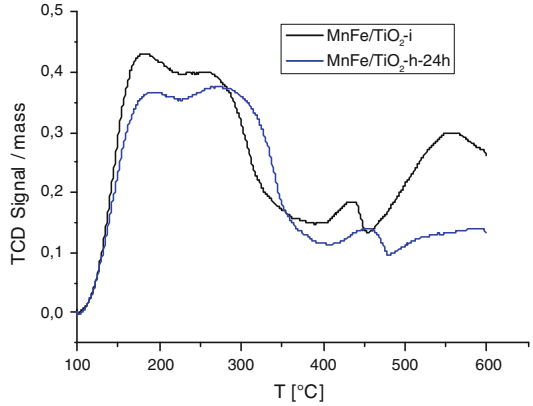

Fig. 11 NH_3–TPD of of MnFe/TiO_2-i and MnFe/TiO_2-h-24 h using a TCD detector

temperature region (>400 °C). The activity data (Fig. 5) suggest that the slightly higher number of surface acid sites of MnFe/TiO_2-i compared to MnFe/TiO_2-h-24 h does not lead to an increased reduction of NO.

4 Conclusion

Mesoporous 30 wt% $Mn_{0.6}Fe_{0.4}/TiO_2$ has been prepared with a structure directing agent containing gel followed by hydrothermal treatment at 120 °C. In terms of textural properties the most striking difference compared to 30 wt% $Mn_{0.6}Fe_{0.4}/TiO_2$ prepared by impregnation is the high fraction of surface area located in mesopores. As this fraction is considerably increased, one can expect pore plugging and therefore deactivation by $(NH_4)_2SO_4$ and $(NH_4)HSO_4$ to be less pronounced. Activity measurements of catalysts loaded with $(NH_4)_2SO_4$ by impregnation confirmed this expectation. In terms of NO reduction activity, there is no significant difference between the catalysts

prepared by impregnation and hydrothermal methods. Though the catalysts prepared in this study have superior activities compared to a commercial VWT reference catalyst at temperatures between 125 and 200 °C, their activities at 200 °C are still low compared to the activity of the VWT reference catalyst at 350 °C. Removal of $(NH_4)_2SO_4$ by heating to 400 °C was ineffective probably due to the formation of metal sulfates whereas water washing proved to be much more effective.

Acknowledgment This work has been financially supported by Energinet.dk through the PSO Project 10521.

References

1. Casapu M, Kröcher O, Elsener M (2009) Appl Catal B 88:413–419
2. Jin R, Liu Y, Wu Z, Wang H, Gu T (2010) Catal Today 153:84–89
3. Zhongyi S, Yuefeng H, Jianming X, Xiaoming W, Weiping L (2012) J Rare Earths 30:676
4. Yu J, Guo F, Wang Y, Zhu J, Liu Y, Su F, Gao S (2010) Appl Catal B 95:160
5. Liu J, An T, Li G, Bao N, Sheng G, Fu J (2009) Microporous Mesoporous Mater 124:197
6. Kim YJ, Kwon HJ, Nam I-S, Choung JW, Kil JK, Kim H-J, Cha M-S, Yeo GK (2010) Catal Today 151:244–250
7. Qi G, Yang RT (2003) J Catal 217:434–441
8. Sing KSW, Everet DH, Haul RAW, Moscou L, Pierotti RA, Rouquérol J, Siemieniewska T (1985) Pure Appl Chem 57:603–619
9. Park KH, Lee SM, Kim SS, Kwon DW, Hong SC (2013) Catal Lett 143:246–253

J Mater Sci (2014) 49:2705–2713
DOI 10.1007/s10853-013-7926-0

Superior DeNO$_x$ activity of V_2O_5–WO_3/TiO_2 catalysts prepared by deposition–precipitation method

Siva Sankar Reddy Putluru · Leonhard Schill · Diego Gardini · Susanne Mossin · Jakob B. Wagner · Anker Degn Jensen · Rasmus Fehrmann

Received: 8 August 2013 / Accepted: 28 November 2013 / Published online: 7 January 2014

Abstract V_2O_5–WO_3/TiO_2 catalysts were prepared by incipient wetness impregnation and deposition–precipitation (DP) methods. The catalysts were characterized by N_2 physisorption, X-ray powder diffraction, Fourier transform infra red spectroscopy, electron paramagnetic resonance spectroscopy, transmission electron microscopy, H_2-temperature programmed reduction and NH_3-temperature programmed desorption. The catalysts exhibited only crystalline TiO_2 phases with the active metal and promoter in highly dispersed or amorphous state. The 3 wt% V_2O_5–10 wt% WO_3/TiO_2 catalyst prepared by DP using ammonium carbamate as a precipitating agent was found to be the most active and selective to N_2. The superior activity of the catalyst can be ascribed to the altered acidic and redox properties of vanadium. The catalysts did not show increased potassium resistance with the change in preparation method or with increasing vanadium concentration. Furthermore, potassium-poisoned catalysts showed above stoichiometric loss of surface acidity. Thus, these modified formulations are suggested to be used in coal/natural gas-fired power plants where there is a demand for high selective catalytic reduction activity and selectivity to N_2.

S. S. R. Putluru · L. Schill · S. Mossin · R. Fehrmann (✉)
Centre for Catalysis and Sustainable Chemistry, Department of Chemistry, Technical University of Denmark, Building 207, 2800 Kgs. Lyngby, Denmark
e-mail: rf@kemi.dtu.dk

S. S. R. Putluru · L. Schill · A. D. Jensen
Combustion and Harmful Emission Control Research Centre, Department of Chemical and Biochemical Engineering, Technical University of Denmark, Building 229, 2800 Kgs. Lyngby, Denmark

D. Gardini · J. B. Wagner
Center for Electron Nanoscopy, Technical University of Denmark, 2800 Kgs. Lyngby, Denmark

Introduction

The selective catalytic reduction (SCR) of NO with ammonia as the reductant is the most common method to eliminate NO_x from flue gases of stationary sources. Several catalysts are reported to be active for the SCR of NO with ammonia. The most well known and commercially used catalyst is vanadia dispersed on a titania support with tungsten oxide as a promoter (V_2O_5–WO_3/TiO_2) [1–3]. Vanadia is the active component and is responsible for the reduction of NO. The vanadium content is generally kept low to limit the oxidation of SO_2 in the flue gases [1]. WO_3 is used (typically around 10 wt%) to increase acidity [1–4], promote SCR activity and most importantly, increase the thermal stability of the catalyst [1–4]. WO_3 addition also helps to further limit the oxidation of SO_2 [1, 4]. The commercial catalyst is installed in the temperature region 300–400 °C, where maximum efficiency of the process can be obtained. To achieve this temperature the vanadium catalysts are placed in high dust (or low dust positions) in most of the configurations [4]. Depending on the fuel type and rate of deactivation, catalysts are also placed in tail-end position where the flue gas is free from dust and SO_2.

The SCR is the most efficient and well-proven technology for the flue gas treatment of stationary sources like gas-, oil- and coal-fired power plants. Despite the success of the SCR technology, some aspects demand improvement. Development of highly active alternative/modified SCR catalysts can be used for both low-temperature and high-temperature regions [5], and extend the application of the SCR technology to biomass and incineration plants.

The use of biomass as an alternative to fossil fuels has achieved increasing interest since it is considered a CO_2 neutral fuel. A main disadvantage of biomass is the fast deactivation of the SCR catalyst [6–8] caused by the presence of high amounts of potassium compounds (up to 2 wt% in straw) which act as a poison to the catalyst. Potassium binds permanently to the catalyst and inhibits the SCR reaction.

Conventional V_2O_5–WO_3/TiO_2 catalysts are prepared by a sequential impregnation method with surface areas around 50–100 $m^2\ g^{-1}$ [3]. Over the last few years there has been great interest in development of highly active vanadium SCR catalysts [9–11]. Djerad et al. [9] studied the influence of 3 and 8 wt% V_2O_5 on 9 wt% WO_3/TiO_2 catalysts prepared by sol–gel method. They found that the well-dispersed and isolated vanadium oxide species (i.e. 3 wt%V_2O_5–9 wt%WO_3/TiO_2) were less active for the SCR reaction but with higher selectivity to N_2. Increasing the vanadium loading favours SCR reaction with poor selectivity to N_2. In order to achieve a high SCR activity and selectivity the vanadium content should be below the monolayer coverage level. Increasing the surface area TiO_2 allows to increase the vanadia loading while keeping high dispersion, hence enhancing both SCR activity and N_2 selectivity. Kompio et al. [10] reported on 5 wt% V_2O_5–10 wt% WO_3/TiO_2 catalysts which showed high SCR activity. These catalysts were prepared by a sequential impregnation method using titania hydrate as a support with high surface area (>250 $m^2\ g^{-1}$). We also reported that 20 wt% V_2O_5/TiO_2 catalysts prepared by a sol–gel method showed high surface area and superior SCR activity [11].

The deposition–precipitation (DP) method using a base for the precipitation step has been applied for the preparation of various catalysts. Upon increasing the pH of the solution, the precipitation of a metal hydroxide onto the support is expected. Deposition of a metal precursor allows better interaction between the metal precursor and the support, and this leads to the formation of a highly dispersed active phase after thermal treatment. To increase the pH of the solution most commonly urea, ammonia and sodium or potassium carbonates are used. Originally, DP was developed to apply high loadings of a catalytically active metal on the surface of a support [12], but it has also been employed more recently to deposit low loadings of extremely small metal particles on the surface of supports [13–15].

In the present work, we studied V_2O_5–WO_3/TiO_2 catalysts prepared by incipient wetness impregnation (IWI) and DP for the SCR reaction. The SCR activities of the catalysts were compared at similar V_2O_5 concentrations and characterized by nitrogen physisorption, X-ray powder diffraction (XRPD), Fourier transform infra red spectroscopy (FTIR), electron paramagnetic resonance (EPR), transmission electron microscopy (TEM), temperature-programmed reduction (H_2-TPR) and NH_3-temperature-programmed desorption (NH_3-TPD) techniques. Finally, the catalysts were tested for potassium resistance for the possible application to biomass-fired units.

Experimental

Catalyst preparation and characterization

Anatase TiO_2 DT-51 (Cristal Global with a sulphur content of $\sim$1.25 wt%, surface area of 87 $m^2\ g^{-1}$) and 10 wt% WO_3/TiO_2 (surface area of 75 $m^2\ g^{-1}$) were used as support materials. 10 wt% WO_3/TiO_2 was prepared by IWI method using ammonium metatungstate (Fluka, 99 %) as a precursor and DT-51 anatase TiO_2. The 10 wt% WO_3/TiO_2 (10WTi) catalyst was dried and calcined at 550 °C for 5 h.

A series of supported vanadium catalysts were prepared using IWI and DP methods. DP catalysts were prepared using ammonium carbamate (1 M solution) or ammonium hydroxide (20 vol%) as the precipitating agents. The required quantity of support (Anatase TiO_2 or 10 wt% WO_3/TiO_2), vanadium oxalate solution and precipitating agents were slowly added under effective stirring until the pH of the solution reached nine. The precipitate was allowed to remain in the basic medium for 1 h followed by evaporation. The obtained solid was oven-dried and calcined for 4 h at 450 °C. The catalysts prepared by DP using ammonium carbamate and ammonium hydroxide were represented as AC and AH, respectively. IWI catalysts were prepared without using the precipitating agents and followed the same drying and calcination steps. The poisoned catalysts were prepared by subsequent impregnation with a solution of KNO_3 (Sigma-Aldrich, 99.9 %) to yield a potassium concentration of 100 μmol g^{-1} catalyst. The potassium-doped catalysts were oven-dried and then calcined for 4 h at 450 °C.

XRPD measurements were performed on a Huber G670 powder diffractometer using CuKα radiation within a 2θ range of 2°–80° in steps of 0.02°. FTIR spectra of the samples were recorded on a Perkin Elmer 1710 spectrometer at ambient conditions in KBr discs (1 in 100 mg). BET surface areas of the samples (100 mg of catalyst) were determined from nitrogen physisorption measurements at liquid nitrogen temperature with a Micromeritics ASAP 2010 instrument.

EPR spectra of the catalysts were recorded ex situ with a Bruker EMX-EPR spectrometer working in the X-band (Bruker ER 041 XGG Microwave Bridge) at microwave frequencies around 9.77 GHz. The measurements were done at room temperature on samples transferred directly

into an exciator after calcination. Data treatment was performed with WIN-EPR software provided by Bruker.

NH_3-TPD experiments were conducted on a Micromeritics Autochem-II instrument. In a typical TPD experiment, 100 mg of dried sample was placed in a quartz tube and pretreated in flowing He at 100 °C for 1 h. The sample was treated at 100 °C with anhydrous NH_3 gas (Air Liquide, 5 % NH_3 in He). After NH_3 adsorption, the sample was flushed with He (50 ml min^{-1}) for 60 min at 100 °C. Finally, the TPD operation was carried out by heating the sample from 100 to 600 °C (10 °C min^{-1}) under a flow of He (50 ml min^{-1}).

H_2-TPR studies were also conducted on a Micromeritics Autochem-II instrument. In a typical experiment, 100 mg of oven-dried sample was placed in one arm of a U-shaped quartz sample tube on a quartz wool plug. The TPR analysis was carried out in a reducing mixture (50 ml min^{-1}) consisting of 4 % H_2 and balance Ar (Air Liquide) from 50 to 850 °C (10 °C min^{-1}). The hydrogen concentration in the effluent stream was monitored by a thermal conductivity detector (TCD) and the H_2 consumption values were calculated from calibration experiments. TEM images were acquired with a FEI Tecnai T20 G2 operating at 200 kV.

Catalytic activity measurements

The SCR activity measurements were carried out at atmospheric pressure in a fixed-bed reactor loaded with 10 mg of fractioned (180–300 μm) catalyst at a flow rate of 300 ml min^{-1} (at room temperature). The inlet concentrations were: NO = 1,000 ppm, NH_3 = 1,000 ppm, O_2 = 4 % and H_2O = 2.3 % with He as balance gas. During the experiments the temperature was increased stepwise from 200 to 450 °C while the NO and NH_3 concentrations were continuously monitored by a Thermo Electron Model 17C chemiluminescent NH_3–NO_x gas analyser. At each set-temperature the N_2O concentration was further measured by gas chromatography (Shimadzu-14 B GC, TCD detection, poraplot column). The activity was measured after attaining steady state and care was taken not to reach 100 % conversion to allow calculation of rate constants. The catalytic activity is represented as the first-order rate constant (cm^3 g^{-1} s^{-1}), since the reaction is known to be first order with respect to NO under stoichiometric NH_3 conditions [8]. Fresh and poisoned catalysts are compared by change in relative activity (%).

The first-order rate constants where obtained from the conversion of NO as:

$$k = -\frac{F}{w} \times \ln(1 - X),$$

where F denotes the flow rate (cm^3 s^{-1}), w the catalyst mass and X the fractional conversion of NO.

Results and discussion

Figure 1 shows the catalytic activity (cm^3 g^{-1} s^{-1}) profiles of 3 wt% V_2O_5/TiO_2 catalysts prepared by IWI and DP methods as a function of reaction temperature. Steady increase in activity was observed for all the catalysts with temperature. Maximum rate constants were observed at 425 °C and decreased thereafter due to the increased rate of ammonia oxidation. At 425 °C, 3VTi-IWI, 3VTi-AH and 3VTi-AC catalysts showed a rate constant value of 466, 634 and 790 cm^3 g^{-1} s^{-1}, respectively. These rate constants correspond to NO conversion values of 60.6 % (3VTi-IWI), 71.9 % (3VTi-AH) and 79.4 % (3VTi-AC), respectively, using 10 mg of catalyst. 3VTi-IWI had the same activity (468 cm^3 g^{-1} s^{-1} at 420 °C) as reported in our previous investigation [16]. Comparison of SCR activity at similar vanadium concentration indicates superior activity of the catalysts using ammonium carbamate and ammonium hydroxide as precipitating agents. The superior activity of DP-prepared catalysts could be due to several factors like change in acidic and redox properties as also reported by Moon et al. [12].

H_2-TPR is frequently used to study the redox properties of V_2O_5 catalysts. In Fig. 2 the TPR patterns of 3 wt% V_2O_5/TiO_2 catalysts are shown. 3VTi-IWI, 3VTi-AH and 3VTi-AC catalysts showed a broad peak with T_{max} at 430, 412 and 414 °C, respectively. The peak corresponded to the reduction of V^{5+} to V^{3+} [10]. Bond et al. [17] reported VO_x monolayer species to be reduced in a single step from V^{5+} to V^{3+} during TPR, if less than four layers of vanadium oxide was deposited. 3VTi-IWI, 3VTi-AH and 3VTi-AC catalysts showed H consumption of 560, 566 and 564 μmol g^{-1}, respectively. Thus, it indicates that a similar vanadium concentration is available in all the catalysts (assuming full reduction of vanadia). The low-temperature reduction peak (i.e. at 412, 414 °C) has been shown to

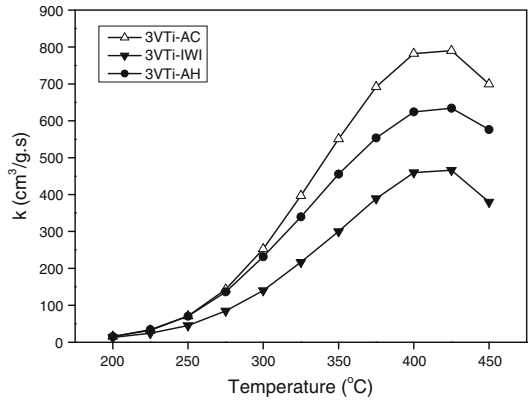

Fig. 1 SCR activity of 3 wt% V_2O_5/TiO_2 catalysts

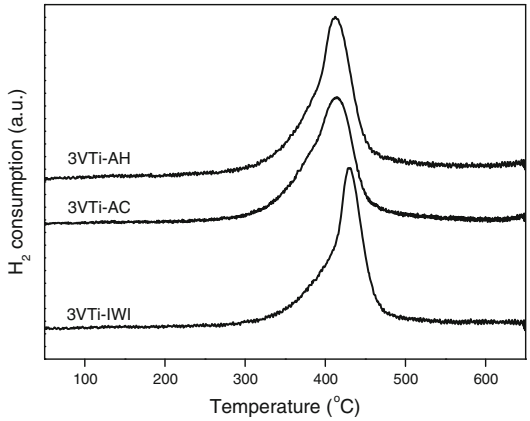

Fig. 2 H_2-TPR profiles of 3 wt% V_2O_5/TiO_2 catalysts

represent the monomeric species or highly dispersed vanadium species [18]. This indicates that ease of reducibility of the DP V_2O_5/TiO_2 catalysts is one of the factor for the superior SCR activity as also observed by Sorrentino et al. [19] using grafting and impregnation methods. With these initial observations, further studies were performed on 10 wt% WO_3/TiO_2 support with 1.5 and 3 wt% V_2O_5 loadings.

Figure 3 shows the SCR activity profiles of 1.5 and 3 wt% V_2O_5–10 wt% WO_3/TiO_2 catalyst prepared by IWI and DP methods. The prepared catalysts are highly active and the optimum operating temperatures are similar i.e. around 425 °C. All the catalysts showed k_{max} value at 425 °C except the 3V10WTi-AC catalyst, which had k_{max} value at 400 °C; and by further increasing reaction temperature to 450 °C the activity decreases due to increasing ammonia oxidation (SCO) over the catalysts. Overall the 1.5V10WTi-IWI, 1.5V10WTi-AH and 1.5V10WTi-AC catalysts showed k_{max} values of 890, 787 and 1,077 $cm^3\ g^{-1}\ s^{-1}$, respectively, at 425 °C reaction temperature. By further increasing the vanadium concentration, the 3V10WTi-IWI, 3V10WTi-AH and 3V10WTi-AC catalysts showed k_{max} values of 1,053, 1,229 and 1,342 $cm^3\ g^{-1}\ s^{-1}$, respectively, at their optimum temperatures. These rate constant values observed for the 3V10WTi catalysts are higher than those for the corresponding 3VTi catalysts as shown in Fig. 1. The rate constants observed for 1.5V10WTi-AC and 3V10WTi-AC catalysts are higher than for the other catalysts. Hence, such a comparison with preparation method, vanadium loading and change of precipitating agent allows choosing an optimum catalyst with better SCR activity. With respect to selectivity 3V10WTi-IWI, 3V10WTi-AH and 3V10WTi-AC catalysts displayed 17, 8 and 0 ppm N_2O formation at 400 °C, respectively. This indicates that the ammonia oxidation reaction, which is responsible for N_2O formation, took place

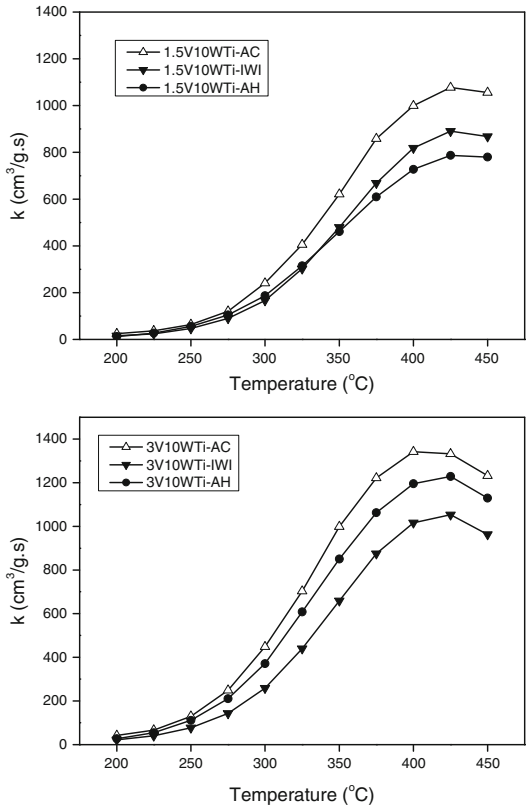

Fig. 3 SCR activity of 1.5 wt% V_2O_5–10 wt% WO_3/TiO_2 and 3 wt% V_2O_5–10 wt% WO_3/TiO_2 catalysts

in the 3V10WTi-AC catalyst. None of the 1.5V10WTi catalysts show N_2O formation at 400 °C.

The results of the N_2-BET surface area and weight percentage of V_2O_5 are shown in Table 1. With an increase in V_2O_5 metal loading from 1.5 to 3 wt%, a slight decrease in surface area is noted. The catalysts showed surface area in the order of AH > AC > IWI for 1.5 and 3 wt% V_2O_5 loadings. Normalized XRPD patterns of 10 wt% WO_3/TiO_2 support and 3V10WTi catalysts are shown in Fig. 4. The presence of a dominating anatase TiO_2 phase (25.3°, 37.9°, 47.8° and 54.3°) was observed in all catalysts. No peaks attributable to rutile TiO_2 (27.4°, 36.1° and 54.2°), WO_3 (17.8°, 20.2° and 23.1°) or V_2O_5 (20.3°, 26.1° and 30.9°) phases were observed. With an increasing V_2O_5 loading there is an increase in vanadium surface coverage ($VO_x\ nm^{-2}$), where the saturation value for the monolayer surface coverage was reported to be 7.9 $VO_x\ nm^{-2}$ [20]. The reported saturation monolayer surface coverage of tungsten was found to be about 4.2 $WO_x\ nm^{-2}$ [20]. In the present case the calculated monolayer surface coverage of

Table 1 Physico-chemical properties of catalysts

Catalyst	V_2O_5 (wt%)	Surface area ($m^2\ g^{-1}$)	Surface density ($VO_x\ nm^{-2}$)	Acidity ($\mu mol\ g^{-1}$)	
				Fresh	K-doped
1.5V10WTi-IWI	1.5	71	1.4	538	393
1.5V10WTi-AC	1.5	72	1.4	475	352
1.5V10WTi-AH	1.5	73	1.3	501	362
3V10WTi-IWI	3.0	65	3.0	594	323
3V10WTi-AC	3.0	68	2.9	454	271
3V10WTi-AH	3.0	70	2.8	448	284

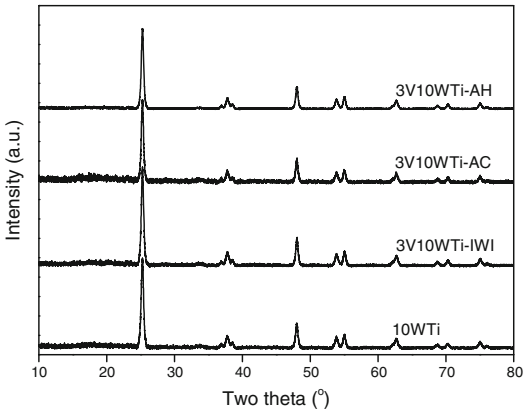

Fig. 4 XRPD patterns of 3 wt% V_2O_5–10 wt% WO_3/TiO_2 catalysts along with 10 wt% WO_3/TiO_2 support

10 wt% WO_3/TiO_2 support was found to be 3.7 WO_x nm^{-2}. It indicates that both vanadium oxide and tungsten oxide are well dispersed and below the monolayer surface coverage on the surface of the TiO_2 support.

FTIR spectra of the 10 wt% WO_3/TiO_2 support and 3V10WTi catalysts are shown in Fig. 5. The broad band observed in the region between 3,200 and 3,600 cm^{-1} and the sharp peak at 1,620 cm^{-1} is due to the stretching and bending vibrations of O–H groups, respectively. The band observed around 470 cm^{-1} can be attributed to the vibrational mode of the skeletal O–Ti–O bonds of the anatase phase [21, 22]. The band at 977 cm^{-1} is associated to W=O stretching of the tungstyl species [23]. The vanadyl species are not detected because of their low concentration compared to tungsten. Furthermore, the bands in the range 1,300–1,000 cm^{-1} can be attributed to different interactions of sulphate and sulphite ions with the TiO_2 surface [22, 23]. Pure V_2O_5 spectra (insert) showed stretching mode of the V=O (vanadyl oxygen) at 1,020 cm^{-1} and V–O–V stretching modes at 830, 585 and 480 cm^{-1} [21, 22].

Ammonia metavanadate as a precursor is expected to form V^{5+} species after calcination [24]. However, the TiO_2 support initiated reduction of a part of the vanadium from

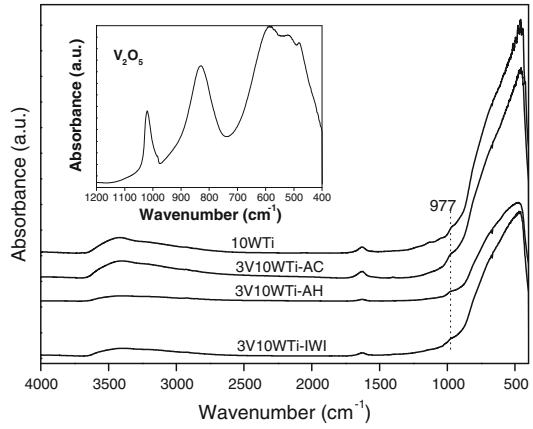

Fig. 5 FTIR spectra of 3 wt% V_2O_5–10 wt% WO_3/TiO_2 catalysts along with 10 wt% WO_3/TiO_2 support

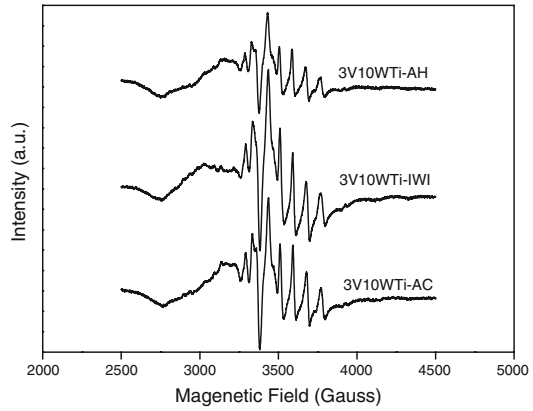

Fig. 6 EPR spectra of 3 wt% V_2O_5–10 wt% WO_3/TiO_2 catalysts recorded at room temperature

V^{5+} to V^{4+}. It was estimated that about 5 % of the total vanadium was reduced from V^{5+} to V^{4+} [24]. EPR has proven to be a powerful technique for detecting the presence of the paramagnetic V^{4+} species in vanadium catalysts. Figure 6 shows the EPR spectra of 3 wt% V_2O_5–10 wt% WO_3/TiO_2 catalysts recorded at room temperature. The EPR spectra revealed a signal from the paramagnetic V^{4+} ($3d^1$) ions with hyperfine structure, originating from the interaction of the unpaired electron with the $^{51}V(I = 7/2)$ to give rise to eight parallel and eight perpendicular components.

Figure 7 shows the H_2-TPR profiles of the 3 wt% V_2O_5–10 wt% WO_3/TiO_2 catalysts. The catalysts showed three reduction peaks around 490 °C (interacted V^{5+} and W^{6+} reduction), 650 °C (W^{6+} reduction to W^{4+}) and 780 °C (W^{4+} reduction to W^0), respectively [10]. Among all

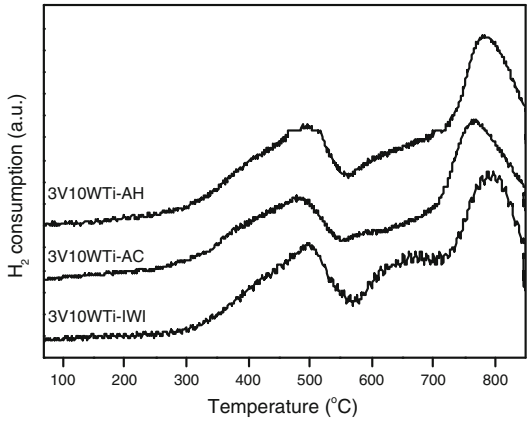

Fig. 7 H_2-TPR profiles of 3 wt% V_2O_5–10 wt% WO_3/TiO_2 catalysts

catalysts the 3V10WTi-IWI catalyst was reducing at slightly higher temperatures. 3V10WTi-IWI, 3V10WTi-AH and 3V10WTi-AC catalysts showed H consumption of 1,671, 1,963 and 1,980 μmol g^{-1}, respectively.

Pure TiO_2 support and 3 wt% V_2O_5–10 wt% WO_3/TiO_2 catalyst particles were investigated by means of TEM. For each sample, several locations on the TEM grid were analysed and representative micrographs of the three catalysts are shown in Fig. 8b–d. When comparing to the pure TiO_2 support (Fig. 8a), the three catalysts reveal a surface modification which appears to be more severe for 3V10WTi-AC. The new features appearing on the surface of the TiO_2 particles did not show any evidence of crystallinity.

Figure 9 shows the NH_3-TPD desorption patterns of 1.5V10WTi and 3V10WTi catalysts prepared by IWI and DP methods. All the catalysts showed broad NH_3-desorption patterns from 150 to 500 °C. The low-temperature peak at around 150 °C is attributed to desorption from the weak acid sites, while the high-temperature broad desorption peaks that appear at 300–500 °C are due to strong interaction of NH_3 with the catalyst. It can be observed that the high-temperature desorption peak is slightly shifted to lower temperatures for 3 wt% V_2O_5 loading compared to the 1.5 wt% sample. The NH_3-TPD results are summarized in Table 1. The acidity of the IWI catalysts increases with vanadium loading from 1.5 to 3 wt%. It is known that acidity of the catalysts is enhanced in the presence of vanadium [25]. On the other hand, slightly decreasing acidity of deposition-precipitated catalysts could be due to the influence of precipitating agents which might be strongly chemisorbed with catalyst even after calcination.

Poisoning the catalysts by doping with potassium (100 μmol g^{-1}) resulted in a decrease in activity and a

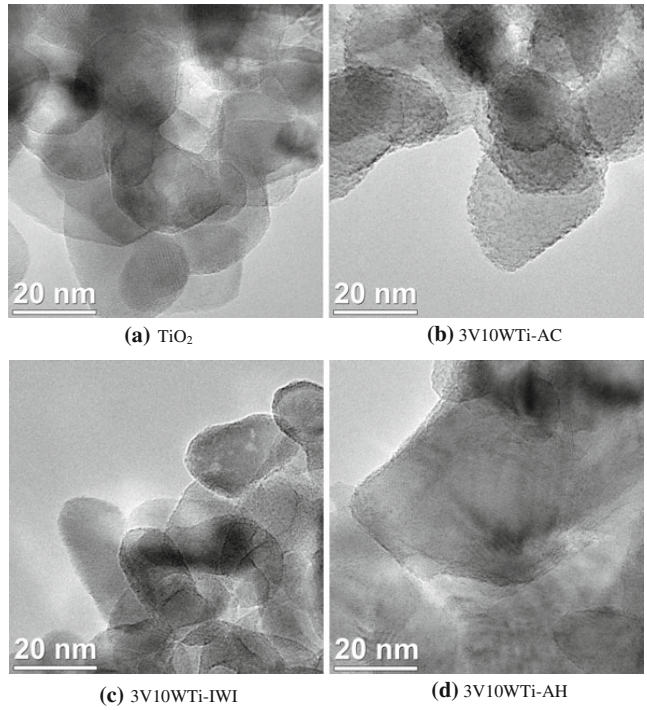

(a) TiO_2 **(b)** 3V10WTi-AC

(c) 3V10WTi-IWI **(d)** 3V10WTi-AH

Fig. 8 Bright-Field TEM micrographs of TiO_2 support and catalysts

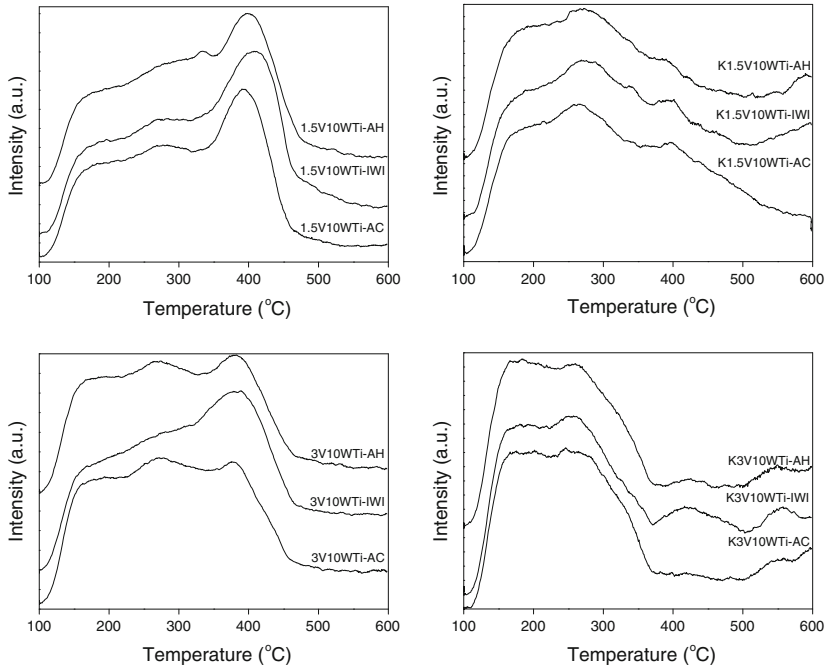

Fig. 9 NH_3-TPD profiles of 3 wt% V_2O_5–10 wt% WO_3/TiO_2 and potassium-doped 3 wt% V_2O_5–10 wt% WO_3/TiO_2 catalysts

small shift of k_{max} towards lower temperature (Fig. 10). The K1.5V10W-IWI, K1.5V10W-AH and K1.5V10W-AC catalysts exhibited k_{max} values of 242, 251 and 342 $cm^3\ g^{-1}\ s^{-1}$, respectively, at 400 °C. The K3V10W-IWI, K3V10W-AH and K3V10W-AC catalysts exhibited k_{max} values of 326, 336 and 334 $cm^3\ g^{-1}\ s^{-1}$, respectively, at 375 °C. The poisoned catalysts exhibited 24–35 % of their initial activity after poisoning, at 400 °C. The considerable decrease in the SCR activity of the poisoned catalysts shows the deactivation potential of potassium. Increasing the vanadium content from 1.5 to 3 wt% results in very little effect in overcoming the deactivation due to potassium.

Figure 9 also shows the NH_3-TPD profiles of potassium-doped catalysts and the results are summarized in Table 1. Overall a significant decrease in total acidity and decrease in the intensity of high-temperature desorption peaks that appear at 300–500 °C are observed. Especially, with increasing vanadium concentration from 1.5 to 3 wt%, the potassium-doped catalysts (100 μmol g^{-1} of potassium) showed above stoichiometric loss of surface acidity. The 1.5V10WTi-IWI and 3V10WTi-IWI catalysts lost 145 and 271 μmol g^{-1} of acidity, respectively, after potassium doping. Thus it indicates that increasing the vanadium concentration does not prevent the loss of surface acidity.

Several authors [26–32] have reported the deactivation effect of alkali metals on the SCR activity of vanadium catalysts followed by a drop in total acidity. The relative drop in SCR activity after potassium doping is known to be well correlated with decrease in total acidity of the catalysts. The potassium is blocking the V_2O_5 Brønsted acid sites permanently. These acid sites are important to initiate the SCR reaction through adsorption of ammonia. Zheng et al. [29] suggested a mechanism with a direct linear correlation between available V–OH sites and catalyst activity. Potassium species may bind irreversibly to V–OH sites leading to loss of activity. Since vanadium is present as both V=O and V–OH species it is not surprising that complete loss of activity is observed experimentally at K/V ratio of around 0.3–0.5 [28, 30]. Furthermore, above stoichiometric loss of acidity can be explained with the recently reported alkali deactivation mechanisms. Potassium metal atom can deactivate up to four active vanadium atoms as reported through DFT calculations by Nicosia et al. [31]. Lewandowska et al. [32] proposed a model including the alkali effect on the support with atomic ratio of $M{:}V{:}Ti_{surface} = 1{:}2{:}4$ using Raman spectroscopy and DFT calculations. Thus, we can assume that the alkali interacts with both the surface vanadium and the support.

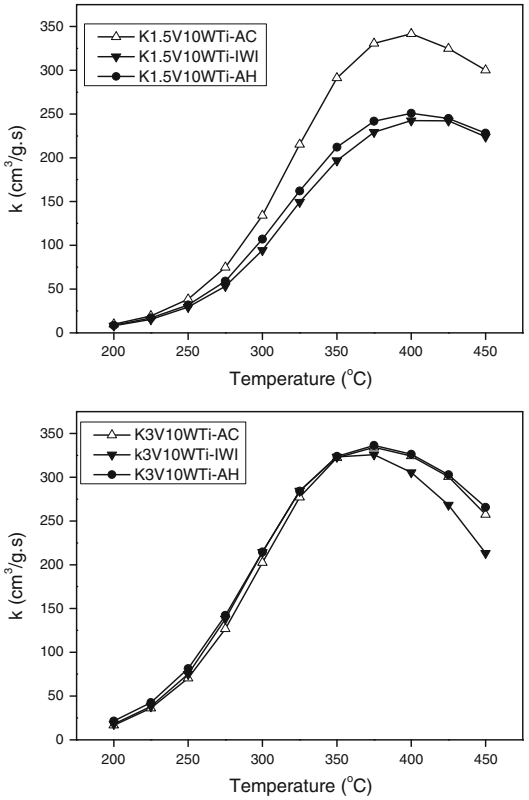

Fig. 10 SCR activity of potassium-doped 1.5 wt% V_2O_5–10 wt% WO_3/TiO_2 and 3 wt% V_2O_5–10 wt% WO_3/TiO_2 catalysts

Conclusions

In summary, V_2O_5/TiO_2 and V_2O_5–10 wt% WO_3/TiO_2 catalysts prepared by IWI and deposition precipitation methods are tested for the SCR of NO with NH_3. 3 wt% V_2O_5–10 wt% WO_3/TiO_2 catalyst prepared by DP method using ammonium carbamate as a precipitating agent was found to be the most active and selective to N_2. The superior activity of the catalyst can be ascribed to the altered acidic and redox properties of vanadium. The catalysts did not show improved alkali resistance, and so these modified formulations are suggested to be useful mainly in coal- or natural gas-fired power plants where the alkali content is less in fly ash and there is a demand for high SCR activity and selectivity to N_2.

Acknowledgements This work is financially supported by Energinet.dk through the PSO project 10521. A. P. Møller and Chastine Mc-Kinney Møller Foundation is gratefully acknowledged for its contribution towards the establishment of the Center for Electron Nanoscopy in the Technical University of Denmark.

References

1. Forzatti P (2001) Present status and perspectives in de-NO*x* SCR catalysis. Appl Catal A 222:221–236
2. Pârvulescu VI, Grange P, Delmon B (1998) Catalytic removal of NO. Catal Today 46:233–316
3. Alemany LJ, Lietti L, Ferlazzo N, Forzatti P, Busca G, Giamello E, Bregani F (1995) Reactivity and physicochemical characterization of V_2O_5–WO_3/TiO_2 De-NO*x* catalysts. J Catal 155:117–130
4. Bosch H, Janssen F (1988) Process development. Catal Today 2:489–506
5. Curtin T (2005) Selective catalytic reduction of NO*x*. In: Grassian VH (ed) Environmental catalysis. CRC Press, Boca Raton, pp 197–210
6. Zheng Y, Jensen AD, Johnsson JE, Thøgersen JR (2008) Deactivation of V_2O_5–WO_3–TiO_2 SCR catalyst at biomass fired plants: elucidation of mechanisms by lab- and pilot-scale. Appl Catal B 83:186–194
7. Due-Hansen J, Boghosian S, Kustov A, Fristrup P, Tsilomelekis G, Ståhl K, Christensen CH, Fehrmann R (2007) Vanadium-based SCR catalysts supported on tungstated and sulfated zirconia: influance of doping with potassium. J Catal 251:459–473
8. Putluru SSR, Kristensen SB, Due-Hansen J, Riisager A, Fehrmann R (2012) Alternative alkali resistant deNO*x* catalysts. Catal Today 184:192–196
9. Djerad S, Tifouti L, Crocool M, Weisweiler W (2004) Effect of vanadia and tungsten loadings on the physical and chemical characteristics of V_2O_5–WO_3/TiO_2 catalysts. J Mol Catal A 208:257–265
10. Kompio PGWA, Brückner A, Hipler F, Auer G, Löffler E, Grünert W (2012) A new view on the relations between tungsten and vanadium in V_2O_5–WO_3/TiO_2 catalysts for the selective catalytic reduction of NO with NH3. J Catal 286:237–247
11. Kristensen SB, Kunov-Kruse AJ, Riisager A, Rasmussen SB, Fehrmann R (2011) High performance vanadia-anatase nanoparticle catalysts for the selective catalytic reduction of NO by ammonia. J Catal 284:60–67
12. Moon SW, Lee G, Park SS, Hong S (2004) Catalytic combustion of chlorobenzene over V_2O_5/TiO_2 catalysts prepared by the precipitation-deposition. React Kinet Catal Lett 82:303–310
13. Babu NS, Lingaiah N, Gopinath R, Reddy PSS, Prasad PSS (2007) Characterization and reactivity of alumina-supported Pd catalysts fort he room-temperature hydrodechlorination of chlorobenzene. J Phys Chem C 111:6447–6453
14. Reddy PSS, Pasha N, Rao MGVC, Lingaiah N, Suryanarayana I, Prasad PSS (2007) Direct decomposition of nitrous oxide over Ru/Al_2O_3 catalysts prepared by deposition-precipitation method. Catal Commun 8:1406–1410
15. Gopinath R, Babu NS, Kumar JV, Lingaiah N, Prasad PSS (2008) Influence of Pd precursor and method of preparation on hydrodechlorination activity of alumina supported palladium catalysts. Catal Lett 120:312–319
16. Putluru SSR, Jensen AD, Riisager A, Fehrmann R (2011) Heteropoly acid promoted V_2O_5/TiO_2 catalysts for NO abatement with ammonia in alkali containing flue gases. Catal Sci Technol 1:631–637
17. Bond GC, Zurita JP, Flamerz S, Gellings PJ, Bosch H, Van Ommen JG, Kip BJ (1986) Structure and reactivity of titania-supported oxides. Part1: vanadium oxide on titania in the sub- and super- monolayer regions. Appl Catal 22:361–378
18. Kwon DW, Park KH, Hong SC (2013) The influence on SCR activity of the atomic structure of V_2O_5/TiO_2 catalysts prepared by a mechanochemical method. Appl Catal A 451:227–235

19. Sorrentino A, Rega S, Sannino D, Magliano A, Ciambelli P, Santacesaria E (2001) Performance of V_2O_5-based catalysts obtained by grafting vanadyl tri-isopropoxide on TiO_2–SiO_2 in SCR. Appl Catal A 209:45–57
20. Wachs IE (1996) Raman and IR studies of surface metal oxide species on oxide supports: supported metal oxide catalysts. Catal Today 27:437–455
21. Chary KVR, Kumar CP, Rajiah T, Srikanth CS (2006) Dispersion and reactivity of monolayer vanadium oxide catalysts supported on zirconia: the influence of molybdena addition. J Mol Catal A 258:313–319
22. Martha S, Das DP, Biswal N, Parida KM (2012) Facile synthesis of visible light responsive V_2O_5/N, S–TiO_2 composite photocatalyst: enhanced hydrogen production and phenol degradation. J Mater Chem 22:10695–10703
23. Cristallo G, Roncari E, Rinaldo A, Trifirò F (2001) Study of anatase-rutile transition phase in monolithic catalyst V_2O_5/TiO_2 and V_2O_5–WO_3/TiO_2. Appl Catal A 209:249–256
24. Srinivas D, Hölderich WF, Kujath S, Valkenberg MH, Raja T, Saikia L, Hinze R, Ramaswamy V (2008) Active sites in vanadia/titania catalysts for selective aerial oxidation of β-picoline to nicotinic acid. J Catal 259:165–173
25. Putluru SSR, Riisager A, Fehrmann R (2010) Vanadia supported on zeolites for SCR of NO by ammonia. Appl Catal B 97:333–339
26. Chen J, Yang R (1990) Mechanism of poisoning oft he V_2O_5/TiO_2 catalysts fort he reduction of NO by NH_3. J Catal 125:411–420
27. Lisi L, Lasorella G, Malloggi S, Russo G (2004) Single and combined deactivating effect of alkali metals and HCl on commercial SCR catalysts. Appl Catal B 50:251–258
28. Kamata H, Takahashi K, Odenbrand CI (1999) The role of K_2O in the selective reduction of NO with NH_3 over $V_2O_5(WO_3)/TiO_2$ commercial selective catalytic reduction catalyst. J Mol Catal A 139:189–198
29. Zheng Y, Jensen AD, Johnsson JE (2004) Laboratory investigation of selective catalytic reduction catalysts: deactivation by potassium compounds and catalyst regeneration. Ind Eng Chem Res 43:941–947
30. Khodayari R, Odenbrand CUI (2001) Regeneration of commercial TiO_2–V_2O_5–WO_3 SCR catalysts used in bio fuel plants. Appl Catal B 30:87–99
31. Nicosia D, Czekaj I, Kröcher O (2008) Chemical deactivation of V_2O_5/WO_3–TiO_2 SCR catalysts by additives and impurities from fuels, lubrication oils and urea solution: part II. Characterization study of the effect of alkali and alkaline earth metals. Appl Catal B 77:228–236
32. Lewandowska AE, Calatayud M, Lozano-Diz E, Minot C, Bañares MA (2008) Combining theoretical description with experimental in situ studies on the effect of alkali additives on the structure and reactivity of vanadium oxide supported catalysts. Catal Today 139:209–213